

**A COMPUTATIONAL FRAMEWORK TO QUANTIFY
NEUROMECHANICAL CONSTRAINTS IN SELECTING
FUNCTIONAL MUSCLE ACTIVATION PATTERNS**

A Thesis
Presented to
The Academic Faculty

by

Mark Hongchul Sohn

In Partial Fulfillment
of the Requirements for the Degree
Doctor of Philosophy in the
Woodruff School of Mechanical Engineering

Georgia Institute of Technology
May 2015

COPYRIGHT © 2015 BY MARK HONGCHUL SOHN

**A COMPUTATIONAL FRAMEWORK TO QUANTIFY
NEUROMECHANICAL CONSTRAINTS IN SELECTING
FUNCTIONAL MUSCLE ACTIVATION PATTERNS**

Approved by:

Dr. Lena H. Ting, Advisor
Wallace H. Coulter Dept. of Biomedical
Engineering
*Emory University and Georgia Institute of
Technology*

Dr. David Hu
Woodruff School of Mechanical
Engineering
Georgia Institute of Technology

Dr. Thomas Burkholder
School of Applied Physiology
Georgia Institute of Technology

Dr. Jun Ueda
Woodruff School of Mechanical
Engineering
Georgia Institute of Technology

Dr. Magnus Egerstedt
School of Electrical and Computer
Engineering
Georgia Institute of Technology

Date Approved: April, 6, 2015

Soli DEO Gloria

ACKNOWLEDGEMENTS

I would like to first thank my advisor, Dr. Lena Ting who has been a patient boss, a generous mentor, an inspiring teacher, an admirable colleague scientist, and a sincere friend to me throughout my graduate years. The word *grace* in a particular worldview of mine refers to a precious gift endowed to one who does not deserve it or have no rights to be endowed, yet solely by the good will of the endower. Lena has always been, and will be, more than I deserve.

I am also grateful to my thesis committee, Dr. Thomas Burkholder, Dr. Magnus Egerstedt, Dr. David Hu, and Dr. Jun Ueda. Their feedback, criticisms have provided a broader aspect to the problem, and have lit the way. Further, I thank Drs. Richard Nichols, Young-Hui Chang, Randy Trumbower, Francisco Valero-Cuevas, and Eric Perreault for leading me into the discussions that were full of insights.

I could not have been where I am now if it were not for the Neuromechanics lab. I thank Lucas McKay who, as my graduate mentor, has taught me how to think, read, write, talk, listen, and become a scientist. I thank Jeff Bingham who always marvels me with his talented skills, and makes me humbled by his noble character. I thank Stacie Chvatal for the warmth in heart she showed me in my times of despairs, helping me to remember that what I have already is enough. I thank Nate Bunderson, Seyed Safavynia, Julia Choi, Keith van Antwerp for their support. I thank Andrew Sawers, Jessica Allen, Yun Seong Song, Kyle Blum, Kim Lang, Aiden Payne, Danny Smith, and Chris Versteeg for always being there for help. I thank Cole Simpson for letting me be assured, once again, that through mentoring one can help another to live and let others live abundant life.

I thank my dearest friends in New Church of Atlanta. In particular I owe a lot to Dr. Jaemin Shin and (soon to be Dr., and a mother) Namin Jeong, who were there from the beginning when I was down on the ground with bare hands. I can never thank them enough for their love and supports.

I have debt of prayers throughout the life to my parents in Korea, Myong Hwan Sohn and Young Soon Shin. I stand in awe of Him who has fulfilled the promises they have received more than 30 years ago here in Atlanta so faithfully. It will be a burden for me for the rest of my life, as I raise my own children, to reflect how great of a parent they were. I would like to acknowledge my sister Hyojin Sohn and my twin brother David Hongsuk Sohn, they are always in my heart.

Lastly, but not the least, I want to thank Jinhee Kim for being there beside me in any circumstances. Ever since she has walked into my life, every day is a miracle, a testimony. I thank her for bringing into our lives our beloved, Yul Junpyo Sohn, who has given me the reasons to take steps forward, who is a reason for my daily breath.

Thank you all.

Studying neural control of movement has always amazed me as I witness the beauty of the design that is all so wondrous. Even though all I could seek for my entire life would still be only a tiny bit of the whole, I shall walk this path humbly in recognition of the Designer who reigns from above. All is Yours, and You are my all.

TABLE OF CONTENTS

	Page
ACKNOWLEDGEMENTS	v
LIST OF TABLES	x
LIST OF FIGURES	xi
SUMMARY	xiii
 <u>CHAPTER</u>	
1 INTRODUCTION	1
1.1 Background	3
1.1.1 Challenges in studying neural control of movement	3
1.1.2 Limitations in current modeling approaches	4
1.1.3 Balance control as a paradigm	7
1.1.4 Muscle synergy hypothesis for balance control	8
1.2 A new computational framework	10
1.3 Thesis overview	11
2 MUSCLE FEASIBLE RANGE DEFINED BY BIOMECHANICAL CONSTRAINT OF THE LIMB AND THE TASK	14
2.1 Introduction	15
2.2 Methods	17
2.2.1 Musculoskeletal model	17
2.2.2 Target endpoint forces	18
2.2.3 Lower and upper bounds on muscle activation	19
2.2.4 Comparison to predicted solutions from suggested neural strategies	20
2.3 Results	20
2.3.1 Bounds on muscle activation during endpoint force production	20
2.3.2 Comparison of identified bounds and predictions of neural strategies	23
2.3.3 Physiological null space at $\alpha=0$	26

2.4 Discussion	26
3 FUNCTIONAL REQUIREMENT FOR GENERALIZABILITY ACROSS BIOMECHANICAL CONDITIONS	30
3.1 Introduction	30
3.2 Methods	33
3.2.1 Experimental synergy force vector data	34
3.2.2 Musculoskeletal model	35
3.2.3 Best-generalizable solution	37
3.2.4 Minimum-effort solution	38
3.2.5 Random solutions	39
3.2.6 Muscle feasible ranges with generalizability constraint	39
3.3 Results	42
3.4 Discussion	50
4 TRADE-OFFS BETWEEN FUNCTIONAL PROPERTIES OF EFFORT AND STABILITY	55
4.1 Introduction	55
4.2 Methods and materials	60
4.2.1 Musculoskeletal model and target endpoint force	60
4.2.2 Defining metrics for effort and stability	62
4.2.3 Mapping the null-path between minimum and maximum-effort solutions	64
4.2.4 Exploring the neighboring solutions	66
4.2.5 Characterization of the local landscape	70
4.2.6 Characterization of the global landscape	71
4.2.7 Investigating redundancy within equivalent functional properties	73
4.3 Results	74
4.3.1 Null-path between minimum and maximum-effort solutions	74
4.3.2 Local landscape explored by the neighboring solutions	75
4.3.3 Global landscape across effort level	81
4.3.4 Redundancy in solutions with equivalent functional properties	83
4.4 Discussion	84

4.A Appendix: Altered mapping due to other potential mechanisms contributing to intrinsic stability	93
4.B Appendix: Effect of signal-dependent noise	96
4.C Appendix: Analysis in muscle activation space	99
5 SIGNIFICANCE	103
5.1 Implications for computational modeling	103
5.1.1 A paradigm: Models as tools for building a map on which to locate one's behavior	103
5.1.2 Finding muscle activation patterns that provide stability to musculoskeletal dynamics	107
5.1 Implications for muscle synergy hypothesis in motor control	109
5.1.1 Guiding principles for acquiring generalizable motor solutions	109
5.1.2 Modular control in real-world applications	112
5.1 Clinical relevance	113
5.1.1 Neuromechanical alterations following stroke	113
5.1.2 Altered kinematics of crouch gait in cerebral palsy	115
5.1.3 Difficulties in training individuals with motor impairments	116
6 CONCLUSION	118
6.1 Limitations and future works	119
6.1.1 Integrating functional requirements for generalizability and stability	119
6.1.2 Task-level control of whole body CoM at global level	120
6.1.3 Experimental validation	122
6.2 Concluding remarks	126
APPENDIX A: EXTENDING MUSCLE FEASIBLE RANGE ANALYSIS TO DYNAMIC TASK OF HUMAN WALKING	128
APPENDIX B: APPLICATION TO IMPAIRED MOTOR CONTROL: EXAMPLES IN STROKE AND AMPUTEES	143
APPENDIX C: TECHNICAL NOTE ON ESTIMATING STATE MATRIX	156
REFERENCES	164
VITA	199

LIST OF TABLES

	Page
Table 2.1: Muscles included in the hindlimb model and abbreviations	18
Table 2.2: Muscle classification in terms of lower bound behavior	24
Table 2.3: Muscle classification in terms of upper bound behavior	25
Table 3.1: Muscles included in the hindlimb model and abbreviations	36
Table 3.2: Force angle deviations in all conditions	43
Table 3.3: Changes in feasible bounds with generalizability constraint with respect to absolute bounds	48
Table 4.C.1: Categorized changes in distribution from perturbed to projected solutions	101
Table 4.C.2: Muscle pairs with high correlation in projected solutions	102
Table A.1: Muscles included in the OpenSim 2392 musculoskeletal model and their abbreviations	142
Table B.1: Muscles included in the musculoskeletal model and their abbreviations	147

LIST OF FIGURES

	Page
Figure 2.1: Experimental data and model	16
Figure 2.2: Target force directions and muscle feasible ranges	21
Figure 2.3: Physiological null space	26
Figure 3.1: Experimental data and model	34
Figure 3.2: Generalizability of simulated endpoint force vectors	44
Figure 3.3: Effort level comparison	46
Figure 3.4: Muscle activation patterns and muscle feasible ranges	47
Figure 3.5: Generalizability of random solutions strictly inside feasible range with generalizability constraint	50
Figure 4.1: Model and the task	61
Figure 4.2: Schematic illustration of null-path	65
Figure 4.3: Schematic illustration of generating neighboring solutions	67
Figure 4.4: Null-path and neighboring solutions	76
Figure 4.5: Local landscape characteristics	78
Figure 4.6: One-way ANOVA multiple comparison across step size	80
Figure 4.7: Sensitivity	81
Figure 4.8: Pareto front	83
Figure 4.A: Null-path in altered conditions	94
Figure 4.B: Task error and stability with SDN	97
Figure 6.1: Proposed experimental study	124
Figure 6.2: Predictions to proposed experimental study	125
Figure A.1: Schematic of methods used to identify feasible ranges of muscle activation during walking	132

Figure A.2: Experimental data used for computing feasible ranges during walking	133
Figure A.3: Computed upper and lower bounds of the feasible ranges of muscle activation as a function of the gait cycle for all 43 muscles of the two legs in the OpenSim 2392 musculoskeletal model	137
Figure A.4: Computed upper and lower bounds of feasible ranges of muscle activation as a function of the gait cycle with experimental EMG data superimposed	139
Figure B.1: Model and target force directions	146
Figure B.2: Feasible force and muscle feasible range	148-149
Figure B.3: FFS in ABLED and TTLL	153
Figure B.4: Redundancy in muscle space	154

SUMMARY

Understanding possible variations in muscle activation patterns and their functional implications to movement and motor control is crucial for rehabilitation. Inter- and intra-subject variability is often observed in muscle activity measured during performance of the same task in both healthy and impaired individuals. However, the extent to which muscle activation patterns can vary under specific neuromuscular conditions and how they may differ functionally are still not well understood. Current musculoskeletal modeling approaches using optimization techniques cannot adequately address such questions because they focus on identifying a unique optimal muscle activation pattern, though many possible patterns exist that could produce the same movement. Therefore, we need an alternative modeling framework to explore and characterize the range of possible muscle activation patterns for a given task and to explain the functional implications of such variations.

Here I developed a novel computational framework that uses a detailed musculoskeletal model to reveal the latitude the nervous system has in selecting muscle activation patterns for a given task with respect to various biomechanical and neural constraints. I specifically focused on an isometric endpoint force generation task relevant to standing balance behavior in cats using a cat hindlimb model. By identifying the explicit bounds on activation of individual muscles defined by biomechanical constraints of the limb and the task, I demonstrate that there exists a wide range of feasible activation patterns that may be sufficient to account for experimentally observed variability. By investigating the possible biomechanical and neural bases of using the same muscle

activation pattern to produce a force across limb postures, I demonstrate that demand for generalization of function can affect the selection of muscle activation patterns that is not granted by limb biomechanics nor a single optimality criterion. By characterizing the landscape of the solution space with respect to two functional properties, effort and stability, I also demonstrate a possible trade-off in neural selection of muscle activation patterns for a given task that may explain individual differences. In addition, I discuss work where I have extended the method to the dynamic task of human walking. Finally, I present preliminary work showing how the modeling framework developed in this thesis can be used for understanding impaired motor control by considering altered biomechanical and neural constraints.

Neuromechanical principles underlying functional and impaired movements can be elucidated by understanding the allowed variability in muscle activation patterns and evaluating the functional consequences of such variations. Specifically, we may gain valuable insights to explaining individual differences in movement strategies, motor learning, or compensation to neuromuscular disorders. Furthermore, this framework can be useful in developing novel biologically-inspired control principles for robots and effective patient-specific treatments and rehabilitation strategies.

CHAPTER 1

INTRODUCTION

In control of movement, humans respond to unexpected perturbations in a robust manner and flexibly adapt to novel tasks. Yet, how the nervous system achieves such graceful control is not fully understood. In particular, redundancy at multiple levels of sensorimotor transformation poses a degrees of freedom problem (Bernstein 1967) in that there are many ways in how the same motor task can be achieved. Accordingly, substantial inter- and intra-subject variability is observed in muscle activity measured during a movement in both healthy and impaired individuals (Gottlieb 1998; Horak and Nashner 1986; Winter and Yack 1987). Understanding this *motor abundance* manifested in such allowed variability is essential to elucidating the neuromechanical control underlying functional and impaired movements.

What determines the differences? That is, what determines which muscle activation pattern is to be used for a given task? The main question that has remained unanswered is the degree to which a muscle activation pattern for a given movement is determined by biomechanical or neural constraints. *Biomechanical constraints* refer to limiting factors owing to the capability of the musculoskeletal system such as the anatomical arrangement of limb musculature, and the task requirements. Musculoskeletal redundancy may allow for ample room in how multiple muscles can be coordinated to achieve a movement under given biomechanical constraints, especially for sub-maximal tasks. Thus, kinematic or morphological differences may not solely account for differences in muscle activity across individuals or trials (Walter et al. 2014). On the other hand, *neural constraints* refer to the principles or control strategies by which the nervous system selects particular solutions to be used. Neural redundancy may, as well, allow for many functionally equivalent solutions, which may not be necessarily optimal

but are “good enough” for a given motor task (Loeb 2012). Specific neuromuscular conditions may affect the possible choices. For example, compromised systems such as weakened muscles or reduced cortico-spinal input due to neurological pathologies may induce a compensatory mechanisms to achieve a functional motor task.

However, it is difficult to understand or interpret variability in muscle activity. Questions may arise: What are the functional differences between one muscle activation pattern and another? What are the possible changes that can be made to muscle activation patterns in individuals with impairment for recovering function? In order to address these types of questions, it is crucial that we understand possible variations in muscle activation patterns and its functional implications to movement and motor control.

Current musculoskeletal modeling approaches use optimization techniques that cannot adequately address such questions because they focus on identifying a unique optimal muscle activation pattern among the many possible patterns that could produce the same movement. Accordingly, optimal predictions often deviate from measured muscle activity and cannot account for experimental variability (Buchanan and Shreeve 1996; Herzog and Leonard 1991; Thelen and Anderson 2006). Nevertheless, detailed musculoskeletal models can be useful tools because they provide high-resolution access to internal variables, such as muscle force, and definitive causal relationships allowing isolated control over parameters of interest (Bunderson and Bingham in press; Hicks et al. 2015). We currently lack a quantitative modeling framework to *explore* the range of possible muscle activation patterns for a given task using musculoskeletal models, and to *predict* the functional implications of such variations.

To this end, this thesis presents a novel computational framework that uses a detailed musculoskeletal model to reveal the latitude the nervous system has in selecting muscle activation patterns for a given task with respect to various biomechanical and neural constraints.

1.1 Background

1.1.1 Challenges in studying neural control of movement

Studying neural control of movement is a difficult problem because it involves complex interaction among neuromechanical elements at multiple hierarchical levels (Nishikawa et al. 2007; Ting et al. 2012). At the execution level, muscle activity is an output of the nervous system that incorporates control signals from multiple sources such as reflexive feedback from spinal circuits and volitional commands descending from higher centers. On the other hand, the transformation from muscle activation to actual movement occurs in a highly nonlinear manner where forces exerted by active muscles result in net moments at the joints that subsequently produce joint movement or limb endpoint forces (Ting and Chiel in press). Biomechanical constraints such as interaction torques (Gribble and Ostry 1999; van Antwerp et al. 2007) and state dependency of muscles' force generation on the dynamics of the body (Gordon et al. 1966; Hill 1953; Rack and Westbury 1969; Zajac 1989) further complicate the problem. What remains largely unknown is the extent to which either biomechanical or neural constraint determines the selection of a particular solution for a given movement.

In particular, understanding the influence of musculoskeletal redundancy on the selection of muscle activation patterns is difficult. Because the number of muscles exceeds the number of joints to be controlled, any movement can be produced with multiple patterns of muscle activation. Accordingly, muscle patterns used during production of similar biomechanical outputs such as joint kinematics or endpoint force varies across individuals and across trials, as measured in substantial variability in electromyography (EMG) (Horak and Nashner 1986; Torres-Oviedo et al. 2006; Torres-Oviedo and Ting 2007). However, it is difficult to interpret such variability with respect to the biomechanical latitude that the nervous system has when selecting muscle activation patterns. There have been only a few studies that have quantitatively examined

the implications of musculoskeletal redundancy on muscle activity (Collins 1995; Kutch and Valero-Cuevas 2011; Martelli et al. 2015; Martelli et al. 2013).

In addition, the functional criteria by which the nervous system may select a specific muscle activation pattern among many possible is not readily identifiable. Variability in neuromotor behaviors results naturally from a large space of equivalent solutions (Klein et al. 2010; Prinz et al. 2004; Raphael et al. 2010). Nevertheless, the nervous system seems to coordinate muscles in a specific manner, exhibiting robust patterns across many functional behaviors (Carlsöö 1972; Elble et al. 1994; Mann et al. 1979; Winter 1987; Winter and Yack 1987). However, multiple objectives and individual habits or preferences that may be involved in such selection (de Rugy et al. 2012; Ganesh et al. 2010; Hasson et al. 2012) obscure the landscape of the solution space.

Furthermore, it is often difficult to evaluate the functional implications of a given muscle activation pattern with respect to a task-level goal of movement. The sensorimotor transformation between abstract goals and execution-level neural commands can be inferred by describing the relationship between experimentally measurable variables. For example, recruitment of muscles has been shown to reflect global task-level variables such as whole-body center of mass in standing balance (Lockhart and Ting 2007; Nashner 1976; 1977; Ting 2007) or angular momentum in walking (Herr and Popovic 2008; Silverman et al. 2012). Local variables such as individual joint angles do not predict well the observed responses in muscle activity or joint torques (Gollhofer et al. 1989; Park et al. 2004; Peterka 2000; Ting and Macpherson 2004). However, these experimental approaches are descriptive such that it is difficult to predict how variations to the observed muscle activation pattern or using different muscle activation patterns will affect the goal of a movement at a global level.

1.1.2 Limitations in current modeling approaches

Realistic musculoskeletal models and simulations can be useful tools in studying movement in that they serve as a test bed on which viability of certain hypothesized neural control strategies can be dissected (Hicks et al. 2015; Zajac 1993). For example, knowing how muscles are coordinated to produce net joint moments that result in a given movement is essential for understanding the underlying neural control. However, because direct measurement of muscle forces is mostly restricted *in vivo* (Fleming and Beynnon 2004), musculoskeletal models can be used to predict muscle activation or force (Erdemir et al. 2007).

Studies using musculoskeletal models to identify muscle patterns required for generating a given movement often utilize optimization techniques to resolve the redundancy problem. There have been mainly three types of approaches: the inverse approach, the forward approach, and the optimal control strategy approach. The inverse approach computes required net joint torques from measured kinematics and external forces (inverse dynamics) and uses optimization to identify a unique muscle activation pattern that satisfies the joint torque requirement. An implicit assumption is made about the criteria by which muscle patterns are organized, represented as a cost function to be minimized, often related to neural effort in terms of muscle forces (Crowninshield and Brand 1981). The forward approach uses forward simulation and dynamic optimization to determine activation patterns that track experimental data (kinematics, kinetics) where the goal is to minimize error from prescribed motion (McLean et al. 2003; Neptune et al. 2001). Sometimes experimental EMG data is directly incorporated in predictions by tracking the activation profiles in subset of muscles that were measured experimentally (Piazza and Delp 1996; 2001). Alternatively, the optimal control strategy approach provides insights to how muscles should be coordinated to maximize the specified performance in a given movement. In this approach, forward simulation and dynamic optimization are used to identify a muscle activation pattern to achieve a goal that needs to be specified explicitly (Pandy 2001). Such an approach has

been successful in predicting various motor behaviors such as human walking (Anderson and Pandy 2001a), maximum-height jumping (Anderson and Pandy 1999) or maximum-speed pedaling (Raasch et al. 1997).

However, the above approaches fail to predict different neural control strategies that can be used to achieve the same motor goal. In both the inverse and forward approaches, the objective is to replicate prescribed experimental data, e.g. motion (kinematics and kinetics) or muscle activity, rather than predicting a behavior *de novo* based on task-level goals. Optimal control approaches are capable of predicting a behavior when a well-defined explicit goal exists for a given motor task. However, optimal control solutions typically converge to a global extremum only when the capability of the model is pushed towards its biomechanical limits such as maximal tasks. Available solutions are highly restricted in such cases, likely leaving only one possibility that may not be relevant to most sub-maximal tasks. An optimal control solution for sub-maximal tasks such as walking likely converges to one of the many local extrema, and thus represents one particular solution from the many that may have similar performance. Overall, these approaches cannot account for variations from an optimum or allowed variability the nervous system possess in selecting muscle activation patterns because they identify only a unique solution from many possible solutions that produce the same movement. Indeed, predicted solutions often deviate from experimentally measured muscle activity (Buchanan and Shreeve 1996; Herzog and Leonard 1991). Therefore, these approaches may not necessarily reveal the underlying neural principles in control of movements beyond biomechanical considerations.

Moreover, simulated movements produced by these optimal solutions are not robust to internal or external perturbations because stability is not considered. Local stability of a musculoskeletal system conferred by the active stiffness and viscosity of muscles can be tuned through the selection of muscle activation patterns producing equivalent motor output (Bunderson et al. 2008). Studies show that animals use viable

solutions that provide intrinsic postural stability, even during the sensorimotor feedback delay (Jacobs and Macpherson 1996), that may not necessarily be the most efficient solution (Bunderson et al. 2010). Because current modeling studies lack neuromechanical principles to guide selection of muscle activation patterns based on physiologically meaningful stability, simulations are often vulnerable to small changes in modeling parameters or variation to the solution, especially for unstable tasks such as walking (John et al. 2013; Risher et al. 1997).

1.1.3 Balance control as a paradigm

Postural control for standing balance is a motor task that is highly suited for studying neural control of movement. Understanding how postural stability is achieved in standing balance has significant clinical importance because falls due to loss of balance often lead to increased morbidity in the elderly (Anderson et al. 2004).

In addition, the contributions of different neuromechanical elements involved can be identified. Delayed responses in muscles elicited by the perturbation can be temporally decoupled into reflexive response (~25ms in cats and ~50ms in humans) and automatic postural response (APR) which occurs around 50 and 100ms, in cats and humans, respectively, after perturbation onset (Horak and Macpherson 1996). Disassociation of the neural command in terms of different control sources is not practically possible for voluntary movements in contrast.

Furthermore, the primary task-level goal for balance control is clearly defined: to maintain the center of mass (CoM) over the base of support (Carpenter et al. 1999; Diener et al. 1988). Moreover, the relationship between the muscle activity and biomechanical output can be assumed to be more direct and linear (Kuo and Zajac 1993; Valero-Cuevas 2000; Valero-Cuevas et al. 1998) because the task can be considered quasi-static, involving small changes in biomechanical parameters (Ting and Macpherson

2004). Nonetheless, redundancy at both kinematic and muscle level provides ample room in which the nervous system can exploit a multitude of viable solutions that achieve the goal. The redundancy of the solution space is illustrated in different strategies used to coordinate multi-joint torques, or variability observed in muscle activity during responses to support perturbation (Horak and Nashner 1986; Runge et al. 1999).

However, studies using computational models to understand balance control have not focused on investigating neural principles underlying spatial coordination across muscles. The majority of studies used simplified models with reduced level of biomechanical complexity, e.g. inverted pendulum or segmental models, to understand the role of sensory feedback, or optimal control strategies in torque space for regulating postural equilibrium (Alexandrov et al. 2001; Bortolami et al. 2003; Kiemel et al. 2002; Kuo 1995; Park et al. 2004; Peterka 2000; Runge et al. 1995; van der Kooij et al. 1999). Only a few studies have used musculoskeletal models to predict experimentally-observed balance behavior assuming various neural feedback mechanisms (Jo and Massaquoi 2004; Mansouri and Reinbolt 2014; Nataraj et al. 2012 ; Nataraj et al. 2010). Yet, these studies still do not address the question of how the nervous system organizes spatial structure of coordination pattern across muscles during balance control.

1.1.4 Muscle synergy hypothesis for balance control

More recent studies examining the underlying structure in coordination of muscles suggest that the nervous system may use a set of a few synchronously activated groups of muscles, called muscle synergies, which can be combined to produce a large repertoire of movement (d'Avella et al. 2003; Hart and Giszter 2004; Ivanenko et al. 2004; Ting and Macpherson 2005; Tresch et al. 1999). Such modular organization may simplify control by reducing the number of independent degrees of freedom to be controlled (Ting 2007) and making the system more linear and controllable.

Experimental studies in balance control also suggests the existence of a modular control scheme where muscle synergies are used in robust manner across a variety of different conditions. In postural behavior during standing balance in cats and humans, muscle synergies were found to produce a specific ground reaction force to exert appropriate acceleration at the CoM (Chvatal et al. 2011; Ting and Macpherson 2005; Torres-Oviedo and Ting 2007). Temporal recruitment of postural muscles synergies have been shown to reflect task-level feedback based on CoM kinematics (Lockhart and Ting 2007; Safavynia and Ting 2013; Welch and Ting 2008). Further, a common set of muscle synergies producing consistent endpoint forces with respect to limb orientation across different postural configurations has been observed in cats (Torres-Oviedo et al. 2006).

However, the criteria by which certain muscle activation patterns may be selected for muscle synergies, as the building blocks for functional movement, remain unknown. Muscle synergy patterns used to produce similar force vectors during balance control varies across individuals in both cats (Torres-Oviedo et al. 2006) and humans (Torres-Oviedo and Ting 2007). The reason for such variations in spatial organization of muscle synergies across individuals could not be explained because experimental approaches have been mainly descriptive (Tresch and Jarc 2009). It is still controversial whether muscle synergies are indeed a choice of the nervous system, as opposed to an emergent structure from biomechanical constraints of the task (Bizzi and Cheung 2013; Kutch and Valero-Cuevas 2012).

In conclusion, how various costs, constraints, and strategies would affect the selection of specific patterns for functional muscle synergies has not been studied. Although musculoskeletal models have been successful in simulating behaviors using muscle synergies (Alessandro et al. 2013; McKay and Ting 2008), patterns for muscle synergies were synthesized in these studies either according to an implicit optimality criteria (McKay and Ting 2012; Steele et al. 2013), or by using experimentally-observed patterns directly (Allen and Neptune 2012; Neptune et al. 2009).

1.2 A new computational framework

I propose a novel computational framework that explores the complete range of muscle activation patterns that can be used for a given movement, and examines the functional implications of possible variations within the multitudes of solutions. The proposed framework overcomes the limitations of experimental approaches that are mainly descriptive (Alessandro et al. 2013; Pandy and Andriacchi 2010; Tresch and Jarc 2009), and the current computational modeling approaches that use optimization techniques to examine only a single solution (Buchanan and Shreeve 1996; Collins 1995; Herzog and Leonard 1991). In essence, this new paradigm maximizes the potential utility of the detailed musculoskeletal models that provide full access and isolated control over neuro-musculoskeletal parameters of interest (Bunderson and Bingham in press; Zajac 1993).

The principle of the proposed framework is to identify the explicit bounds in the solution space defined purely by the biomechanical constraints. These bounds represent the biomechanical latitude that the nervous system has in selecting muscle activation patterns, and quantifies the range in which all theoretically possible solutions lie. The biomechanical constraints for a given movement are determined by the torque-producing capability of the muscles and net joint torque requirements (task demand) from measured or specified kinematics and kinetics.

Next, the proposed framework imposes additional constraints or considers costs that may narrow the range of possible solutions, based on hypothesized principles by which the nervous system organizes the spatiotemporal structure of muscle activation patterns. This identifies sub-ranges in muscle activation space, or subsets of solutions that meet certain functional criteria or confer a certain functional property to the system. Different constraints and costs can be considered such as generalization of movement across multiple biomechanical conditions, neural criteria regarding energetic cost or control strategies, or neuromuscular impairments.

Finally, the proposed framework evaluates and compares muscle activation patterns in terms of function. Neuromechanical constraints and costs that affect the selection of muscle activation patterns are used as quantitative metrics to evaluate and compare different solutions in terms of functional implications of using a particular solution. Using these metrics, high-dimensional muscle activation space can be mapped with respect to their functional properties. By constructing a map that can be visualized in low-dimensional (two or three) functional property space, one can predict how certain variations to muscle activation pattern result in differences in functional implications, both in terms of the direction (qualitative measure of what kind of change) and distance (quantitative measure of how much different).

The proposed computational framework provides quantitative tools that can be used for elucidating the underlying neuromechanical principles by which the nervous system selects particular functional muscle activation patterns, and to explain individual differences. Sources of variability in muscle activation patterns that can be used to produce the same movement may arise from neural selection (Bernstein 1967). Therefore, examining variability is crucial for understanding the neural control of functional and impaired movements. In particular, the proposed framework can be used to identify the full range of possible variations – the way in which neuromuscular redundancy shapes the bounds on how different solutions can be, and predict the functional implications of such variations – predicting the consequences of using certain solutions as well as to explain why one solution is chosen versus another.

1.3 Thesis overview

In this thesis, I seek to investigate the principles by which the nervous system may explore and select viable muscle activation patterns used in the functional behavior of balance control. In particular, I focused on an isometric endpoint force generation task

relevant to muscle synergies used for standing balance behavior in cats. To this end, I developed a novel computational framework to reveal the latitude the nervous system has in selecting muscle activation patterns for a given task with respect to various biomechanical and neural constraints. In particular, I used a highly redundant musculoskeletal model of the cat hindlimb to characterize the solution space available for a given task. In addition, I utilized forward dynamic simulations to evaluate the functional properties of given solutions with respect to dynamics of the whole limb.

My overall hypothesis is that the nervous system flexibly selects muscle patterns for functional muscle synergies that are “good enough” regarding energetic efficiency, stability, and generalizability. A further implication is that biomechanical constraints nor a single optimality criterion alone are insufficient to define muscle activation patterns for producing an observed force during reactive balance behavior. I predict that biomechanical redundancy confers a multitude of functionally equivalent solutions that are energetically suboptimal but provides stability and generalizable function.

In order to test this hypothesis, I addressed three relevant, yet independent, questions. The general scheme is to consider from pure biomechanical constraints to more neural constraints in selecting muscle activation patterns for a given task: I examine the range of possible muscle activation patterns to satisfy a single biomechanical condition (chapter 2), multiple biomechanical conditions (chapter 3), and multiple neural criteria regarding cost and implication to local dynamics of the body (chapter 4).

In **Chapter 2**, I asked: *To what extent can activation of individual muscles vary for a given task?* This question tests whether biomechanical constraint is sufficient to define muscle activation pattern for a muscle synergy with a given biomechanical function, e.g. isometric force generation. By identifying the explicit bounds on activation of individual muscles defined by biomechanical constraints of the limb and the task, I demonstrated that there exists a wide range of feasible activation patterns, which may sufficiently account for experimentally observed variability.

In **Chapter 3**, I asked: *How does a functional requirement for generalization across biomechanical conditions affect the range of possible solutions?* This question tests whether a limited range of viable solutions for muscle synergy patterns emerges from a requirement for generalization of function across different conditions. By investigating the possible biomechanical and neural bases of using the same muscle activation pattern to produce a force across limb postures, I demonstrated that a demand for generalization of function can affect the selection of muscle activation patterns that are not granted merely by limb biomechanics nor a single optimality criterion.

In **Chapter 4**, I asked: *How do neural criteria regarding the intrinsic properties of muscle activation patterns affect the selection?* This question tests whether a functional property of muscle activation patterns relevant to the task determines the way in which one solution is selected over another. By characterizing the landscape of the solution space with respect to two functional properties, effort and stability, I demonstrated a possible trade-off in neural selection of muscle activation patterns for a given task that may explain individual differences.

CHAPTER 2

MUSCLE FEASIBLE RANGE DEFINED BY BIOMECHANICAL CONSTRAINTS OF THE LIMB AND THE TASK

This chapter was originally published as an article in the *Journal of Biomechanics*:

Sohn MH, McKay JL, and Ting LH. Defining feasible bounds on muscle activation in a redundant biomechanical task: practical implications of redundancy. *J Biomech* 46: 1363-1368, 2013.

Used with permission by Elsevier.

Measured muscle activation patterns often vary significantly from musculoskeletal model predictions that use optimization to resolve redundancy. Although experimental muscle activity exhibits both inter- and intra-subject variability we lack adequate tools to quantify the biomechanical latitude that the nervous system has when selecting muscle activation patterns. Here, we identified feasible ranges of individual muscle activity during force production in a musculoskeletal model to quantify the degree to which biomechanical redundancy allows for variability in muscle activation patterns. In a detailed cat hindlimb model matched to the posture of three cats, we identified the lower and upper bounds on muscle activity in each of 31 muscles during static endpoint force production across different force directions and magnitudes. Feasible ranges of muscle activation were relatively unconstrained across force magnitudes such that only a few (0~13%) muscles were found to be truly “necessary” (e.g. exhibited non-zero lower bounds) at physiological force ranges. Most muscles were “optional” having zero lower bounds, and frequently had “maximal” upper bounds as well. Moreover, “optional” muscles were never selected by optimization methods that either minimized muscle stress, or that scaled the pattern required for maximum force generation. Therefore,

biomechanical constraints were generally insufficient to restrict or specify muscle activation levels for producing a force in a given direction, and many muscle patterns exist that could deviate substantially from one another but still achieve the task. Our approach could be extended to identify the feasible limits of variability in muscle activation patterns in dynamic tasks such as walking.

2.1 Introduction

Musculoskeletal redundancy (Bernstein 1967) in biomechanical models is often addressed through optimizations that identify a unique muscle activation pattern among many possible. One popular criterion is minimizing muscle stress (Crowninshield and Brand 1981) which has been widely applied to predict muscle coordination in simulations (Anderson and Pandy 2001b; Erdemir et al. 2007; Thelen et al. 2003). However, measured muscle activity often varies significantly from these predictions (Buchanan and Shreeve 1996; Herzog and Leonard 1991; Thelen and Anderson 2006; van der Krogt et al. 2012). We currently lack methods for analyzing high-dimensional musculoskeletal models that would allow us to quantify the degree to which muscle activity may feasibly vary for a given motor task.

A first step to understanding the variability in muscle activity with respect to musculoskeletal redundancy is to identify absolute biomechanical constraints on muscle activity for a given task. In contrast to optimization, this approach seeks to find the full range of possible solution sets available to the nervous system (Kutch and Valero-Cuevas 2011). In particular, identifying the explicit bounds on muscle activation can reveal whether predicted or measured muscle activity is due to biomechanical requirements necessary to perform the task, or because of allowable variability in how the task can be achieved. Identifying feasible bounds of muscle activity can also describe the degree to which muscle activity may deviate from optimal solutions.

This study was motivated by experimentally-observed inter- and intra-subject variability during reactive balance control (Horak and Nashner 1986; Torres-Oviedo et al. 2006; Torres-Oviedo and Ting 2007). For example in cats, when producing an extensor force vector (Fig. 2.1A, F_{EXT}), knee extensor *vastus medialis* (VM) was recruited consistently across animals, but hip and knee flexor *medial sartorius* (SARTm) was recruited at different levels across animals (Fig. 2.1B, F_{EXT}). Conversely, when producing a flexor force vector (Fig. 2.1A, F_{FLEX}), VM recruitment varied across animals but SARTm was recruited consistently in all animals (Fig. 2.1B, F_{FLEX}).

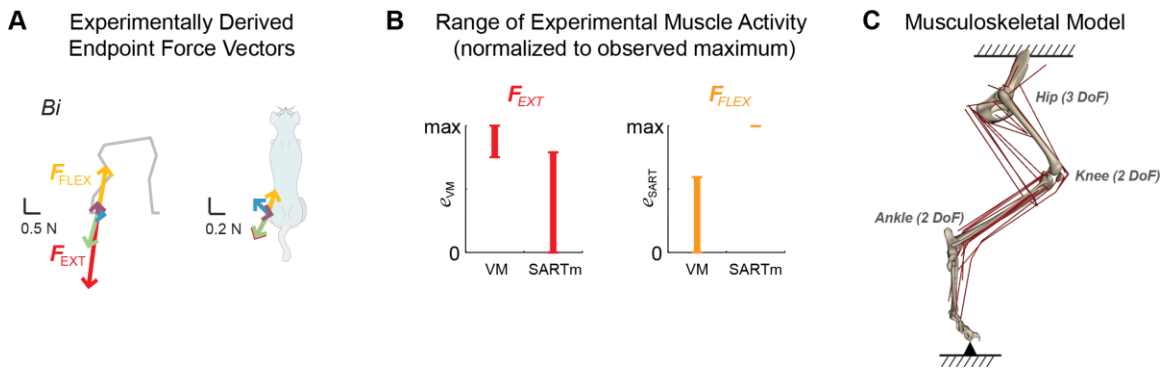


Figure 2.1: Experimental data and model. (A) Experimentally-measured hindlimb endpoint force vectors in *cat Bi* from Torres-Oviedo et al. (2006). Extensor force vector (F_{EXT} , red) and flexor force vector (F_{FLEX} , yellow) vectors were essentially identical across cats. (B) Range of experimental muscle activity across producing F_{EXT} and F_{FLEX} across three cats. When producing F_{EXT} , VM was consistently activated in all animals, whereas the activation level of SARTm varied across animals. For F_{FLEX} , SARTm was activated consistently in all animals and VM was activated at varying levels across animals. (C) Musculoskeletal model of the cat hindlimb (Burkholder and Nichols, 2004) with seven rotational degrees of freedom (3 at the hip, 2 each at the knee and ankle) and 31 muscles. In this static model, the pelvis was fixed to the ground and the endpoint, defined at the MTP joint, was connected to the ground via gimbal joint where moments were constrained to be zero.

Here, we identified feasible ranges of muscle activation during static force production in a detailed model of the cat hindlimb (Fig. 2.1C; (Burkholder and Nichols 2004; McKay and Ting 2008). We identified the upper and lower bounds on muscle activity in each of 31 muscles during endpoint force production in different directions

and magnitudes. Muscles with non-zero lower bounds were classified as “necessary”, whereas muscles with zero lower bounds were classified as “optional”. Muscles were further classified to have “sub-maximal upper bound” or “maximal upper bound”. To examine the degree to which feasible muscle activation patterns could deviate from an optimal solution, we compared these bounds to muscle activation patterns predicted by minimizing muscle stress (Crowninshield and Brand 1981), or scaling the pattern required for maximum force generation (Valero-Cuevas 2000).

2.2 Methods

2.2.1 Musculoskeletal model

The static three-dimensional musculoskeletal model of the cat hindlimb (Burkholder and Nichols 2004) included seven rotational degrees of freedom (Fig. 2.1C). 31 muscles (Table 2.1) produced net joint torque $\bar{\tau}$ (7×1), and a resulting endpoint wrench (force and moment vector) \bar{F}_{End} (6×1) at the metatarsophalangeal (MTP) joint. The MTP was connected to the ground via a gimbal joint (Fig. 2.1C), representing the experimental condition of a freely standing cat where the foot never lost contact or slipped with respect to the ground (Jacobs and Macpherson 1996). Endpoint moments were constrained to be zero, a conservative approximation of the small moments that can be supported by the contact area of cat’s foot (McKay et al. 2007). The model defined the mapping from muscle activation vector \bar{e} (31×1) to endpoint wrench \bar{F}_{End} :

$$\mathbf{R}\mathbf{F}_{AFL}\bar{e} = \bar{\tau} = \mathbf{J}^T\bar{F}_{End}, \quad (2.1)$$

where \mathbf{J} is a geometric Jacobian (6×7), \mathbf{R} is a moment arm matrix (7×31) that maps muscle forces to joint torques, and \mathbf{F}_{AFL} is a diagonal matrix (31×31) of scaling factors based on the active force-length property of muscle (Zajac 1989). To approximate the operating region on the force-length relationship curve commonly observed in habitual

postures, all muscles were set to 95% optimal fiber length (Burkholder and Lieber 2001; Roy et al. 1997; Sacks and Roy 1982). We found matrices **J** and **R** for each of 3 cats B_i , N_i , and R_u based on their average kinematic configuration measured during quiet standing (McKay et al. 2007) using Neuromechanic software (Bunderson et al. 2012).

Table 2.1. Muscles included in the hindlimb model and abbreviations

Name	Abbreviation	Name	Abbreviation
<i>Adductor femoris</i>	ADF	<i>Plantaris</i>	PLAN
<i>Adductor longus</i>	ADL	<i>Iliopsoas</i>	PSOAS
<i>Biceps femoris anterior</i>	BFA	<i>Peroneus tertius</i>	PT
<i>Biceps femoris posterior</i>	BFP	<i>Pyriformis</i>	PYR
<i>Extensor digitorum longus</i>	EDL	<i>Quadratus femoris</i>	QF
<i>Flexor digitorum longus</i>	FDL	<i>Rectus femoris</i>	RF
<i>Flexor hallicus longus</i>	FHL	<i>Sartorius</i>	SART
<i>Gluteus maximus</i>	GMAX	<i>Semimembranosus</i>	SM
<i>Gluteus medius</i>	GMED	<i>Soleus</i>	SOL
<i>Gluteus minimus</i>	GMIN	<i>Semitendinosus</i>	ST
<i>Gracilis</i>	GRAC	<i>Tibialis anterior</i>	TA
<i>Lateral gastrocnemius</i>	LG	<i>Tibialis posterior</i>	TP
<i>Medial gastrocnemius</i>	MG	<i>Vastus intermedius</i>	VI
<i>Peroneus brevis</i>	PB	<i>Vastus lateralis</i>	VL
<i>Pectineus</i>	PEC	<i>Vastus medialis</i>	VM
<i>Peroneus longus</i>	PL		

2.2.2 Target endpoint forces

Five experimentally-derived force vectors in each cat measured during postural responses to translational support perturbation (Torres-Oviedo et al. 2006) were used as target endpoint force vector directions (Fig. 2.1A). These force vectors represented the active response of the cats following perturbation, measured as the change in the ground reaction force from the background level, averaged over the postural response period 150-200 ms following the perturbation (Jacobs and Macpherson 1996), where only small angular deviations in joint angles ($\leq 2^\circ$) are observed (Ting and Macpherson 2004). To

examine biomechanical constraints across force magnitudes, we scaled each force vector from 0 to the maximum feasible level that could be produced by the model, identified using linear programming. We found the muscle activation pattern $\bar{e}^{-\text{MAX}}$ that maximized force magnitude:

$$\bar{e}^{-\text{MAX}} : \text{Find } \bar{e} \text{ s.t. } \left\| (\mathbf{RF}_{AFL} \bar{e}) \cdot (\mathbf{J}^T \bar{F}_{Exp}) \right\| \text{ is maximized, while } (\mathbf{RF}_{AFL} \bar{e}) \times (\mathbf{J}^T \bar{F}_{Exp}) = 0, \quad (2.2)$$

where the cross product constraint in Eq. (2.2) ensured the preservation of force direction. Activation of each muscle was constrained between 0 and 1, and endpoint moments were constrained to be zero. The maximum feasible force in direction of the experimental force vector is given by:

$$\bar{F}_{Exp}^{\text{MAX}} = \frac{\left\| \mathbf{RF}_{AFL} \bar{e}^{-\text{MAX}} \right\|}{\left\| \mathbf{J}^T \bar{F}_{Exp} \right\|} \bar{F}_{Exp}. \quad (2.3)$$

2.2.3 Lower and upper bounds on muscle activation

We used linear programming to identify the lower bound (e_m^{LB}) and the upper bound (e_m^{UB}) on the feasible activation level of each muscle as the magnitude (α) of each of the target endpoint force vectors was scaled from 0 to 1 (Eq. (2.4) and (2.5)). Grid spacing $\Delta\alpha=0.1$ was used from $\alpha=0.0$ to 0.9, and grid spacing $\Delta\alpha=0.02$ from $\alpha=0.9$ to 1.0 because initial tests revealed rapid changes for higher values of α . For each muscle and each value of α , the lower and upper bound was identified as follows:

$$e_m^{\text{LB}} : \text{Find } \bar{e} \text{ s.t. } |e_m| \text{ is minimized, while } \mathbf{RF}_{AFL} \bar{e} = \alpha \cdot \mathbf{J}^T \bar{F}_{Exp}^{\text{MAX}}, \quad (2.4)$$

$$e_m^{\text{UB}} : \text{Find } \bar{e} \text{ s.t. } |e_m| \text{ is maximized, while } \mathbf{RF}_{AFL} \bar{e} = \alpha \cdot \mathbf{J}^T \bar{F}_{Exp}^{\text{MAX}}. \quad (2.5)$$

Each muscle was classified as *necessary* or *optional* based on whether, and at what force magnitude the muscle became biomechanically required to generate endpoint force, corresponding to a nonzero lower bound. Similarly, we classified muscles as

having *sub-maximal upper bound* or *maximal upper bound* based on whether the upper bound was less than or equal to full activation. Considering all combinations of animals, muscles, bounds, endpoint force vectors, and levels of α resulted in 13,206 separate linear programming calls.

Lower and upper bounds identified at $\alpha=0$ were considered a special case because they do not depend on direction of the endpoint force vector and reveal the feasible muscle activation patterns associated with zero net torque production, which we call the *physiological null space*.

2.2.4 Comparison to predicted solutions from suggested neural strategies

We compared the feasible range of individual muscle activity to solutions for muscle activation patterns identified by 1) minimizing muscular stress (Crowninshield and Brand 1981) in the form of sum-squared muscle activation (Thelen et al. 2003) and 2) scaling the muscle activation pattern for the maximal task (Valero-Cuevas 2000). For the minimum stress strategy, muscle patterns $\bar{e}^{-\min}$ were identified for each level of α via quadratic programming as follows:

$$\bar{e}^{-\min} : \text{Find } \bar{e} \text{ s.t. } \sum_{m=1}^{31} e_m^2 \text{ is minimized, while } \mathbf{RF}_{AFL} \bar{e} = \alpha \cdot \mathbf{J}^T \bar{F}_{Exp}^{\text{MAX}}. \quad (2.6)$$

For the scaling strategy, $\bar{e}^{-\text{MAX}}$ identified in Eq. (2.2) was scaled proportional to α .

2.3 Results

2.3.1 Bounds on muscle activation during endpoint force production

The feasible range of muscle activity for each muscle changed non-uniformly as force magnitude α increased from zero to maximal in a given target endpoint force direction (e.g. Fig. 2.2B, shaded region). This range was defined by the difference

between the lower bound (Fig. 2.2B, bottom trace) and upper bound (Fig. 2.2B, top trace) at a given α . In each animal, similar patterns of the feasible range of muscle activity was identified across muscles and force directions. Therefore, two force directions are used for detailed illustration of the results: an extensor force F_{EXT} (Fig. 2.2A, red) and a flexor force F_{FLEX} (Fig. 2.2A, yellow).

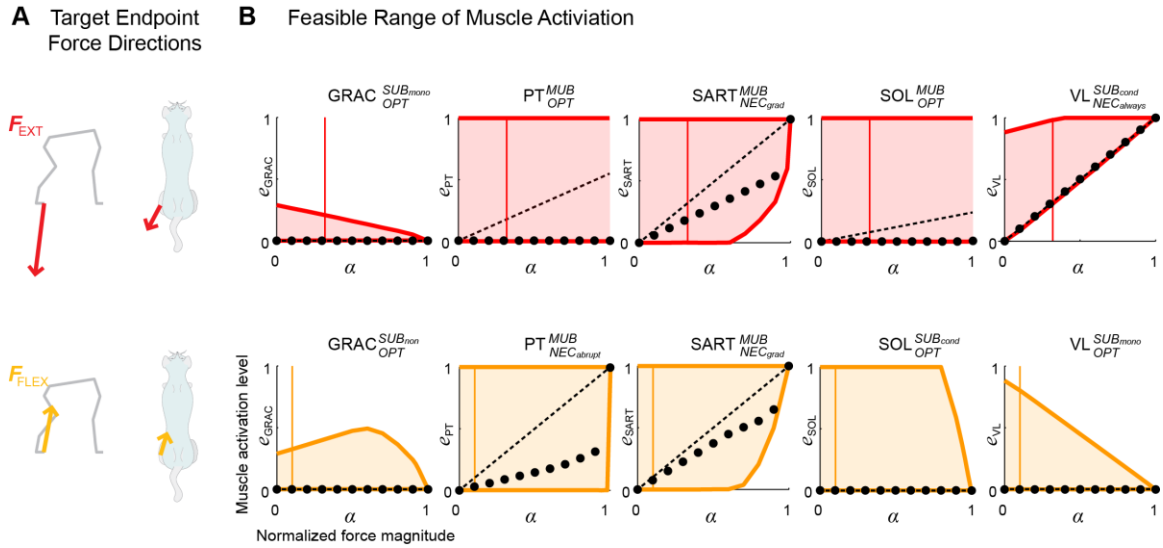


Figure 2.2: Target force directions and muscle feasible ranges. (A) Two representative target endpoint force directions for cat *Bi*: F_{EXT} (red, top row) and F_{FLEX} (yellow, bottom row). (B) Identified feasible range of activation as a function of normalized force magnitude (α) for five muscles in cat *Bi*: GRA, PT, SART, SOL and VL. Feasible range (shaded) is defined by the difference between the lower bound (e_m^{LB} , bottom trace) and the upper bound (e_m^{UB} , top trace). Muscles with zero lower bounds were categorized as optional (*OPT*), e.g. GRAC, PT, SOL for F_{EXT} , and GRAC Sol and VL for F_{FLEX} . Muscle were categorized as necessary if they were nonzero at any force level, and further subdivided into categories of becoming necessary gradually (grad), e.g. SART for F_{EXT} and F_{FLEX} ; only near maximal force, e.g. PT for F_{FLEX} ; or always, e.g. VL for F_{EXT} . Muscles were also classified as having maximal (*MUB*) upper bounds e.g. PT, SART, SOL for F_{EXT} and PT, SART, for F_{FLEX} ; or having sub-maximal (*SUB*) upper bounds, either monotonically, e.g. GRAC in F_{EXT} and VL in F_{FLEX} ; nonmonotonically, e.g. GRAC in F_{FLEX} ; or conditionally, e.g. VL in F_{EXT} and SART in F_{FLEX} . The vertical line indicates the experimental force levels at which most muscles had zero lower bound and were practically “optional”; of the muscles shown, only VL for F_{EXT} was truly “necessary”. Feasible ranges were wide in general, where activity of a muscle could deviate substantially from the solutions predicted by either minimizing muscle stress (dots), or scaling the pattern required for maximal force (dashed lines). Note that neither strategy predicted the recruitment of optional muscles.

Most muscles had zero lower bound for all force magnitudes ($e_m^{\text{LB}}=0$ for all α) and were classified as optional (*OPT*). Muscles for which lower bound became nonzero for some α were classified as necessary; they were either always necessary (*NEC_{always}*: $e_m^{\text{LB}}>0$ for all α), or became gradually necessary as α increased (*NEC_{grad}*: $e_m^{\text{LB}}>0$ at $0<c<\alpha<1$), or became necessary only at the maximum force level (*NEC_{abrupt}*: $e_m^{\text{LB}}>0$ only at $\alpha\approx 1$). Across cats, $71\pm 7\%$ of muscles were optional for the generation of F_{EXT} , and 58%—but not the same muscles—were optional for generation of F_{FLEX} (Table 2.2). For example, in cat *Bi* (Fig. 2.2B), GRAC, PT, SOL were *OPT* for F_{EXT} , and GRAC, SOL, VL were *OPT* for F_{FLEX} . VL was *NEC_{always}* for F_{EXT} , SART was *NEC_{grad}* in both F_{EXT} and F_{FLEX} , and PT was *NEC_{abrupt}* for F_{FLEX} .

Less than 1/3 of muscles had an upper bound of one for all force magnitudes and were classified as having maximal upper bound (*MUB*: $e_m^{\text{UB}}=1$ for all α). Muscles with upper bound less than one for some range of α were classified as having sub-maximal upper bound conditionally (*SUB_{cond}*: $e_m^{\text{UB}}<1$ for $0<\alpha<c$ or $c<\alpha<1$). Muscles for which the upper bound was always less than one were classified as having sub-maximal upper bound ($e_m^{\text{UB}}<1$ for all α), but were further categorized based on whether the upper bound changed monotonically (*SUB_{mono}*) or non-monotonically (*SUB_{non}*). Across cats, $32\pm 3\%$ of the muscles had maximal upper bound for generating F_{EXT} , $22\pm 2\%$ had sub-maximal upper bound for generating F_{FLEX} (Table 2.3). For example, PT, SART, SOL were *MUB* for F_{EXT} , and PT and SART were *MUB* for F_{FLEX} in cat *Bi* (Fig. 2.2B). VL was *SUB_{cond}* and GRAC was *SUB_{mono}* for F_{EXT} , whereas SOL was *SUB_{cond}*, VL was *SUB_{mono}*, and GRAC was *SUB_{non}* for F_{FLEX} .

Muscle classification in terms of the lower and upper bounds depended on the target endpoint force direction (Tables 2.2 and 2.3). In total, 20 muscles in *Bi*, 20 in *Ni*, 19 in *Ru*, showed different behavior for F_{FLEX} as compared to F_{EXT} . The classification of muscles was relatively consistent across cats for a given force direction: for the upper bound, only 4 muscles were categorized differently across 3 cats for both F_{EXT} and F_{FLEX} ,

and for the lower bound, only 3 muscles were categorized differently across all cats for both F_{EXT} and F_{FLEX} . Because the direction of endpoint force vectors was very consistent ($\cos\theta > 0.998$) across cats for both F_{EXT} and F_{FLEX} , these differences in the categorization were due to differences in posture.

Regardless of classifications, the feasible range of muscle activity at physiological levels of force did not identify a clear pattern of muscle activity necessary to achieve the task. At experimentally-observed force magnitudes (Fig. 2B, vertical lines), lower bounds were often zero, suggesting that most muscles were optional at those force levels. Across animals, α_{exp} was 0.32, 0.77, 0.19 in *Bi*, *Ni* and *Ru* for F_{EXT} and 0.12, 0.11, 0.11 for F_{FLEX} .

2.3.2 Comparison of identified bounds and predictions of neural strategies

Because of the large feasible range, muscle activity could deviate substantially from two commonly suggested muscle coordination strategies. Both solutions fell within the feasible ranges of muscle activity, and typically near—but not necessarily at—the lower bound. Both the scaling strategy (Fig. 2.2B, dashed line) and the minimum stress strategy (Fig. 2.2B, dotted line) recruited necessary muscles at the earliest nonzero α even though the lower bounds on feasible muscle activity were typically zero at low force magnitudes (e.g. Figure 2.2B, VL for F_{EXT} and SART for F_{FLEX}). Optional muscles were never selected in either strategy (e.g. Figure 2.2B, GRAC for F_{EXT} and VL for F_{FLEX}). Although the upper and lower bounds typically converged on a unique solution for maximum force production (Fig. 2.2B, bottom row), this was not always the case in ankle muscles for F_{EXT} (Fig. 2.2B, top row, PT and SOL), indicating that redundancy remained even at maximum force magnitudes. This resulted from low ankle torque ($\sim 0.004\text{N}\cdot\text{m}$) compared to knee torque ($\sim 0.5\text{N}\cdot\text{m}$) required to produce F_{EXT} .

Table 2.2. Muscle classification in terms of lower bound (e_m^{LB}) behavior

	<i>Bi</i>		<i>Ni</i>		<i>Ru</i>	
	F_{EXT}	F_{FLEX}	F_{EXT}	F_{FLEX}	F_{EXT}	F_{FLEX}
ADF	<i>OPT</i>	<i>OPT</i>	<i>OPT</i>	<i>OPT</i>	<i>OPT</i>	<i>OPT</i>
ADL	<i>OPT</i>	<i>OPT</i>	<i>OPT</i>	<i>OPT</i>	<i>OPT</i>	<i>OPT</i>
BFA	<i>OPT</i>	<i>OPT</i>	<i>OPT</i>	<i>OPT</i>	<i>OPT</i>	<i>OPT</i>
BFP	<i>NEC_{always}</i>	<i>NEC_{grad}</i>	<i>NEC_{always}</i>	<i>NEC_{grad}</i>	<i>NEC_{grad}</i>	<i>NEC_{grad}</i>
EDL	<i>OPT</i>	<i>NEC_{grad}</i>	<i>OPT</i>	<i>NEC_{grad}</i>	<i>OPT</i>	<i>NEC_{grad}</i>
FDL	<i>OPT</i>	<i>OPT</i>	<i>OPT</i>	<i>OPT</i>	<i>OPT</i>	<i>OPT</i>
FHL	<i>OPT</i>	<i>OPT</i>	<i>OPT</i>	<i>OPT</i>	<i>OPT</i>	<i>OPT</i>
GMAX	<i>OPT</i>	<i>OPT</i>	<i>OPT</i>	<i>OPT</i>	<i>OPT</i>	<i>OPT</i>
GMED	<i>NEC_{abrupt}</i>	<i>NEC_{grad}</i>	<i>NEC_{grad}</i>	<i>NEC_{grad}</i>	<i>NEC_{grad}</i>	<i>NEC_{grad}</i>
GMIN	<i>OPT</i>	<i>OPT</i>	<i>OPT</i>	<i>OPT</i>	<i>NEC_{abrupt}</i>	<i>NEC_{abrupt}</i>
GRAC	<i>OPT</i>	<i>OPT</i>	<i>OPT</i>	<i>OPT</i>	<i>OPT</i>	<i>OPT</i>
LG	<i>OPT</i>	<i>NEC_{grad}</i>	<i>OPT</i>	<i>NEC_{grad}</i>	<i>OPT</i>	<i>NEC_{grad}</i>
MG	<i>OPT</i>	<i>NEC_{abrupt}</i>	<i>OPT</i>	<i>NEC_{abrupt}</i>	<i>OPT</i>	<i>OPT</i>
PB	<i>OPT</i>	<i>NEC_{abrupt}</i>	<i>OPT</i>	<i>NEC_{grad}</i>	<i>OPT</i>	<i>OPT</i>
PEC	<i>OPT</i>	<i>OPT</i>	<i>OPT</i>	<i>OPT</i>	<i>OPT</i>	<i>OPT</i>
PL	<i>OPT</i>	<i>NEC_{abrupt}</i>	<i>OPT</i>	<i>NEC_{grad}</i>	<i>OPT</i>	<i>NEC_{abrupt}</i>
PLAN	<i>OPT</i>	<i>OPT</i>	<i>OPT</i>	<i>OPT</i>	<i>OPT</i>	<i>OPT</i>
PSOAS	<i>NEC_{grad}</i>	<i>NEC_{grad}</i>	<i>NEC_{grad}</i>	<i>NEC_{grad}</i>	<i>NEC_{grad}</i>	<i>NEC_{grad}</i>
PT	<i>OPT</i>	<i>NEC_{abrupt}</i>	<i>OPT</i>	<i>NEC_{abrupt}</i>	<i>OPT</i>	<i>NEC_{abrupt}</i>
PYR	<i>NEC_{grad}</i>	<i>NEC_{grad}</i>	<i>NEC_{grad}</i>	<i>NEC_{grad}</i>	<i>NEC_{grad}</i>	<i>NEC_{grad}</i>
QF	<i>NEC_{grad}</i>	<i>NEC_{grad}</i>	<i>NEC_{grad}</i>	<i>NEC_{grad}</i>	<i>NEC_{grad}</i>	<i>NEC_{grad}</i>
RF	<i>OPT</i>	<i>OPT</i>	<i>OPT</i>	<i>OPT</i>	<i>NEC_{grad}</i>	<i>OPT</i>
SART	<i>NEC_{grad}</i>	<i>NEC_{grad}</i>	<i>NEC_{grad}</i>	<i>NEC_{grad}</i>	<i>NEC_{grad}</i>	<i>NEC_{grad}</i>
SM	<i>OPT</i>	<i>OPT</i>	<i>OPT</i>	<i>OPT</i>	<i>OPT</i>	<i>OPT</i>
SOL	<i>OPT</i>	<i>OPT</i>	<i>OPT</i>	<i>OPT</i>	<i>OPT</i>	<i>OPT</i>
ST	<i>OPT</i>	<i>OPT</i>	<i>OPT</i>	<i>OPT</i>	<i>OPT</i>	<i>NEC_{abrupt}</i>
TA	<i>NEC_{abrupt}</i>	<i>NEC_{grad}</i>	<i>OPT</i>	<i>NEC_{grad}</i>	<i>NEC_{abrupt}</i>	<i>NEC_{grad}</i>
TP	<i>OPT</i>	<i>OPT</i>	<i>OPT</i>	<i>OPT</i>	<i>OPT</i>	<i>OPT</i>
VI	<i>NEC_{abrupt}</i>	<i>OPT</i>	<i>OPT</i>	<i>OPT</i>	<i>NEC_{grad}</i>	<i>OPT</i>
VL	<i>NEC_{always}</i>	<i>OPT</i>	<i>NEC_{always}</i>	<i>OPT</i>	<i>NEC_{grad}</i>	<i>OPT</i>
VM	<i>OPT</i>	<i>OPT</i>	<i>OPT</i>	<i>OPT</i>	<i>OPT</i>	<i>OPT</i>

OPT: e_m^{LB} is always zero; *NEC_{always}*: e_m^{LB} is always non-zero; *NEC_{grad}*: e_m^{LB} becomes non-zero gradually; *NEC_{abrupt}*: e_m^{LB} becomes non-zero abruptly at maximal force magnitude. Muscle that changed classifications of *necessary* versus *optional* across the two force directions are shown in bold black. Muscles that differ in sub-classifications across force directions are shown in bold gray.

Table 2.3. Muscle classification in terms of upper bound (e_m^{UB}) behavior

	<i>Bi</i>		<i>Ni</i>		<i>Ru</i>	
	F_{EXT}	F_{FLEX}	F_{EXT}	F_{FLEX}	F_{EXT}	F_{FLEX}
ADF	<i>SUB_{mono}</i>	<i>SUB_{mono}</i>	<i>SUB_{mono}</i>	<i>SUB_{mono}</i>	<i>SUB_{mono}</i>	<i>SUB_{non}</i>
ADL	<i>SUB_{cond}</i>	<i>SUB_{cond}</i>	<i>SUB_{cond}</i>	<i>SUB_{cond}</i>	<i>SUB_{cond}</i>	<i>SUB_{cond}</i>
BFA	<i>SUB_{mono}</i>	<i>SUB_{mono}</i>	<i>SUB_{mono}</i>	<i>SUB_{non}</i>	<i>SUB_{mono}</i>	<i>SUB_{non}</i>
BFP	<i>SUB_{mono}</i>	<i>SUB_{non}</i>	<i>SUB_{mono}</i>	<i>SUB_{non}</i>	<i>SUB_{mono}</i>	<i>SUB_{non}</i>
EDL	<i>SUB_{cond}</i>	<i>MUB</i>	<i>SUB_{cond}</i>	<i>SUB_{non}</i>	<i>SUB_{cond}</i>	<i>MUB</i>
FDL	<i>MUB</i>	<i>SUB_{cond}</i>	<i>MUB</i>	<i>SUB_{cond}</i>	<i>MUB</i>	<i>SUB_{cond}</i>
FHL	<i>SUB_{cond}</i>	<i>SUB_{cond}</i>	<i>SUB_{cond}</i>	<i>SUB_{cond}</i>	<i>SUB_{cond}</i>	<i>SUB_{cond}</i>
GMAX	<i>SUB_{cond}</i>	<i>SUB_{cond}</i>	<i>SUB_{cond}</i>	<i>SUB_{cond}</i>	<i>SUB_{cond}</i>	<i>SUB_{cond}</i>
GMED	<i>SUB_{mono}</i>	<i>SUB_{mono}</i>	<i>SUB_{mono}</i>	<i>SUB_{non}</i>	<i>SUB_{non}</i>	<i>SUB_{mono}</i>
GMIN	<i>SUB_{cond}</i>	<i>SUB_{cond}</i>	<i>SUB_{cond}</i>	<i>SUB_{cond}</i>	<i>MUB</i>	<i>MUB</i>
GRAC	<i>SUB_{mono}</i>	<i>SUB_{non}</i>	<i>SUB_{mono}</i>	<i>SUB_{non}</i>	<i>SUB_{mono}</i>	<i>SUB_{non}</i>
LG	<i>SUB_{mono}</i>	<i>SUB_{non}</i>	<i>SUB_{mono}</i>	<i>SUB_{non}</i>	<i>SUB_{mono}</i>	<i>SUB_{mono}</i>
MG	<i>SUB_{mono}</i>	<i>SUB_{non}</i>	<i>SUB_{mono}</i>	<i>SUB_{non}</i>	<i>SUB_{mono}</i>	<i>SUB_{mono}</i>
PB	<i>MUB</i>	<i>SUB_{cond}</i>	<i>MUB</i>	<i>SUB_{cond}</i>	<i>MUB</i>	<i>SUB_{cond}</i>
PEC	<i>SUB_{cond}</i>	<i>SUB_{cond}</i>	<i>SUB_{cond}</i>	<i>SUB_{cond}</i>	<i>SUB_{cond}</i>	<i>SUB_{cond}</i>
PL	<i>MUB</i>	<i>MUB</i>	<i>MUB</i>	<i>MUB</i>	<i>MUB</i>	<i>SUB_{cond}</i>
PLAN	<i>SUB_{mono}</i>	<i>SUB_{non}</i>	<i>SUB_{mono}</i>	<i>SUB_{non}</i>	<i>SUB_{mono}</i>	<i>SUB_{mono}</i>
PSOAS	<i>MUB</i>	<i>MUB</i>	<i>MUB</i>	<i>MUB</i>	<i>MUB</i>	<i>MUB</i>
PT	<i>MUB</i>	<i>MUB</i>	<i>MUB</i>	<i>MUB</i>	<i>MUB</i>	<i>MUB</i>
PYR	<i>MUB</i>	<i>MUB</i>	<i>MUB</i>	<i>MUB</i>	<i>MUB</i>	<i>MUB</i>
QF	<i>SUB_{cond}</i>	<i>SUB_{cond}</i>	<i>MUB</i>	<i>SUB_{cond}</i>	<i>SUB_{cond}</i>	<i>SUB_{cond}</i>
RF	<i>SUB_{mono}</i>	<i>SUB_{non}</i>	<i>SUB_{mono}</i>	<i>SUB_{non}</i>	<i>SUB_{cond}</i>	<i>SUB_{cond}</i>
SART	<i>MUB</i>	<i>MUB</i>	<i>MUB</i>	<i>MUB</i>	<i>MUB</i>	<i>MUB</i>
SM	<i>SUB_{mono}</i>	<i>SUB_{non}</i>	<i>SUB_{mono}</i>	<i>SUB_{non}</i>	<i>SUB_{mono}</i>	<i>SUB_{non}</i>
SOL	<i>MUB</i>	<i>SUB_{cond}</i>	<i>MUB</i>	<i>SUB_{cond}</i>	<i>MUB</i>	<i>SUB_{cond}</i>
ST	<i>SUB_{mono}</i>	<i>SUB_{non}</i>	<i>SUB_{mono}</i>	<i>SUB_{non}</i>	<i>SUB_{mono}</i>	<i>SUB_{non}</i>
TA	<i>MUB</i>	<i>MUB</i>	<i>MUB</i>	<i>MUB</i>	<i>MUB</i>	<i>MUB</i>
TP	<i>SUB_{mono}</i>	<i>SUB_{mono}</i>	<i>SUB_{mono}</i>	<i>SUB_{mono}</i>	<i>SUB_{mono}</i>	<i>SUB_{mono}</i>
VI	<i>SUB_{cond}</i>	<i>SUB_{cond}</i>	<i>SUB_{cond}</i>	<i>SUB_{cond}</i>	<i>MUB</i>	<i>SUB_{cond}</i>
VL	<i>SUB_{cond}</i>	<i>SUB_{mono}</i>	<i>SUB_{cond}</i>	<i>SUB_{mono}</i>	<i>SUB_{cond}</i>	<i>SUB_{mono}</i>
VM	<i>SUB_{mono}</i>	<i>SUB_{non}</i>	<i>SUB_{mono}</i>	<i>SUB_{non}</i>	<i>SUB_{cond}</i>	<i>SUB_{cond}</i>

MUB: e_m^{UB} is always one (maximal); *SUB_{cond}*: e_m^{UB} is sub-maximal only at certain range of α ; *SUB_{mono}*: e_m^{UB} is always sub-maximal and changes monotonically; *SUB_{non}*: e_m^{UB} is always sub-maximal and changes non-monotonically. Muscle that changed classification of *sub-maximal upper bound* versus *maximal upper bound* across the two force directions are shown in bold black. Muscles that differ in sub-classifications across force directions are shown in bold gray.

2.3.3 Physiological null space at $\alpha=0$

Approximately 1/3 of muscles had upper bounds of less than one for zero net torque production, defining the physiological null space (Fig. 2.3). Because the torque generated by each muscle must be counterbalanced by activation of other muscles, those producing large torques (e.g. large moment arms and maximum isometric force) typically had low upper bounds (≤ 0.53) because of the lower torque-generating capabilities of their antagonists (Ait-Haddou et al. 2004; Jinha et al. 2006).

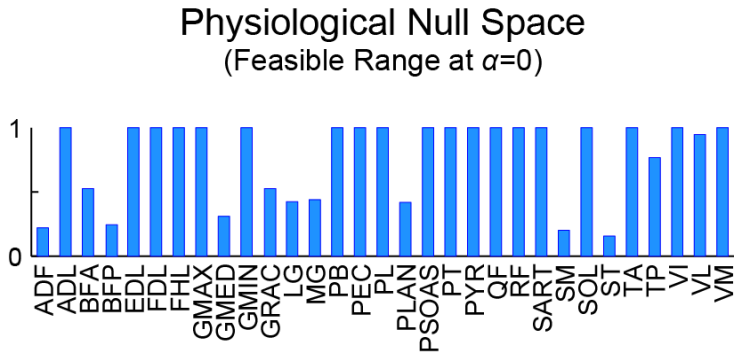


Figure 2.3: Physiological null space. Physiological null space, defined as the feasible range at $\alpha=0$ in cat *Ru*. While many muscles could be maximally activated, several muscles were limited in the maximum activation that would allow zero net torque production. Upper bounds of muscles that produce large torques (e.g. BFP) were typically limited, because of the lower torque-generating capabilities of their antagonists.

2.4 Discussion

Here, we identified the feasible ranges of individual muscle activation during endpoint force generation as a way of understanding the degree to which biomechanical redundancy allows for variability in muscle activation patterns. Feasible ranges of muscle activation were relatively unconstrained across force magnitudes in a cat hindlimb model (7 non-orthogonal DoF's, 31 muscles). Although we identified muscles that became biomechanically “necessary” at higher levels of force (e.g. nonzero lower bound), few muscles were found to be truly “necessary” at physiological force ranges. Thus,

biomechanical constraints were generally insufficient to specify muscle activation levels, demonstrating that many possible muscle patterns exist that could deviate substantially from one another. In contrast, the biomechanical bounds on muscle activity in finger force generation (4 orthogonal DoF's, 7 muscles) was shown to be highly constrained, even at sub-maximal force magnitudes (Kutch and Valero-Cuevas 2011), demonstrating differences in the biomechanical redundancy of the cat hindlimb limb versus the index finger.

The ubiquity of “optional” muscles in both agonist and antagonists across most force levels highlights the necessity to understand neural strategies governing selection of muscle activation patterns. The large space of functionally equivalent solutions is consistent with variations in neural and muscular activity observed across individuals in a variety of neuromotor behaviors (Klein et al. 2010; Prinz et al. 2004; Raphael et al. 2010). Moreover, “optional” muscle were never selected by typical methods that resolve biomechanical redundancy, e.g. minimizing stress (Thelen et al. 2003), or scaling patterns that produce maximal force (Valero-Cuevas 2000), suggesting that other optimization criteria may need to be considered, such as impedance (Burdet et al. 2001), stability (Bunderson et al. 2008), fiber velocity (Prilutsky et al. 1997; Walmsley et al. 1978), metabolic energy (Alexander 2005; 1989; Hoyt and Taylor 1981), or more likely a combination of multiple goals in interplay (Franklin et al. 2008; Ganesh et al. 2010; Todorov 2004). Alternatively, variations in muscle activation patterns may be due to neural constraints of activating muscles in groups (d'Avella et al. 2006; Hart and Giszter 2004; Ting and Macpherson 2005), or habitual movement patterns (de Rugy et al. 2012). One implication is that altering the biomechanical properties of a muscle, e.g. via weakening or surgery (Arnold et al. 2005; Correa et al. 2012; Hicks et al. 2008; Valero-Cuevas and Hentz 2002), in a highly redundant system may not affect muscle activation patterns even if the limb's force generating capabilities are altered (Damiano et al. 2010 ; Scianni et al. 2009).

Despite some limitations in our modeling assumptions, our estimates of feasible muscle range are likely robust and somewhat conservative. Although we specified zero endpoint moment, specifying a different moment values is not likely to alter our results. However, allowing a range of small endpoint moments would increase the set of redundant solutions (McKay et al. 2007), increasing the feasible range of muscle activity. Further, individual variations in morphology of each animal compared to our generic musculoskeletal model (Burkholder and Nichols 2004) are not expected to change the basic categorizations found. Torque-generating capabilities of muscles based on 95% optimal fiber length were only altered by -9 to +3% when physiological ranges of 80-110% optimal fiber length (Burkholder and Lieber 2001) were used, and would not change significantly if tendon elasticity were included (Biewener et al. 1998). Finally, the activation-dependent changes in the force-length relationship (Rack and Westbury 1969), would alter the mapping from muscle force to activation, but would only minimally affect the bounds on feasible muscle activation.

Comparing the predicted feasible muscle activation ranges to experimental data is still difficult due to differences between the model and experimental conditions. Direct comparisons of EMG to feasible limits were not possible because a reference level of muscle force was unknown (and could be estimated by maximum voluntary contraction). Further, because our technique only examines the feasible limits of a single muscle, we cannot use the predictions to identify specific multi-muscle patterns to perform a given task. The measured EMGs may not correspond exactly to the muscles or muscle groupings represented in the model. Finally, for direct comparison to our specific experimental data, we need to take into account background force for standing, which required that the pre-existing force level be considered. For standing, this would decrease extensor force redundancy, increase flexor force redundancy, and likely have a small effect in other directions.

Nonetheless, our approach provides important insight as to the relative variability allowed for a muscle activity that is applicable to both static and dynamic tasks. In contrast to the dimension of the solution space (Bunderson et al. 2008), our approach identifies explicit constraints on muscle activation patterns. The identified bounds could be used to assess confidence of predicted muscle activity as well as possible variations when alternate cost functions or strategies are considered. The feasible muscle range also quantifies the degree to which measured muscle activity is expected to be variable or deviate from predictions. An advantage of our method is that the number of muscles that can be solved is not limited and can be applied to any high-dimensional musculoskeletal models. Our method could also be extended to analysis of dynamic tasks (Ackland et al. 2012; Thelen and Anderson 2006; van der Krogt et al. 2012) that use methods where each time step of a movement is solved independently, e.g. inverse dynamics or static optimization (Anderson and Pandy 2001b).

CHAPTER 3

FUNCTIONAL REQUIREMENT FOR GENERALIZABILITY

ACROSS BIOMECHANICAL CONDITIONS

3.1 Introduction

It has been suggested that the nervous system may use a repertoire of fixed muscle patterns called muscle synergies that can be flexibly combined to achieve functional motor goals. Muscle synergies have been shown to account for experimentally observed variability in muscle activity across different motor behaviors in various species (Chvatal et al. 2011; d'Avella et al. 2006; Hart and Giszter 2004; Raasch and Zajac 1999; Roh et al. 2012; Ting and Macpherson 2005). Each muscle synergy is hypothesized to produce a consistent biomechanical sub-task (Giszter and Kargo 2000; McKay and Ting 2008). The level of recruitment during any given task is dependent on the spatiotemporal requirements of the task-level goal (Safavynia and Ting 2013). For example, muscle synergies used for standing balance in cats and humans produced ground reaction force vectors that have distinct functions for controlling the center-of-mass (Chvatal et al. 2011; Ting and Macpherson 2005). Muscle synergies used in human walking are associated with biomechanical sub-tasks such as body support, forward propulsion, or leg-swing (Allen and Neptune 2012; Lacquaniti et al. 2012; Neptune et al. 2009).

The degree to which biomechanical versus neural constraints organize the spatial structures of muscle synergies is widely debated. Experimental evidence suggests substantial inter-subject variability in muscle synergy structure despite similar motor outputs (Chvatal et al. 2011; Clark et al. 2010; Frere and Hug 2012; Torres-Oviedo et al. 2006; Torres-Oviedo and Ting 2007). While some studies suggest that biomechanical constraints may largely define the structure of muscle synergies (Kutch and Valero-

Cuevas 2012), our recent work suggests that muscle activity for performing a motor task in a *single condition* is largely unconstrained (Sohn et al. 2013). A wide range of activations for individual muscles was found to be feasible for generating experimentally-observed endpoint forces in a static cat hindlimb model. Similarly, a large number of “good-enough” solutions can be identified to perform any motor task (Loeb 2012; Raphael et al. 2010), demonstrating our ability to take advantage of the highly redundant motor solution space. Thus, it should be no surprise that computational approaches that rely on a single optimization criteria to mimic neural control mechanisms cannot predict experimentally-observed variability across subjects (Buchanan and Shreeve 1996; Herzog and Leonard 1991; Sohn et al. 2013; van der Krogt et al. 2012). It is likely that multiple criteria are required to explain neural principles for determining muscle synergy patterns (Ganesh et al. 2010).

Muscle synergies may represent a set of motor solutions that are selected based on their ability to be generalized across different contexts. The structure, or pattern, of muscle synergies has been shown to be robust across a variety of motor behaviors and biomechanical conditions. In cats, consistent muscle synergies and the ground reaction forces they produce (Ting and Macpherson 2005) robustly explained the reactive balance responses across a variety of postures (Torres-Oviedo et al. 2006). In humans, common muscle synergies are observed across variations in standing postures, reactive balance strategies (Chvatal et al. 2011; Torres-Oviedo and Ting 2010), walking with altered loads (McGowan et al. 2010), reaching in various dynamic and postural conditions (d'Avella et al. 2006), as well as during isometric force generation in multiple directions at different postures in human arm (Roh et al. 2012). Further evidence suggests that muscle synergies may even be shared across different motor tasks, such as reactive balance and walking (Chvatal and Ting 2013), forward and backward locomotion (Raasch and Zajac 1999; Ting et al. 1999), and a range of different lower limb motor tasks in frogs, such as

jumping, swimming, kicking, and reflexive wiping in the frog (Cheung et al. 2005; Cheung et al. 2009; d'Avella and Bizzi 2005; Hart and Giszter 2004; Roh et al. 2011).

In particular, we were interested in functional muscle synergies associated with force production during balance control across several different postural configurations in cats (Ting and Macpherson 2005; Torres-Oviedo et al. 2006). Based on prior experimental findings, we previously demonstrated the rotation of the muscle synergy force vectors could be predicted by applying a common simulated muscle synergy pattern across different postures (McKay and Ting 2008). While the results were largely similar across widely varying muscle synergy patterns that produced the same force, the differences in the generalizability of different muscle synergy patterns was not explicitly tested. Further, we predicted that functional requirements for generalizability would narrow the range of possible muscle activation patterns for muscle synergies. Our prior method for identifying feasible ranges in muscle activation (Sohn et al. 2013) considered only biomechanical constraints for a single task, but the range of feasible solutions may become significantly restricted when multiple task constraints are superimposed (Keenan et al. 2009; Loeb 2000; Racz et al. 2012). That is, the selection of a particular muscle synergy could be influenced by its ability to satisfy biomechanical task constraints across a range of limb postures.

Here we used a musculoskeletal model of the cat hindlimb to investigate possible biomechanical and neural bases of using a consistent muscle synergy to produce a force across different limb postures. In particular, we explicitly tested a hypothesis, along with two alternate hypotheses, by which generalizability of muscle activation pattern across biomechanical conditions may arise from. First, we hypothesized that generalizability reflects the selection of specific muscle activation pattern that provide similar functions across postures. This hypothesis predicts that muscle activation patterns that can be used across different biomechanical configurations are sub-optimal at any single configuration, and further that the generalizability constraint will reduce the range of possible solutions.

Second, we hypothesized that generalizability is a property of an optimal (e.g. minimum-effort) solution for a single posture. Finally, we hypothesized that generalizability is a property of limb biomechanics such that all muscle activation patterns are predicted to generalize their function across postures. To test these hypotheses, we examined muscle activation patterns that produced the experimentally-observed ground reaction force vector at a preferred stance posture according to three different selection criteria: a best-generalizable solution that minimizes deviations from the experimentally-observed force vectors across all postures, a minimum-effort solution, and random solutions. We found that only a few selected muscle activation patterns could be generalized across postures. Our results demonstrate that functional demand for generalization across postures can affect the selection of muscle activation patterns, and does not arise from limb biomechanics or a single optimality criterion alone.

3.2 Methods

In summary, we used a detailed musculoskeletal model of the cat hindlimb to test the generalizability of muscle activation patterns across stance postures based on three different selection criteria: (1) a solution that explicitly minimized deviation from the experimentally-observed forces across all postures, (2) an optimal solution minimizing muscle effort at preferred posture, and (3) a set of random solutions. For each selection criteria, we generated muscle activation patterns that produced the experimentally-observed force vectors at preferred stance posture. We then applied these muscle activation patterns to three other stance postures and simulated the resulting endpoint force vectors. We assessed generalizability of each muscle activation pattern by measuring the angular deviations in the simulated force vectors from the experimentally-observed force vectors. We further tested whether feasible range of activation in individual muscles for producing the experimentally-observed force vector at preferred posture is reduced with a generalizability constraint.

3.2.1 Experimental synergy force vector data

Experimentally-observed force vectors were taken from a previous study investigating reactive balance behavior in cats (Torres-Oviedo et al. 2006). Cats stood quietly at four different postures with varying fore-hindlimb stance distances: shortest, short, preferred and long (Macpherson 1994). Across all stance distances, five muscle synergies ($W_1 \sim W_5$) in each cat robustly explained active changes in muscle activity and hindlimb forces in response to multi-directional horizontal support-surface perturbations. Experimental synergy force vectors (\bar{F}_{W_i}) were found by extracting three-dimensional endpoint force vector components that were co-modulated with recruitment level of each muscle synergy. These synergy force vectors rotated with the limb axis across postures (Fig. 3.1A).

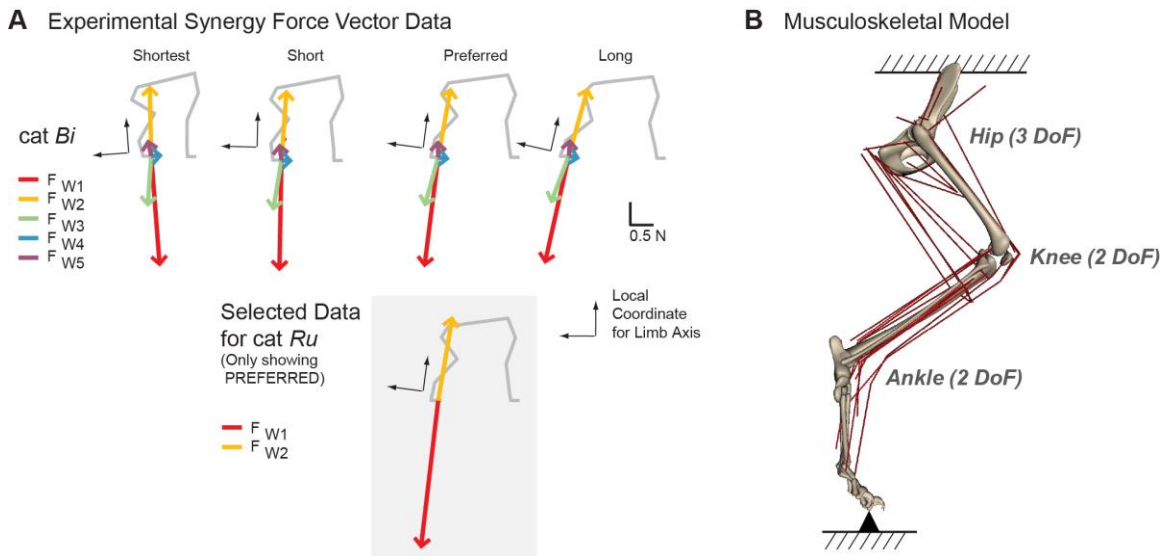


Figure 3.1: Experimental data and model. (A) Experimental synergy force vector ($F_{W_{1-5}}$) data in two cats *Bi* and *Ru* from Torres-Oviedo et al., (2006). A common set of muscle synergies ($W_1 \sim W_5$) that explained reactive balance behavior in cats across different postural configuration (Shortest, Short, Preferred, and Long stance) produced consistent endpoint force vectors with respect to limb orientation, i.e., synergy force vectors that rotated with the limb axis across postures. Two force vectors, the extensor synergy force vector (red) and the flexor synergy force vector (yellow), were selected as representative conditions for detailed results. Note that for cat *Ru* only selected data at Preferred stance is shown here. (B) Musculoskeletal model of the cat hindlimb (Burkholder and Nichols, 2004) with seven rotational degrees of freedom (3 at the hip, 2 each at the knee and ankle) and 31 muscles. In this static model, the pelvis was fixed to the ground and the endpoint (MTP joint) was connected to the ground via gimbal joint.

3.2.2 Musculoskeletal model

We used a previously developed three-dimensional musculoskeletal model of the cat hindlimb (Fig. 3.1B; (Burkholder and Nichols 2004). Details of this model are described elsewhere in both static (McKay et al. 2007; Sohn et al. 2013) and dynamic conditions (Bunderson et al. 2008; Bunderson et al. 2010). Briefly, the model included 7 degrees-of-freedom at anatomical joints (3 at the hip, 2 at the knee, 2 at the ankle) and 31 hindlimb muscles (list and abbreviations in Table 3.1). The posture of the model was matched to kinematics of each cat at each of the stance configurations (McKay and Ting 2008). The pelvis was fixed to ground and the endpoint was defined at the metatarsal-phalangeal joint (MTP), which was connected to the ground via gimbal joint. At static equilibrium, the model defined a linear mapping between muscle activation and endpoint force:

$$\mathbf{R}\mathbf{F}_{AFL}\bar{e} = \mathbf{J}^T \bar{F}_{End} \quad (3.1),$$

where \mathbf{R} is the moment arm matrix (7×31), \mathbf{F}_{AFL} is the diagonal matrix (31×31) of scaling factors for active muscle force generation, \bar{e} is the muscle activation vector (31×1), \mathbf{J} is the geometric Jacobian (3×7), and F_{End} is the endpoint force vector (3×1). Muscle moment arm (\mathbf{R}), geometric Jacobian (\mathbf{J}), and muscle parameters required to characterize active muscle force generation (\mathbf{F}_{AFL}), i.e, maximum isometric force and force-length relationship (Zajac 1989), were acquired using *Neuromechanic*, a previously developed and freely-available software (Bunderson et al. 2012). Muscle fiber lengths were set at 65% of optimal fiber length for all muscles at preferred posture so that muscles operated on the ascending slope on force-length relationship curve and were at physiological operating ranges across all postures.

The experimental synergy force vector at preferred posture in each of two *cats* (*Bi* and *Ru*) was used as the target endpoint force vector to simulate in the model. Synergy force vectors at the other three postures (shortest, short and long) were used to define the

desired directions to which simulated endpoint forces in the model were compared (see 3.2.2 Musculoskeletal model). Because cats were highly trained in experiments for the particular task of postural balance, their behavior was most consistent and robust in a normative condition, e.g. preferred postures. Therefore, we tested whether muscle activation patterns specifically used for this posture could generalize its function across other conditions.

Muscle activation patterns that produced a given target force, i.e., synergy force vector at preferred posture, were found using the static linear model (Eq. 3.1). Endpoint force vectors produced by given muscle activation patterns at other postures were simulated using *Neuromechanic*; the full dynamic model was integrated forward a small time step (1ms) such that reaction forces satisfying the kinematic constraints were computed but before any acceleration and thus other inertial and velocity-dependent forces were developed.

Table 3.1. Muscles included in the hindlimb model and abbreviations

Name	Abbreviation	Name	Abbreviation
<i>Adductor femoris</i>	ADF	<i>Plantaris</i>	PLAN
<i>Adductor longus</i>	ADL	<i>Iliopsoas</i>	PSOAS
<i>Biceps femoris anterior</i>	BFA	<i>Peroneus tertius</i>	PT
<i>Biceps femoris posterior</i>	BFP	<i>Pyriformis</i>	PYR
<i>Extensor digitorum longus</i>	EDL	<i>Quadratus femoris</i>	QF
<i>Flexor digitorum longus</i>	FDL	<i>Rectus femoris</i>	RF
<i>Flexor hallicus longus</i>	FHL	<i>Sartorius</i>	SART
<i>Gluteus maximus</i>	GMAX	<i>Semimembranosus</i>	SM
<i>Gluteus medius</i>	GMED	<i>Soleus</i>	SOL
<i>Gluteus minimus</i>	GMIN	<i>Semitendinosus</i>	ST
<i>Gracilis</i>	GRAC	<i>Tibialis anterior</i>	TA
<i>Lateral gastrocnemius</i>	LG	<i>Tibialis posterior</i>	TP
<i>Medial gastrocnemius</i>	MG	<i>Vastus intermedius</i>	VI
<i>Peroneus brevis</i>	PB	<i>Vastus lateralis</i>	VL
<i>Pectineus</i>	PEC	<i>Vastus medialis</i>	VM
<i>Peroneus longus</i>	PL		

3.2.3 Best-generalizable solution

In order to determine the degree to which a single solution can be generalized across different conditions, we explicitly searched for a single muscle activation pattern that best approximated experimental synergy force vectors across postures. We formulated a nonlinear optimization problem to identify a unique muscle activation pattern ($\bar{e}^{-\text{Best}}$) that produced experimental synergy force vector at preferred posture ($\bar{F}_{W_i}^{\text{Preferred}}$) while minimizing the deviation between simulated and experimentally-observed synergy force vector at other postures ($\bar{F}_{W_i}^{\text{Shortest}}$, $\bar{F}_{W_i}^{\text{Short}}$, and $\bar{F}_{W_i}^{\text{Long}}$):

$$\begin{aligned} & \text{minimize } \sum \left| \Delta \theta_{W_i}^{\text{Posture}} \right|^2, \\ & \text{subject to } \mathbf{RF}_{AFL} \bar{e} = \mathbf{J}^T \bar{F}_{W_i}^{\text{Preferred}}, \text{ and } \bar{lb} \leq \bar{e} \leq \bar{ub} \end{aligned} \quad (3.2),$$

where $\Delta \theta_{W_i}^{\text{Posture}}$ is a force angle deviation calculated from vector angle difference between the experimental synergy force vector ($\bar{F}_{W_i}^{\text{Posture}}$) and simulated endpoint force in the model ($\bar{F}_{End}^{\text{Posture}}$) at a given posture. Force angle deviations were computed using the angle defined by the inverse cosine of the dot product between the two 3-dimensional force vectors:

$$\Delta \theta_{W_i}^{\text{Posture}} = \cos^{-1} \left(\frac{\bar{F}_{W_i}^{\text{Posture}} \bullet \bar{F}_{End}^{\text{Posture}}}{\left\| \bar{F}_{W_i}^{\text{Posture}} \right\| \cdot \left\| \bar{F}_{End}^{\text{Posture}} \right\|} \right) \quad (3.3).$$

We also computed muscle feasible ranges (MFR; (Sohn et al. 2013)) for producing experimental synergy force vectors at preferred posture to specify the absolute lower and upper bounds in individual muscles. This nonlinear optimization problem (Eq. 3.2) was solved using *fmincon* in Matlab (Mathworks, Natic, MA). In order to ensure convergence to a global minimum solution, we performed the search using 100 random initial conditions (\bar{e}^{-0}) in which activation levels of individual muscles were uniformly distributed between 0 and 1, which is the physiological range.

3.2.4 Minimum-effort solution

To test whether a solution that is optimal for a single posture can be generalized across postures, we assessed force angle deviations of an optimal solution at preferred posture across all stance configurations. The optimal solution was selected based on the criteria used most often in musculoskeletal modeling (Erdemir et al. 2007), minimizing sum of squared muscle activations (Eq. 3.4) (Anderson and Pandy 2001b; Crowninshield and Brand 1981; Thelen et al. 2003). For each synergy, we used quadratic programming to identify a unique muscle activation pattern ($\bar{e}^{\text{-minE}}$) that minimized sum of squared muscle activations while matching experimental synergy force vector at preferred stance:

$$\begin{aligned} & \text{minimize } \bar{e}^{\text{-T}} \bar{e}, \\ & \text{subject to } \mathbf{RF}_{AFL} \bar{e} = \mathbf{J}^T \bar{F}_{W_i}^{\text{Preferred}}, \quad \text{and} \quad \bar{l}b \leq \bar{e} \leq \bar{u}b \end{aligned} \quad (3.4).$$

Force angle deviations of the minimum effort solutions ($\bar{e}^{\text{-minE}}$) from simulated forces across all other postures were computed as in Eq. 3.3, and were compared to that of the best-generalizable solution.

To determine how much more effort is required for the best-generalizable solutions, we evaluated their effort levels and compared to the minimum-effort solutions at each posture (Eq. 3.4). To compare across conditions, we normalized the effort levels of each muscle activation pattern to that of the maximum-effort solution at each posture found using an optimization similar to Eq. 3.4 but subject to maximizing instead of minimizing the sum of squared muscle activations. The effort level of the best-generalizable solution at the preferred stance distance was applied uniformly across postures without scaling the activation patterns to match the magnitude of simulated forces vectors to the experimental synergy force vectors. We did not control for the magnitude of simulated force vector because force vector direction is a more relevant performance measure for the given task or reactive balance; nonetheless, simulated force magnitudes ranged around 75~155% of the experimental synergy force vectors.

3.2.5 Random solutions

In order to demonstrate that generalizability may be a functional constraint that the nervous system may consider, rather than a pure anatomical constraint of the hindlimb, we tested the generalizability of random solutions found at preferred posture to other stance conditions. We first generated 100 random muscle activation patterns that produced the experimental synergy force vectors at preferred posture. These random solutions were generated by finding the nearest solution to each of the 100 random patterns that were used as initial conditions (\bar{e}^{-0} , see 3.2.2 Best generalizable solutions), projecting them to a solution manifold in least-square sense. This optimization problem was solved using quadratic programming (*quadprog* in Matlab):

$$\begin{aligned} & \text{minimize } (\bar{e} - \bar{e}^{-0})^T (\bar{e} - \bar{e}^{-0}), \\ & \text{subject to } \mathbf{RF}_{AFL} (\bar{e} - \bar{e}^{-0}) = \mathbf{J}^T \bar{F}_{W_i}^{\text{Preferred}} - \mathbf{RF}_{AFL} \bar{e}^{-0}, \quad \text{and} \\ & \quad \quad \quad \bar{lb} - \bar{e}^{-0} \leq \bar{e} - \bar{e}^{-0} \leq \bar{ub} - \bar{e}^{-0} \end{aligned} \quad (3.5).$$

These random solutions were then applied to the other postures and the resulting force angle deviations were computed and compared to that of the best-generalizable solution.

3.2.6 Muscle feasible ranges with generalizability constraint

In order to test whether a functional requirement for generalizability across tasks restricts the feasible range of activation in individual muscles, we identified sub-range of muscle activation patterns that are more generalizable than others. We computed the feasible bounds on individual muscles for which a muscle activation pattern satisfied production of experimental synergy force vectors at preferred posture while deviations in force directions at other postures were kept within a given tolerance (*Tol*). Based on the results from force angle deviations of best-generalizable solutions which was typically less than $\sim 10^\circ$, the tolerance (*Tol*) was defined to be 10° . In one case where the maximum

force angle deviation of the best-generalizable solution exceeded 10° in certain posture, the tolerance was set to 110% of the maximum: 11.6° at shortest stance for the flexor synergy force vector in cat *Bi*. Tolerance of 10° was comparable to expected variability in active forces generated across trials during experiment, which should be greater than variability observed in the total ground reaction force vector during initial passive period of 100 ms of $\sim 5^\circ$ (Ting and Macpherson 2004).

The minimum allowable activation for generalizability in a muscle was found by solving a nonlinear optimization:

$$\begin{aligned}
 & Gen_m^{lb}: \text{Find } \bar{e} \text{ such that } e_m \text{ is minimized,} \\
 & \text{subject to } \mathbf{RF}_{AFL} \bar{e} = \mathbf{J}^T \bar{F}_{w_i}^{\text{Preferred}}, \quad \bar{lb} \leq \bar{e} \leq \bar{ub}, \quad \text{and} \\
 & \Delta\theta_{w_i}^{\text{Posture}} \leq Tol \text{ for all postures shortest, short, and long} \quad (3.6).
 \end{aligned}$$

Similarly, the maximum allowable activation for generalizability in each muscle was found by solving a nonlinear optimization:

$$\begin{aligned}
 & Gen_m^{ub}: \text{Find } \bar{e} \text{ such that } e_m \text{ is maximized,} \\
 & \text{subject to } \mathbf{RF}_{AFL} \bar{e} = \mathbf{J}^T \bar{F}_{w_i}^{\text{Preferred}}, \quad \bar{lb} \leq \bar{e} \leq \bar{ub}, \quad \text{and} \\
 & \Delta\theta_{w_i}^{\text{Posture}} \leq Tol \text{ for all postures shortest, short, and long} \quad (3.7).
 \end{aligned}$$

In total, 62 independent optimizations were run (two empirical bounds for each of 31 muscles), resulting in 62 muscle activation patterns for each synergy.

We qualitatively examined at preferred posture whether the muscle feasible ranges are reduced in each muscle with the functional requirement for generalizability, across postures compared to the absolute muscle feasible ranges for producing the experimental synergy force vectors. In particular, we categorized the difference in each muscle in terms of an increased lower bound, decreased upper bound, or both. Although these bounds represent the limit regarding activation level of individual muscles for which a generalizable solution can be found, note that it is only a necessary (not

sufficient) condition that a pattern within this range is always generalizable within the specified tolerance.

To test whether the muscle feasible ranges computed with the generalizability constraint could represent a reduced solution space for muscle activation patterns that are more generalizable, we compared the dimensionality and generalizability of a set of random solutions that were inside these constrained muscle feasible ranges versus a control set in which muscle activations were allowed to violate these muscle feasible ranges. Specifically, we generated 100 random solutions satisfying the synergy force vector at preferred posture as in Eq. 3.5, but using the feasible range with the generalizability constraint as the bounds for each muscle. For the control set, we used the previously generated random solutions (see 3.2.5 Random solutions), because most of these solutions were found to lie outside the feasible range with generalizability constraint. Only a few solutions for the extensor synergy force vector in both cats (1 in cat *Bi*, and 3 in cat *Ru*) were strictly inside the feasible range with generalizability constraint; more than one muscle violated the feasible range with generalizability constraint in all other cases.

Dimensionality was compared by computing the rank of a matrix composed of each set of 100 random solutions. Further, in order to test whether narrowing of the ranges imposes more constraints in terms of co-variation across muscles, correlation coefficient (R^2 , Pearson coefficient of correlation, evaluated at significance level $\alpha=0.05$) was computed for activation levels of all muscle pairs in each of the two sets. Furthermore, in order to test whether muscle feasible ranges identified with generalizability constraint within a given tolerance could be indicative of a sufficient condition for the generalizability requirement, we compared force deviations in solutions that were within the feasible range with generalizability constraint and those that violated the feasible range with generalizability constraint using one-way ANOVA ($\alpha=0.05$).

3.3 Results

Only specific muscle patterns could be generalized across postures, suggesting that generalizability can be a functional constraint. This was consistent across all conditions (each cat and each synergy force vector) (Table 3.2). Therefore, for detailed illustration of the results, we selected two synergy force vectors that were the most consistent in force direction across cats in all postures: the extensor synergy force vector (\bar{F}_{w_1} ; Fig. 3.1A, red) and the flexor synergy force vector (\bar{F}_{w_2} ; Fig. 3.1A, yellow). For each case we were able to find a single solution that produces the experimental synergy force vector at the preferred posture and approximates the direction of the synergy force vectors at the three other postures, which we refer to as the best-generalizable solutions.. In general, deviations in the simulated forces produced by the best-generalizable solutions (Fig. 3.2, blue force vectors) were small, always less than 12° across all conditions (cats, synergies, and postures). For example, deviations in the simulated forces produced by the best-generalizable solution for the extensor synergy force vector in the model matched to cat *Ru* were less than 4° in all three postures (Fig. 3.2C). The largest deviation was found for the flexor synergy force vector in model matched to cat *Bi* (Fig. 3.2B) at shortest stance, which was 12° . Across all cats and synergies, force angle deviations of the best-generalizable solutions were always greatest at the shortest stance, indicating that more controlled selection may be required for muscle activation patterns to be generalizable at this more extreme posture.

Most searches for the best-generalizable solution converged to the same local minimum solution, regardless of the different initial conditions from which the search was started, suggesting that we were able to find the global minimum. In these cases the nonlinear optimization yielded essentially the same solution: the standard deviations in individual muscle activations for all conditions (cats and synergies) were always less than less than 10^{-10} in most cases (always less than 10^{-4}) and the average standard deviations in

force angle deviations across all postures were less than $10^{-3\circ}$ in most cases (always less than $10^{-2\circ}$). There were only a few cases when the search converged to a different local minimum given different initial conditions. Further analyses were based on the solutions where the maximum deviation in force were the smallest across all initial conditions.

The optimal solutions minimizing effort at preferred postures were not generalizable across postures. When applied to the other postures, the force angle deviations (Fig. 3.2, black force vectors with dotted lines) were generally greater than the best-generalizable solutions (Fig. 3.2, blue force vectors), especially at the short and shortest stance. For example, force angle deviations for the flexor synergy force vector at shortest stance was 39° (Fig. 3.2B) and 44° (Fig. 3.2D) in cat *Bi* and *Ru*, respectively. On the other hand, at long stance, force angle deviations of the minimum-effort solution were

Table 3.2. Force angle deviations in all conditions

		<i>Bi</i>			<i>Ru</i>		
		Best-G	Min-E	Random	Best-G	Min-E	Random
F_{W1}	Shortest	6.90°	29.8°	43.3°±17.2°	3.53°	24.5°	23.5°±16.6°
	Short	2.97°	11.0°	9.75°±4.08°	1.10°	15.3°	11.4°±6.83°
	Long	5.54°	4.04°	9.51°±2.32°	0.38°	5.35°	7.76°±2.37°
F_{W2}	Shortest	11.6°	39.4°	63.2°±26.7°	9.98°	44.2°	67.8°±23.3°
	Short	2.50°	30.1°	109°±35.4°	4.57°	26.5°	44.3°±17.3°
	Long	5.93°	19.1°	133°±31.3°	6.21°	8.77°	97.0°±56.0°
F_{W3}	Shortest	3.20°	17.7°	53.1°±25.1°	4x10 ⁻⁴ °	6.09°	26.2°±14.6°
	Short	1.65°	8.96°	9.36°±6.25°	6x10 ⁻⁴ °	7.58°	27.9°±15.7°
	Long	2.06°	0.89°	13.7°±3.82°	2x10 ⁻⁴ °	53.1°	80.9°±6.82°
F_{W4}	Shortest	3.93°	9.61°	63.0°±12.2°	0.34°	7.01°	115°±20.1°
	Short	2.41°	7.21°	69.4°±17.9°	0.45°	2.58°	112°±30.1°
	Long	3.08°	24.8°	101°±7.12°	0.03°	3.47°	92.1°±27.1°
F_{W5}	Shortest	7.67°	41.1°	78.4°±27.0°	1.85°	39.0°	76.4°±35.0°
	Short	2.50°	38.9°	149°±8.87°	1.79°	25.0°	61.0°±36.3°
	Long	0.06°	67.0°	149°±13.8°	0.12°	21.1°	153°±6.73°

Best-G: Best-generalizable solutions, Min-E: Minimum-effort solutions, Random: Random solutions

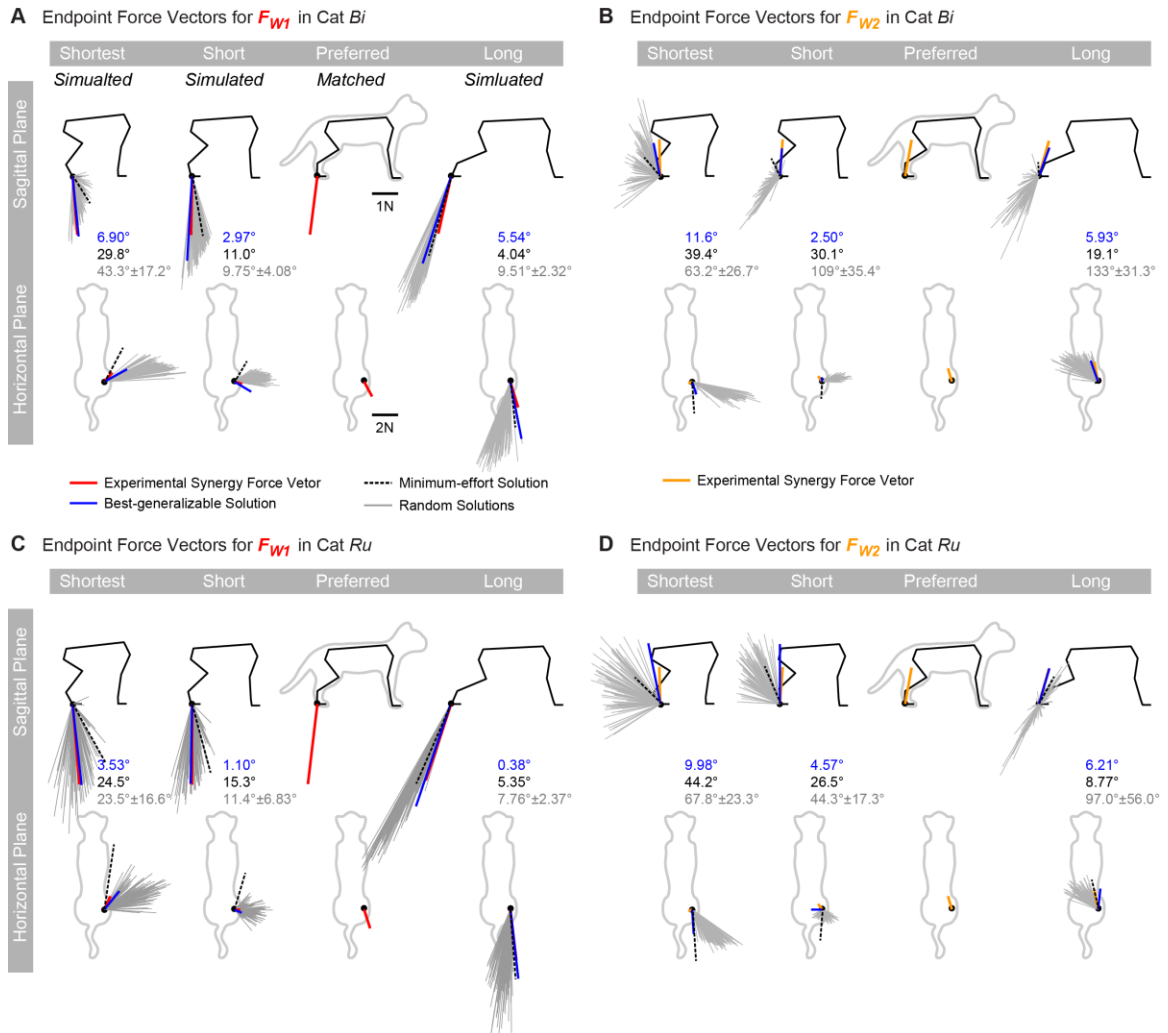


Figure 3.2: Generalizability of simulated endpoint force vectors. Simulated endpoint force vectors for F_{W1} in (A) cat *Bi* and (B) cat *Ru*, and for F_{W2} in (C) cat *Bi* and (D) cat *Ru*. Muscle activation patterns were found to match the experimental synergy force vector at Preferred stance, and were applied to other postures to generate endpoint force vectors. At Shortest, Short, and Long stances, force angle deviations compared to experimental synergy force vectors of the best-generalizable solution (blue force vectors), optimal minimum-effort solution (black force vectors), and 100 random solutions (gray force vectors) were found for F_{W1} (red) and F_{W2} (yellow). Force angle deviations of the best-generalizable solution was small ($<10^\circ$) in general (numbers in blue). Force angle deviations in all other solutions (numbers in black for the minimum-effort solution and in gray for random solutions) were generally greater, especially at Shortest stance.

relatively small and comparable to that of the best-generalizable solutions. For example, force deviations for the extensor synergy force vector at long stance were only 4.0° (Fig.3.2A) and 5.4° (Fig.3.2C) in cat *Bi* and *Ru*, respectively.

In addition, randomly selected solutions did not generalize across postures, suggesting that generalizability is not a property of biomechanics of the limb. Deviations in forces at other postures with random solutions (Fig. 3.2, gray force vectors) that produced the experimental synergy force vector at the preferred posture were, in general, substantially greater than the best-generalizable solution (see Table 3.2 for detailed numbers). Similar to solutions selected with other criteria, the force angle deviations were greatest at shortest stance. For example, force angle deviations of the random solutions for the extensor synergy force vector were $43^\circ \pm 17^\circ$ in cat *Bi* and $24^\circ \pm 17^\circ$ in cat *Ru*.

The best-generalizable solutions were always sub-optimal in terms of effort. The relative effort level of the best-generalizable solution was greater than the minimum-effort solution in all conditions (Fig. 3.3). For example, in cat *Ru*, effort level of the best-generalizable solutions were around 50% for both synergy force vectors, compared to the minimum-effort solutions with $\sim 10\%$ (Fig. 3.3 right, blue solid lines versus black dotted lines). The smallest difference between the effort level of the best-generalizable solution and the minimum-effort solutions was found in cat *Bi*, for extensor synergy force vector (Fig. 3.3 left, red dots on blue solid lines and black dotted lines). Increased effort of the best-generalizable solutions was due to high activation levels in only a few muscles. In particular, the activation level of some muscles in the best-generalizable solutions were at physiological maximum, e.g. 4 muscles for the flexor synergy force vector in cat *Bi* (Fig. 3.4A, bottom row).

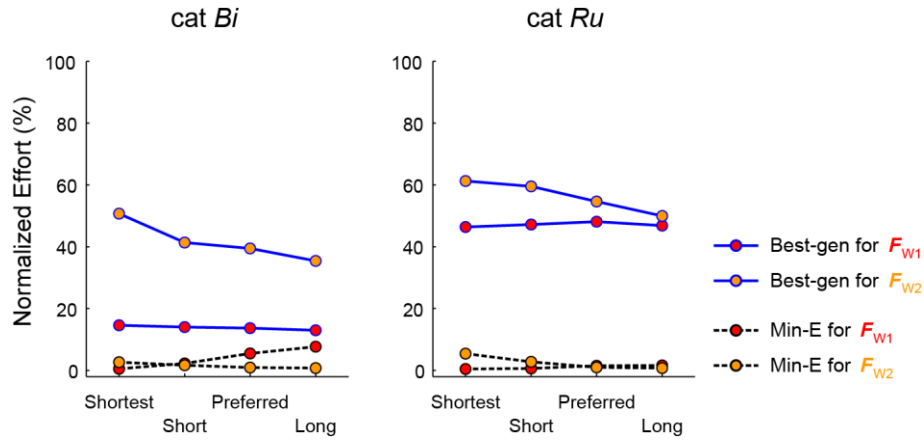


Figure 3.3: Effort level comparison. Normalized effort levels of the best-generalizable solution (Best-gen) and optimal solution (minimum-effort, Min-E) for cat *Bi* (left) and cat *Ru* (right). Effort levels were normalized to the maximum value that can be found for corresponding experimental synergy force vector at each posture. Best-generalizable solutions were always sub-optimal: effort levels of the best generalizable solutions were greater than the optimal solutions across all condition, i.e., cats and forces.

The requirement for generalizability across different tasks restricted the feasible range of activation levels in some muscles but many retained a wide feasible range (Fig. 3.4B, filled boxes). Overall, muscle feasible ranges identified with the generalizability constraint, (i.e., tolerance in force angle deviations $<10^\circ$) were smaller than the absolute muscle feasible range for the experimental synergy force vector at preferred posture in many of the muscles: $71 \pm 30\%$ and $62 \pm 37\%$ across muscles for the extensor and flexor synergy force vector, respectively, in cat *Bi*; $93 \pm 14\%$ and $61 \pm 36\%$ in cat *Ru*. Reduction in feasible ranges with the generalizability constraint was due to decreased upper bounds (Fig. 3.4B, left, e.g. BFP, MG, or VM), increased lower bounds (Fig. 3.4B, left, e.g. TA), or both (2 muscles for the flexor synergy force vector in cat *Ru*, not shown). However, many muscles had no change in their feasible range when the generalizability constraint was added, such that activation levels were still allowed to vary from 0 to 1 (Fig. 3.4B, left, e.g. ADL, PSOAS, or SOL). Specific changes for each cat and synergy force vector are summarized in Table 3.2.

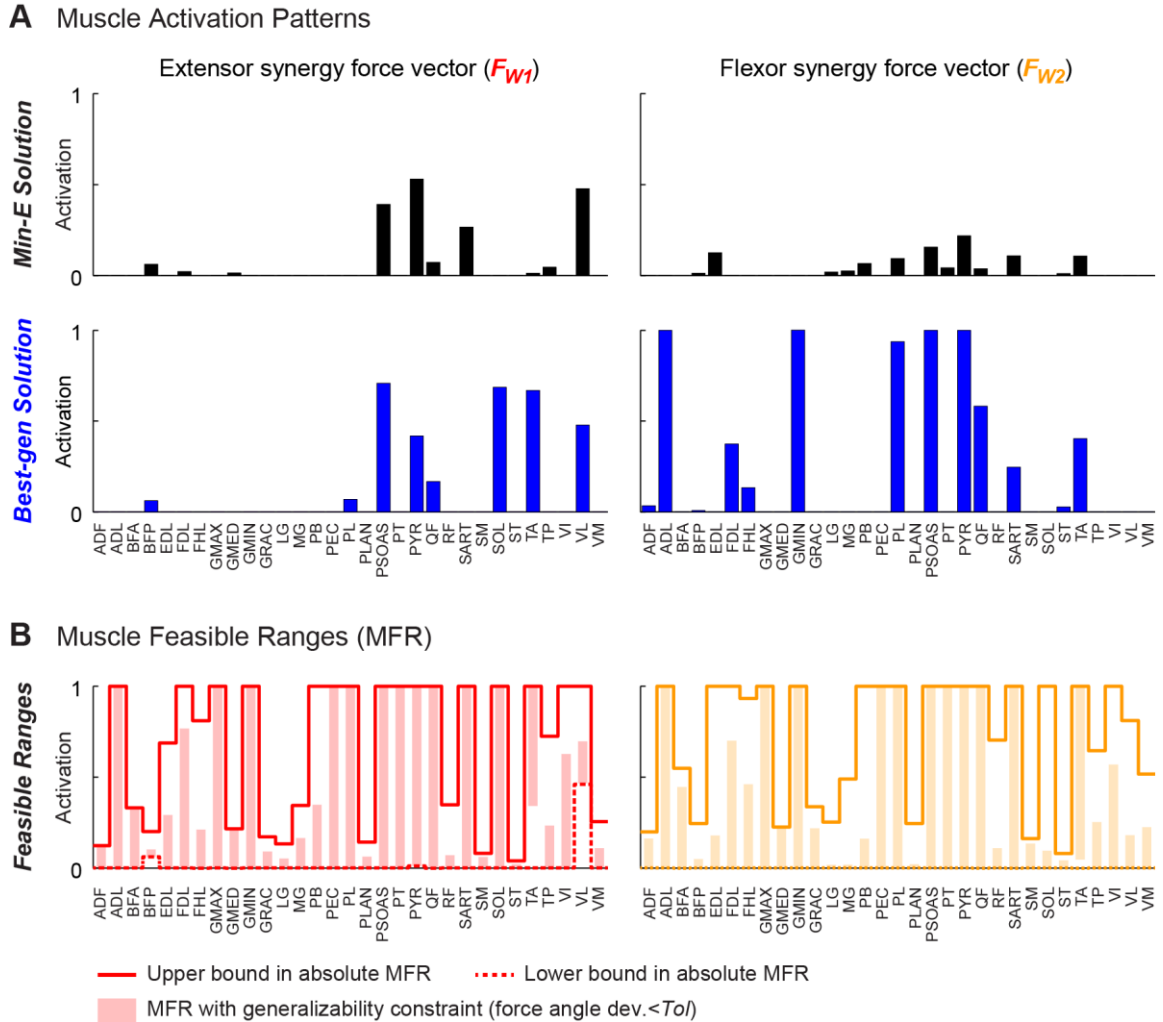


Figure 3.4: Muscle activation patterns and muscle feasible ranges. (A) Muscle activation patterns of minimum-effort solutions (top row) and best-generalizable solutions (bottom row) for F_{W1} (left) and F_{W2} (right) in cat *Bi*. Some muscles in the best-generalizable solution for F_{W2} have activation levels at physiological maximum of 1, resulting in high level of effort compared to the minimum-effort solution. (B) Absolute muscle feasible ranges (thick lines) for producing experimental synergy force vector at preferred stance, muscle feasible range with the generalizability constraint in each muscles (filled boxes), i.e., keeping the force angle deviations $< Tol$ across all postures. The requirement for generalizability ($< Tol$) narrowed the feasible range of activation in some muscles: e.g. BFP, MG, or VM by decreasing the upper bound, and TA by increased lower bound for F_{W1} (left). However, many muscles were still allowed to vary from 0 to 1 (e.g. ADL, SOL, PSOAS, or SOL for F_{W1}), illustrating redundancy in muscle activation space even with requirement for generalization of function across postures.

Table 3.3. Changes in feasible bounds with the generalizability constraint compared to absolute bounds

	<i>Bi</i>				<i>Ru</i>			
	F_{W1}		F_{W2}		F_{W1}		F_{W2}	
	<i>UB</i>	<i>LB</i>	<i>UB</i>	<i>LB</i>	<i>UB</i>	<i>LB</i>	<i>UB</i>	<i>LB</i>
ADF	-	-	↓	-	-	-	↓	-
ADL	-	-	-	-	-	-	-	-
BFA	-	-	↓	-	-	-	↓	-
BFP	↓	-	↓	-	↓	-	↓	-
EDL	↓	-	↓	-	-	-	↓	-
FDL	↓	-	↓	-	-	-	↓	-
FHL	↓	-	↓	-	↓	-	↓	↑
GMAX	-	-	-	-	-	-	-	-
GMED	-	-	-	-	↓	-	↓	-
GMIN	-	-	-	-	-	-	-	-
GRAC	↓	-	↓	-	-	-	↓	-
LG	↓	-	↓	-	↓	-	↓	-
MG	↓	-	↓	-	↓	-	↓	-
PB	↓	-	↓	-	-	-	-	-
PEC	-	-	-	-	-	-	-	-
PL	-	-	-	-	-	-	-	↑
PLAN	↓	-	↓	-	↓	-	↓	-
PSOAS	-	-	-	-	-	-	-	-
PT	-	-	-	-	-	-	-	↑
PYR	-	-	-	-	-	-	-	-
QF	-	-	-	-	-	-	-	-
RF	↓	-	↓	-	↓	-	↓	-
SART	-	-	-	-	-	-	-	-
SM	↓	-	↓	-	-	-	↓	-
SOL	-	-	↓	-	-	-	↓	-
ST	↓	-	↓	-	-	-	↓	-
TA	-	↑	-	↑	-	-	-	↑
TP	↓	-	↓	-	-	-	↓	↑
VI	↓	-	↓	-	-	-	↓	-
VL	↓	-	↓	-	-	↑	↓	-
VM	↓	-	↓	-	-	-	↓	-

↓: decreased upper bound ↑: increased lower bound -: same upper or lower bound

The space of feasible ranges with the generalizability constraint was reduced in dimension. Dimension, or rank, of the random solutions that violate the feasible range with generalizability constraint was 25 in all conditions, whereas the rank of the random solutions that were inside the feasible range with generalizability constraint was 18 and 20 for the extensor synergy force vector in cat *Bi* and *Ru*, respectively, and 23 in both cats for the flexor synergy force vector. The modest reduction in dimension was likely due to increased co-variations across muscles in random solutions that were inside the feasible range with generalizability constraint. For example, for the extensor synergy force vector in cat *Bi*, there were five muscle pairs that had R^2 greater than 0.50 ($p < 0.05$) with the generalizability constraint, compared to only one pair in solutions that violated the feasible range with generalizability constraint.

The feasible ranges with the generalizability constraint did not always predict solutions that are generalizable to a given tolerance (Fig. 3.5, dotted lines). Force angle deviations of the solutions that were inside the feasible range with the generalizability constraint could often be substantially greater than the specified tolerance in most conditions (Fig. 3.5, light bars).

The feasible ranges with the generalizability constraint did not always predict solutions that are generalizable to given tolerance (Fig. 3.5, dotted lines). Force angle deviations of the solutions that were inside the feasible range with the generalizability constraint could often be substantially greater than the specified tolerance in most conditions (Fig. 3.5, light bars). However, in many cases, the solutions inside the feasible range with the generalizability constraint had smaller force angle deviations than the solutions that violated the constrained feasible range (Fig. 3.5, dark bars). For example, force angle deviations of the 100 random solutions that were inside the feasible range found with the generalizability constraint were always smaller ($p < 0.05$) than the other 100 random solutions that violated the feasible range with generalizability constraint at all stance distances in both cats for the flexor synergy force vector (Fig. 3.5, right).

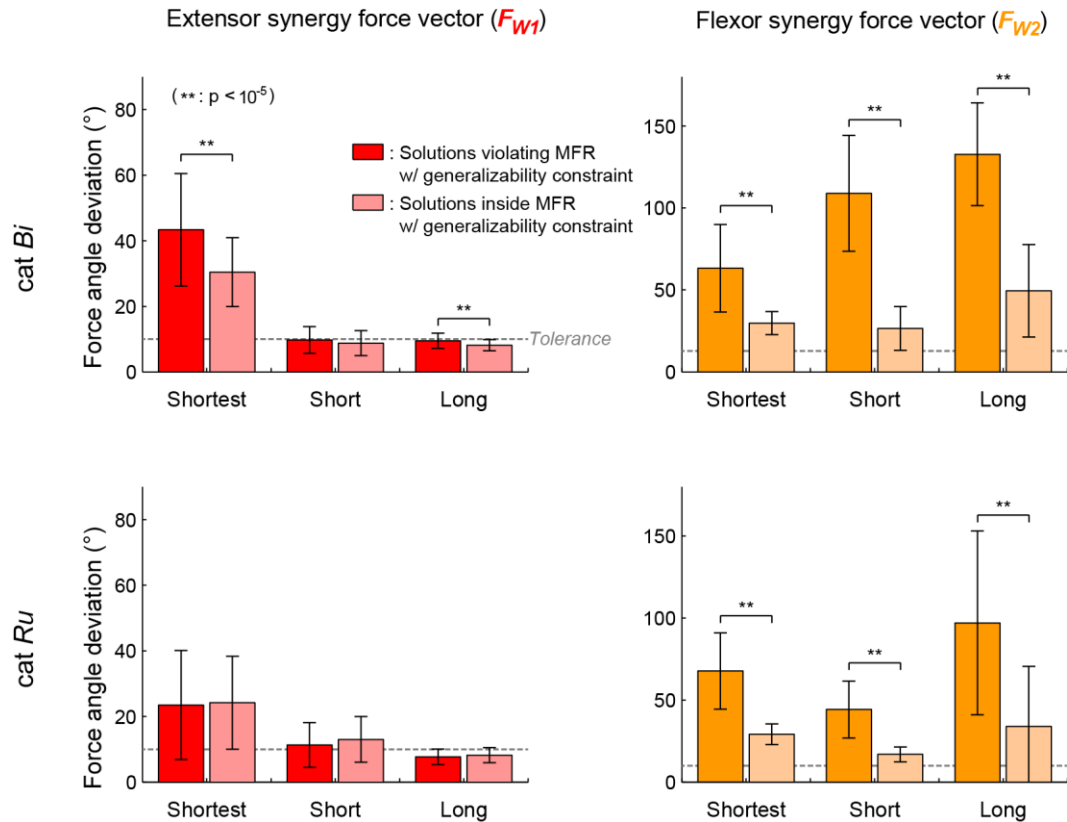


Figure 3.5: Generalizability of random solutions inside feasible range with generalizability constraint. Force angle deviations of 100 random solutions that were strictly inside the feasible range with generalizability constraint (light bar) compared to random solutions that violated the feasible range with generalizability constraint (dark bar) for the extensor synergy force vector (left column) and the flexor synergy force vector (right column) in cat *Bi* (top) and cat *Ru* (bottom). Force angle deviations of solutions that were strictly inside the feasible range with generalizability constraint could often be substantially greater than the specified tolerance (dotted lines) in most conditions. In many case, solutions that were inside the feasible range with the generalizability constraint were more generalizable, i.e., smaller force angle deviations ($p < 0.05$), than solutions that violated the feasible range with the generalizability constraint.

3.4 Discussion

In this study, we demonstrated that a functional requirement of generalizability across biomechanical conditions reduces the range of feasible muscle activation patterns for force generation. Our results reject two alternative hypotheses about the origin of generalizability of muscle activation patterns observed experimentally. By showing that most solutions at one posture do not generalize across postures, we demonstrate that

generalizability is not granted merely by anatomical arrangement and function of limb musculature (i.e., biomechanical constraints) (Kutch and Valero-Cuevas 2012). Second, by showing that the optimal solution based on a minimum-effort criteria does not generalize across postures we demonstrate that a single optimization criterion (Todorov 2004) may not be sufficient for the nervous system to organize the spatial structure of muscle synergies. In contrast, it is possible to select solutions that are generalizable across postures. This supports our hypothesis based on experimental observations that muscle synergies represent fixed entities that are neurally encoded, or selected from, among many possible solutions. We also showed that solutions explicitly selected to be generalizable across postures, i.e., the best-generalizable solutions, were always sub-optimal at a given posture in terms of effort. Our results further showed that even with functional requirements for generalizability within a given tolerance, feasible ranges of muscles were wide. This may explain inter-subject variability in muscle synergy patterns that produce essentially same biomechanical output (Chvatal and Ting 2012; Clark et al. 2010; Torres-Oviedo et al. 2006), as well as deviations of optimal predictions from experimentally-observed muscle patterns (Buchanan and Shreeve 1996; Thelen and Anderson 2006). Our framework of using computational models to predict and evaluate muscle activation patterns according to functional properties and optimality criteria may be useful in examining possible variations in range of solutions that are functional in various contexts.

Consideration of biomechanical constraints from multiple conditions narrows the range of possible muscle activation patterns that can be generalized across conditions. Biomechanical constraints such as muscle's function and capability as well as task demands (Bunderson et al. 2010; Delp and Loan 2000; Kaya et al. 2008; Valero-Cuevas 2009; van Antwerp et al. 2007) determine how much room is allowed for motor control solutions. Available solutions may be more strictly constrained in less redundant systems such as human finger (Kutch and Valero-Cuevas 2011), or for a maximal task (Valero-

Cuevas 2000). Alternate task demands such as the need to modulate limb impedance (Hu et al. 2012; Perreault et al. 2001; 2002) may require adjustment in the biomechanical condition itself, such as change in postures (Franklin et al. 2013; Trumbower et al. 2009). In general, however, the latitude the nervous system has in selecting muscle activation pattern for a single sub-maximal task is wide (Martelli et al. 2015; Martelli et al. 2013; Sohn et al. 2013). Nevertheless, superimposition of multiple task constraints may restrict the feasible range of solutions (Keenan et al. 2009; Loeb 2000; Racz et al. 2012). Our results show that only a few of the redundant muscle activation patterns that satisfy a single task constraint can generalize to other conditions and meet the subsequent task constraints. A tight regulation in force production was required for muscle activation patterns to be generalized in certain conditions such as short stance. Therefore, identifying motor solutions that can be generalized across conditions cannot be guaranteed by satisfying a single task constraint or biomechanical changes corresponding to each task. The reduction in feasible ranges of muscle activation patterns we identified with a generalizability constraint may reflect the sensitivity of muscles' torque-producing characteristics across changes in posture. For example, the recruitment of muscles that undergo substantial changes in moment arm length due to changes in hip angle may have been suppressed, as indicated by the decrease in their upper bound. The robustness of muscle synergies that can be generalized across conditions that vary in biomechanical constraints (Cheung et al. 2005; Chvatal and Ting 2013; d'Avella and Bizzi 2005; Hart and Giszter 2004) may support the neural origin hypothesis of muscle synergies, a topic that has been widely debated (Bizzi and Cheung 2013; Hart and Giszter 2010; Kutch and Valero-Cuevas 2012; Tresch and Jarc 2009).

Muscle synergies may be sub-optimal in terms of a single criterion such as effort for a given motor task, but optimal in a more global sense. The best-generalizable solutions found in this study were always sub-optimal in terms of effort. On the other hand, effort-wise optimal solutions that were selected for a single posture were not

generalizable across conditions. They were less generalizable than most of the randomly selected solutions. Therefore, it is unlikely that spatial patterns of muscle synergies are organized based on the single optimality principle of minimizing effort. Rather, muscle synergies may be optimal in a more global sense. They may result from a balance between multiple goals and criteria such as generalizability (Tsianos et al. 2014), computational efficiency or the facilitation of motor learning (Berger et al. 2013; Berniker et al. 2009; Byadarhaly et al. 2012; Giszter et al. 2007; McKay and Ting 2012; Mussa-Ivaldi and Giszter 1992; Mussa-Ivaldi et al. 1994). However, if muscle synergies are neural entities that have been acquired over an extended period of learning and refinement (Lacquaniti et al. 2013; Loeb 2012; McKay et al. 2007; Wu et al. 2014), they may also be near optimal regarding single criterion. Many modeling studies have shown that spatial organization of muscle synergies resemble solutions obtained from optimal control process such as minimizing errors or control effort (De Groote et al. 2014; Steele et al. 2013; Todorov and Jordan 2002), or that exploits natural limb dynamics (Berniker et al. 2009). Thus, muscle synergies may represent “good enough” solutions (Loeb 2012) that can be flexibly used across different conditions.

The redundancy remaining in the functionally equivalent solutions that can be generalized across conditions may account for individual differences, and suggests that additional neural criteria are likely involved in selection of muscle activation patterns for muscle synergies. Our results showed that even when imposing constraint for generalization, the feasible range of activations in many muscles were allowed to vary substantially. This suggests that there can be many different muscle activation patterns that are equally generalizable, but differ in their spatial structures. This is consistent with experimental variability observed in muscle synergy patterns that are used for same biomechanical function across biomechanical conditions (Chvatal and Ting 2012; Clark et al. 2010; Torres-Oviedo et al. 2006). Variability in muscle synergy patterns across individuals may therefore reflect individual differences in habits or preferences (de Ruyg

et al. 2012; Ganesh et al. 2010), or additional selection criteria regarding energetics (Alexander 2005; 1989; Huang and Kuo 2014; Neptune et al. 2008) or stability (Bunderson et al. 2008; Liao et al. 2013; Sohn et al. 2013).

CHAPTER 4

TRADE-OFFS BETWEEN FUNCTIONAL PROPERTIES OF EFFORT AND STABILITY

4.1 Introduction

Variability is commonly observed in experimental muscle activation patterns used for performing a motor task (Gottlieb 1998), but little is known about neural principles underlying variability. Musculoskeletal redundancy allows for individuals to exploit many different ways to produce a same movement (Bernstein 1967). Accordingly, even for stereotypical patterns of movement (e.g. joint kinematics and kinetics) such as in walking, muscle activity as measured by electromyography (EMG) exhibit both inter- and intra-subject variability (Liu et al. 2008; Winter and Yack 1987). Likewise, during standing balance in both humans and animals, different muscle patterns are used across individuals to produce similar reactive force at the endpoint (Horak and Nashner 1986; Torres-Oviedo et al. 2006; Torres-Oviedo and Ting 2007). Such variability reflects a large space of equivalent solutions that can achieve the same task, suggesting that neural selection of muscle activation patterns may involve multiple criteria that vary according to the context (Loeb 2012). For example, minimization of metabolic energy or control effort has often been proposed as a governing principle for tasks such as reaching (Alexander 1997; Nakano et al. 1999; Soechting et al. 1995; Todorov 2004; Todorov and Jordan 2002; Torres and Zipser 2002; Uno et al. 1989) or walking (Alexander 2005; 1989; Zarrugh et al. 1974). However, when similar tasks are performed in dynamically unstable environments, functional requirements for stability elicit changes in the solutions that are used. During reaching in a divergent force field (Franklin et al. 2008) or walking down-slope (Hunter et al. 2010), subjects increased co-activation across muscles

to stiffen the joints and gain stability, but at the cost of increased effort. On the other hand, pathological motor deficits (Dietz and Sinkjaer 2007) or preference for habitual patterns (de Rugy et al. 2012; Ganesh et al. 2010; Hasson et al. 2012; Kistemaker et al. 2010) may prevent individuals from using a solution with a better functional property, e.g. either a more efficient or a more stable one. Understanding possible variations in muscle activation patterns for a given task, and thus the neural selection in a redundant muscle space requires examination of multiple functional criteria that may be involved and possible trade-offs between them.

Current computational approaches using musculoskeletal models and single optimization criterion such as minimizing effort are insufficient to address variability. These approaches inherently forbid explicit exploration of various solutions that can be used for a given task because it identifies a unique solution based on an optimality criterion. Among many of the various criteria proposed in literature (Anderson and Pandy 1999; Harris and Wolpert 1998; Hogan 1984), one popular cost function that has been widely used is to minimize neural effort, often in terms of muscle forces or activations (Anderson and Pandy 2001b; Crowninshield and Brand 1981; Erdemir et al. 2007; Thelen et al. 2003). However, measured muscle activity often deviates from these optimal predictions (Buchanan and Shreeve 1996; Herzog and Leonard 1991; Thelen and Anderson 2006; van der Krogt et al. 2012). These deviations may contradict studies suggesting that musculoskeletal system significantly constrains the possible motor patterns such that all of the feasible motor solution are substantially similar (Kutch and Valero-Cuevas 2011). We recently demonstrated that in a musculoskeletal model of a cat hindlimb, muscle activation patterns for generating an isometric endpoint force could deviate substantially from one another (Sohn et al. 2013). Importantly, a great deal of biomechanical latitude was revealed, and minimizing effort could not explain the recruitment of muscles often observed experimentally. Therefore, in order to account for natural variability in selection of motor solution (Martelli et al. 2013; Prinz et al. 2004;

Raphael et al. 2010), physiologically relevant criteria other than just effort need to be considered.

Stability of the musculoskeletal system conferred by active muscles is a critical functional requirement for producing physiological behaviors. Neural control of movement can be inherently unstable because sensorimotor feedback is delayed due to slow neural conduction (Hasan 2005; Miall et al. 1993). Intrinsic stability, i.e. the capability of the *open-loop* musculoskeletal system to be stable, may ensure functionally robust behavior by prolonging the time until feedback corrections need to occur. Maintaining posture in response to perturbations illustrates the necessity for open-loop stability (Crevecoeur and Scott 2014; Perreault et al. 2004). Reactive responses in muscles elicited by perturbations during standing balance occur around 50 and 100ms after perturbation onset in cats and humans, respectively (Horak and Macpherson 1996). Thus, background muscle activation patterns used during quiet standing in cats are sufficient to provide intrinsic stability such that joint angle deviations are $<5^\circ$ in absence of any active control or sensorimotor feedback (Jacobs and Macpherson 1996). It is also known that cats with spinal cord transaction can be trained to bear weight in quiet standing and withstand small perturbations (De Leon et al. 1998), but lack appropriate directional responses at longer latency that are mediated by supraspinal circuitry (Macpherson and Fung 1999). Open-loop stability in musculoskeletal systems has mainly been attributed to intrinsic viscoelastic properties in active muscles (Burdet et al. 2001; Franklin et al. 2008; Hogan 1984). Intrinsic stability at the joint or whole-limb level can be achieved solely by preferential selection of muscle activation patterns (Bunderson et al. 2008). Nevertheless, other intrinsic mechanisms such as muscle short-range stiffness (Cui et al. 2008; Epstein and Herzog 2003) or proprioceptive length feedback (Burkholder and Nichols 2000; Nichols 1989 ; Wilmink and Nichols 2003) can contribute to stability at relatively short timescales, and prevent having excessive levels of muscle tone.

Whether the two functional properties effort and stability reflect a true trade-off in high dimensional muscle activation space for a redundant musculoskeletal system has not been explicitly tested. In multi-muscle systems effort and stability may compete against each other, since increased effort owing to muscle co-activation generally results in improved stability by stiffening the joints (Osu et al. 2002). To our knowledge, however, no study has quantitatively examined the landscape of effort and stability across the space of possible muscle activation patterns for a given task. Studies investigating feed-forward control of arm stability have mostly examined regulation of limb stiffness due to changes in muscle co-activation in terms of the resulting task error or variability (Burdet et al. 2006; Franklin et al. 2008; Hu et al. 2012; Selen et al. 2009). Few studies have explicitly examined stability conferred by active muscles during simulated behavior in musculoskeletal models. Recently, the open-loop stability conferred by muscle activation patterns was examined in a human arm model to assess possible improvements in stability for functional electrical stimulation (Liao et al. 2013). For a given posture, it was demonstrated that the maximum-effort solution, which had a high level of muscle co-activation, drastically improved stability compared to the minimum-effort solution. It has been shown that different muscle activation patterns that produce equivalent motor output in a cat hindlimb model can have widely varying local stability, as measured by time constants of the linearized system, or Lyapunov stability (Bunderson et al. 2008). A three-dimensional simulation of human walking was used show that intrinsic muscle properties play a role in stabilization against a disturbance (John et al. 2013). However, none of the above studies have examined how much cost, in terms of effort, is necessary to achieve certain level of stability.

Analytical tools and frameworks to explore the landscape of the solution space with respect to effort and stability may provide insight into how the nervous system finds a solution, or solutions, that satisfy certain functional properties. Furthermore, we may be

able to predict how easy or difficult it is, or what kind of a change needs to be made in a muscle pattern, to find another solution with a desired level of effort and stability.

Developing neuromechanical principles to guide selection of muscle activation patterns based on physiologically-meaningful stability metrics also has important implications for using models to study neural control of movement. Open-loop stability is important for forward dynamic simulations because it provides dynamic responses of the body that are more physiologically-relevant, and a numerically-stable basis for testing neural controllers (Ting et al. 2009). However, intrinsic stability is often lacking in simulations using musculoskeletal models. Solutions predicted from optimization are not robust in that simulations are vulnerable to small changes in modeling parameters or variation to the solution, especially for unstable tasks such as walking (John et al. 2013; Risher et al. 1997). For example, when a minimum-effort solution for producing an experimentally observed endpoint force was used in a cat hindlimb model, a slight change in configuration leads to unrecoverable joint angle deviations in forward dynamic simulations (Bunderson et al. 2010). Stable solutions can be useful for generating simulations that are robust to sources of instability such as noise, numerical round-off error, disturbances or inaccuracies in the modeling parameters (Alexandrov et al. 2005; Higginson et al. 2006; Risher et al. 1997).

Here, we sought to explore the landscape of the solution space with respect to the two functional properties of effort and stability during an isometric task of endpoint force production in a cat hindlimb model. We evaluated a multitude of possible muscle activation patterns in terms of sum-squared activation for effort versus stability predicted from linearized system using the Lyapunov indirect method, and mapped them onto a two-dimensional functional property space. In order to characterize the landscape of this space, we examined how variations in redundant muscle activation patterns change functional properties. Finally, we investigated whether effort and stability show reciprocal relationships and thus demonstrate a true trade-off by searching for the Pareto

front that illustrates the optimal border for maximizing stability while minimizing effort. Our results suggest that a large space of equivalent solutions is also reflected in vastly different functional properties of the solutions that can be explored by changing muscle activity within the constraint of the task. Further, differences in sensitivity of stability to changes in muscle pattern according to different region of the functional property space implies that there are multiple ways of finding a “better” solution, e.g. more stable solution with small increase in effort, which may explain difference in how individuals learn or acquire new solutions, e.g. optimal patterns in athletes versus pathological patterns in patients.

4.2 Methods and materials

4.2.1 Musculoskeletal model and target endpoint force

We used a detailed musculoskeletal model of a cat hindlimb (Burkholder and Nichols 2004) to examine muscle activation patterns to produce an experimentally observed endpoint force during postural response in a cat (Torres-Oviedo et al. 2006). Details of this three-dimensional model are described elsewhere (Bunderson et al. 2008; Bunderson et al. 2010; McKay and Ting 2008; Sohn et al. 2013), but briefly, the model included seven rotational degrees of freedom at the anatomical joints and 31 Hill-type muscles (Fig. 4.1A). The pelvis was fixed to the ground and endpoint of the limb defined at the metatarsophalangeal (MTP) joint was modeled as a gimbal joint. Model posture was matched to experimentally-measured kinematics of a cat during quiet standing (McKay et al. 2007; Torres-Oviedo et al. 2006). The equations of motion describing the dynamics of the limb using joint angles as generalized coordinates (\vec{q}) can be given as:

$$\mathbf{M}(\vec{q})\ddot{\vec{q}} = \vec{V}(\vec{q}, \dot{\vec{q}}) + \mathbf{R}(\vec{q})\vec{F}_M(\vec{q}, \dot{\vec{q}}, \vec{e}) - \mathbf{J}(\vec{q})^T \vec{F}_{End} \quad (4.1),$$

where $\vec{\dot{q}}$ and $\vec{\ddot{q}}$ are joint velocity and acceleration vector respectively; \vec{e} is a vector of muscle activation; \mathbf{M} is the inertia matrix; \mathbf{R} is the moment arm matrix; \mathbf{J} is the endpoint Jacobian; \vec{F}_M is a vector of muscle forces; \vec{F}_{End} is the target endpoint force vector; \vec{V} is the Coriolis force vector. Note that the model corresponds to generation of endpoint forces based on no background activity and in the absence of gravity, similar to previous models examining the feasible forces that can be generated by a limb (McKay et al. 2007; Schmidt et al. 2003; Valero-Cuevas 2000).

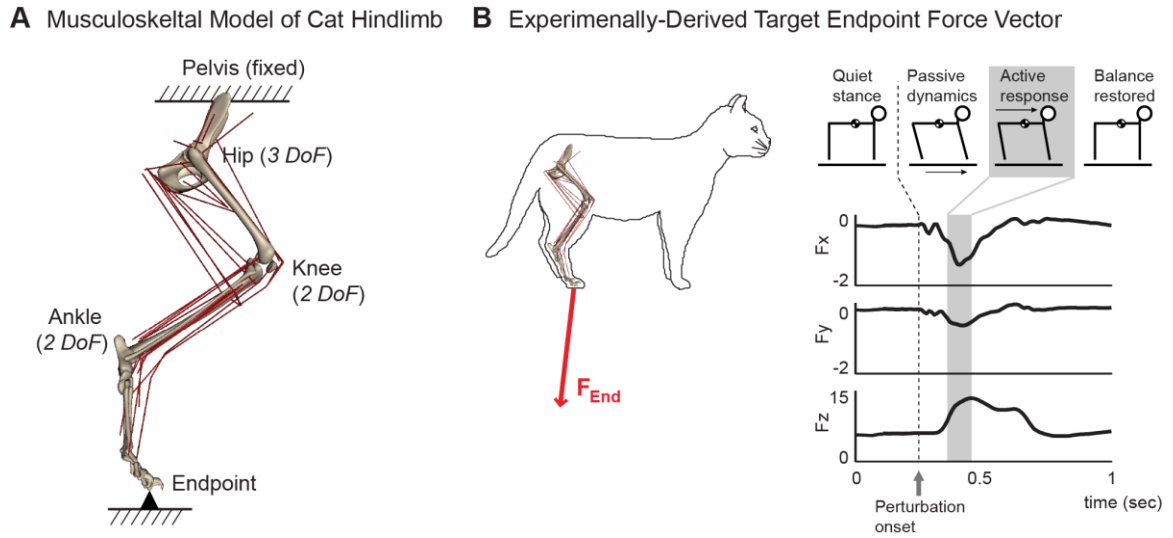


Figure 4.1: Model and task. (A) Musculoskeletal model of the cat hindlimb with seven rotational degrees of freedom (3 at the hip, 2 each at the knee and ankle) and 31 muscles. In this dynamic model, the pelvis was fixed to the ground and the endpoint (MTP joint) was connected to the ground via gimbal joint. (B) Target endpoint force vector (red) derived from active postural responses (gray box) during reactive balance task in cats. Kinematic changes were small during this active response period (80ms window following 120ms after onset of perturbation), and the task could be approximated quasi-static.

We defined a linear mapping from muscle activation vector to the net joint torque vector required to produce the target endpoint force vector to represent this model at static equilibrium ($\vec{\ddot{q}} = \vec{\dot{q}} = \vec{0}$):

$$\mathbf{R}\vec{F}_M = \mathbf{R}\mathbf{F}_{AFL}\vec{e} = \vec{\tau} = \mathbf{J}^T\vec{F}_{End} \quad (4.2).$$

Note that muscle force vector ($\bar{\mathbf{F}}_M$) is further factored into a diagonal scaling matrix for isometric force generation (\mathbf{F}_{AFL}) based on the force-length relationship (Zajac, 1989), multiplied by muscle activation (\bar{e}). All muscles were set at 65% optimal fiber length in ascending region of the force-length relationship curve (Gordon et al. 1966) to avoid inherent instability owing to lack of intrinsic stiffness in muscles (Bunderson et al. 2008).

For the target endpoint force vector, we used an extensor force vector (Fig. 4.1B) that was experimentally measured in active response of a cat following translational support perturbation (Torres-Oviedo et al. 2006). This force vector represented the change in the ground reaction force from the background level, averaged over 120-200 ms following the perturbation (Jacobs and Macpherson 1996), in which posture of the cat could be approximated quasi-static (Ting and Macpherson 2004).

4.2.2 Defining metrics for effort and stability

In order to evaluate functional properties of redundant muscle patterns that generate the same endpoint force and to map a functional property space in terms of effort and stability, we defined quantitative metrics for each criterion. We defined the metric for effort (E) to be the sum of squared activations (Eq. 4.3), which is equivalent to summing muscle stress (Anderson and Pandy 2001b; Crowninshield and Brand 1981; Thelen et al. 2003):

$$E = \sum_{m=1}^{31} e_m^2 \quad (4.3).$$

To normalize the level of effort across different muscle activation patterns, we identified the global minimum-effort solution ($\bar{e}^{-\min E}$) and maximum-effort solution ($\bar{e}^{-\max E}$) for the static mapping (Eq. 4.2), using quadratic programming. The effort for any muscle activation pattern examined in this study was then normalized to percent of the global maximum, i.e., E of the maximum-effort solution.

We defined the metric for stability using Lyapunov stability of the linearized model. The full nonlinear system (Eq. 4.1) was linearized about a static equilibrium point, defined by a muscle activation pattern that satisfies the endpoint force generation (Eq. 4.2), using software *Neuromechanic* (Bunderson et al. 2012). Specifically, the system equation incorporated joint torques generated by muscles:

$$f = \ddot{q} = \mathbf{M}^{-1}(\bar{V} + \mathbf{R}\bar{F}_M - \mathbf{J}^T \bar{F}_{End}) \quad (4.4).$$

The system was linearized by numerically computing the partial derivatives with respect to kinematic states using first-order Taylor-series expansion to obtain the state space representation:

$$\begin{bmatrix} \Delta \dot{q} \\ \Delta \ddot{q} \end{bmatrix} = \mathbf{A} \begin{bmatrix} \bar{q} \\ \bar{\dot{q}} \end{bmatrix}, \quad \text{where,} \quad \mathbf{A} = \begin{bmatrix} \mathbf{0} & \mathbf{I} \\ \frac{\partial f}{\partial \bar{q}} & \frac{\partial f}{\partial \bar{\dot{q}}} \end{bmatrix} \quad (4.5).$$

The state matrix (\mathbf{A}) was used to calculate the eigenvalues (λ) of the linearized system. For a given muscle activation pattern, the metric for stability (S) was defined as the maximum real part of the 14 eigenvalues of \mathbf{A} such that

$$S = \max\{\text{Re}(\lambda)\} \quad (6).$$

We only considered 8 out of 14 eigenvalues that had the largest real parts in magnitude, which correspond to the 8 modes (or eigenvectors) that are relevant to the dynamics of the system in physiological timescale. Due to the constraint that eliminates endpoint translation in 3 directions, effective degrees of freedom of the model is reduced from 7 to 4. As a result, 6 of the 14 eigenvectors are modes that do not affect the dynamics of the system, corresponding to the 6 eigenvalues that are near zero (similar to rigid-body modes) which are very small in magnitude. These 6 eigenvalues typically were less than 10^{-5} in magnitude, and thus were not relevant in physiological time scales: the time at which the magnitude of a perturbed response is reduced to 50% is longer than 6.9×10^4 seconds. In contrast, the 8 eigenvalues that were considered in S for a given solution were typically larger than 10^{-3} in magnitude.

A solution of the system defined by a given muscle activation pattern was determined “stable” if $S < 0$, and “unstable” if $S > 0$. Further, because the magnitude of S predicts the rate at which a perturbed system will return to (if $S < 0$), or deviate from (if $S > 0$) the equilibrium, a solution is to be “less stable” for greater value of S , and “more stable” for smaller value of S . This metric from system theory, i.e., Lyapunov indirect or linearization method, has been shown to predict the behavior of perturbed nonlinear systems in simulations (Bingham and Ting 2013; Bunderson et al. 2008; Bunderson et al. 2010; Sohn 2011).

4.2.3 Mapping the null-path between minimum and maximum-effort solutions

In order to explicitly examine how stability changes along a given direction in the null space across all possible effort levels, we evaluated effort (E) and stability (S) of 49 intermediate solutions that were evenly spaced between the minimum- and maximum-effort solutions in muscle activation space. These solutions (e_{nth}^{-null}) were computed by linearly scaling the difference between the minimum-effort solution ($e^{-min E}$) and the maximum-effort solution ($e^{-max E}$):

$$e_{nth}^{-null} = e^{-min E} + n(e^{-max E} - e^{-min E})/50 \quad (4.7).$$

Note that difference between any two solutions that satisfy the torque requirement (Eq. 4.2) belongs to the 24-dimensional null space defined by the linear mapping matrix (\mathbf{RF}_{AFL}), i.e., the vector difference will produce zero torque (e.g. $\mathbf{RF}_{AFL}(e^{-max E} - e^{-min E}) = \bar{0}$). Therefore, solutions generated as above (Eq. 4.7) lie along the “null direction” defined by the vector difference ($e^{-max E} - e^{-min E}$). Here, we defined the unique path between any two solutions in the muscle activation space as a “null-path” (schematically illustrated in Fig. 4.2).

We mapped the null-path onto the functional property space by evaluating the effort (E) and stability (S) of each intermediate solution, revealing the projection from the linear muscle activation space to the functional property space. In particular, we were interested in whether the minimum-effort solution, representing the least amount of co-activation for a given task, is unstable, and whether the maximum-effort solution, with highest level of co-activation, is stable. Further, this null-path was used to demonstrate whether an unstable solution can be made stable by following a defined direction in muscle activation space, and to quantify the amount of effort necessary to make the

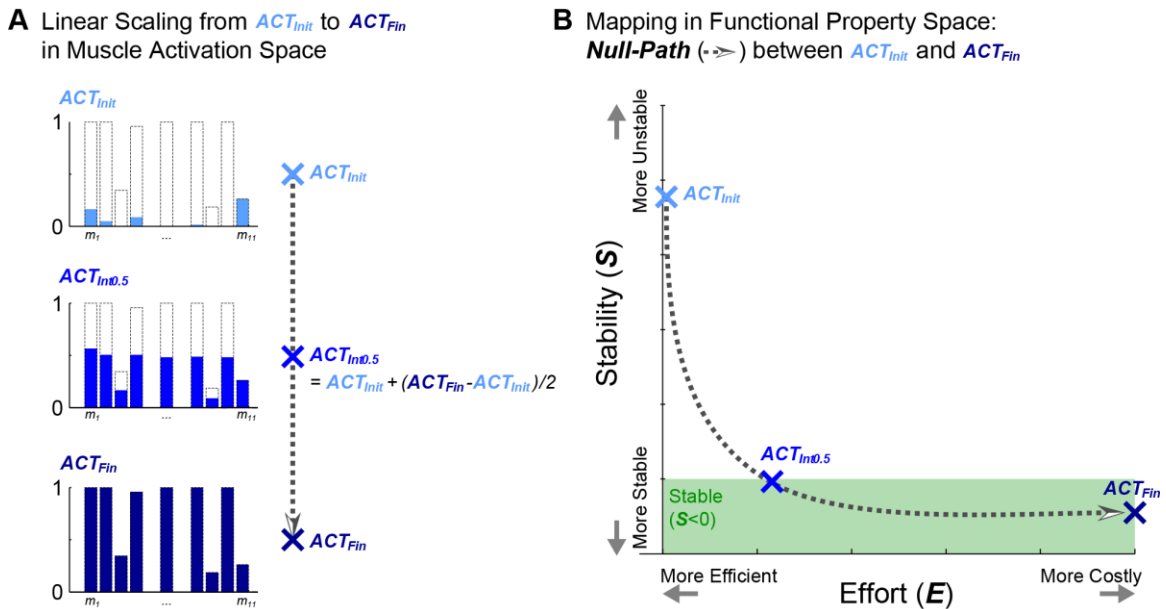


Figure 4.2: Schematic illustration of a null-path. (A) Linear scaling of a muscle activation pattern. The vector difference between two solutions belongs to null space defined by linear mapping in Eq. 4.2. Thus, intermediate solutions between any two solutions can be generated by linearly scaling from one solution, e.g. initial activation pattern (ACT_{Init} , light blue), to another solution, e.g. final activation pattern (ACT_{Fin} , dark blue). For example, the intermediate solution $ACT_{Int0.5}$ (blue) is half way from ACT_{Init} to ACT_{Fin} . (B) Mapping of the null-path (thick gray dotted line) on the functional property space. The functional property space is a 2-dimensional space on which functional properties of muscle activation patterns are evaluated in terms of effort (E , on x-axis) and stability (S , on y-axis). A unique path in functional property space can be found by mapping the linearly scaled solutions as described in (A). For example, the null-path between solutions that is very efficient but unstable (ACT_{Init} , 'x' in light blue) and a solution that is very stable but costly (ACT_{Fin} , 'x' in dark blue) can be defined by evaluating effort and stability of intermediate solutions, e.g. $ACT_{Int0.5}$ ('x' in blue).

minimum-effort solution stable. For these 51 solutions on the null-path (e_{nth}^{-null}) between the minimum and the maximum effort solutions, we further investigated how altering the muscle force-length relationship and other possible intrinsic muscle properties that contribute to stability affect the mapping in the functional property space (see 4.A Appendix: Altered mapping due to other factors contributing to stability).

4.2.4 Exploring the neighboring solutions

In order to reveal the local landscape of the solution space with respect to effort and stability, we explored the *neighboring solutions* around the null-path (e_n^{-null}) between the minimum- and maximum-effort solution, and mapped them onto the functional property space. The *seed* (e^{-seed}) for each exploration was defined as each of the 51 solutions on the null-path (minimum- and maximum-effort solutions, and 49 intermediate solutions). We defined *neighboring solutions* ($e^{-neighbor}$) as the solutions that were pseudo-randomly distributed around the *seed* in muscle activation space in which the amount of change, either positive or negative, in any muscle from the *seed* was constrained to be within a given *step size* specified for each muscle:

$$\left| e_m^{neighbor} - e_m^{seed} \right| \leq \text{step size} \quad (4.8).$$

The *step size* was defined for each muscle as a percentage of the muscle feasible range (MFR) of activation (Sohn et al. 2013) for the target endpoint force production, so that the amount of change in any muscle is normalized. To vary the extent to which area in the functional property space is explored by the neighboring solutions around a given seed solution, we used step sizes of 1, 2, 5, 10, 25, 50, and 100% MFR.

We generated 262 neighboring solutions ($e^{-neighbor}$) for each seed and step size using the following four steps (schematically illustrated in Fig. 4.3). In summary, our goal was to explore the functional property space in every possible direction around a

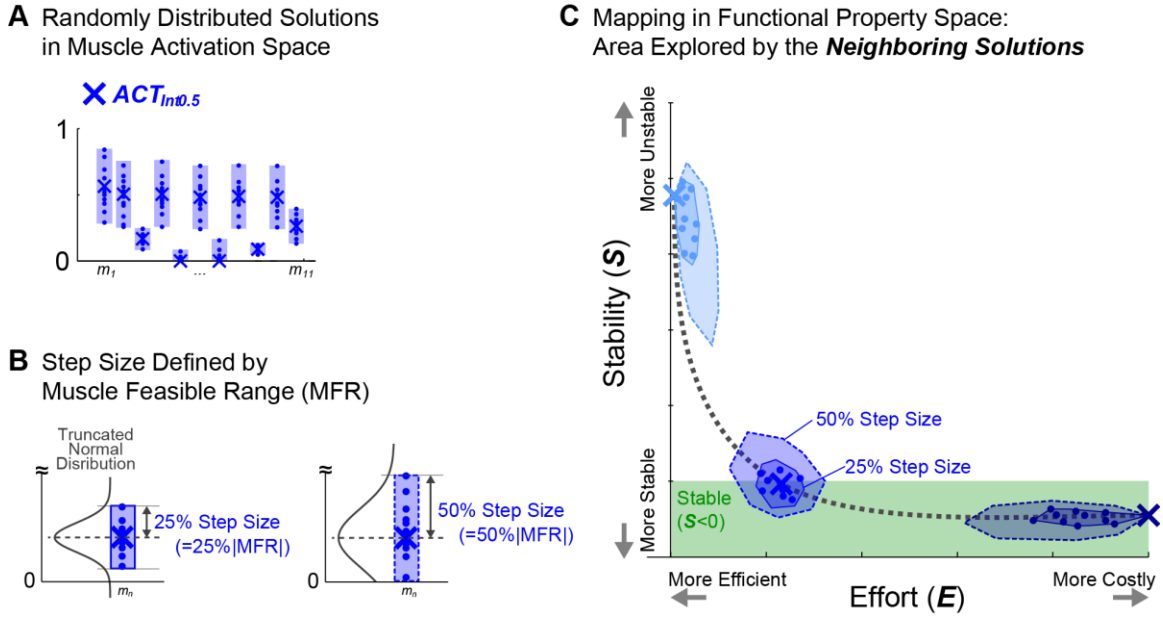


Figure 4.3: Schematic illustration of generating neighboring solutions. (A) Randomly distributed solutions around a seed muscle activation pattern. We generated solutions that were randomly distributed around a given seed on the null-path, e.g. $ACT_{Init0.5}$ ('x' in blue). Note that activation level in each muscle is distributed randomly, whereas the patterns themselves are all solutions that satisfy the joint torque requirement. (B) Step size defined using muscle feasible range (MFR). For each muscle, we defined the step size, i.e., the extent to which activation of a muscle in the neighboring solution can vary from the level of corresponding muscle in the seed solution. For a given seed, we used different step sizes at varying magnitudes which was defined with respect to MFR, e.g. 25% or 50% MFR. Depending on the step size, normal distribution was truncated at physiological bounds in muscle activation (e.g. step size 50% MFR). (C) Neighboring solutions mapped on the functional property space. Region in the functional property space explored by the neighboring solutions can be represented with convex polygon that encapsulates all of the neighboring solution for a given seen and step size. Dots inside the convex polygon show individual neighboring solutions mapped on the functional property space (e.g. shown for 25%MFR). Importantly, the distance and the shape of the area explored in the functional property space depends on the seed, e.g. ACT_{Init} (convex polygons in light blue) and ACT_{Fin} (convex polygons in dark blue), and the step size, e.g. 25% MFR (convex polygon with solid line) and 50% MFR (convex polygon with dotted line).

given seed, reaching the maximum extent in distance for a given amount of changes allowed in the muscle activation space. To this end, we generated sets of solutions that were randomly distributed around a given seed with varying distance in muscle activation space controlled by the step size:

- 1) In order to induce random deviations to muscle activations near each of the seed solutions, we first generated 200 perturbed patterns (\bar{e}^{pert}), in which each element in \bar{e}^{pert} , i.e., e_m^{pert} , was randomly drawn from a normal distribution with mean (μ) at activation level of the seed (e_m^{seed}) and variance (σ^2) equal to the muscle-specific step size:

$$e_m^{pert} \in N(\mu, \sigma^2) \quad (4.9),$$

where $\mu = e_m^{seed}$ and $\sigma^2 = step\ size$.

However, in order to examine perturbed patterns in which e_m^{pert} was always within physiological limits (0, 1), we limited the range from which the values were drawn using an algorithm for simulating a truncated normal distribution on a finite interval (Chopin 2011), implemented in MATLAB (Mazet 2012). The interval of each muscle was defined as the smaller value of physiological limits (0,1) or two times the step size away from the seed:

$$interval = [\max\{0, e_m^{seed} - 2 \times (step\ size)\}, \min\{1, e_m^{seed} + 2 \times (step\ size)\}] \quad (4.10).$$

- 2) We then identified the nearest solutions (\bar{e}^{proj}) to all \bar{e}^{pert} that produced the specified force. To find projections of \bar{e}^{pert} to the solution manifold in a least-squares sense, we performed optimizations to find muscle activation patterns (\bar{e}^{proj}) that minimized sum-squared difference to each of the perturbed patterns:

$$\text{minimize } c = (\bar{e}^{proj} - \bar{e}^{pert})^T \mathbf{Q} (\bar{e}^{proj} - \bar{e}^{pert}) \quad (4.11).$$

Note that we used a scaling matrix \mathbf{Q} , which is a diagonal matrix that penalizes the difference between perturbed and projected muscle activation. Elements of \mathbf{Q} were weighted inversely to the feasible range to prevent projection only occurring in muscles with small feasible ranges. Each

optimization was subject to an equality constraint for satisfying the torque requirement:

$$\mathbf{RF}_{AFL}(\bar{e}^{-proj} - \bar{e}^{-pert}) = \mathbf{J}^T \bar{F}_{End} - \mathbf{RF}_{AFL} \bar{e}^{-pert} \quad (4.12),$$

and inequality constraints specifying the search limits (\overline{lim}^{lower} and \overline{lim}^{upper}) defined either by the step size or the bounds from the feasible range identified for given task:

$$\overline{lim}^{lower} - \bar{e}^{-pert} \leq (\bar{e}^{-proj} - \bar{e}^{-pert}) \leq \overline{lim}^{upper} - \bar{e}^{-pert} \quad (4.13),$$

$$(\overline{lim}_m^{lower} = \max\{lb_m^{FR}, e_m^{seed} - step\ size\}; \overline{lim}_m^{upper} = \min\{ub_m^{FR}, e_m^{seed} + step\ size\}).$$

We then evaluated the induced changes in muscle activation patterns with respect to different muscles, step sizes and seed solutions, where we compared the spatial structure of the projected solutions (\bar{e}^{-proj}) to both the perturbed patterns (\bar{e}^{-pert}) and the initial seed solution (\bar{e}^{-seed}) (see 4.C Appendix: Analysis in muscle activation space).

- 3) To search the functional property space, we defined a new null-path between \bar{e}^{-seed} and each \bar{e}^{-pert} , and found extrapolated solutions (\bar{e}^{-ext}) along those paths until muscle activation met the search limits. Null-paths were computed in a same way described above (see 4.2.3 Mapping the null-path between minimum and maximum-effort solutions), where the change ($\bar{e}^{-proj} - \bar{e}^{-seed}$) was further extrapolated along the null direction until any of the muscles reached either the lower or upper bound (Eq. 4.13) for given step size. Extrapolated solutions (\bar{e}^{-ext}) generated this way are true solutions that satisfy the torque requirement, with at least one of the muscle activations lying on the search limits. These were defined as the *neighboring solutions* of the initial seed solution for a given step size. To visualize the path in the functional property space to get to the corresponding neighboring solution, we also computed four

intermediate solutions linearly interpolated along the null-path from the seed to each of the neighboring solutions.

- 4) Finally, in order to encourage the generated neighboring solutions to span the full possible range in muscle activation space for a given step size, we further generated solutions ($e^{-limits}$) that lie on the search limits (Eq. 4.13). Limit solutions were computed by specifying activation level of each muscle at its lower (lim_m^{lower}) and upper limit (lim_m^{upper}), and pushing the other 30 muscles as close as possible to their lower and upper limits. This optimization is similar to that for projected solution (Eq. 4.11-13), where the problem is reduced to solving for a 30-dimensional muscle activation vector that minimizes the distance to either lower or upper limit vector (Eq. 4.13), specified for a given step size. Although solutions generated this way were not guaranteed to satisfy the torque requirement, especially when small step sizes were allowed, more than 57 (60 ± 1.1 across seed and step size) limit solutions were generated for each seed and added to the set of neighboring solutions of the seed for a given step size.

4.2.5 Characterization of the local landscape

We examine the local landscape around each seed solution using the neighboring solutions mapped in the functional property space. For each seed and each step size, we identified a convex polygon that encompassed all points in the two dimensional functional property space mapped by a given set of neighboring solutions and the seed, using a ‘convhull’ algorithm in MATLAB. We further characterized the shape of the area explored by the neighboring solutions, we computed radial distance (r) and angle (θ ; rightward direction of effort axes is 0° and clockwise direction is positive) from the seed

to each of the neighboring solutions, and was compared across different step sizes for a given seed:

$$r = \sqrt{(E^{neighbor} - E^{seed})^2 + (S^{neighbor} - S^{seed})^2} \quad (4.14),$$

$$\text{and } \theta = \cos^{-1}\left(\frac{S^{neighbor} - S^{seed}}{E^{neighbor} - E^{seed}}\right) \quad (4.15).$$

Although Euclidian distance in the functional property space may be an arbitrary measure because the effort and stability metrics have different units, r determines the extent to which the neighboring solutions are explored the functional property space in a given direction (θ). More importantly, θ represents the distribution of qualitative changes in the solutions and determines whether the neighboring solutions for a given seed explored the full possible range of changes in the functional property space. For example, $-90^\circ < \theta < 0^\circ$ means that solution became “more stable and more costly”, whereas $-180^\circ < \theta < -90^\circ$ means that solution became “more stable and less costly”. In particular, we examined whether the change to the neighboring solutions spanned the full range of possible directions ($-180^\circ < \theta < 180^\circ$), and the relative distributions of solutions that became more stable versus more unstable.

To examine how step size determines the degree to which solutions with different functional properties can be explored, we compared effort and stability values of the neighboring solutions found for a given seed, across different step sizes. Differences in the effort (E) and stability (S) values of neighboring solutions found with different step sizes were compared using one-way ANOVA evaluated with a significance level of $\alpha=0.05$ adjusted with a Bonferroni correction for multiple comparison.

4.2.6 Characterization of the global landscape

To determine whether differences in effort (E) or stability (S) explored by the neighboring solutions depend on the location of the seed solution is in functional property

space, we conducted two-way ANOVA (*step size* \times *seed*) on the differences in each effort (E) or stability (S) of the neighboring solutions evaluated with a significance level of $\alpha=0.05$ adjusted with a Bonferroni correction for multiple comparisons.

We also computed the sensitivity of stability to changes in muscle pattern across the seeds. For each set of neighboring solutions, sensitivity was defined as change in stability (ΔS) over sum-squared amount of changes in the muscle activation pattern ($\Delta \bar{e}$):

$$Sensitivity = \left(\frac{\Delta S}{\|\Delta \bar{e}\|} \right)_{seed} \quad (4.16).$$

Sensitivity was computed using neighboring solutions generated with 1% FR step size. Sensitivity was averaged across neighboring solutions for each seed solution and were examined across the effort level. However, in order to examine how sensitivity changes as amount of allowed variation is increased, we computed sensitivity for 2, 5, and 10% step sizes. Step sizes bigger than 10% were disregarded because changes in both muscle activation and stability were substantial and no longer represented differential changes.

We found a global maximum-stability and defined the edge that connected the minimum-effort solution, global maximum-stability solution as the Pareto front and compared the values and shape to the null-path between the minimum- and maximum-effort solutions. To examine an explicit trade-off for minimizing effort while maximizing stability, we identified Pareto front that quantifies the maximum level of stability that can be achieved for a given amount of effort, or vice versa, the minimum amount of effort required to achieve certain level of stability. Along the perimeter of the area in the functional property space that is explored by all of the solutions examined, the most important edge regarding the trade-off between effort and stability is the outer-most edge connecting the minimum-effort solution, the global maximum-stability solution. To define this edge, we first performed a heuristic search that identified the global

maximum-stability solution (most stable with smallest S). Across all solutions we found the solution with smallest values of S ($e^{-\max S}$) to explore neighboring solutions (see 4.2.4 *Exploring the neighboring solutions*). If solutions that were more stable was found, it was assigned as the new global maximum-stability solution and the search was repeated with the new seed. Even when no solution more stable than $e^{-\max S}$ was found in a given iteration, we continued the search using the same until there were no change in maximum stability for 20 consecutive iterations.

To determine the extent to which solutions for a given task can be unstable, we also performed a heuristic search that identified the global minimum-stability solution (most unstable solution with largest S). The search was similar to that for finding the global maximum-stability solution, where here any solution that was more unstable compared to the current minimum-stability solution was assigned as the new seed in each iteration.

4.2.7 Investigating redundancy within equivalent functional properties

In order to examine the extent to which solutions can vary and still have similar functional properties, we compared multiple solutions that are within a small range of effort (E) and stability (S). Specifically, we were interested in whether near-maximal stability could be achieved using vastly different muscle patterns. Thus, among all neighboring solutions investigated, we examined solutions that were nearest to the local maximum stability solution on the null-path between the minimum- and maximum-effort solutions. We chose the local maximum stability solution instead of global maximum stability solution because it possibility to find solutions that are around in all possible directions in the functional property space. In order to avoid selecting solutions that are inherently similar in muscle activation pattern, we first sorted five solutions that were nearest in distance (Eq. 4.14) to the local maximum stability solution from each set of

neighboring solutions around a given seed, across step sizes. Among these 255 solutions (5 from each of 51 seeds), we selected solutions that had both effort and stability within 10% difference from the local maximum stability solution. This resulted in total 105 solutions near the local maximum stability solution. To characterize the difference, we computed the range of cosine angle differences of the selected solutions to the local maximum stability solution on the null-path between the minimum- and maximum-effort solutions. We also examined range of activation levels in the 31 muscles with respect to feasible range for each muscle. Further, to determine whether similar level of stability was achieved by different types of stiffening across the joints, we computed the level of co-activation in each joint for the 108 selected solutions using a co-activation index (*c.i.*) for a given degrees of freedom (DoF):

$$c.i._{DoF} = \frac{|\tau_{exc}|}{|\tau_{net}|} \left(= \frac{|\tau_{ago} - \tau_{ant}|}{|\tau_{ago} + \tau_{ant}|} \right) \quad (4.17),$$

where τ_{ago} is sum of torques produced by all muscles that are agonistic in terms of requirement for the task, and τ_{net} is the net torque requirement. This index gives a measure of excessive torque (τ_{exc}) at a joint relative to the net required torque, that is, the resulting torque balanced out by the antagonistic muscles (τ_{ant}). We then constructed a single 7-dimensional vector $\overline{C.I.}$ with co-activation indices for all of the 7 DoFs.

4.3 Results

4.3.1 Null-path between minimum and maximum-effort solutions

The null-path from the minimum-effort solution to the maximum-effort solution revealed a reciprocal relationship between effort and stability (Fig. 4.4, dotted line), and demonstrated that stable solution can be found with small increase in effort. The

minimum-effort solution was unstable ($S=18.9$) with effort (E) being 0.77% of the maximum (Fig. 4.4, 'x' in light blue), whereas the maximum-effort solution (Fig. 4.4, 'x' in black) was stable ($S=-2.25$ and $E=100\%$). Solutions on the null-path when mapped on the functional property space demonstrated a reciprocal change in stability (S) as a function of effort (E). Overall, S was decreased (i.e., stability was improved) drastically as effort increased near minimum effort region and flattened out as it approached the maximum-effort solution. Among the solutions on the null-path, the lowest S ($S=-2.34$, i.e., local maximum stability) was found at moderately low effort level $E=14.9\%$ (Fig. 4.4, 'x' in dark blue). The first solution on the null-path that became stable ($S<0$) was found at $S= -0.0066$ and $E=2.77\%$ (Fig. 4.4, 'x' in blue), which had only 2% increase in effort from the minimum-effort solution.

4.3.2 Local landscape explored by the neighboring solutions

We found that the extent to which solutions with different functional properties can be found depended on the step size, representing the amount of change in the activation of each muscle, and the seed, the initial solution from which a change is made. The local landscape explored around the seed solutions with the neighboring solutions was represented by characteristics of the convex polygon that encompasses all of the neighboring solutions explored for a given step size (Fig.4.4, sub-figures). In general, the size of the convex polygons, which represents the distance reached in the functional property space, increased as step size increased. For example, the area explored with a 10% step size (Fig.4.4, convex polygon with dotted line) was larger and encapsulated the area explored with a 5% step size (Fig.4.4, convex polygon with dotted line). The far right and left edge of the convex polygons were comprised mostly of the limit solutions, where limit solutions pushed to the lower and upper search limits were distributed towards low and high effort regions, respectively, within a given convex polygon. On the

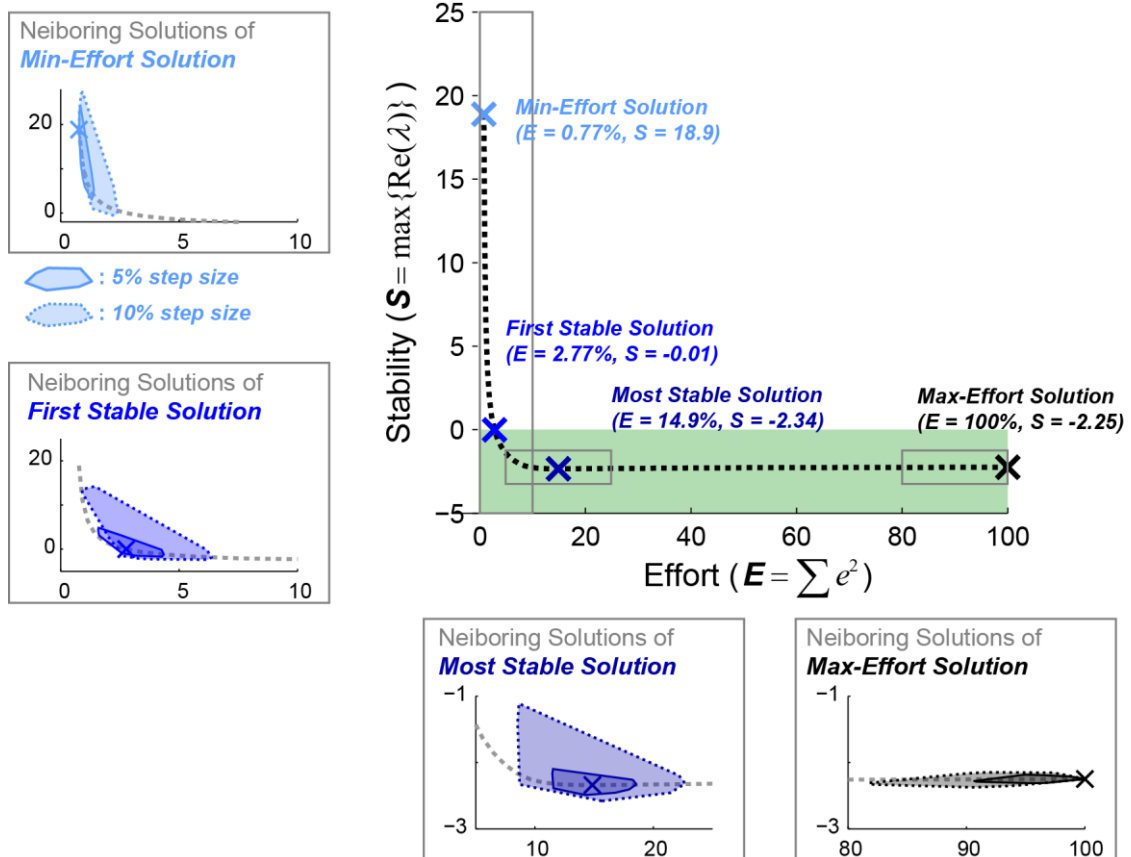


Figure 4.4: Null-path and neighboring solutions. Null-path between the minimum- and the maximum-effort solution revealed a reciprocal relationship between effort and stability (thick dotted line in main figure, top right corner). The minimum-effort solution ('x' in light blue) was unstable and the maximum-effort solution ('x' in black) was stable. A stable solution, i.e., $S < 0$ (shaded region in green) could be found with small increase in effort from the minimum-effort solution (first stable solution, 'x' in blue). The most stable solution ('x' in dark blue) had moderately low effort level. Examples of neighboring solutions (sub-figures in gray boxes) show explored regions in functional property space around four seed solutions on the null-path with 5% (convex polygon with solid line) and 10% step size (convex polygon with dotted line). Note that different scales are used for better visualization of the convex polygons encapsulating the neighboring solutions; axis limits in each figure correspond to the window, on the global functional property space (top right corner), boxed around a given solution with gray lines. The shape of the convex polygon depended on the seed and step size. In general, the size of the convex polygons, which represents the distance reached in the functional property space, increased as step size increased. For example, area explored with 10% step sizes (convex polygon with dotted line) was larger and encapsulated the area explored with 5% step size (convex polygon with dotted line). Across the seeds at varying effort level, the shape of the convex polygon was slender near low effort region (e.g. around min-effort solution, in light blue), relatively round in intermediate effort levels (e.g. around first stable solution, in blue), and became flat in high-effort region (e.g. around max-effort solution, in black). The shape, however, was more distinct across different seeds with smaller steps size.

other hand, the shape of the convex polygons illustrated how the explored neighboring solutions were distributed around the seed and became more spread across the functional property space as step size increased, always converging to a shape similar to that of the null-path.

More specifically, the shape of the convex polygons, especially with smaller step sizes, showed distinct characteristics across seed solutions at different effort levels (Fig. 4.4, sub-figures in gray boxes). In general, the shape was more slender near low effort regions (e.g. around minimum-effort solution, Fig. 4.4, convex polygon in light blue) in which the neighboring solutions mainly varied in stability. The shape gradually changed to be more flat towards higher effort levels (e.g. around maximum-effort solution, Fig. 4.4, convex polygon in black) where the change in functional property occurred mostly in effort. Here, we describe the details of the local landscape from four representative seed solutions at varying effort levels characterized with radial distance (r) and angle (θ): the minimum-effort solution, the first stable solution, locally most stable solution (inflection point of the null-path), and the maximum-effort solution. Around the minimum-effort solution (Fig. 4.5A), convex polygons were in general slender, indicating that neighboring solutions were mostly more stable than the seed with small change in effort. The shape was more slender for smaller step size (e.g. 5% step size, features with solid line in Fig. 4.5A), where θ was mostly concentrated around -90° (more stable with no change in effort). As step size increased, θ became more evenly distributed between -90° to 0° (becoming more stable with increase in effort) where r increased in all of these directions (e.g. 10% step size, features with dotted line in Fig. 4.5A). Across step size, there were only a few neighboring solutions near 90° (more unstable with no change in effort). Around the first stable solution (Fig. 4.5B), the shape of the convex polygons were oriented diagonally with negative slope, following the curvature of the null-path at this point. The neighboring solutions were distributed in all possible directions around the seed in the functional property space; this was true for all seed solutions on the null-path

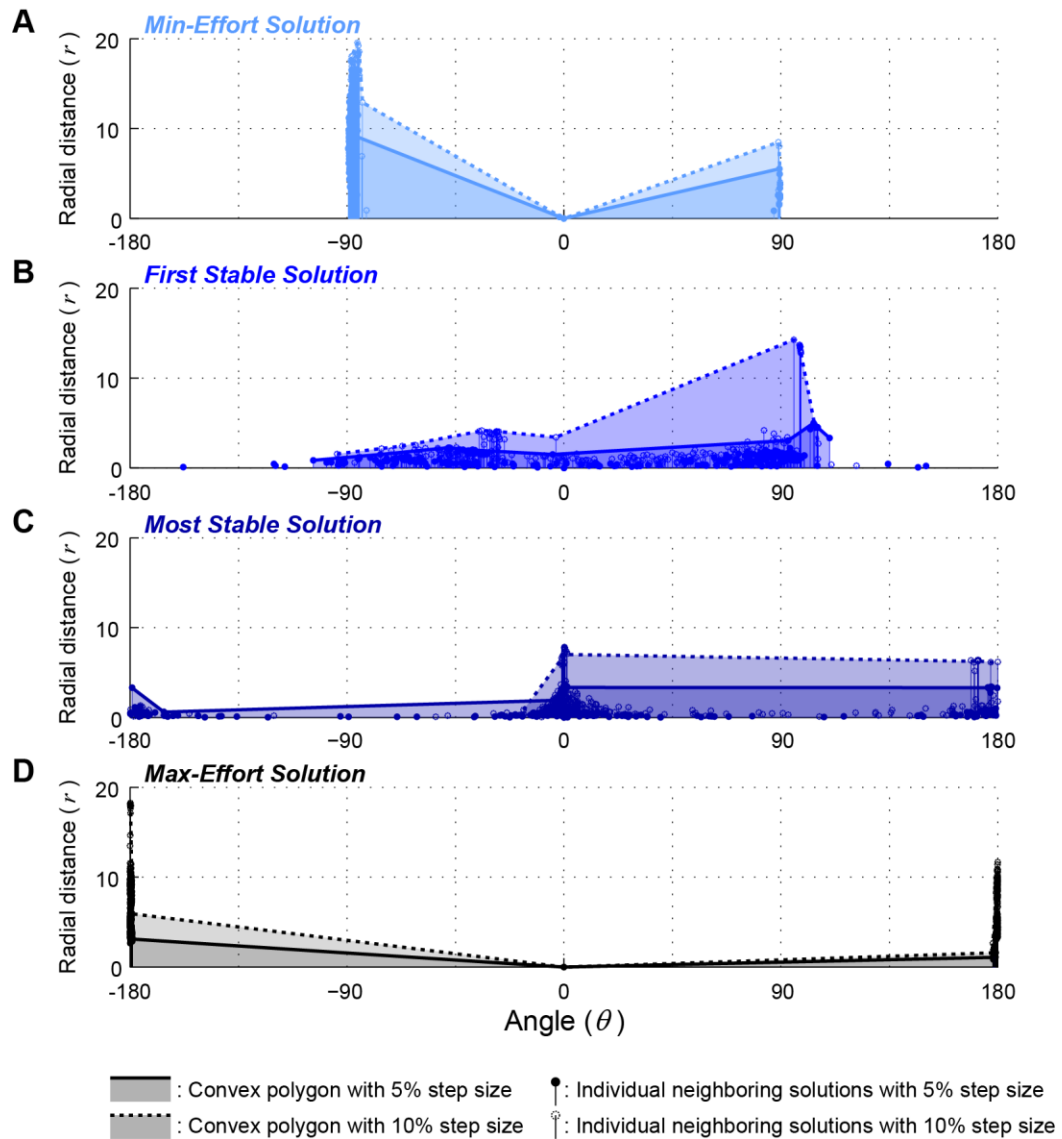


Figure 4.5: Local landscape characteristics. Convex polygons (shaded region) encapsulating the neighboring solutions (circles on top of line segments) of selected seed solutions. Around the minimum-effort solution (A), convex polygons were slender, where the neighboring solutions were distributed mostly near -90° (more stable region with almost no change in effort). The shape was more slender for smaller step size (e.g. 5% step size, solid line), where distance (r) was greater as step size increased (e.g. 10% step size, dotted lines). Few neighboring solutions existed near 90° (more unstable with no change in effort). Around the first stable solution (B), convex polygons were diagonally oriented. The neighboring solutions were distributed in all possible directions around the seed in the functional property space, but concentrated near -45° (becoming less stable with decrease in effort) and 135° (becoming more stable with increase in effort). Around the most stable solution (C), convex polygons were round, spanning all possible directions in the functional property space (from -180° to 180°). Around the maximum-effort solution (D), convex polygons were mostly flat, where the neighboring solutions were highly concentrated near -180° and near 180° (decrease in effort but with small changes in stability).

except the minimum- and maximum-effort solutions. The majority of the neighboring solutions, however, were concentrated around -45° (becoming less stable with decrease in effort) and 135° (becoming more stable with increase in effort). Around the most stable solution (Fig. 4.5C), the shape of the convex polygons were generally round spanning all possible directions in the functional property space (from -180° to 180°), where distance r was more consistent across direction θ for smaller step sizes (e.g. 5% step size). Consistently across step sizes, r could be greater in directions from -90° to -180° , indicating that neighboring solutions could reach out further to more unstable regions. Around the maximum-effort solution (Fig. 4.5D), the shape of the convex polygons was mostly flat, where neighboring solutions decreased in effort but with small changes in stability. Because no solutions can have greater effort than the seed, θ could only span from 90° to 180° , and -180° to -90° . However, θ was highly concentrated near -180° and 180° consistently across step sizes, where r increased with increasing step size (e.g. compare 5% and 10% step size).

Step size determined whether different values of effort and stability were found by the neighboring solutions in functional property space for a given seed in most cases. Overall, for 48 of 51 seed solutions, both effort and stability of the neighboring solutions were different across different step size ($p < 0.05$). For one seed solution with $E = 2.76\%$ and $S = -0.0066$, stability was not different ($p = 0.025$), and for two seed solution with $E = 37.8\%$ and $S = -2.30$, and $E = 40.2\%$ and $S = -2.29$, effort was not different ($p = 0.023$ and $p = 0.200$, respectively) across step size.

However, multiple comparisons across step sizes ($\alpha = 0.05$, with a Bonferroni correction) of the differences in effort and stability level of the neighboring solutions from the seed had different characteristics depending on the locations of the seed solution in the functional property space (Fig. 4.6). In terms of effort, solutions with more distinct levels of effort were discovered across different step sizes for seeds near low and high effort regions (Fig. 4.6A). For example, effort levels of the neighboring solutions around

the minimum-effort solution with 1, 2, 5, and 10% step size were significantly different ($p < 0.05$) from those with 25, 50, and 100% step size, whereas those with 25, 50, and 100% step size were different from all other step sizes; this was same for the first and the most stable solutions (Fig. 4.6A). On the other hand, for an intermediate seed with $E = 37.8\%$ and $S = -2.30$, effort levels of the neighboring solutions were not significantly different from each other for any step size. In terms of stability, solutions with more distinct levels of stability were discovered across different step sizes for seeds at lower effort regions and less distinct towards high effort regions (Fig.4.6B). For example, stability levels of the neighboring solutions around the minimum-effort solution found were significantly different across step sizes ($p < 0.05$) except for 25% and 50% and

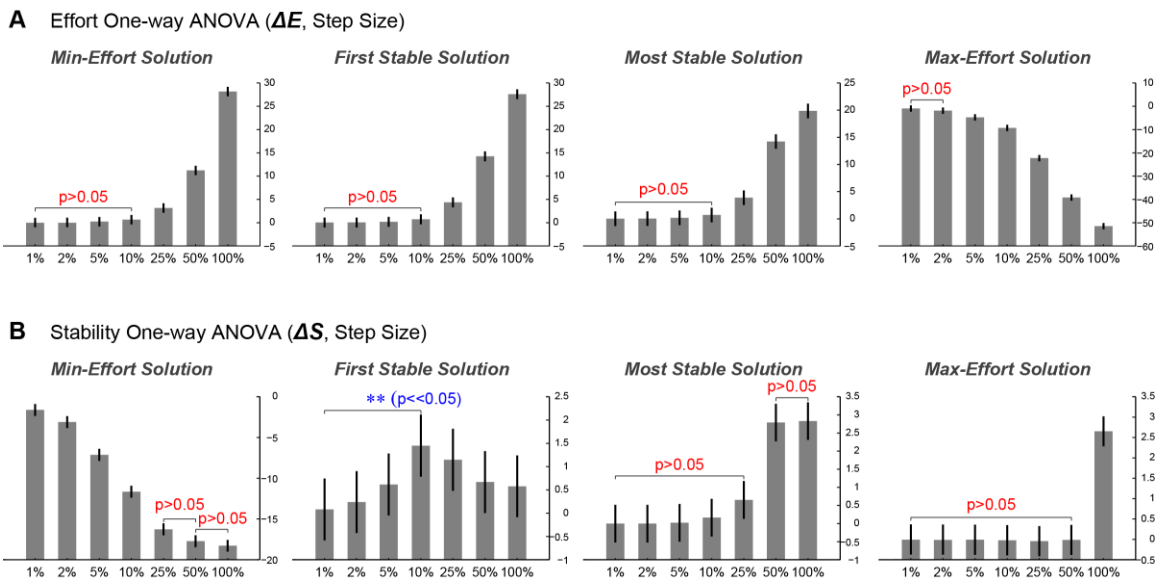


Figure 4.6: One-way ANOVA multiple comparison across step size. Difference in effort (A) and stability (B) level of the neighboring solutions to the seed compared across step sizes. Only statistically significant ($p < 0.05$) comparisons are shown in blue (i.e., otherwise not significant) or statistically insignificant ($p > 0.05$) comparisons are shown in red (i.e., otherwise significant). For seed solutions at relatively low-effort region (around $< 10\%$), effort levels of the neighboring solutions found with small step sizes (e.g. 1, 2, 5, and 10%) were not different from each other (e.g. min-effort, first stable, and most stable solutions). Neighboring solutions with more distinct stability level were found for seed solutions in low-effort region (e.g. min-effort solution). For seed solutions at relatively high-effort region (around $> 30\%$), stability levels of neighboring solutions were not different from each other across step sizes, except for the 100% step size (e.g. max-effort solution).

between 50% and 100% step size (Fig. 4.6B, min-effort solution). However, beyond the seed solution with $E = 37.8\%$ and $S = -2.30$, stability levels found with only 100% step size were different from all other step sizes ($p < 0.05$), which was also true for the maximum-effort solution (Fig. 4.6B, max-effort solutions).

4.3.3 Global landscape across effort level

Two-way ANOVA (*step size x seed*) showed that seed solutions at different levels of effort determined whether solutions with different effort and stability were explored by the neighboring solutions ($p < 0.05$ with Bonferroni correction).

Sensitivity of stability to change in muscle activity for the solutions on the null-path varied globally across effort level in the functional property space (Fig. 4.7). In general, sensitivity of stability to change in muscle activity was greater in the low-effort

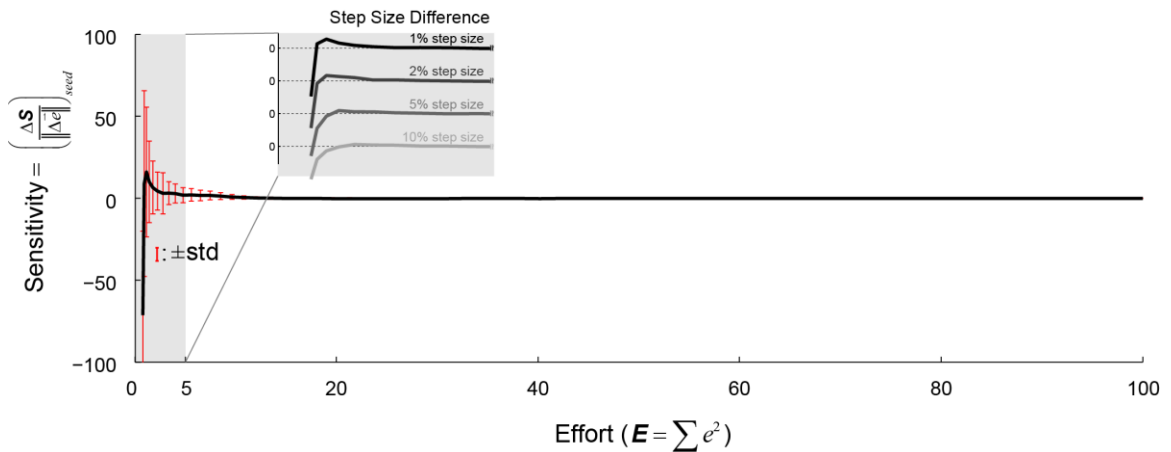


Figure 4.7: Sensitivity. Sensitivity of stability to change in muscle activation. Sensitivity of stability to change in muscle activation was greater in low-effort region. For example, sensitivity on average (black solid line) was highly negative, however with large variability (standard deviation in red error bars). This indicates that very small changes in muscle activation may cause large decrease in stability, i.e., increased stability. In contrast, stability was nearly insensitive (zero) to changes in muscle activation in high-effort region, e.g. beyond effort region greater than 10%. This means that for stable solutions with high effort, it is difficult to induce any change in level of stability by varying muscle activations. Sensitivity calculated using step sizes greater than 1% had diminishing effect only near small effort region (gray box). Sensitivity calculated using 2%, 5%, and 10% step size are shown on top, up to 5% effort level.

region, indicating that small changes in muscle activation may cause large difference in resulting stability. In contrast, stability was nearly insensitive to changes in muscle activation in the high-effort region, suggesting that for stable solutions with high effort, it is difficult to induce any change in stability by varying muscle activation. More specifically, for seed solutions that were in very low-effort region (<1%), sensitivity had very large negative values on average (Fig. 4.7, black solid line), but with large variability (Fig. 4.7, standard deviation in red error bars). Sensitivity values on average became positive once effort exceeded 1% and gradually approached zero with drastic decrease in variability near 5% effort (Fig. 4.7, gray-boxed region). Beyond 10% effort, sensitivity was essentially zero, with almost no variability. However, high sensitivity near low effort region became diminished, i.e., negative value in smaller magnitude, and converged to zero value with less overshoot when sensitivity was calculated using greater step sizes (Fig. 4.7, sensitivity calculated using 2%, 5%, and 10% step size in gray lines).

The Pareto front, defined by all of the solutions examined in this study, illustrated an explicit trade-off in optimality for minimizing effort while maximizing stability (Fig. 4.8). The heuristic search for a global maximum-stability solution was terminated after 144 iterations, and reached at $S=-3.56$ and $E=20.2\%$ (Fig. 4.8, 'x' in green). The Pareto front generated between the minimum-effort solution (Fig. 4.8, 'x' in light blue) and the maximum-stability solutions reflected a reciprocal relationship (Fig. 4.8, bold black line) similar to the null-path between the minimum- and maximum-effort solutions (Fig. 4.8, white dotted line), where it closely followed the null-path near very low effort region. However, the Pareto front was more stable, i.e., lower S , at lower effort levels.

Increased co-activation was not always stabilizing; therefore effort may not provide sufficient stability information. The most unstable solution found heuristically had $S = 50.3$ and $E = 31.0\%$. Search parameters (e.g. initial seed, stop criteria) were manually adjusted due to the bumpy landscape in functional property space with many local extrema. Nevertheless, multitudes of such unstable solutions with effort higher than

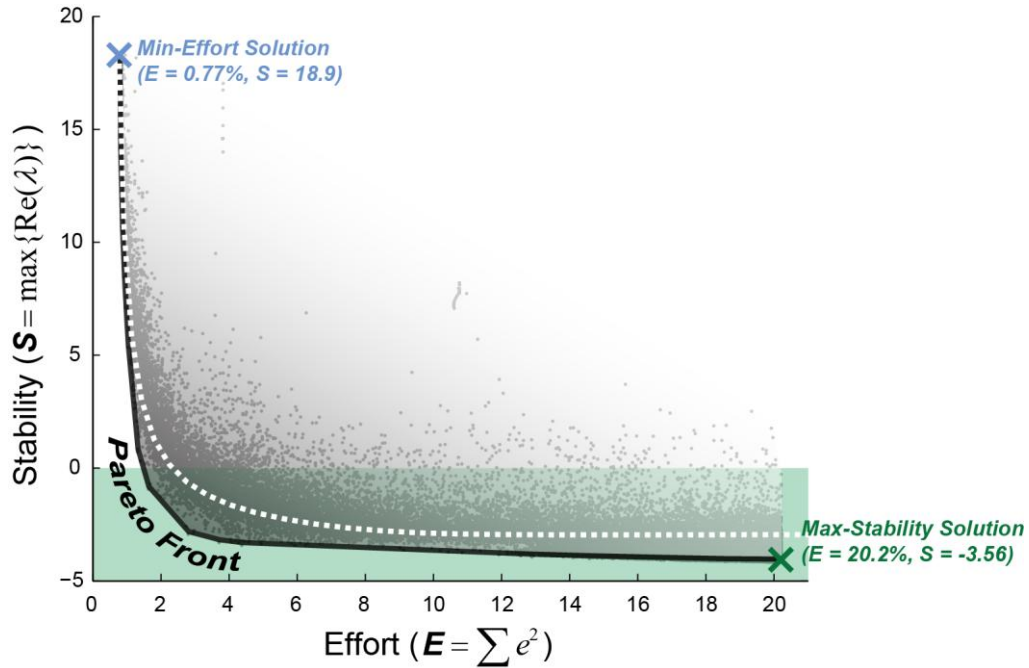


Figure 4.8: Pareto front. Pareto front illustrating explicit trade-off between effort and stability. Global maximum-stability solution ('x' in green) was found with heuristic search. The Pareto front (bold black line) generated between the minimum-effort solution ('x' in light blue) and the global maximum-stability solution reflected the reciprocal relationship between minimizing effort and maximizing stability. The Pareto front reached more efficient and more stable regions compared to the null-path between the minimum- and maximum-effort solutions (white dotted line). Among all solutions examined, solutions near the Pareto front (e.g. more stable than the min-effort solution and more efficient than the max-stability solution) are shown with gray dots.

the minimum-effort solution demonstrated that increased effort can be sometimes destabilizing and does not always reflect the trade-off between effort and stability.

4.3.4 Redundancy in solutions with equivalent functional properties

Multiple solutions can have similar functional properties, e.g. low effort and near-maximal stability. Substantial redundancy was observed in spatial structures of muscle activation patterns that are close in functional property space, e.g. low effort and near-maximal stability. For 105 solutions that were nearest to the local maximum-stability solution on the null-path between the minimum- and maximum-effort solutions had E of $14.9 \pm 0.314\%$ and S of -2.33 ± 0.108 . However, how such functional properties were

achieved in terms of muscle pattern could be vastly different. Angle difference in muscle activation patterns of these 105 solutions to the local maximum-stability solution was $15 \pm 10^\circ$ and ranged from 0.63° to 35° . The range in activation level in each of the 31 muscles was $38 \pm 14\%$ of the feasible range. Interestingly, the way in which these solutions achieved stability through co-activation at the joints was similar. The majority of co-activation occurred at the ankle: co-activation index for ankle extension was 121 ± 16 , compared to 14 ± 1.9 and 3.4 ± 0.57 and for hip flexion and knee extension, respectively. Nevertheless, solutions that were similar in functional property could be achieved by different type of co-activation across joints. For example, one solution (e.g. ACT1) that was 26.5° from the local maximum-stability solution achieved S of -2.25 with co-activation index 18.1, 4.73 and 94.4 at hip, knee and ankle extension, whereas another solution (e.g. ACT2) with 28.6° cosine angle achieved S of -2.54 with co-activation index of 12.1, 3.68 and 167.4 at hip, knee and ankle extension. The muscle activation patterns differed across these two solutions. For example, activation of *vastus medialis* (knee extensor) was absent and activation level of *gluteus minimus* (hip flexor) and *sartorius* (hip and knee flexor) was very low in ACT2 compared to ACT1. On the other hand, activation level of *tibialis anterior* (ankle flexor) was high in ACT2, but very low in ACT1.

4.4 Discussion

Here, we used a novel computational framework to explicitly map out trade-offs between effort and intrinsic stability in a redundant muscle activation space for an isometric force production task. In contrast to current modeling approaches that only examine an optimal solution with respect to single criterion (Anderson and Pandy 2001b; Crowninshield and Brand 1981; Thelen and Anderson 2006; Todorov 2004; Todorov and Jordan 2002), our framework seeks to explore a multitude of solutions and evaluates

them in terms of multiple functional criteria. To this end, we characterized the landscape of the solution space in terms of how variations in muscle activation patterns are mapped onto a two-dimensional functional property space of effort and stability. Thorough and extensive exploration of this space revealed a general reciprocal relationship between effort and stability. More importantly, the nature of functional changes that can be made by altering muscle activation patterns depended on the location of the current solution in functional property space and the size of the deviations in muscle activity. In particular, the sensitivity of stability to changes in muscle activation differed between solutions with low and high effort. Sensitivity provided a measure of how difficult or easy it is to find a new solution with altered functional properties. Our framework reveals the way in which changes to a given muscle activation pattern result in functional changes in performing the same task. Thus, it can be used to examine possible variations in muscle activation patterns for a given motor task and predict their functional implications in various contexts. Ultimately, it may explain individual differences in finding a new motor solution with different functional properties, e.g. more stable or efficient, which has important implications for motor learning in general and rehabilitation for individuals with pathological motor patterns.

The high sensitivity of stability to changes in muscle activity in the low-effort region demonstrates that stable *sub-optimal* solutions can be “easily” found near the globally optimal minimum-effort solution, which may be unstable. Optimal minimum-effort muscle activation patterns result in the least amount of co-activation across muscles (Collins 1995; Herzog and Leonard 1991) which may provide only provide low levels of joint stiffness (Gomi and Osu 1998; Hu et al. 2012; Liao et al. 2013; Milner and Leger 1995). Therefore, a musculoskeletal system using effort-wise optimal solutions are likely to be dynamically unstable in response to perturbations, as shown here and elsewhere (Bunderson et al. 2010; John et al. 2013). However, we found that small variations in the global minimum-effort solution can result in large increase in stability. This suggests that

it is relatively “easy” to find an intrinsically stable solution with near-minimum effort even with relatively conservative exploration. Thus individuals who perform a task in an energetically optimal way such as highly trained athletes may have adapted to such near-optimal motor solutions from stable solutions. Subtle difference in cost in terms of effort or metabolic energy, however, may not be distinguishable in experimentally measured muscle activity or from metabolic cost, and thus may have been regarded as optimal (Alexander 1989).

On the other hand in high-effort regions, the low sensitivity of stability and to changes in muscle activation suggests that that making functional changes can be “difficult” when searching from a high-effort solutions. High cost in terms of effort results co-contracting antagonistic muscles that stiffen the joint. This may be the most intuitive feed-forward mechanism of stabilization in tasks, such as maintaining limb (McIntyre et al. 1996; Mussa-Ivaldi et al. 1985; Perreault et al. 2008; Selen et al. 2009) or upright trunk posture (Gardner-Morse and Stokes 1998; McGill et al. 2003), or reaching (Franklin et al. 2008; Osu et al. 2002). Accordingly, voluntary or involuntary use of more stable solutions is commonly observed in the presence of environmental instability (Franklin et al. 2004). Increased stability at the cost of increased effort is also commonly observed in individuals with low back pain (Hansen and Anders 2014; Jones et al. 2012). However, prolonged use of costly solutions requiring high effort can be problematic because it may induce muscle fatigue or joint loading, which be detrimental to dynamic stability (Granata and Gottipati 2008; Granata and Marras 2000). Interestingly, our results revealed potential barriers to changing functional properties in high-effort solutions by varying muscle activation patterns. Deviations in muscle activation patterns in the high-effort region hardly affected stability and also were limited in reaching to lower-effort regions. The low sensitivity of high-effort solutions may explain difficulties commonly experienced in training individuals with neurological disorders (Fisher and Sullivan 2001; Fisher et al. 2008; Will et al. 2004), low back pain (Dubois et al. 2011;

Stokes and Gardner-Morse 2001) who often exhibit high-level of co-contraction that can be irrelevant to the task demands.

Substantial redundancy across solutions that have similar functional properties may account for intra- and inter-subject variability in muscle activation patterns that produce similar behavioral output. Our results demonstrate a bumpy landscape with many local minima where muscle patterns with similar effort and stability can vary significantly from each other even near various optima, e.g. minimum effort or maximum stability solutions. This may explain observed variability in muscle activation patterns used across individuals that achieve the same task with qualitatively similar performance (McGill et al. 2003). For example, in standing balance task in cats, different animals were able to maintain balance using the same extensor force vector, as used in this study. However, the experimentally-recorded muscle activity used to produce the same force vector varied across animals (Torres-Oviedo et al. 2006). A large set of functionally equivalent solutions is consistent with natural variability in many neuromotor solutions (Klein et al. 2010). Although such motor solutions are not necessarily strictly optimal, they may represent families of solutions that are “good enough” for a given task (Loeb 2012).

Our current approach of mapping the redundant solution space in terms of functional properties relevant to the task can be useful tool for describing the exploratory behavior during motor learning. When performing the same task repeatedly, individuals learn to use solutions with a better functional properties. For example, humans adapt to environmental instability by adjusting the mechanical impedance of limb endpoint along the direction of instability (Krutky et al. 2013; Selen et al. 2009). A redundant solution space provides a multitude of muscle activation patterns that have similar functional properties, and individuals may exploit such allowed variability to discover new patterns during motor learning (Pekny et al. 2015; Tsianos et al. 2014; Wu et al. 2014). Similar exploratory processes of motor learning have been shown in studies with other species

such as song birds (Sober et al. 2008; Tumer and Brainard 2007), rodents (Costa 2011) and primates (Mandelblat-Cerf et al. 2009 ; Takikawa et al. 2002). This further implies that variability in muscle activation patterns cannot be simply attributed to noise (see 4.B Appendix: Effect of signal-dependent noise) inherent in the sensorimotor system (Harris and Wolpert, 1998), but may reflect individual differences in selection amongst the abundance of functionally equivalent motor solutions (Latash 2012; Loeb 2012). By evaluating motor solutions with respect to functional properties relevant to the task, the landscape over which one searches heuristically to acquire a new motor solution can be described. For example, the bumpiness of the landscape may explain why habitual versus optimal patterns are preferred (de Rugy et al. 2012; Ganesh et al. 2010; Hasson et al. 2012; Kistemaker et al. 2010). Although we used two functional properties of effort and stability, other multi-objective criteria can be used (see later discussion), such as minimizing trajectory error, energetics (Krishnaswamy et al. 2011), and ability to generalize (Thoroughman and Shadmehr 2000; Tsianos et al. 2014) or switch (Zenzeri et al. 2014) across motor tasks.

The ability to make desired functional changes in muscle activation patterns for a given task could be further limited by other biomechanical or neural constraints. When searching for neighboring solutions in this study, we allowed random changes to muscle activation patterns assuming independent control of each muscle. Hence, the range space of the neighboring solutions spanned all theoretically-possible directions in the null space. The corresponding area in the functional property space also reached in all possible directions for most sub-optimal cases, meaning that any direction of changes in functions were possible by varying muscle activation. However, the control of muscle may not be so independent. First, biomechanical constraints in musculoskeletal system such as tendinous connections (Valero-Cuevas 2005; Valero-Cuevas et al. 2007), force transmission through connective tissues (Huijing 2003; Maas and Sandercock 2010), or mechanical coupling of joints (Debicki and Gribble 2004; Gribble and Ostry 1999; van

Antwerp et al. 2007; Yamasaki et al. 2008) may restrict independent variations in muscle activation patterns and thus changes in functional properties. Second, neural constraints in healthy individuals, or due to pathology may affect the possible changes that can be made to a given muscle activation pattern. For example, individuals (d'Avella et al. 2006; Ting and Macpherson 2005) have more difficulty in adapting to task demands that are incompatible with the coordination of muscles within muscle synergies (Berger et al. 2013). Neuromuscular impairments may further impose pathological constraints. Saturation in activation of muscles due to weakness (McCrea et al. 2005) or abnormal coupling across muscles are often present (Brunnström 1970; Dewald and Beer 2001; Dewald et al. 1995) in individuals with stroke. Such constraints can limit available muscle activation pattern for altering functional properties of the limb, and may account for compensatory behaviors that requires additional change in the biomechanical configuration (Beer et al. 2004; Beer et al. 2007; Reisman and Scholz 2006).

Although we examined a relatively simple task and feed-forward control of isometric endpoint force generation, consideration of more complex tasks or control mechanisms is not likely to alter our findings. Other intrinsic mechanisms such as short-range stiffness (Cui et al. 2008; Loram et al. 2009; Rack and Westbury 1969) or stretch reflexes (Burkholder and Nichols 2000; Nichols 1989 ; Wilmink and Nichols 2003) may further contribute to limb stability (see 4.A Appendix: Altered mapping due to other potential mechanisms contributing to intrinsic stability). However, we predict that how changes in functional properties occur by altering feed-forward commands for voluntary tasks will not be qualitatively different if these additional mechanisms are considered. For example, the ease or difficulty of inducing changes to functional property of a given solution will still depend on where the initial solution was located and how far one reaches out from it. In addition, redundancy remains in that there can be many different ways to obtain similar functional properties. In fact, consideration of more complex tasks or control mechanisms adds more flexibility in terms of available motor solutions to

produce a functionally “better” behavior. For example, dynamic tasks such as arm reaching or walking requires coordination of multiple joints over time, which adds kinematic redundancy to how a motor goal can be achieved. On the other hand, feedback mechanisms contributing to early reactions in resisting external perturbations provide stability in the absence of volitional intervention or integrated neural correction. For example, long-latency stretch reflexes have been suggested as an involuntary neural mechanism for impedance modulation, which can be highly adaptable in context-dependent manner (Krutky et al. 2010; Perreault et al. 2008). Such additional mechanisms may enable the nervous system to cope with more complicated tasks that may involve multiple goals (Shemmell et al. 2010).

Different metrics for effort and stability, or additional functional properties could also be considered using our method. For example, metabolic energy consumption based on mechanistic or phenomenological models of muscle contraction (Bhargava et al. 2004; Ma and Zahalak 1987) or respiratory process (Ellis et al. 2013; Huang et al. 2012) may more closely represent the energetic cost relevant for many motor tasks such as walking (Donelan et al. 2001 ; Donelan et al. 2002 ; Ralston et al. 1976).

More behavior-based metrics for stability may better explain functional motor tasks. Adopting a metric of stability from classical control theory in biological systems can be problematic because stability in behavioral contexts often contradicts with mathematical definitions of stability (Hasan 2005). For example, stride-to-stride variability (Hausdorff 2007) or extrapolated CoM position (Hof et al. 2005) have been used as stability measures during walking. Dynamic postural instability has also been examined using a center of mass time-to-contact measure (Hasson et al. 2008). Nevertheless, mathematical measures from systems control theory have been shown to predict local dynamic behavior. For example, a local divergence exponent or maximum Floquet multipliers for orbital trajectories during walking have been used to examine whole-body stability (Bruijn et al. 2013; Dingwell and Kang 2007; Kao et al. 2014;

McAndrew et al. 2011). The maximum Lyapunov exponent has also been extensively used for examining the stability of the lumbar spine (Dupeyron et al. 2013; Graham et al. 2014; Granata and Gottipati 2008). Stability radius, which is a single measure that represents the relative sensitivity of eigenvalues to system parameters based on pseudo-spectra analysis has been used to explain selection of different biomechanical configurations during standing balance (Bingham and Ting 2013). Because tasks considered in this study, i.e., production of endpoint force during quiet standing, can be considered quasi-static, the maximum real part of the eigenvalues of linearized system matrix closely predicts local dynamic behavior of the nonlinear system (Sohn 2011). More importantly, the novelty is in that our stability metric accounts for how active muscles contribute to whole limb dynamics, which is readily applicable to systems that incorporate muscle activation dynamics, elasticity in tendons, and feedback control (Bunderson et al. 2012). In contrast, previous approaches using torque-controlled systems cannot examine contributions of muscle activity to stability.

In conclusion, our approach serves as a first step in establishing methodology to explore the functional landscape of a redundant motor solution space. In addition to revealing principles by which a muscle activation pattern with desirable functional properties can be found, it has important implications in many aspects. First, our framework can be generalized to other musculoskeletal systems and tasks, used to design with experiments. For example, motor solutions for dynamic tasks such as arm reaching or orbital trajectories during walking (Holmes et al. 2006) can be evaluated with respect to relevant functional criteria. Further, an experiment can be designed to explicitly test whether humans exploit variability in varying task demands and varying environmental stability. Second, being able to find and use stable muscle activation patterns in muscle-driven musculoskeletal models may be beneficial in forward dynamic simulations. Whereas unstable muscle activation patterns drive the system to deviate from desired states rapidly under numerical perturbations (Higginson et al. 2006; Risher et al. 1997),

stable muscle activation patterns may allow system dynamics to tolerate such perturbation and facilitates optimization. Intrinsic stability of musculoskeletal dynamics conferred by muscle activation pattern can be also useful for testing neural feedback controllers that regulates a perturbed behavior on top of more physiological muscle tone. Finally, understanding the possible variations in motor solutions and their functional consequences has important implication for rehabilitation. By using computational tools to predict functional outcomes of possible alterations to given motor solutions, we may gain valuable insights to explaining individual differences in strategies, learning, or compensation in neuromuscular disorders. This is especially critical for developing novel and effective patient-specific treatments and rehabilitation strategies.

4.A Appendix: Altered mapping due to other potential mechanisms contributing to intrinsic stability

For the 51 solutions on the null-path (e_{nth}^{-null}) between the minimum and the maximum effort solutions, we investigated how altered condition force-length relationships and other possible intrinsic mechanisms that can contribute to stability affect the mapping in functional property space.

First, we computed a set of solutions that constituted a null-path but with a modified model where fiber lengths of all muscles were set at 95% optimal fiber length, i.e., the plateau region of the force-length relationship curve (Zajac 1989) and thus more prone to destabilization. Note that these solutions are not the same as the original solutions, because the scaling matrix for isometric force generation (\mathbf{F}_{AFL}) in Eq. 4.2 is different. However, each of the 51 solutions in the two models (65% and 95%) was very similar (cosine of the angle between the two muscle activation vectors was 0.998 ± 0.002 across 51 solution pairs). These solutions were mapped on the functional property space, where the effort was scaled to that of the maximum found in the 65% model.

Secondly, stability of the original 51 solutions on the null-path was evaluated in a model implemented with a short-range stiffness (SRS) in muscles (Cui et al. 2008; Hu et al. 2011) to represent the instantaneous force-length behavior upon muscle stretch. However, the SRS model was slightly modified because we assumed tendons to be inelastic in the static mapping in Eq. 4.2. Hence, our SRS model represented the instantaneous stiffness solely from the muscle, assuming infinite stiffness in the tendons in series with the muscle. As a result, we used a force-relationship curve with constant slope (value was adopted from that estimated in Cui et al., 2008) that was significantly greater than that of the generic force-length relationship curve. In addition, we included the force-velocity relationship that provided damping as in the generic model because its contribution may be large in the numerical process for linearization.

Third, we used another model with autogenic length feedback with no delay in each muscle fiber (Bunderson et al. 2010; Burkholder and Nichols 2000), and evaluated the stability of the same 51 solutions from the original null-path. Here, on top of the constant activation in the 51 solutions, each muscle received an additional neural input that was proportional to the change in muscle fiber length. We adopted the length feedback gains for each muscle from a previous study (Bunderson et al. 2010) which used data from ramp-and-hold experiments in decerebrate cats (Burkholder and Nichols 2000; Nichols 1989 ; Wilmlink and Nichols 2003).

The stability of the null-path between the minimum- and maximum-effort solutions could be altered when the model was varied with mechanisms affecting the intrinsic stability conferred by given muscle activation pattern (Fig. 4.A). For the 95%

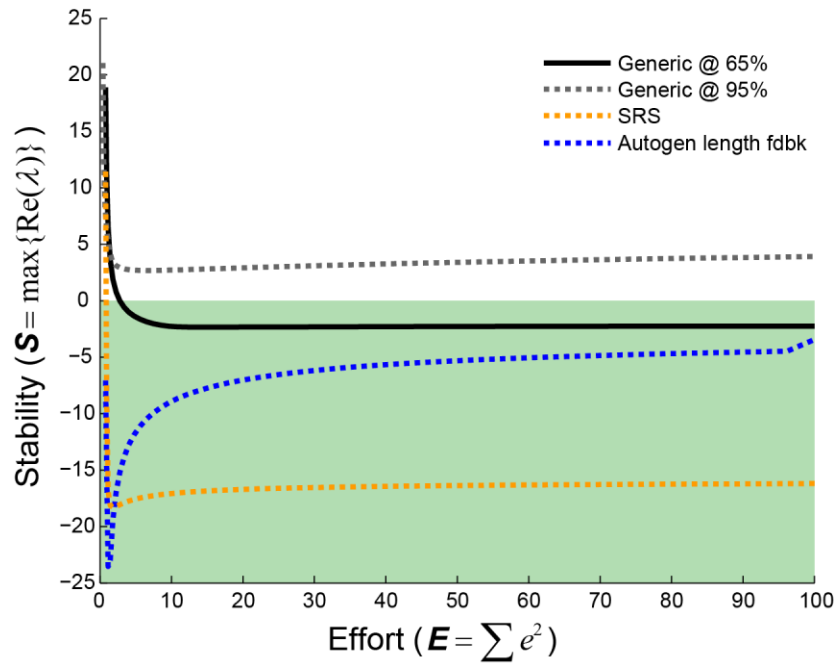


Figure 4.A: Null-path in altered conditions. Change in the null-path between the minimum- and maximum-effort solutions when other potential mechanisms affecting intrinsic stability were considered. Solutions on the original null-path (black solid line) were shifted towards more unstable regions when provided with unstable force-length relationship, e.g. 95% optimal fiber length on the force-length (f-l) relationship curve (gray dotted line). On the other hand, adding intrinsic stabilizing mechanisms such as short-range stiffness (orange dotted line) or autogenic length feedback (blue dotted line) shifted the solutions towards more stable region.

model in which all muscles operated on the plateau region of the force-length relationship curve, the null-path was shifted up in the functional property space (Fig. 4.A, gray dotted line), i.e., solutions on the null-path became more unstable. For the 95% model, solutions on the null-path were always unstable ($S > 0$) including the minimum-effort solution with $S = 21.1$ (compare to $S = 18.9$ for the 65% model) and the maximum-effort solution with $S = 3.92$ (compare to $S = -2.25$ for the 65% model).

When other intrinsic stabilizing mechanisms such as short-range-stiffness (SRS) and autogenic length feedback were considered, the null-path was shifted down towards a more stable region in the functional property space. For the SRS model (Fig. 4.A, orange dotted line), the minimum-effort solution was still unstable ($S = 11.4$) but more stable than the 65% model using the generic force-length relationship curve, with $S = 18.9$. However, the null-path entered the stable region with a sharp change and solutions on the null-path became stable. The local minimum for stability $S = -18.3$ occurred at $E = 1.80\%$ level, and the null-path flattened out until it reached to $S = -16.2$ for the maximum-effort solution. The null-path for the model with an autogenic length feedback (Fig. 4.A, blue dotted line) was always within in the stable region, where the minimum-effort solution was at $S = -7.07$. Stability was further improved until it reached the local minimum for stability $S = -23.5$ which occurred at $E = 1.14\%$, similar to the SRS model. However, beyond the local minimum, solutions on the null-path soon became less stable, even less stable than the minimum-effort solution, and gradually reached to the maximum-effort solution which was at $S = -3.43$.

In summary, we investigated how the mapping of the set of solutions along the null-path between the global minimum- and maximum-effort solutions is altered when other mechanisms potentially affecting stability were considered. As expected, solutions shifted towards more unstable region with unstable force-length relationships, and towards more stable region with adding intrinsic stabilizing mechanisms.

4.B Appendix: Effect of signal-dependent noise

In order to investigate the possible trade-offs between effort and robustness of solutions to noise, stability, and task performance, we selected subset of muscle activation patterns from the perturbed patterns generated across seeds and step size. Note that the perturbed patterns (\bar{e}^{-pert}) in Eq. 4.9 do not meet the torque requirement for producing the specified force (Eq. 4.2), and thus are not “true” solutions for the task. Nevertheless, these patterns can be considered as solutions contaminated by signal-dependent noise (Harris and Wolpert 1998), when the variance of the noise ($\bar{e}^{-pert} - \bar{e}^{-seed}$) across muscles have a proportional relationship to the effort level of corresponding seed solution. A subset of these perturbed patterns were used to further investigate implications to signal-dependent noise (SDN).

Among all of the perturbed patterns across all seeds and different step sizes, we selected muscle patterns that approximately met the criteria that variance within the noise ($\bar{e}^{-pert} - \bar{e}^{-seed}$) is proportional to effort where mean is close to zero:

$$\bar{w} = \bar{e}^{-pert} - \bar{e}^{-seed} = N(\sim 0, \sigma^2). \text{ where } \sigma^2 = k(\bar{e}^{-seed})^T \bar{e}^{-seed} = kE^{seed} \quad (4.B.1)$$

The proportionality constant k and threshold for deviation from zero mean were manually chosen ($k = 1.36\%$; threshold: 0.075) so that these patterns were sampled from all 51 effort levels of the seed on the null-path between the minimum- and the maximum-effort solutions. More than 10 solutions were selected for all 51 levels of effort. Stability of these patterns were evaluated with the metric (S). Task error was defined as the deviations in the endpoint force vectors from the target force direction, simulated using the selected patterns as input. For each effort level, we further investigated whether the task error due to SDN can be correlated with stability.

An additional trade-off for minimizing effort was found for robustness in production of the endpoint force in the presence of SDN. Solutions on the null-path from

the minimum-effort to the maximum-effort solution no longer produced the specified endpoint force when contaminated with SDN. The extent to which endpoint force vectors deviated from the original vector increased with effort level. In general, error in the task space as measured by force angle deviation from the desired direction increased with the levels of noise (Fig. 4.B, left). All muscle activation patterns were unstable after signal-dependent noise injection ($S > 0$), and level of instability tended to increase with effort level (Fig. 4.B, right). However, there was substantial variability in both the task error and stability across different muscle activation patterns selected for a given effort level (Fig. 4.B, shaded area; \pm standard deviations in red lines, where values for actual muscle activation patterns are shown with gray dots). Thus, even for muscle activation patterns with high level of noise, both task error and stability could be similar to ones with low level of noise.

However, task error (force angle deviation) and stability across noise-injected muscle activation patterns at a given effort level were negatively correlated. Among 51 effort levels, negative correlations between task error and stability ($p < 0.05$) were found in 29 effort levels with $R^2 = 0.20 \pm 0.07$ ($R^2 = 0.14 \pm 0.09$ across all 51 effort levels).

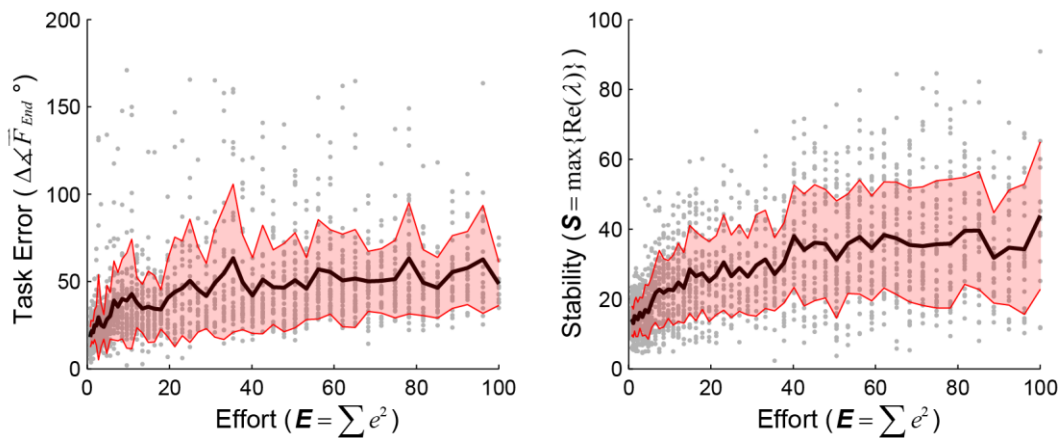


Figure 4.B: Task error and stability with SDN. Error in the task space in terms of force angle deviation to target force direction (left) and stability (right) with signal-dependent noise (Harris and Wolpert, 1998). In general, both task error and instability (positive S) increased with level of effort, and thus the level of noise. However, variability was large in all effort levels (black bold line: mean, shaded area in red: \pm std, gray dots: actual muscle activation pattern).

These results imply that task error due to signal-dependent noise may not always result in destabilization. For example, although all muscle activation patterns themselves were unstable, actual values of S had decreased (i.e., became “less unstable”) in many muscle activation patterns compared to the seed solution, especially in low-effort regions. Further, there may be muscle activation patterns that deviate from a solution inducing only small errors in the task space as well as providing increased stability. Although such case may be very rare from the limited set of selected muscle activation patterns examined here, it can be further speculated that noise may not always be detrimental in neuromotor system (Herzfeld and Shadmehr 2014; Wu et al. 2014), provided that large redundancy exists.

4.C Appendix: Analysis in muscle activation space

In order to characterize the changes that occurred in muscle activation patterns between the perturbed patterns (\vec{e}^{-pert}) to the projected solutions (\vec{e}^{-proj}), we examined the changes in distribution and range of activation levels, cosine of the angle between solutions, and the dimensions of each set of 200 patterns for given step size and seed. However, to simplify the comparison, we chose 5 seeds that were spaced approximately 25% apart in effort level including the minimum and the maximum effort level, and step sizes of 1, 10 and 100%. In particular, the effect of the projection was examined mainly with respect to step size, and values for comparison were averaged across seeds at different effort levels for a given step size.

To characterize how the normal distribution in the perturbed patterns change by projection, we categorized the distribution of activation in the projected solutions into “normal distribution”, “condensed at lower limit”, “condensed at upper limit”, “condensed at both limits”, based on the percentiles of activation in the projected solutions. In order to measure the extent to which distribution of activation in the projected solutions resembled the distribution of activation in the perturbed patterns, we computed R^2 between the percentiles of each set of 200 activation levels in perturbed patterns and projected solutions. Further, for a given step size, we determined whether distribution of activation levels in each muscle spanned the full search limit or not.

In order to determine the extent to which each perturbed patterns and projected solutions deviate from the seed in terms of vector direction, we computed the vector difference as cosine angle (Eq. 4.C.1) between each of the 200 patterns in each set and the seed solution for a given step size:

$$\cos \theta = \frac{\vec{e}^{-pert} \bullet \vec{e}^{-seed}}{\|\vec{e}^{-pert}\| \cdot \|\vec{e}^{-seed}\|} \quad \text{and} \quad \cos \theta = \frac{\vec{e}^{-proj} \bullet \vec{e}^{-seed}}{\|\vec{e}^{-proj}\| \cdot \|\vec{e}^{-seed}\|} \quad (4.C.1).$$

To test whether there mean difference in the cosine of the angles between perturbed patterns and projected solutions, we performed paired t-test with a significance level of $\alpha=0.05$ for given seed and step size.

We examined the reduction in dimension as perturbed patterns were projected onto the solution manifold. Dimensionality was computed as the rank of the data matrix constructed by stacking the 200 patterns into columns (31x200). In order to test whether the reduction in dimension in solution space involves any correlation in terms of changes in of any two muscles, we computed R^2 between all muscle pairs from the data matrix constructed by stacking the 200 difference patterns, i.e., difference between projected solutions and seed, which represented the 200 samples in the null space.

We found that projections of the perturbed patterns to the solution manifold imposed constraints in spatial structure due to net joint torque requirement. Distributions of activation for a muscle in the projected solutions were changed from the perturbed patterns, which was initially a truncated normal distribution about the seed. Overall, change occurred in more muscles for smaller step sizes and about the seed solutions near the extreme effort levels.

Distributions of muscle activations in projected solutions was more condensed at the limits (lower, upper, or both) for smaller step size, and more closely maintained the original normal distribution for greater step size. For example, the number of muscles categorized as “condensed at both limits” was 9.0 ± 2.8 across effort levels for 1% step size ($R^2 = 0.94\pm 0.04$), 8.6 ± 2.8 for 10% step size ($R^2=0.94\pm 0.04$), and 0.4 ± 0.54 for 100% step size ($R^2 = 0.99\pm 0.0002$). On the other hand, number of muscles categorized as “normal distribution” was 3.8 ± 0.83 across effort levels for 1% step size ($R^2 = 0.98\pm 0.03$), 3.8 ± 0.45 for 10% step size ($R^2 = 0.98\pm 0.02$), and 5.4 ± 0.89 for 100% step size ($R^2 = 0.97\pm 0.03$). R^2 value was in general small for the “condensed at lower limit” distribution category. Detailed categorization of muscles based on changes in distribution from perturbed solution to projected solution are listed in Table 4.C.2.

Table 4.C.1. Categorized changes in distribution from perturbed to projected solutions

Categorization	# of muscles across effort level	(R ² value)
normal distribution	3.8±0.83 for 1% step size	(0.98±0.03)
	3.8±0.44 for 10% step size	(0.98±0.02)
	5.4±0.89 for 100% step size	(0.97±0.03)
condensed at lower limit	13.8±2.6 for 1% step size	(0.65±0.23)
	14.0±2.9 for 10% step size	(0.68±0.22)
	18.4±0.55 for 100% step size	(0.77±0.21)
condensed at upper limit	4.4±2.5 for 1% step size	(0.94±0.05)
	4.6±2.8 for 10% step size	(0.91±0.08)
	6.8±0.45 for 100% step size	(0.92±0.07)
condensed at both limits	9.0±2.8 for 1% step size	(0.94±0.04)
	8.6±2.8 for 10% step size	(0.94±0.04)
	0.4±0.55 for 100% step size	(0.99±0.0002)

Activation level of muscles in the projected solutions less likely spanned the full possible range, i.e., from lower limit to upper limit, for greater step size. The number of muscles that spanned the full range of activation was similar for 1% and 10% step sizes, but was substantially smaller for 100% step sizes. Across effort levels, 17.6±3.85 muscles spanned the full possible range for 1% step size, 18.2±5.01 muscles for 10% step size, and 3.6±0.55 muscles for 100% step size.

Patterns became more similar to the seed solution in terms of vector direction in 31-dimensional space. The cosine of the angle between the seed solutions and perturbed patterns changed from 1.93±2.34° to 1.15±1.29° across effort levels for 1% step size, from 15.5±16.1° to 10.2±10.3° for 10% step size, from 46.4±12.1° to 35.4±10.9° for 100% step size in projected solutions. Differences in all conditions were significantly different statistically ($p < 0.05$).

The dimension of the solution sets was always reduced from 31 to 25. We found 4 sets of muscle pairs in which change in activation levels of two muscles were correlated and thus may contribute to reduction in dimensionality. These muscle pairs were *biceps*

femoris posterior and *rectus femoris*, *flexor digitorum longus* and *tibialis posterior*), *gluteus medius* and *quadratus femoris*), *gluteus medius* and *sartorius* (R^2 values across conditions are listed in Table 4.C.2).

Table 4.C.2. Muscle pairs with high correlation in projected solutions

Muscle Pairs	R^2 across effort level	p value
<i>biceps femoris posterior</i> and <i>rectus femoris</i>	0.81±0.05 for 1% step size 0.84±0.04 for 10% step size 0.81±0.03 for 100% step size	p<<0.05 in all conditions
<i>flexor digitorum longus</i> and <i>tibialis posterior</i>	0.38±0.10 for 1% step size 0.45±0.04 for 10% step size 0.40±0.04 for 100% step size	p>0.05 at min-effort level for 1% step size (p<<0.05 otherwise)
<i>gluteus medius</i> and <i>quadratus femoris</i>	0.50±0.10 for 1% step size 0.50±0.04 for 10% step size 0.50±0.05 for 100% step size	p<<0.05 in all conditions
<i>gluteus medius</i> and <i>sartorius</i>	0.55±0.16 for 1% step size 0.47±0.13 for 10% step size 0.55±0.03 for 100% step size	p<<0.05 in all conditions

CHAPTER 5

SIGNIFICANCE

5.1 Implications for computational modeling

5.1.1 A paradigm: Models as tools for building a map on which to locate one's behavior

The framework developed in this thesis proposes a paradigm in which detailed musculoskeletal models can be most useful for revealing neuromechanical principles underlying neural control of movement: *using models to build a map that lays out complete range of motor solutions (or behaviors) with respect to costs, constraints, goals and strategies relevant to the task*. The essential utility of such map is to evaluate where an individual's motor solution is located and thereby infer the principles that may have guided such specific choice. On the same basis, different motor solutions across individuals or conditions can be compare, providing explanation for such variations in selection (e.g. in healthy individuals) or compensation (e.g. in individuals with movement disorders).

One serious critique that can be given to a particular line or research using musculoskeletal models is inferring muscles' function during movement based on optimal predictions. "Measuring" biomechanical functions of individual muscles based on the exerted force on body segments (or torque at the joints) during movement is practically not plausible *in vivo* (Fleming and Beynnon 2004; Pandy and Andriacchi 2010). Therefore, muscle forces (or activations) predicted using optimization techniques in musculoskeletal models are often used to infer their role during movement (Erdemir et al. 2007; Hicks et al. 2015). For example, the contribution of muscles to leg swing, propulsion or body support in terms of CoM acceleration during human walking or

running (Anderson and Pandy 2003; Dorn et al. 2012; Hamner and Delp 2013; Hamner et al. 2010; Liu et al. 2008) have been extensively examined based on muscle activation patterns predicted by minimizing effort (Thelen et al. 2003). However, spatiotemporal discrepancy between optimal predictions and experimentally-observed muscle activity is often neglected (Thelen and Anderson 2006; van der Krogt et al. 2012); an optimal solution is merely one of many muscle activation patterns that replicate measured movement. Therefore, any conclusion drawn from such inferences should be taken with caution because they may not reflect the actual neural control, and thus may not be valid scientifically. For example, optimal solutions may deviate substantially from the pathological muscle activation patterns observed in impaired movements such as crouch gait in children with cerebral palsy (Steele et al. 2012a; Steele et al. 2010; Steele et al. 2012b) or hemiparetic gait in individuals with stroke (Jansen et al. 2014).

The proposed paradigm suggests an alternative approach: rather than making predictions based on a particular assumption (e.g. optimality) and comparing it to actual behavior (e.g. measured EMG), models can be used to identify and explicitly map out the window in which a viable solution may lie. The first step here is to identify the full range of possible solutions that satisfy the biomechanical task constraint (chapter 1). Previously, musculoskeletal models have been used to identify the set of feasible solutions in motor output space, e.g. biomechanical variables such as limb endpoint force (Valero-Cuevas 2009). For example, feasible forces that can be generated at the endpoint have been shown in a human lower limb (Gruben et al. 2003; Schmidt et al. 2003) and finger (Valero-Cuevas 2000; Valero-Cuevas et al. 1998), and a cat hindlimb (McKay et al. 2007). Similarly, the set of all feasible acceleration that muscles can induce at the joints or and hand had been examined in human lower limb (Kuo and Zajac 1993) and whole-body models (Khatib et al. 2009). A need for applying this type of explorative approach at a muscle level has recently been recognized. For example, possible range of muscle fiber length, which is one of the key determinants of a muscle's mechanical capability,

has been examined in walking and running (Arnold and Delp 2011). In a few recent studies, the feasible set of solutions for a given movement in muscle activation space has been investigated (Kutch and Valero-Cuevas 2011; Martelli et al. 2015; Martelli et al. 2013; Simpson et al. in review; Sohn et al. 2013); see Appendix A for Simpson et al., in review.

The most significant potential of the proposed paradigm is in its ability to provide a range of predicted motor solutions to which experimentally-observed behavior can be compared. A motor solution an individual currently uses is a product of the selection process which may involve various costs, constraints, goals, and strategies (Loeb 2012; Tsianos et al. 2014). Experimental evidence suggests that in motor learning, individuals exploit the allowed variability, actively exploring the vastly redundant solution space to efficiently search for a viable solution (Wu et al. 2014). Detailed musculoskeletal models can be used first as a substrate on which a multitude of solutions that vary in their properties regarding various certain costs, constraints, goals, or strategies can be generated and evaluated (chapter 2 and chapter 3). By placing the experimentally-observed motor solution (or behavior) on this map, the properties of particular selections can be examined quantitatively and compared across individuals and conditions. Such investigation further provides viable bases on which one can infer the principles by which a specific solution was selected over the other.

The following studies illustrate examples of how conceptually similar approach had been used to answer important questions of motor control: Bingham et al., (2011) used a planar biomechanical model of standing balance to investigate how altered biomechanics (e.g. stance width) affects the range of possible feedback gains to stabilize the system in frontal plane (Bingham et al. 2011). Specifically, by mapping out the full range of stabilizing feedback gains with respect to stance width, they could explain the changes in behavior in both healthy and neurologically impaired individuals. Hu et al., (2012) explored biomechanical constraints on the ability to modulate endpoint stiffness

across a variety of conditions using an upper extremity model (Hu et al. 2012). The resulting functional map could explain the limited voluntary modulation of endpoint stiffness observed in experiments (Perreault et al. 2001). Franklin et al., (2013) showed that subjects' selection of limb posture in an unstable virtual environment reflected solutions that ensured stability in the presence of motor noise while maximizing energetic efficiency, which was mapped and evaluated across the work space using neuromechanical simulations (Franklin et al. 2013). Similarly, Liao et al., (2014) showed that selected postures could be explained by the cost map that incorporates the stability criterion evaluated using a musculoskeletal model, and built across the joint space (Liao et al. 2014). Further, a cost map for a different force field could predict the variability of arm postures observed in experiments (Trumbower et al. 2009).

Meanwhile, a range of predicted motor solutions or behavior in a model may not always encompass physiological behavior because models are too “strict” in that variations in parameters are not allowed, unless intended. Such rigidity results, inevitably, from modeling effort to mathematically and deterministically representing physiological features of the neuro-musculoskeletal system with inherent variability and uncertainty (Higham and Biewener 2011; Lieber and Ward 2011). For example, many muscles insert into a broad area on the bone, or have varying moment arm due to functional and architectural complexity that cannot be simply modeled with cable actuators (Ting and Chiel in press; Yeo et al. 2011; Yeo et al. 2008). Hard constraints on biomechanical parameters in a model has important implications when linking model predictions to experimental data. In particular, experimentally-derived control signals, e.g. muscle activation pattern, may produce substantial errors in the task space (de Rugy et al. 2013). Vice versa, flexible recruitment in experimental muscle activity may not be present in predicted muscle activation patterns (Steele et al. 2015). Sensitivity analysis has been the gold standard validating the predictions and was applied in studies using musculoskeletal models (Hicks et al. 2015), or in studies explicitly testing the validity of such approaches

(Ackland et al. 2012; De Groot et al. 2010). Nevertheless, they still suffer from the possibility of lacking relevance to actual neural control if results were predicted using muscle activation patterns based on single optimal criterion, as discussed above.

An approach that is more coherent with the paradigm suggested here has been proposed more recently. This framework seeks to explicitly explore the range of feasible predictions of a model itself to mirror the distribution of experimental data (Santos et al. 2009; Valero-Cuevas et al. 2009). In addition to systematic exploration of the parameter space, its use can be extended for testing neural control hypotheses (Kutch et al. 2008). Adding to the proposed paradigm which gives range of predicted behaviors using an individual model, exploration of the possible variations in the model itself may provide more abundant space to represent a behavior, and thus lend more relevance to the experimental data that it is to be overlaid with.

5.1.2 Finding muscle activation patterns that provide stability to musculoskeletal dynamics

One practical implications of computational methods developed in chapter 4 is that more stable solutions can be found for forward dynamic simulations. Stable solutions may confer robustness to sources of instability such as numerical round-off error or noise in simulations (Alexandrov et al. 2005; Higginson et al. 2006; Risher et al. 1997). Intrinsic stability is often lacking in simulations using muscle-driven musculoskeletal models, in which case the system states deviate catastrophically from desired states under numerical perturbations (Bunderson et al. 2010; John et al. 2013). Being able to find and use stable muscle activation patterns in muscle-driven forward dynamic simulations is beneficial, especially for dynamic optimizations in inherently unstable tasks such as walking or running (Anderson and Pandy 2001a; Neptune 1999). Dynamically stable

initial conditions conferred by active muscles in forward simulations may allow system dynamics to tolerate such instability and facilitates the search.

The method used here to evaluate local dynamic stability conferred by active muscles can be extended, in general, to dynamic tasks such as walking or arm reaching. Although I examined local dynamic stability of the cat hindlimb system linearized with respect to a static equilibrium point (chapter 4), linearized system dynamics at any instance predicts the local response characteristics of the states with respect to the original dynamic equilibrium point on the movement trajectory. A similar approach using systems theory has been used to quantify and characterize local orbital stability in human walking, e.g. short-term local divergence exponent or maximum Floquet multipliers which represents the response of a system to small discrete perturbations from cycle to cycle (Bruijn et al. 2013; Dingwell and Kang 2007; Kao et al. 2014; McAndrew et al. 2011). However, such measures examine stability with respect to trunk motion, e.g. kinematic states at C7, which does not address how stability is achieved through functional coordination of the limb, and ultimately by the muscles. On the other hand, extension to arm reaching tasks provides novel opportunities to examine neural control strategies for stabilization at muscle level that has previous been studied extensively in the framework of endpoint impedance regulation at joint torque level (Burdet et al. 2001; Burdet et al. 2006).

More generally, understanding neuromechanical principles to guide selection of muscle activation patterns based on physiologically meaningful stability also has important implication for using models to study neural control of movements. Ensuring the dynamics of the body that is more physiologically relevant and numerically stable provides ground on which viability of any hypothesized neural controller can be tested (Ting and Chiel in press).

5.2 Implications for muscle synergy hypothesis in motor control

5.2.1 Guiding principles for acquiring generalizable motor solutions

Muscle synergies are hypothesized to be the building blocks of movement that can generalize its function across tasks and flexibly combined to produce a large repertoire of movements (Cheung et al. 2005; Cheung et al. 2009; Chvatal and Ting 2013; Chvatal et al. 2011; d'Avella et al. 2006; d'Avella and Bizzi 2005; Hart and Giszter 2004; Roh et al. 2011; Roh et al. 2012; Torres-Oviedo et al. 2006; Torres-Oviedo and Ting 2010). However, the actual existence of such modular entities as neural substrate is constantly debated (Bizzi and Cheung 2013; Kutch et al. 2008; Kutch and Valero-Cuevas 2012; Tresch and Jarc 2009). Nevertheless, structure and function in various parts of the nervous system involved in development, motor learning, skill acquisition, and adaptation constitute evidence for utility of such pre-selected primitives for motor control (Callebaut and Rasskin-Gutman 2005; Giszter and Hart 2013; Minai 2015; Ting et al. in press; Wagner et al. 2007). Regardless of its origin, understanding muscle synergies as *acquired motor solutions* is a useful framework for explaining the fundamental organization underlying motor behaviors.

One crucial premise for the very idea of flexibly combining few muscle synergies to generate a vast range of complex movements is that each muscle synergy itself must be functionally robust. Although spatial structure of muscle synergies with a specific biomechanical function can be pre-organized at multiple time-scales (d'Avella et al. 2003; Tresch et al. 1999), the coordinated recruitment across muscle synergies is modulated spatially or temporally according to the task-level goals. For example, recruitment level of muscle synergies used during postural balance tasks are tuned, spatially, to the direction of perturbation (Ting and Macpherson 2005; Torres-Oviedo and Ting 2007). On the other hand, recruitment level of muscle synergies used during human walking are modulated temporally during specific episodes of the gait cycle (Chvatal and Ting 2013).

For both cases, however, the biomechanical condition at which a muscle synergy is actively performing its function may change due to alterations in the body configurations or task requirements. Further necessity for robustness in using muscle synergies across varying conditions arise when muscle synergies are required to generalize their function across different tasks (Cheung et al. 2005; Chvatal and Ting 2013; d'Avella and Bizzi 2005; Hart and Giszter 2004), or when they are subject to regulation through feedback mechanisms (Lockhart and Ting 2007; Safavynia and Ting 2013).

In this thesis, I examined the principles, and possibly the processes, by which a neural selection could be guided towards a motor solution that meets functional demands for generalizability (chapter 3) and intrinsic stability (chapter 4). In particular, I demonstrated in chapter 3 the possibility of finding muscle activation patterns that can generalize its function, e.g. isometric endpoint force, across a range of postures. Sub-optimality of such generalizable solutions further supported the idea that the process of acquiring a pattern for a muscle synergy is more likely through learning and refinement (Ting et al. in press), rather than online optimization, e.g. optimal feedback control (Todorov 2004; Todorov and Jordan 2002). In addition, muscle activation patterns that provide intrinsic stability at local joint-levels over a physiological range of variation in biomechanical configuration are more likely to ensure the linear mapping from activation of a muscle synergy to its motor output. Moreover, superposition of the output from multiple input in linear fashion, e.g. linearly combining few synergies, is more likely to be expected in stable systems. The heuristic exploration algorithm developed in chapter 4 can be used to search for sets of solutions that are intrinsically stable.

Furthermore, muscle synergies themselves can evolve over time. New muscle synergies can be developed (Dominici et al. 2011 ; Lacquaniti et al. 2013) or learned (Kargo and Nitz 2003 ; Ruckert and d'Avella 2013). Alternatively, spatiotemporal recruitment of pre-existing or acquired muscle synergies can be adapted to novel task requirement or challenges (Berger et al. 2013; Cheung et al. 2009; Clark et al. 2010). The

landscape of the solution space with respect to functional properties of a muscle activation pattern which I explored in chapter 4 may possibly illustrate such search or adaptation processes. I showed that functional properties of an acquired solution after making a change in muscle activation may depend critically on where one is at, i.e., the current solution, and how radical or conservative one is in making changes, i.e., the step size. Redundancy in muscle patterns across different solutions with similar functional properties further suggests a possible explanation for observed variability in the spatial structure of muscle synergies of a similar function, across individuals (Chvatal and Ting 2012; Clark et al. 2010).

Lastly, and more practically, the method developed to identify muscle feasible range in chapter 2 can extend its application for predicting feasible range in unobserved muscles during experiments. The number of muscles that can be recorded are often limited in experiments for studying the organization of coordinated movement using muscle synergy analysis. However, the number and choices of muscles included in muscle synergy analysis may affect the structure of extracted muscle synergies, e.g. over-estimating variance accounted for with smaller number of muscles (Steele et al. 2013). Furthermore, the missing contributions from muscle that were not measured in experiments has been one of the main limiting factors in using experimentally-observed muscle synergy patterns directly in detailed musculoskeletal models (Kargo et al. 2010; McKay and Ting 2008; 2012; Neptune et al. 2009). In the framework of muscle feasible range analysis, we can use observed coordination in a subset of muscles, e.g., muscle synergy patterns, as a constraint to infer the possible range of variations within a synergy for muscles that were not measured during the experiment (see Appendix B for preliminary results). The effect of a synergy constraint will be reflected in muscle activation space, i.e., feasible ranges, as well as motor output space, e.g. feasible forces (Valero-Cuevas et al. 1998), which may predict the physiological behavior observed in experiments (Borzelli et al. 2013; McKay and Ting 2008; 2012).

5.2.2 Modular control in real-world applications

The computational framework developed in this thesis can be useful for developing novel biologically-inspired control principles in many applications such as robotics or functional electrical stimulations (FES). Constructing complex movements from a few sets of modules is an appealing control scheme. By reducing the number of control variables it grants the nervous system computational efficiency (Byadarhaly et al. 2012; McKay and Ting 2012) which facilitates learning and adaptation (Alessandro et al. 2013; Ting et al. in press; Tsianos et al. 2014). In implementing a modular controller in any real-world applications, challenges remain in the same vein as what the nervous system faces when selecting an activation pattern for functional muscle synergies: selecting from among many, and selecting the ones that are functionally robust.

In robotics, ‘movement primitives’, or kinematic synergies, has been commonly used in the framework of reinforcement motor skill learning, and has been successfully applied in controlling high DoF robots for complex movements (Hauser et al. 2011; Ijspeert et al. 2003; Meier et al. 2011). On the other hand, physiological behavior has been successfully reproduced in computer simulations using musculoskeletal models, with synergy-based controllers in a variety of motor tasks (Berniker et al. 2009; Kargo et al. 2010; McKay and Ting 2008; 2012). However, only a few actual robotic applications exist that directly borrows control from muscle synergy in biological systems (Alessandro et al. 2013; Chhabra and Jacobs 2006; Ison and Artemiadis 2015). Understanding the principles of how the nervous system may organize muscle synergies that are functionally robust provides insights into synthesizing modular solutions that can control the dynamics of robots in real physical world (de Rugy et al. 2013).

Furthermore, the ability to find functional muscle activation patterns such as muscle synergies can inform the design of functionally viable control for an FES paradigm (Davoodi et al. 2003; Denis et al. 2013; Muceli et al. 2010) or myoelectric control in powered prostheses (Hargrove et al. 2009; Parker et al. 2006).

5.3 Clinical relevance

Understanding the functional implications of neuromechanical alterations in movement disorders is crucial for developing effective rehabilitation interventions and treatments. To this end, the computational framework developed in this thesis can be a very powerful tool for predicting the effects of specific pathological constraints to functional behavior. Such predictions made in models can provide insights to better understand the neuromuscular impairments afflicting individuals with neuromuscular and sensory disorders such as stroke, cerebral palsy, or spinal cord injury.

5.3.1 Neuromechanical alterations following stroke

Many of the motor deficits in individuals with stroke can be simulated in detailed musculoskeletal models. In particular, the deficits in impaired multi-joint limb control following stroke involve muscle weakness (Chang et al. 2013), spasticity (Dietz and Sinkjaer 2007), impaired joint individuation (Zackowski et al. 2004), as well as systematically disturbed feed-forward control (Beer et al. 2000).

For example, spasticity, phenomenologically, is regarded as hyper-excitability in muscle spindle reflexes, and can be simulated in models by increasing the feedback gains to length and velocity changes in muscles (Jansen et al. 2014; Mansouri and Reinbolt 2014). The adverse effect of this altered sensorimotor feedback on the overall behavior in motor tasks such as postural control or walking can be evaluated in terms of changes in dynamic stability at the local limb level or the whole body level (chapter 4). Further, limitations in possible compensatory corrections predicted under such simulated impairments may explain the impaired stretch reflex behavior in stroke patients that is exaggerated and insensitive to changes in task demand.

Abnormal co-activation of muscles often present in individuals with stroke (Brunnström 1970; Dewald and Beer 2001; Dewald et al. 1995) can be modeled simply

by the coupling of muscles, i.e., certain muscles are constrained to receive and be activated with a single command. Such neural constraint at the muscle level may explain the difficulty stroke patients have in producing antigravity torque in the upper limb, beyond the biomechanical constraints of the limb (see Appendix B). Alternatively, together with muscle weakening which induces saturation in the activation of muscles in stroke patients (McCrea et al. 2005), the model may predict the alteration of postures, e.g. out-of-plane movements in arm reaching (Beer et al. 2004; Beer et al. 2007; Reisman and Scholz 2006), as a biomechanical compensatory strategy.

Finally, the functional consequences of altered muscle synergy patterns can be assessed in musculoskeletal models. During human walking, altered muscle synergies in individuals with stroke were found to be a resultant of merging of two different synergies observed in healthy control (Clark et al. 2010). Using dynamic simulation of musculoskeletal model using muscle synergies, Allen et al., (2013) has examined the influence of merged synergies on walking performance in terms of the altered contributions to body support, forward propulsion, mediolateral control and leg swing (Allen et al. 2013). On the other hand, during an isometric force generation task in a human arm, the spatial structure of muscle synergies was altered in individuals with stroke, compared to healthy controls (Roh et al. 2013). Muscle feasible range analysis (chapter 2) can be used to predict the functional consequences of such alterations in spatial organization of muscle synergy patterns. For example, coupled activation of deltoid muscles in muscle synergy from individuals with stroke (Roh et al. 2013) may limit the biomechanical capability of the limb in producing forces in certain directions. Furthermore, abnormal coordination pattern in subset of muscles may also influence the spatial organization of other muscles, revealing how the other muscles must compensate for such pathology (see Appendix B for preliminary results).

5.3.2 Altered kinematics of crouch gait in cerebral palsy

Crouch gait is an impaired movement pattern typically observed in individuals with cerebral palsy. Such altered kinematics is often characterized by excessive hip, knee and ankle flexion during the stance phase (Wren et al. 2005). This impaired gait is known to be energetically inefficient (Rose et al. 1989; Waters and Mulroy 1999), to induce pain in the joints (Jahnsen et al. 2004) and induce deformation of bones (Graham and Selber 2003). Muscle weakness, which is common in individuals with cerebral palsy, has been suggested as a potential cause for crouch gait (Damiano et al. 1995; Wiley and Damiano 1998). Thus, strength training has been the one focus for remedying crouch gait (Dodd et al. 2002; Mockford and Caulton 2008; Pippenger and Scalzitti 2004). However, its outcomes are variable or questionable at some times (Damiano et al. 2010 ; Kerr et al. 2006; Liao et al. 2007), and the underlying mechanisms remain unclear. Short hamstrings due to spasticity have been suggested as another potential mechanism for this abnormal gait pattern in cerebral palsy (Baumann et al. 1980; Crenna 1998 ; Tuzson et al. 2003). The remedy for this has been surgical lengthening of the hamstrings. However, the outcomes of these procedures are inconsistent (Abel et al. 1999; DeLuca et al. 1998; Kay et al. 2002; Novacheck et al. 2002), which critically impedes the prediction of which patient will benefit from such treatment (Arnold et al. 2006a).

Previously, musculoskeletal models have been used to examine altered muscle contributions to body acceleration during crouch gait (Correa et al. 2012; Steele et al. 2012a; Steele et al. 2010). Further, the extent to which specific muscle groups can be weakened before alteration to unimpaired kinematics occurs were predicted (Steele et al. 2012b). However, in these studies optimal solutions minimizing effort (Thelen and Anderson 2006) have been used to simulate muscle forces during crouch gait. As discussed before, the discrepancy between the actual neural control versus optimal prediction was ignored. As expected, simulations of unimpaired gait controlled with optimal solutions exhibited robustness to muscle weakness (van der Krogt et al. 2012).

Alternatively, models were also used to examine the difference in the force-generating capacities of muscles due to altered kinematics (Arnold et al. 2006b; Hicks et al. 2008) that may or may not be reflected in how muscles are actually used.

Muscle feasible range analysis explicitly identifies the full possible range of muscle activation, and thus possible compensations. Results shown in chapter 2 suggests that even with muscle weakness, muscle activation patterns may not be determined by biomechanics, and thus can deviate substantially from optimal solutions. Muscle feasible ranges for normal walking (Martelli et al. 2015; Simpson et al. in review) further verified such speculation, where most muscles were “unnecessary” for the most part. A wide muscle feasible range also suggests that morphological (biomechanical) changes in a muscle, e.g. lengthening of the hamstring, may not necessarily elicit changes in the functional use of the muscle in terms of neural control. Known neuromuscular pathologies involved in cerebral palsy can be further incorporated, on top of muscle feasible range identified for patient-specific kinematics, to investigate potential mechanisms for crouch gait and provide predictive outcome measures for treatments.

5.3.3 Difficulties in training individuals with motor impairments

Clinicians often experience difficulties in training individuals with motor impairments to replicate functional, or “normal”, movement patterns. Intuitively, this is because what would be an optimum in a healthy individual may not be an optimum for an individual with neuromuscular deficits. Ignoring the possible neuromechanical differences in such compensated systems may be the reason why rehabilitation strategies to enforce a stereotyped movement pattern is unsuccessful. One obvious example can be illustrated in inconsistent outcomes from robot-assisted gait training in individuals with impaired gait or balance such as stroke or Parkinson’s disease patients (Cao et al. 2014; Hussain 2014; Picelli et al. 2014; Swinnen et al. 2014).

The computational framework developed in this thesis can address the fundamental questions of what is “possible”, and what is a “better” solution for an individual with a particular neuromuscular alteration. Muscle feasible ranges (chapter 2) can explain the difference in the space in which activation of individual muscles can vary (see Appendix B), as well as the extent of possible deviation from an optimal solution. Further, the landscape of the solution space with respect to functional and altered neural constraints (chapter 3 and 4) may explain the limitations in what functional changes one can make from the current pathological state (Dubois et al. 2011; Fisher and Sullivan 2001; Fisher et al. 2008; Stokes and Gardner-Morse 2001; Will et al. 2004). Ultimately, by taking into account of the way in which possible changes affect functional outcomes in an individual, patient-specific treatments and rehabilitation strategies can lead to successful restoring of function, not necessarily “a pattern”.

CHAPTER 6

CONCLUSION

My long-term goal is to understand how the human nervous system coordinates feed-forward (e.g. postural configuration, muscle tone, voluntary activation) and feedback (e.g. stretch reflex, automatic postural responses) mechanisms to generate the natural repertoire of movements and postures used in everyday life. As a first step towards this goal, in this thesis I developed a novel computational framework that explores the complete range of motor solutions for a given task, and evaluates functional implications of multitudes of solutions.

This work advances the utility of detailed musculoskeletal models in elucidating neuromechanical control principles underlying functional and impaired movements. The computational framework developed here provides useful modeling tools to examine allowed variability in muscle activation patterns for a given task with respect to various biomechanical and neural constraints. For example, it can aid in interpreting variability in measured muscle activity, or explaining individual differences in motor strategies and motor learning (de Rugy et al. 2012; Hasson et al. 2012). It can also be used for assessing confidence of predicted muscle activity as well as for evaluating possible variations when alternate cost functions or strategies are considered. This may provide important principles for designing functionally viable control for stimulation paradigms (Denis et al. 2013), prosthetic devices, and bio-inspired control for robots (Hauser et al. 2011; Ruckert and d'Avella 2013). Finally, predicting the possible variations in motor solutions and their functional consequences, we may gain valuable insights to explaining differences in individuals with motor deficits (Dietz and Sinkjaer 2007), which is crucial for developing novel and effective patient-specific treatments and rehabilitation strategies.

In the following sections, I discuss limitations in scope of this thesis, as well as possible directions in which future investigations can be pursued to fill in the gaps. I end with concluding remarks on desired attitudes towards taking neuromechanical approaches in unveiling the principles of neural control of movement.

6.1 Limitations and future works

6.1.1 Integrating functional requirements for generalizability and stability

Generalizability and stability, which are both experimentally-observed functional property of a muscle synergy, have not previously been considered simultaneously. In chapter 3, I demonstrated that only suboptimal muscle activation patterns for muscle synergies generalize motor function across postures; effort-wise optimal solution was not generalizable. On the other hand, I showed in chapter 4 that optimal solution in terms of effort is dynamically unstable. Thus, chapter 3 and 4 together strongly suggests that minimum-effort criterion is not likely the only consideration in determining how the spatial structure of a muscle synergy is organized. However, whether generalizable solutions provide intrinsic stability, or vice versa, stable solutions are generalizable has not been tested explicitly.

The two functional requirements of generalizability and stability can be integrated to further narrow down the range of viable muscle activation patterns for functional muscle synergies. More specifically, additional constraints regarding stability evaluated for the linearized system under a given muscle activation pattern can be considered within the feasible range considering a generalizability constraint in chapter 3. Remaining redundancy in muscle activation space after considering either of the functional constraints, i.e. generalizability (chapter 3) or stability (chapter 4), suggest a possibility for existence of subset of solutions that meet both requirements. Alternatively,

generalizable solutions may not be stable due to biomechanical differences in the model across configurations and allowed error in the output space. In such case, the possible role of task-level feedback mechanisms can be investigated using dynamic simulations and model implemented with controller for stabilization of the task.

6.1.2 Task-level control of whole-body CoM at global level

In this thesis, the biomechanical task and dynamic behavior of the system were examined only at local level (single limb), and hierarchical feedback control of postural behavior at global level, i.e., controlling whole-body CoM dynamics, was not considered. Neuromechanical models have been used to demonstrate feasibility of achieving observed task performance with muscle synergies (Kargo et al. 2010; Neptune et al. 2009), and not necessarily predicting a behavior, in a forward way, based on extrinsic goal for a given motor task. In order to genuinely test the viability of producing functional behavior using muscle synergies in models, predictions made in models controlled with muscle synergies must be examined at a behavioral level (Alessandro et al. 2013). However, for balance control, task-level control of CoM based on sensorimotor feedback has only been demonstrated in simple models, e.g. an inverted pendulum (Lockhart and Ting 2007; Welch and Ting 2009; Welch and Ting 2008). On the other hand, using muscle synergies in detailed musculoskeletal model to predict global behavior of CoM control has only been shown in static condition (McKay and Ting 2012).

Challenges in using muscle synergy for balance control in a complex dynamic model is that intrinsic stability is required during both a passive period in absence of any sensorimotor corrections (Jacobs and Macpherson 1996), and during an active period when muscle synergies are recruited as active neural control inputs on top of an existing background muscle activity. Moreover, the multiple modular control inputs need to work in linear fashion even though the transformation to output occurs through highly

nonlinear musculoskeletal dynamics. For such linearity, output of each and combined muscle synergies at CoM must be preserved robustly over range of neuromechanical alterations: variability in kinematic posture, signal-dependent noise in muscle activity, and ongoing biomechanical changes due to the dynamics of the whole body.

The above questions can be adequately addressed using computational tools developed in this thesis, as well as insights gained from the studies. In particular, we can investigate to what extent functional consequence of muscle synergy patterns with different level of intrinsic stability can be kept *effective* and *linear* over ranges of disturbance to the system. We can hypothesize that muscle synergy patterns with greater intrinsic stability provide more linear mapping from input, active response in muscle activation, to output CoM kinematics. In order to investigate functional consequences of activating given muscle synergy patterns in cats in terms of whole-body dynamics, however, a dynamic multi-limb model would need to be developed (Martin 2013).

One specific question that can be investigated is whether muscle synergy patterns selected with different functional properties at local limb-level exhibit different level of performance in controlling whole-body CoM. Muscle synergy patterns that have varying levels of effort and intrinsic stability can be selected (chapter 4) for each of the five experimental synergy force vectors (Torres-Oviedo et al. 2006). The task output of these muscle synergy patterns can be simulated by activating each pattern, e.g. by Gaussian pulses individually and measuring simulated CoM kinematics as a global output measure. The extent to which task space outputs of each synergy can be combined linearly, can be assessed by applying pair-wise combination of the synergy patterns and examining the resulting CoM behavior compared to predicted CoM behavior by linear superposition.

Further challenges in the task-level behavior of balance control can be tested if muscle synergy patterns selected with certain level of functional stability indeed ensures linear behavior over certain range. For example, translational support perturbation can be simulated to induce alterations in kinematic states, similar to those experienced in

experiments (Jacobs and Macpherson 1996; Macpherson 1988a; b). Signal-dependent noise (Harris and Wolpert 1998) can be applied to each synergy activation pattern to test robustness to alteration in muscle activation. We can also test whether effective noise rejection, in the presence of disturbance torque at the joints, in quiet standing (Peterka 2000) can be achieved by feedback control using identified synergies. Alternatively, we can test whether desired CoM trajectory can be produced by activating sets of muscle synergies in linear combination. Here, the activation profile, or temporal recruitment of each synergy can be defined by projecting a specified CoM trajectory onto task space output of each synergy. Finally, we can implement an optimal feedback controller with delayed CoM kinematics to model the balance control behavior using synergy patterns that provides intrinsic stability at both local and global level.

6.1.3 Experimental validation

The contribution of this thesis using computational models can be augmented by validation through actual experiments. In particular, a detailed musculoskeletal model of the cat hindlimb predicted that there exists a redundant solution space that allows for variability in how muscles can be coordinated for an isometric endpoint force generation, and produce different functional properties of the limb. This was true, in general, in a biomechanically redundant task using both human lower (see Appendix A) and upper extremity (see Appendix B). However, what has not been shown is whether people actually utilize the full space and thus exploit the allowed variability in their muscle patterns for achieving the same motor task. More specifically, the extent to which different levels of variability should be attributed to biomechanical constraint defined by the limits of the musculoskeletal system, or neural constraint owing to functional requirement, is unknown.

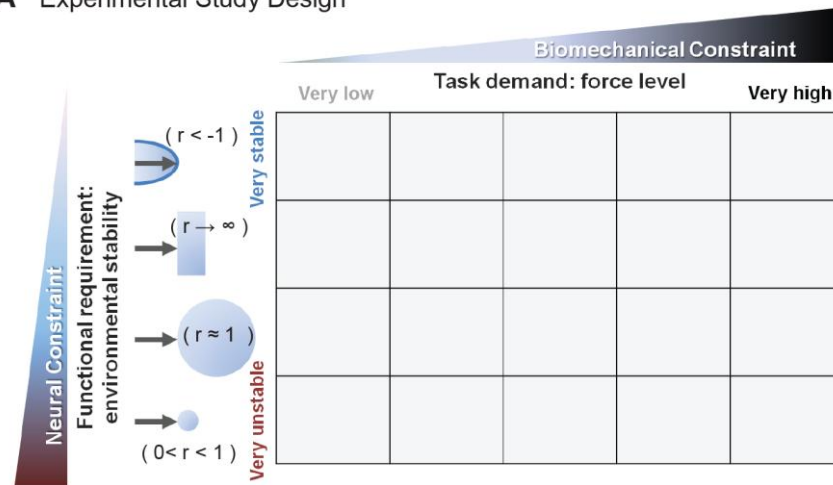
A plausible goal for an experimental study could be to investigate whether and to what extent subjects exploit musculoskeletal redundancy in upper extremity while performing isometric force generation task in different functional contexts, e.g. task demand and environmental stability (Fig. 6.1A). We can hypothesize that less variability will be exploited for more demanding task and increased functional requirement for stability. This hypothesis can be tested by examining variability in muscle patterns measured during the same motor task at varying force level, and in different levels of environmental stability rendered by robotic manipulator (Fig. 6.1B; e.g. Haptic-Master; Moog-FCS Control Systems, Nieuw-Vennep, The Netherlands).

More specifically, in order to test whether task demand affects variability in muscle activity measured during isometric force generation, force magnitude that subjects needs to produce can be varied at different levels in a given direction. In order to test whether functional requirement affects variability in muscle activity measured during isometric force generation, environmental stability in which subjects perform the task can be varied at different levels by rendering the haptic interaction with different surface geometry (Fig. 6.1A). The experimental protocol can be similar to that used previously in studies which examined context-dependent modulation of limb impedance (Krutky et al. 2013; Trumbower et al. 2009) and contributions of long-latency stretch reflex (Krutky et al. 2010; Perreault et al. 2008; Trumbower et al. 2010). The modeling framework here (Fig. 6.1C) can be further applied using an existing upper extremity model (Holzbaur et al. 2005) to provide theoretical map for muscle feasible range across force magnitude (chapter 1) and trade-off between effort and stability (chapter 3).

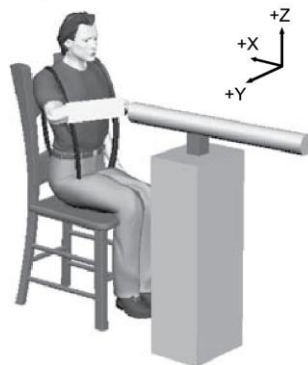
I propose four specific questions that can be addressed with this experimental design, and corresponding analyses to answer these questions. First, whether task demands and functional requirements affect intra/inter-subject variability can be tested by comparing variability in experimental muscle activity (EMG) across force levels and stability conditions. Second, whether environmental instability (functional requirement)

imposes additional limits beyond biomechanical capabilities can be tested by comparing maximum voluntary force (MVF) in a given direction across stability conditions. Third, the pattern of variation in measured muscle patterns with respect to biomechanical redundancy defined in the model can be quantified by comparing experimental variability in muscle activity across force levels with respect to the muscle feasible ranges computed at corresponding force level in the model.

A Experimental Study Design



B Experimental Setup: Haptic Interaction



C Modeling Framework: Musculoskeletal Model

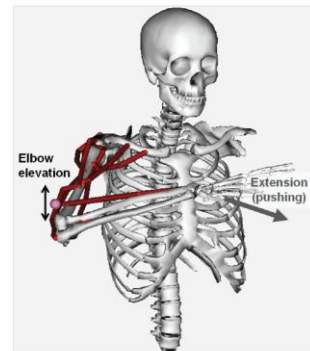


Figure 6.1: Proposed experimental study. (A) Experimental study design. We can investigate whether and to what extent subjects exploit musculoskeletal redundancy in upper extremity while performing isometric force generation tasks in different functional contexts. (B) Experimental setup. Environmental stability can be rendered by haptic interaction with robotic manipulandum. (C) Modeling framework. A detailed musculoskeletal model of upper extremity can be used to provide theoretical map for muscle feasible range across force magnitude, and functional properties of effort and stability.

I predict that, variability in muscle activity for generating force in a given direction will be high for low force level, and less variable for high force level (Fig. 6.2A). In addition, variability in muscle activity for generating same level of force will be higher in stable condition than unstable conditions, which require additional control for ensuring stability (Fig. 6.2B). Further, maximum force that can be generated in a given direction will be lower in magnitude in unstable condition than stable condition. Finally, ranges in experimental muscle activity may be smaller, even for low force levels, compared to models because feasible ranges in the model using the method presented in chapter 2 is computed for individual muscles, i.e., not regarding coordination, and thus does not reflect any control strategy beyond biomechanical demand.

The same protocol can be used to examine how altered neuromuscular conditions affect the ability to exploit musculoskeletal redundancy, i.e., the allowed variability, in individuals with stroke. I predict that inability to independently control muscles (Dewald and Beer 2001; Dewald et al. 1995) will restrict the range of variability and impair limb function.

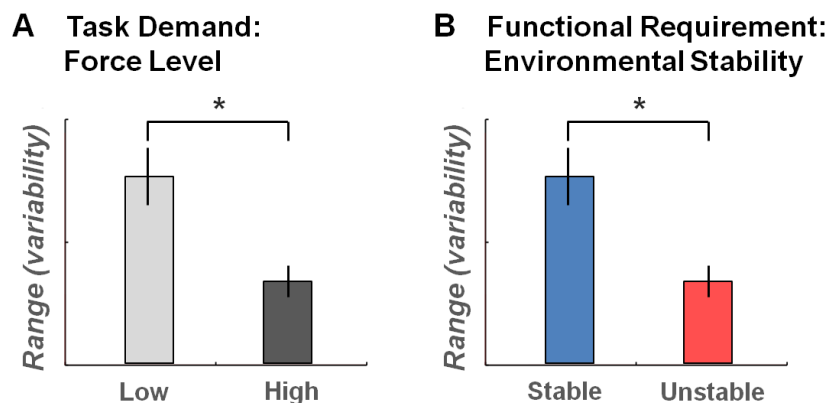


Figure 6.2: Predictions to proposed experimental study. (A) Predicted experimental variability in muscle activity across force level. Variability in muscle activity (EMG) for generating force in a given direction will be high for low force level, and less variable for high force level. (B) Predicted experimental variability in muscle activity across environmental stability. Variability in muscle activity (EMG) for generating same level of force will be higher in stable condition than unstable condition, which requires functional stability.

6.2 Concluding remarks

Neuromechanics is an integrative approach that seeks to understand control principles underlying functional motor behavior with respect to complex, flexible, and context-dependent interactions among the brain, the body, and the environment (Chiel et al. 2009; Nishikawa et al. 2007; Ting and Chiel in press). In pursuit of such goals, one may choose to use experimental investigation, e.g. examining how individuals achieve a given motor task with different strategies, behavior, or execution at muscle level. On the other hand, one may choose to use computational models, e.g. using simulations of a behavior to make predictions, which can be compared and interpreted with respect to physiological behavior. The two approaches can be, and often are, used together to augment each other. Regardless of the approach, however, and whether the underlying motivation is a scientific question or an engineering problem, two attitudes (that may have been too often ignored perhaps) are required for researchers in the field of neuromechanics:

- 1) *We must appreciate variability.* Interpreting variability in experimental data, e.g. EMG, can be difficult and one may be tempted to examine the data averaged across trials, or even across subjects, to make a unifying explanation. However, we can be different, and we are different. Understanding the differences is the key to elucidating the principles underlying one's choice, either voluntary or involuntary, in a behavior.
- 2) *We must appreciate discrepancies.* Models can be useful if they act as expected, producing or predicting an experimentally observed behavior it was supposed to model. However, when our models start fail to match the experimental data, that is precisely the moment when one can ask “why”, presenting an opportunity to reveal the mechanisms underlying such discrepancies. Thus, we must not ignore the “disagreements”, and not be afraid of our models falling apart because that is when it helps for real.

In conclusion, our questions in studying neural control of movements should be focused on examining ‘what we *actually* do’ on the basis of understanding ‘what we *can* do’, not ‘what we *ought to* do’.

APPENDIX A

EXTENDING MUSCLE FEASIBLE RANGE ANALYSIS TO DYNAMIC TASK OF HUMAN WALKING

This chapter was submitted to the *Journal of Biomechanics* and is currently in review.

Simpson CS, Sohn MH, Allen JL, and Ting LH. Muscle feasible ranges in human walking are unconstrained by biomechanics. *J Biomech* (in review)

Although it is possible to produce the same movement using an infinite number of different muscle activation patterns owing to musculoskeletal redundancy, both biomechanical and neural mechanisms may also impose limits on the possible variations in muscle activity observed during movements. However, the extent to which biomechanics allow for variations in muscle activation patterns has not been explicitly characterized for dynamic motor tasks such as walking. Therefore the degree to which observed experimental variability reflects neural versus biomechanical constraints in walking is not known. Here, we examined the range of biomechanically permitted muscle activations in human walking by identifying muscle feasible ranges using a detailed musculoskeletal model combined with experimentally observed kinematics and kinetics. Muscle feasible ranges were computed at each time point by performing optimizations on a linear equation mapping muscle activations to required joint torques. Our results demonstrate that biomechanics are insufficient to constrain muscle activation patterns for walking; more than 72% of muscles had muscle feasible ranges of greater than 95% of the total range for more than 95% of the gait cycle during walking. Comparison with electromyography data revealed that experimental variability in muscle activation

patterns was much less than that permitted by the biomechanics, suggesting the influence of common neural strategies. Muscle feasible ranges may provide a useful way to compare different neural strategies for movement in both healthy and motor impaired individuals.

A.1 Introduction

The biomechanical constraints of a task imposes limitations on feasible motor patterns for movement, but at the same time, musculoskeletal redundancy (Bernstein 1967) allows for an infinite number of combinations of muscle activation patterns for performing a given task. Neuromotor systems are also thought to have preferred structures in the patterning of movements and yet are highly flexible and capable of producing a wide range of motor patterns. Accordingly, while common features of motor patterns are observed in many motor tasks such as walking, variability both within and across individuals is also a feature of biological movement (Liu et al. 2008; van der Krogt et al. 2012; Winter and Yack 1987). Currently, we lack tools to interpret whether experimentally observed variability results from neural versus biomechanical constraints.

Current modeling approaches typically assume an optimization criterion as a proxy for neural constraints of muscle activation, but these cannot explain experimentally observed variations in muscle activation. Typically, a single set of muscle activations is selected from the entire range of possible solutions using physiologically based criteria, such as minimizing muscle stress (Crowninshield and Brand 1981; Thelen et al. 2003). Optimal muscle activation solutions frequently deviate from experimentally recorded patterns (Buchanan and Shreeve 1996; Liu et al. 2008; van der Krogt et al. 2012). It has been suggested that deviation of optimal solutions from experimental data is due to differences in body morphology and biomechanics (Buchanan and Shreeve 1996; Kutch and Valero-Cuevas 2011). However, biomechanical constraints do not appear to

adequately resolve redundancy, as improved matches to measured data can be achieved by adding neural constraints on muscle activation patterns (McKay and Ting 2008; 2012; Walter et al. 2014).

In order to better understand the role that biomechanical versus neural constraints play in shaping muscle activation patterns for movement, the full range of possible muscle activation patterns based on biomechanics must first be defined. For instance, in situations where the range defined by biomechanical constraints is commensurate with observed variability, neural strategy likely has little influence in determining muscle activation. If biomechanical models allow considerably more variability than is exhibited in recorded data, a neural strategy may be the factor constraining the variability. However, the level of model complexity also affects the degree of biomechanical redundancy. For example, Kutch and Valero-Cuevas (2011) demonstrated a limited range of possible muscle activation patterns during finger force production in a 4 degrees of freedom (DoF) model with 7 muscles, suggesting that biomechanics largely defines observed muscle activation pattern. Similarly, using a simplified planar leg model with 14 muscles and three DOF they also demonstrated that loss of a single muscle would greatly reduce force production capabilities of the leg. In contrast, using more detailed musculoskeletal models both Martelli et al. (2013) and Sohn et al. (2013) have demonstrated very wide feasible solution spaces in early stance during human walking (10 DoFs, 82 muscles) and in a model of isometric force production in the cat hindlimb (7 DoFs, 31 muscles). This suggests that in the human leg, biomechanics allow a great deal of variability in choosing muscle activation patterns. However it is not known whether similar variability extends to a dynamic task such as walking.

Here, our goal was to extend the methods of Sohn et al. (2013) to a dynamic task, to define the range of feasible muscle activation patterns during a full gait cycle of human walking. Previous studies of muscle feasible ranges examined isometric force productions, except Martelli (2013), where only a single timepoint in the gait cycle was

examined and the full range of activation was not explicitly found. We identified muscle feasible ranges during human walking using experimental data (John et al. 2013) and a detailed musculoskeletal model of the human lower extremity with 23 DoF and 92 muscles (Delp et al. 2007; Delp et al. 1990). We extended Sohn's (2013) method such that each time point in the gait cycle was treated as an independent optimization problem where muscle activation patterns were identified to satisfy dynamic equilibrium (Anderson and Pandy 2001b). The upper and lower bounds on muscle activation, defining the muscle feasible ranges, were identified for each muscle at each time point and were compared to experimentally recorded electromyographic (EMG) data reported in literature (Perry 1992; van der Krogt et al. 2012).

A.2 Methods

A.2.1 Experimental data

We used experimental kinematic and ground reaction force data (Fig. A.1) of a single subject (male; height, 1.83 m; body mass, 65.9 kg) walking at self-selected speed (1.36 m/s) on an instrumented treadmill as inputs to the muscle feasible range analyses. This data is publically available at <https://simtk.org/home/muscleprops> (John et al. 2013).

A.2.2 Extraction of parameters from walking simulation

Parameters required to calculate the biomechanical constraints (Fig. A.1, model outputs) that define the task, i.e. required joint torques and force-producing capability of muscles were extracted from a three-dimensional OpenSim musculoskeletal model of the human lower extremity with 23 DoF and 92 musculotendon actuators. Built-in OpenSim tools were used to scale the model to match subject anthropometrics (Scale Tool), calculate joint angles (Inverse Kinematics Tool, Fig. A.2B), and joint torques (Inverse

Dynamics Tool, Fig. A.2C). Musculotendon lengths and moment arms, R , were extracted based on the motion from inverse kinematics analysis. Additional muscle parameters such as optimal fiber length and maximum isometric muscle forces required in computing muscle force capabilities were extracted directly from the model file.

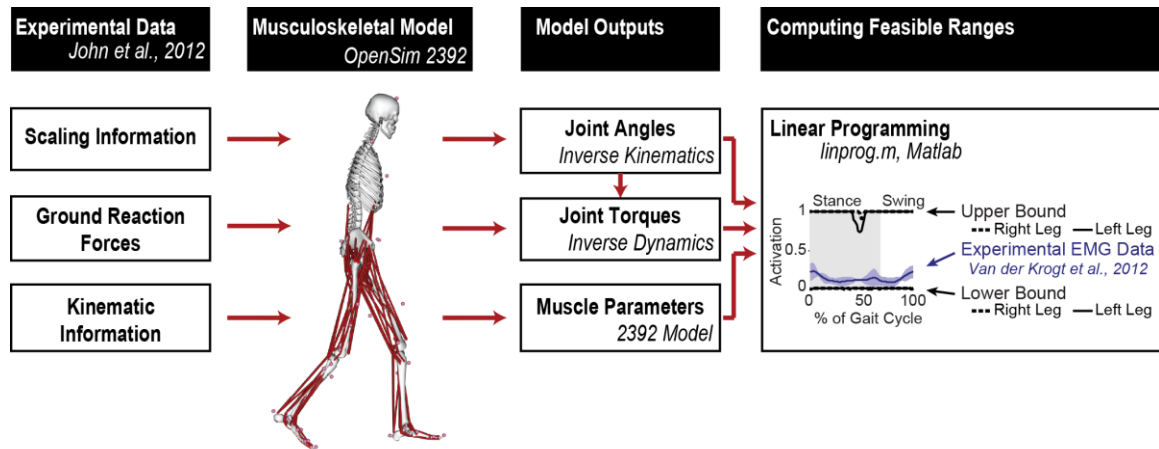


Figure A.1: Schematic of methods used to identify feasible ranges of muscle activation during walking. Experimental data from John et al. (2012) was fed into an OpenSim human lower limb musculoskeletal model with 23 degrees of freedom and 92 muscles (Delp et al., 1990, 2007). Native OpenSim tools (Inverse Kinematics and Inverse Dynamics) were used to calculate joint angles and torques as well as to define additional properties necessary to compute muscle force production capabilities. Feasible ranges were then computed using linear programming (linprog.m) in Matlab. Experimental EMG data (van der Krogt et al., 2012) was superimposed onto the feasible ranges for available muscles.

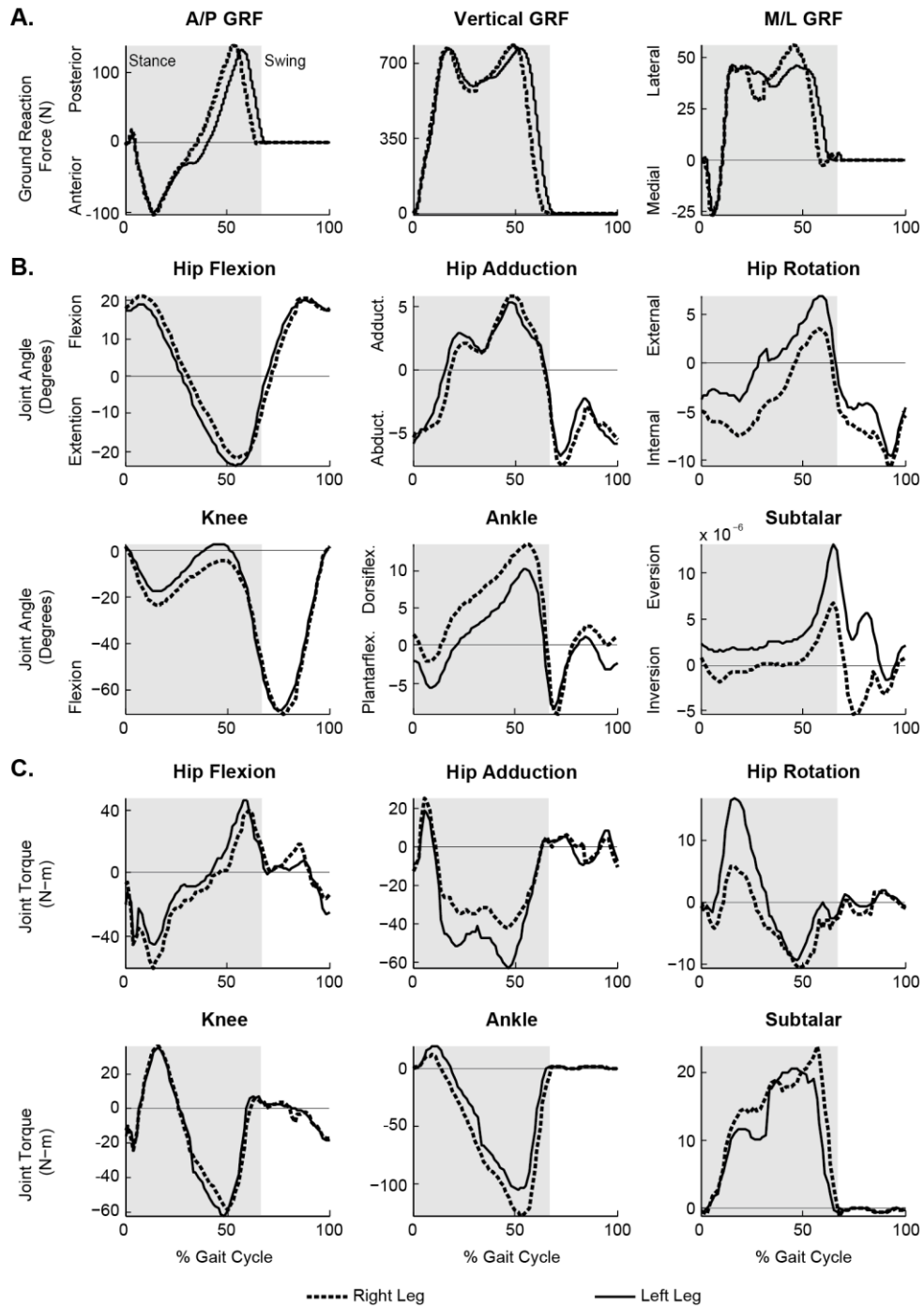


Figure A.2: Experimental data used for computing feasible ranges during walking. (A) Ground reaction forces data for one gait cycle from John et al. (2012) and freely available on www.simtk.org. The shaded grey region indicates the stance phase of the gait cycle. (B) Joint angles computed using the Inverse Kinematics Tool in OpenSim using marker data from John et al. (2012). Joint angles were used for computing kinematic properties of muscles, i.e. force-length and force-velocity relationships. (C) Joint torques computed using the Inverse Dynamics Tool in OpenSim with the ground reaction forces shown in A and the joint angles shown in B. These joint torques were used as task requirements for which feasible ranges of muscle activation were identified.

A.2.3 Muscle feasible range calculations

A linear mapping was defined between muscle activations (e) and joint torques ($\bar{\tau}$) required to produce the dynamic task:

$$\mathbf{R}[\bar{q}(T)] \cdot \mathbf{AMF}[\bar{q}(T), \dot{\bar{q}}(T)] \cdot \bar{e}(T) = \bar{\tau}(T) - \mathbf{R}[\bar{q}(T)] \cdot \mathbf{PMF}[\bar{q}(T)] \quad (\text{A.1})$$

where \mathbf{R} is the moment arm matrix dependent on joint angle, \mathbf{AMF} is the active muscle force contribution (maximum isometric force scaled using the active force length and fiber velocity curves), and \mathbf{PMF} is the passive muscle force (muscle stretch) contribution. Both \mathbf{AMF} and \mathbf{PMF} were computed according to the force-length and force-velocity relationships in a Hill-type muscle model (Thelen 2003). The tendons were assumed to be inelastic (Zajac and Gordon 1989).

Muscle feasible ranges were computed for each leg at each discretized time point for two complete gait cycles (one cycle for each leg; 1.2 seconds at 72 Hz). Linear optimizations were performed using the `linprog.m` function in Matlab on the equation mapping muscle activations (\bar{e}) to joint torque requirements ($\bar{\tau}$). For each muscle and each time point, the lower (e_M^{LB}) and upper (e_M^{UB}) bounds of muscle activation were identified as follows (Sohn et al., 2013):

e_M^{LB} : Find \bar{e} such that $|e_M|$ is minimized, while

$$\mathbf{R}[\bar{q}(T)] \cdot \mathbf{AMF}[\bar{q}(T), \dot{\bar{q}}(T)] \cdot \bar{e}(T) = \bar{\tau}(T) - \mathbf{R}[\bar{q}(T)] \cdot \mathbf{PMF}[\bar{q}(T)]$$

e_M^{UB} : Find \bar{e} such that $|e_M|$ is maximized, while

$$\mathbf{R}[\bar{q}(T)] \cdot \mathbf{AMF}[\bar{q}(T), \dot{\bar{q}}(T)] \cdot \bar{e}(T) = \bar{\tau}(T) - \mathbf{R}[\bar{q}(T)] \cdot \mathbf{PMF}[\bar{q}(T)] \quad (\text{A.2})$$

while satisfying the constraint: $0 \leq e^M \leq 1$. While muscle feasible ranges were calculated for all 92 musculotendon units in the musculoskeletal model, only the 86 musculotendon units of the legs were examined.

A.2.4 Analysis

Each muscle was classified as “necessary” or “optional” and “limited” or “unlimited” based on the characteristics of the lower and upper bounds, respectively. If a muscle exhibited lower bounds greater than “zero” (i.e. 10^{-8} , which was the resolution of the optimization software) at any point, that muscle was required to be active in order to satisfy the dynamics of the system and was therefore classified as “necessary” to perform the action. “Optional” muscles exhibited lower bounds close to zero ($<10^{-8}$) at every time point. In the case that a muscle exhibited upper bounds less than “one” (i.e. $1-10^{-8}$), that muscle was constrained to produce less than its maximal force and was therefore classified as “limited” rather than “unlimited”.

A.2.5 Comparison to experimental muscle activity

Constraints on muscle activations were compared between time points when each muscle was active versus inactive. Each muscle was classified as “active” or “inactive” at every time point based on previously published normative human walking data (Perry 1992). The upper bounds during time points when each muscle was classified as active were compared with upper bounds during time points when each muscle was classified as inactive. This comparison was performed using single-tailed two-sample t-tests with 95% confidence levels to examine whether differences in muscle recruitment by the nervous system correspond to changes in biomechanically dictated constraints on muscle activations.

To examine the explicit range defined by biomechanical constraints with respect to observed variability in experimental muscle activity, the computed muscle feasible ranges were superimposed on experimental EMG data. Since EMG data was not available for the subject from whom the kinetic, kinematic, and scaling data came, normative EMGs were taken from another study. That study consisted of 5 healthy subjects aged 16 ± 1 years that weighed 68 ± 5 kg and were 175 ± 9 cm tall walking at self-

selected speed (1.08 ± 0.16 m/s) (van der Krogt et al. 2012). To estimate the relative level of muscle activation recorded, EMG data was scaled to the peak value from the simulated muscle activity identified using the computed muscle control algorithm in OpenSim (Thelen and Anderson 2006).

A.3 Results

A.3.1 Muscle feasible ranges

We found that most muscles were not restrained in their muscle feasible ranges based on biomechanical constraints of the limb and the torque requirements during walking (Fig. A.3). Seventy-three percent (63 out of 86) of muscles had fully unconstrained muscle feasible ranges with upper bounds of 1 and lower bounds of 0 for the entire gait cycle. Differences in the kinematics and kinetics (Fig. A.2) between the two legs resulted in slightly different muscle feasible ranges between legs in some muscles (Fig. A.3). Overall, the muscle feasible ranges in the right leg were found to be larger than those of the left leg.

Almost no muscles were “necessary”, defined as having non-zero lower bound (Fig. A.3, lower traces). All muscles in the right leg had a lower bound of zero throughout the gait cycle (Fig. A.3, lower traces with dotted lines). Only two left-leg muscles, the tibialis anterior (TA) and the anterior compartment of gluteus medius (GMED1), had non-zero lower bounds at some point during the gait cycle (Fig. A.3, lower traces with solid lines). The left TA was necessary shortly after the initiation of stance, consistent with controlling the descent of the toe. The left GMED1 was necessary at 50% of the gait cycle, where the hip abduction torque in late stance was also larger in the left leg (Fig. A.2C, dotted versus solid line). However, the GMED has not typically been reported to be active (Fig. A.3, red lines) in gait during late stance.



Figure A.3: Computed upper and lower bounds of the feasible ranges of muscle activation as a function of the gait cycle for all 43 muscles of the two legs in the OpenSim 2392 musculoskeletal model. Red lines plotted above select plots indicate when muscles are known to be active during gait from normative data (Perry, 1992). The shaded grey region indicates the stance phase of the gait cycle. The feasible ranges are all of the activations bounded by the upper and lower bounds. Feasible ranges were generally very wide, showing that muscle activation is virtually unconstrained by biomechanical considerations.

Overall, 73% (63 out of 86) of muscles were “unlimited” in their feasible level of activity, i.e. have an upper bound (Fig. A.3, upper traces) of 1, at every time point in the gait cycle. Several muscles with action about the hip were limited in their upper bounds in late stance phase, e.g. gluteus maximus (GMAX) and gluteus medius (GMED), but never in swing phase. Several ankle plantarflexors, e.g. medial gastrocnemius (MG) and lateral gastrocnemius (LG), were also constrained in early stance and late swing phase. The soleus (SOL), the strongest muscle in the model, was the most limited muscle.

A.3.2 Comparison to experimental data

Overall, 44% (8 out of 18) of “limited” muscles had smaller upper bounds when they are typically inactive. For example, upper bounds on GMED3 were higher when it is typically active (early stance, Fig. A.3, red bars) than when it is inactive (late stance). Only 11% (2 out of 18, the left LG and the left ADL) of “limited” muscles were found to have lower upper bounds when they are typically active than when they are inactive.

Comparing the muscle feasible ranges with sample experimental EMG data revealed that the observed variability is much smaller than the identified muscle feasible range based on biomechanical considerations (Fig. A.4).

A.4 Discussion

Our results demonstrate that instantaneous biomechanical constraints are not sufficient to define the muscle activation patterns during human walking in healthy individuals. Based on musculoskeletal properties and joint torque requirements, we identified muscle feasible ranges that define the possible solution space from which the nervous system can select muscle activation patterns. The largely unconstrained muscle feasible ranges indicate a large degree of musculoskeletal redundancy during healthy

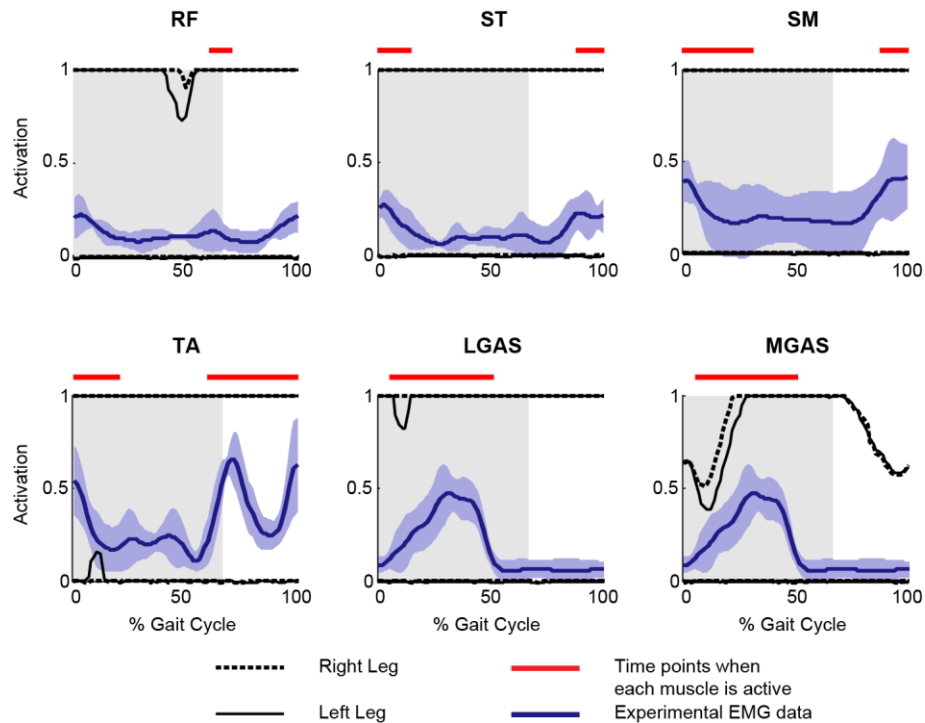


Figure A.4: Computed upper and lower bounds of feasible ranges of muscle activation as a function of the gait cycle with experimental EMG data (Van der Krogt et al., 2012) superimposed. Red lines plotted above select plots indicate when muscles are known to be active during gait from normative data (Perry, 1992). The shaded grey region indicates the stance phase of the gait cycle. The variability of EMG data is much less than that permitted by biomechanically determined feasible ranges.

human walking, suggesting a wide range of allowable variability in muscle activation patterns. However, observed variability in muscle activation patterns was more limited than the muscle feasible ranges, revealing the influence of neural constraints on motor variability. Muscle feasible ranges may be a useful tool for examining the effects of musculoskeletal and neurological impairments on feasible motor patterns for movement.

Here, we extend the computation of muscle feasible range methods developed by Sohn et al. (2013) for static force production to dynamic tasks by including the effects of inertial and velocity-dependent forces. Our analysis was posed as a linear programming problem independently for each muscle at each time point in the gait cycle using joint torque requirements from inverse dynamics computations. While this method does not account for muscle activation dynamics, prior work has demonstrated that independent

static optimization at each time point produces similar results to dynamic optimization in sub-maximal tasks such as human walking (Anderson and Pandy 2001b). Our linear programming method can be applied to more complex systems than methods relying on computational geometry that are limited to small muscle sets (Kutch and Valero-Cuevas 2011). Further, linear programming also identifies the extrema of the muscle feasible ranges, which is not guaranteed in Monte Carlo methods (Martelli et al. 2013).

In a complex model of human walking, we found virtually no limitations on muscle activation, suggesting a great deal of robustness to variation in motor patterns. Prior experiments on cadaveric human hands have demonstrated limited robustness to muscle weakness that suggests very little musculoskeletal redundancy (Kutch and Valero-Cuevas 2011; Valero-Cuevas and Hentz 2002). However, simulations of healthy subjects in normal gait showed surprising robustness to muscle weakness, suggesting ample redundancy (van der Krogt et al. 2012). The wide muscle feasible ranges suggest that almost any deviation from an optimal solution is likely feasible (Buchanan and Shreeve 1996; Liu et al. 2008; van der Krogt et al. 2012), to the point that individual muscles can be completely silenced in walking without reducing the ability to meet the biomechanical demands of the task.

The lower bound of the muscle feasible range shows the minimum activation and by extension, the minimum strength permissible for each individual muscle to complete the simulation. Other methods have examined musculoskeletal redundancy using trial and error methods of weakening or eliminating muscles or muscle groups to show whether deficits in task performance occur (Arnold et al. 2005; Correa et al. 2012; Steele et al. 2012b; van der Krogt et al. 2012). Further, whereas these studies still use a muscle activation pattern from computed muscle control (CMC) optimizations (Crowninshield and Brand 1981; Thelen et al. 2003) to identify an optimal compensation for muscle weakness, the muscle feasible range identifies the possible variability in such compensations.

We recognize that possible variations in muscle activity identified using muscle feasible ranges do not allow for the dynamics of the system to be altered. For example, muscle weakening or neural constraints might alter kinematics or motor control strategies, which could not be investigated using our approach. Optimal control models that simulate human walking (Ackermann and van den Bogert 2010; Anderson and Pandy 2001a) could be used to identify changes in the dynamics of walking due to muscle weakness, but also rely on a relevant objective function to identify a single muscle activation pattern from among many. Considerable advances in computational methods are necessary to combine muscle feasible range analyses with dynamic optimization. However, it is likely that even more latitude in muscle activation patterns would be revealed due to the ability of the model to select dynamics most suitable to its force producing capabilities.

We explicitly sought to identify the muscle feasible ranges for muscle activation in the absence of any neural constraints on muscle activation as a basis to understand the degree to which neural constraints could influence muscle activation patterns. Further reductions in muscle feasible ranges would be predicted by grouping muscles to assume a common neural drive, as it would eliminate compensation within synergistic muscle groups. Muscle feasible ranges could be further narrowed by including additional neurally-inspired constraints to the muscle feasible range optimizations such as modular activation of multiple muscles across different joints (Ivanenko et al. 2004; Ting and Macpherson 2005), generalizability of muscle patterns across tasks (Chvatal et al. 2011; Torres-Oviedo et al. 2006; Torres-Oviedo and Ting 2010; Walter et al. 2014), multiple task constraints (Keenan et al. 2009; Racz et al. 2012), or stability considerations (Bunderson et al. 2008). Identifying muscle feasible ranges may thus provide an important foundation for understanding actual and possible variations in motor patterns in both healthy and impaired populations.

Table A.1: Muscles included in the OpenSim 2392 musculoskeletal model and their abbreviations.

<u>Name</u>	<u>Abbreviation</u>	<u>Name</u>	<u>Abbreviation</u>
<i>Adductor brevis</i>	ADB	<i>Peroneus brevis</i>	PB
<i>Adductor longus</i>	ADL	<i>Peroneus longus</i>	PL
<i>Adductor magnus</i>	ADM	<i>Peroneus tertius</i>	PT
<i>Biceps femoris long head</i>	BFLH	<i>Piriformis</i>	PIR
<i>Biceps femoris short head</i>	BFSH	<i>Iliopsoas</i>	PSOAS
<i>Extensor digitorum</i>	ED	<i>Quadratus femoris</i>	QF
<i>Extensor hallucis</i>	EH	<i>Rectus femoris</i>	RF
<i>Flexor digitorum</i>	FD	<i>Sartorius</i>	SAR
<i>Flexor hallucis</i>	FH	<i>Semimembranosus</i>	SM
<i>Gemellus</i>	GEM	<i>Soleus</i>	SOL
<i>Gluteus maximus</i>	GMAX	<i>Semitendinosus</i>	ST
<i>Gluteus medius</i>	GMED	<i>Tibialis anterior</i>	TA
<i>Gluteus minimus</i>	GMIN	<i>Tibialis posterior</i>	TP
<i>Gracilis</i>	GRAC	<i>Tensor fasciae latae</i>	TFL
<i>Iliacus</i>	ILI	<i>Vastus intermedius</i>	VI
<i>Lateral gastrocnemius</i>	LG	<i>Vastus lateralis</i>	VL
<i>Medial gastrocnemius</i>	MG	<i>Vastus medialis</i>	VM
<i>Pectineus</i>	PEC		

APPENDIX B

APPLICATION TO IMPAIRED MOTOR CONTROL:

EXAMPLES IN STROKE AND IN AMPUTEES

Here, I present preliminary works showing how the modeling framework developed in this thesis can be used for understanding impaired motor control by considering altered biomechanical and neural constraints. I illustrate this with two specific examples. First, I consider a pathological neural constraint of abnormal co-activation typically observed in individuals following stroke and examine how it affects feasible range in muscle space and biomechanical output space. Second, I consider biomechanical impairment owing to transtibial amputation in the lower limb and examine its effect on feasible range in muscle space and biomechanical output space. Thorough investigation is needed to develop each of these examples to an independent study. Nevertheless, they serve as examples that demonstrate the possible utility of our modeling framework applied in compensated systems with neuromuscular impairments.

B.1 Imposing clinical synergy of shoulder and elbow muscles in stroke

B.1.1 Background and motivation

The ability to properly recruit and coordinate muscles determines performance and set of possible solutions that can be used in functional motor task. In stroke survivors, abnormal co-activation across shoulder and elbow muscles and thus coupling of torque across these joints is commonly observed (Dewald and Beer 2001; Dewald et al. 1995). Such *clinical synergy* typically involves coupling of elbow flexion with shoulder abduction-extension-external rotation, and to a lesser extent, coupling of elbow

extension with shoulder adduction-flexion-internal rotation (Brunnström 1970). Impaired function due to this abnormal coupling is most evident in difficulty in anti-gravitational torque generation during isometric (Ellis et al. 2007) or reaching tasks (Beer et al. 2004; Reisman and Scholz 2006; Sukal et al. 2007).

Muscle weakness may be a potential contributor for clinical synergy in stroke patients (Beer et al. 2007). Such biomechanical alteration can be reflected in task or output space (Kuo and Zajac 1993; Valero-Cuevas 2000; Valero-Cuevas et al. 1998). For example, elimination of particular muscles may affect the feasible set of endpoint forces to large extent (Kutch and Valero-Cuevas, 2011). On the other hand, biomechanical limiting factor from muscle weakening can also affect muscle activation space for a given task, mainly demanding altered coordination in other muscles as a compensation (McCrea et al. 2005; Steele et al. 2012b; van der Krogt et al. 2012).

However, clinical synergy itself as a pathological neural constraint can affect both biomechanical output space as well as muscle activation space. Abnormal coupling of muscles following stroke may attributed as a neural constraint, emerging from altered descending pathways such as corticospinal tract due to lesion (Dawes et al. 2008; Stinear et al. 2007; Ward et al. 2006). It has been shown that functional neural constraint of synchronous activation of groups of muscles reduces the range in motor output space, which more closely resembled physiological behavior than when muscles are activated independently (McKay and Ting 2008; 2012). Likewise, pathological neural constraint of abnormal muscle co-activation is likely to affect the biomechanically feasible motor outputs as wells as muscle activation space (Wang and Gutierrez-Farewik 2014).

Here, I investigated how abnormal coupling of shoulder and elbow muscles activation affect the range of feasible endpoint forces that can be produced in the human arm as well as feasible ranges in activation levels muscles (Sohn et al. 2013). I hypothesized that abnormal coupling of shoulder and elbow muscles limits the maximum force that can be produced in a given direction, and restricts feasible ranges of activation

in other muscles for given task. As a proof of concept, I tested this hypothesis by imposing a co-activation constraint across subset of muscles involved in clinical synergy, and examining the resulting maximum feasible forces and feasible ranges of activations in muscles compared to a control case where all muscles were independently controlled.

B.1.2 Approach

I used an existing detailed musculoskeletal model of human upper extremity (Holzbaur et al. 2005), which was modified (Steele et al. 2013) to reflect experimental conditions in Roh et al., (2012; 2013), where wrist joint movement was restrained. Briefly, the model had 4 degrees of freedom (DoF) at the anatomical joints of shoulder (3 DoF: shoulder elevation, flexion/extension, internal/external rotation) and elbow (1 DoF: flexion/extension), controlled by 30 muscles (Table B.1). The posture of the model, however, was matched to resemble a different experimental setup (Trumbower et al. 2010): 70° shoulder elevation, 50° shoulder flexion, 90° elbow flexion (Fig. B.1). This setup explicitly provided specified posture in accordance to the DoFs defined in the model, and did not required further inverse kinematic analysis. The torso was fixed to the ground where the endpoint was defined approximately at the 5th metacarpophalangeal joint in the model (Liao et al. 2013).

In particular, 8 muscles were considered to be involved in clinical synergy as reported in literature (Dewald et al. 1995): *anterior deltoid* (DEL_{ANT}), *medial deltoid* (DEL_{MED}), *posterior deltoid* (DEL_{POST}), clavicular head of *pectoralis* ($PECM_{CLAV}$), *triceps long head* (TRI_{LONG}), *biceps brachii longhead* (BIC_{LONG}), *brachioradialis* (BRD), and *pronator teres* (PT). The clinical synergy constraint was simply implemented by having muscles within a clinical synergy group to be activated with single control value, while rest of the muscles were left to be independently activated. Although coupling was most evident for shoulder abductors/adductors with elbow flexors/extensors in the

experimental data, I tested 14 different combinations which ranged from a group only involving a muscle pair that showed significant co-variation in the experiments (e.g. and DEL_{ANT} and BIC_{LONG}) to an extreme case where all 8 muscles were included as a group.

The task was defined simply to produce isometric endpoint force in 4 orthogonal directions in the horizontal plane: anterior, posterior, medial, and lateral (Fig. B.1, blue arrows). Maximum feasible forces and muscle feasible ranges (MFR) were computed for the control case, where all muscle were assumed to be independently controlled, as described in our previous study (Sohn et al. 2013). In particular, MFR were identified for each target force direction while varying the force magnitude linearly scaled from 0 to the maximum value possible in given direction. Similarly, MFR were identified for the clinical synergy group and remaining muscles across force magnitude.

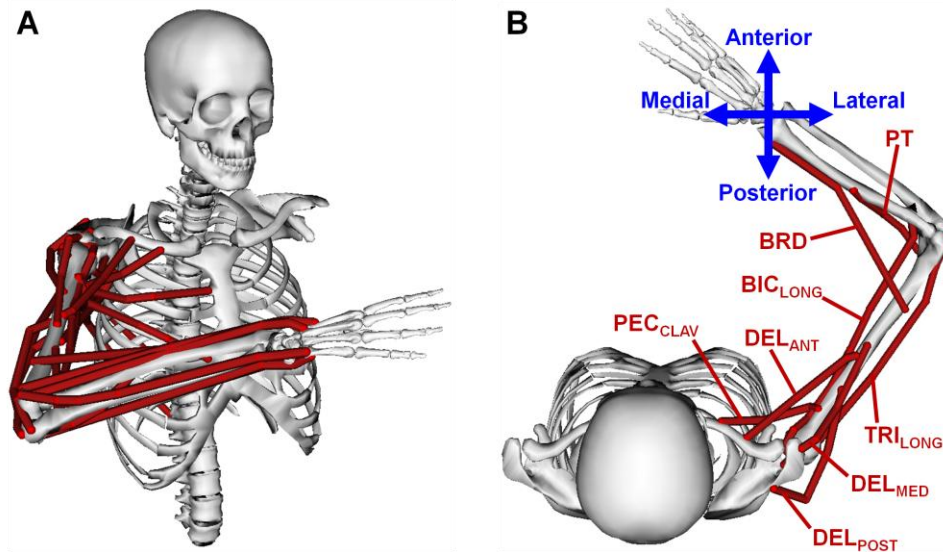


Figure B.1: Model and target force directions. (A) Detailed musculoskeletal model of human upper extremity (Holzbauer et al., 2005) simplified to 4 DoF and 29 muscles (Steele et al., 2013). The posture of the model resembled experimental condition in Trumbower et al., (2010). The torso was fixed to the ground, and the endpoint was defined at the wrist joint which was locked in this simplified model. (B) Target force directions and 8 muscles involved in clinical synergy. The task was defined as isometric endpoint force generation in 4 orthogonal direction in the horizontal plane (blue arrows), for which maximum feasible force and muscle feasible range were computed (Sohn et al., 2013). Only the 8 muscles involved in clinical synergy, reported in Dewald et al., (1995) is shown.

Table B.1: Muscles included in the musculoskeletal model and their abbreviations.

Name	Abbreviation	Name	Abbreviation
<i>Anterior deltoid</i>	DELT _{ANT} *	<i>Coracobrachiali</i>	CORB
<i>Medial deltoid</i>	DELT _{MED} *	<i>Triceps long head</i>	TRI _{LONG} *
<i>Posterior deltoid</i>	DELT _{POST} *	<i>Triceps lateral head</i>	TRI _{LAT}
<i>Supraspinatus</i>	SUPSP	<i>Triceps medial head</i>	TRI _{MED}
<i>Infraspinatus</i>	INFSP	<i>Anconeus</i>	ANC
<i>Subscapularis</i>	SUBSC	<i>Supinator</i>	SUP
<i>Teresminor</i>	TMIN	<i>Biceps long head</i>	BIC _{LONG} *
<i>Teresmajor</i>	TMAJ	<i>Biceps short head</i>	BIC _{SHORT}
<i>Pronator teres</i>	PT *	<i>Brachialis</i>	RRA
<i>Pectoralis major clavicular</i>	PECM _{CLAV} *	<i>Brachioradialis</i>	BRD *
<i>Pectoralis major medial</i>	PECM _{MED}	<i>Extensor carpi radialis longus</i>	ECRL
<i>Pectoralis major inferior</i>	PECM _{INF}	<i>Extensor carpi radialis brevis</i>	ECRB
<i>Latissimus dorsi superior</i>	LAT1	<i>Extensor carpi ulnaris</i>	ECU
<i>Latissimus dorsi medial</i>	LAT2	<i>Flexor carpi radialis</i>	FCR
<i>Latissimus dorsi inferior</i>	LAT3	<i>Flexor carpi ulnaris</i>	FCU

*: muscles involved in clinical synergy reported in Dewald et al., (1995)

B.1.3 Findings

In the control case, maximum feasible forces (Fig. B.2, blue arrows) were found to be largest in posterior direction (378.8N) and smallest in the lateral direction (125.2N). This was consistent with experimental observation that lateral force was the weakest direction especially in individuals with stroke (Roh et al., 2012). Across all target force directions, muscle feasible ranges were wide in general, across force magnitudes (Fig. B.2, gray area enveloped with bold black traces). Upper and lower bounds in some muscles did not converge even at maximum force level in particular directions, indicating substantial redundancy even for maximal task. For example, MFR spanned full possible range, from 0 to 1, in anterior and medial directions in muscle SUPSP (Fig. B.2A, top and left), posterior and lateral direction in muscle TRI_{LAT} (Fig. B.2B, bottom and right). This was also in agreement with previous results from cat hindlimb during biomechanically redundant task of isometric force generation (Sohn et al. 2013).

With the *clinical synergy* constraint, both feasible forces and muscle feasible ranges were restricted compared to independently controlled condition (Fig. B.2, red area enveloped with bold red traces). Here, I selected the most restricted case in which all 8 muscles are co-activated as a representative example to illustrate the effect of the clinical synergy constraint; other combinations that may be more relevant physiologically had essentially the same features qualitatively, but was less prominent.

Although maximum feasible force in each target force direction was not computed explicitly, model with clinical synergy constraint could not achieve maximal endpoint force generation in given direction in many cases. For example, lower bound exceeded 1 at sub-maximal level of force in posterior and medial directions in muscle SUPSP (Fig. B.2A, bottom and left), and in posterior and lateral directions in muscle TRI_{LAT} (Fig. B.2B, bottom and right).

A Muscle SUPSP: Feasible Force and Muscle Feasible Range (MFR)

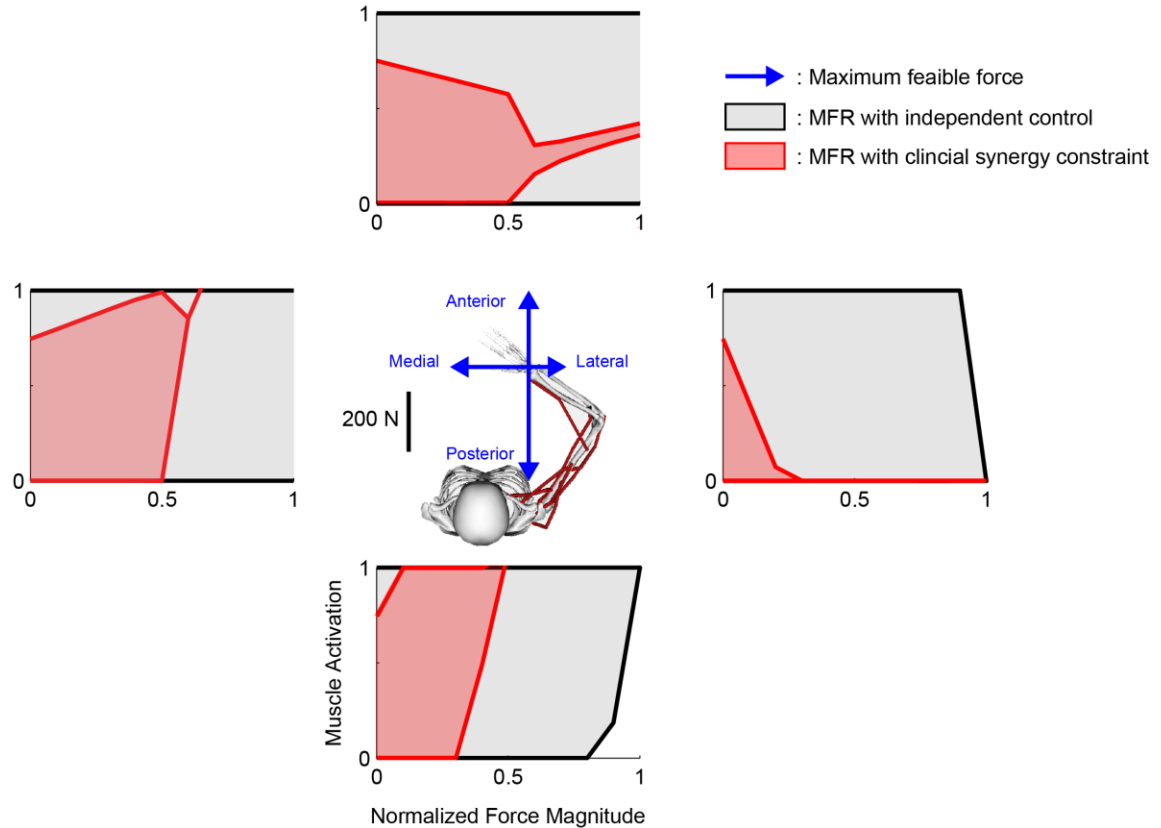


Figure B.2: Feasible force and muscle feasible range (cont. on next page). (A) Muscle SUPSP.

B Muscle TRI_{LAT}: Feasible Force and Muscle Feasible Range (MFR)

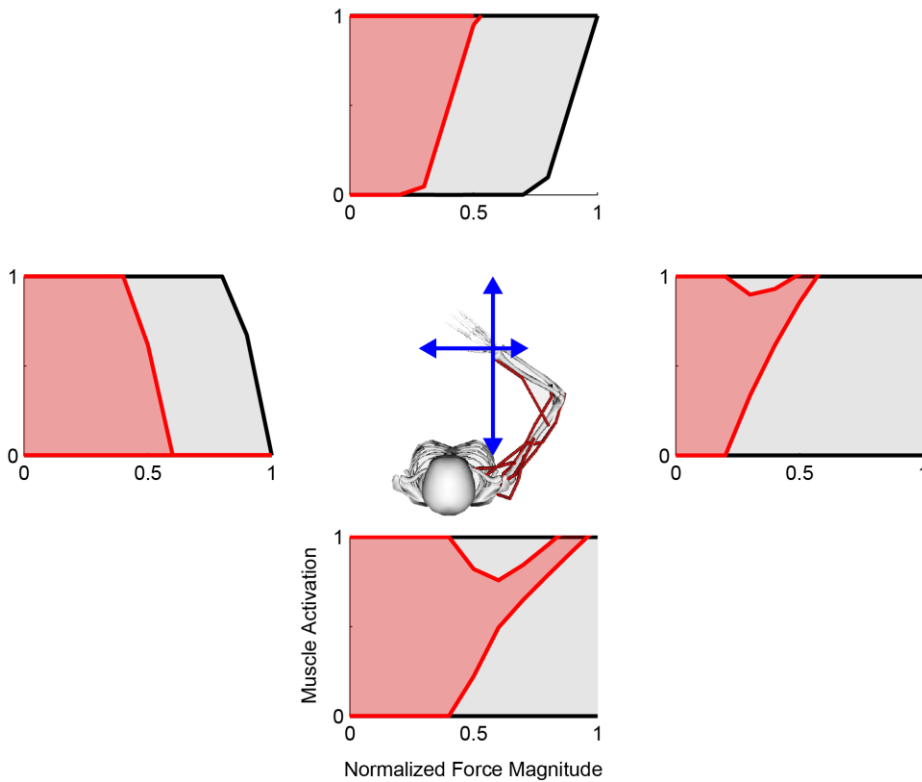


Figure B.2: Feasible force and muscle feasible range (cont. from previous page). (B) muscle TRI_{LAT}. Maximum feasible force in each direction was computed (blue arrows) in the control condition, i.e., independent control. All force levels examined were normalized to this value in each condition. Muscle feasible ranges (MFR) were identified in both control (gray area enveloped with bold black traces) and clinical synergy constraint condition (red area enveloped with bold red traces). Clinical synergy constraint significantly restricted both feasible forces and MFR in muscles that were not included.

Feasible ranges of activation in muscles that were not included in the clinical synergy group became significantly more narrow. Muscles became constrained (smaller upper bound) earlier at low force magnitudes, e.g. in muscle SUPSP (Fig. B.2A, in all directions, upper traces in red). Muscles became necessary (lower bound >0) earlier, e.g. in anterior, posterior, and medial directions in muscle SUPSP (Fig. B.2A, top, bottom, and left, lower traces in red), and in anterior, posterior, and lateral directions in muscle TRI_{LAT} (Fig. B.2B, top, bottom, and right, lower traces in red). However, some muscles such as TRI_{LAT} remained redundant at lower force magnitudes (Fig. B.2B).

Interestingly, clinical synergy constrained the solution space, specifying a pattern, as force magnitude increased. A muscle activation pattern was becoming more uniquely defined towards higher forces force: e.g. in medial direction in muscle SUPSP (Fig. B.2A, top). Sometimes, muscle feasible ranges defined a narrow window showing linear slope as force magnitude increased: e.g. in anterior direction in muscle SUPSP (Fig. B.2A, top), and in posterior and lateral directions in muscle TRI_{LAT} (Fig. B.2B, bottom and right).

B.1.4 Conclusions

In summary, I examined how abnormal co-activation of shoulder and elbow muscles typically observed in stroke affect the feasible force and muscle feasible range during isometric endpoint force generation. Results demonstrated that clinical synergy, or pathological coupling, in feed-forward control of muscles adversely affects the biomechanical capability of the limb and restricts the flexibility of choices by the nervous system.

Muscle feasible ranges were wide in general at lower force levels. It may explain the absence of clinical synergies during muscle synergy analysis for individuals with stroke who performed isometric force generation tasks at low force levels (Roh et al. 2012; Roh et al. 2013). Further, wide range in activation of muscles implies that substantial deviation from any single optimal solution, e.g. minimum-effort (Steele et al. 2013), is possible.

Clinical muscle synergy may constrain the solution space to a “typical” pathological pattern that may impair motor function or have poor functional properties, especially at relatively higher force levels. In contrast, wide ranges in the control case suggest that there may need a neural strategy such as functional muscle synergy (Roh et al. 2012) which might serve to constrain windows for more functionally robust solutions.

By imposing muscle synergy constraint from healthy people, we may define a restricted range of solutions with better functional properties, e.g. efficient and stable.

The approach of identifying muscles feasible ranges using observed coordination as a constraint has further implication to how measured muscle pattern can be used to infer possible variations in unrecorded muscles; practically, not all muscles can be measured in experiments.

B.2 Modeling how amputation limits biomechanical capability of the lower limb

B.2.1 Background and motivation

Physical impairments in the musculoskeletal system such as amputated limb can alter both biomechanical and neural control strategies for functional movement such as balance control or gait (Prinsen et al. 2011; Soares et al. 2009 ; Vrieling et al. 2008; Waters and Mulroy 1999). Despite biomechanical deficiencies, the central nervous system remains intact in individuals with limb loss, and may adapt compensatory control mechanisms. For example, asymmetry in inter-limb coordination often observed in individuals with unilateral transtibial limb loss (TTLL) during gait (Childers and Kogler 2015 (In press); Hak et al. 2014) or reactive balance tasks (Bolger et al. 2014) may be attributed to functional compensation. However, contribution from biomechanical constraints imposed by the prosthesis or missing joint, is not readily distinguishable from experimentally observed behavior, e.g. from kinematics or ground reaction forces.

Musculoskeletal models can be used to dissociate different contributions from biomechanical and neural constraints. In particular, biomechanical capability of the limb in generating endpoint force can be quantified with feasible force set (FFS), which represents a manifold of all possible endpoint force vectors that can be produced (McKay et al. 2007; Valero-Cuevas et al. 1998). By exploring these biomechanically feasible

solutions (FFS) available to able-bodied individuals and individuals with TTLL, we can infer whether asymmetries represent a biomechanical deficit or a neural control strategy.

I hypothesized that “biomechanical constraint alone is insufficient to determine asymmetric inter-limb coordination in individuals with TTLL”. I predict that FFS is larger than the range of experimentally-observed forces during movement. Further implication is that muscle activity during asymmetric inter-limb coordination in individuals with TTLL reflects selected neural control strategies, among many solutions in the redundant muscle activation space. As a first step to testing this hypothesis, I am testing how TTLL may affect the capability of the limb in producing endpoint forces.

B.2.2 Approach

I use a musculoskeletal model of the human leg with 7 degrees of freedom (DoF) and 43 muscles in each leg (described in detail elsewhere), and considered only the right leg. The posture of the model was put to a single static configuration, a slightly flexed posture to avoid singularity. Pelvis was fixed to the ground and endpoint was defined as gimbal joint and was located at the MTP joint.

In a control, *Able-bodied* model (ABLED), MTP joint was discarded to prevent additional constraint imposed by this joint, which had no effect on the endpoint force. In result, ABLED model had 6 DoF and 43 muscles. TTLL was modeled by locking distal DoF beyond the knee (ankle and subtalar joints) and removing the muscles crossing those joints. As a result, the *simulated transtibial limb loss* model (TTLL) had 4 DoF and 33 muscles.

FFS in both models were computed using methods similar to that described in our previous work (Sohn et al., 2013). Maximum feasible force was computed for a given set of desired endpoint force directions: 289 directions uniformly distributed around 3-dimensional unit sphere.

Because of redundancy, muscle activation pattern that produce maximal endpoint force in a given direction is not unique. Therefore, I used 25 different initial conditions for the search: a pattern with all zeros, another pattern with all ones, and 23 random patterns with uniform distribution between 0 and 1. The same set of initial conditions were used for both ABLED and TTLL models. Relative redundancy in each case was examined with the range in activation spanned by converged solutions.

B.2.3 Findings

The biomechanical capability of the lower limb in isometric endpoint force generation was limited particularly in leg extension in TTLL (Fig. B.3B, downward).

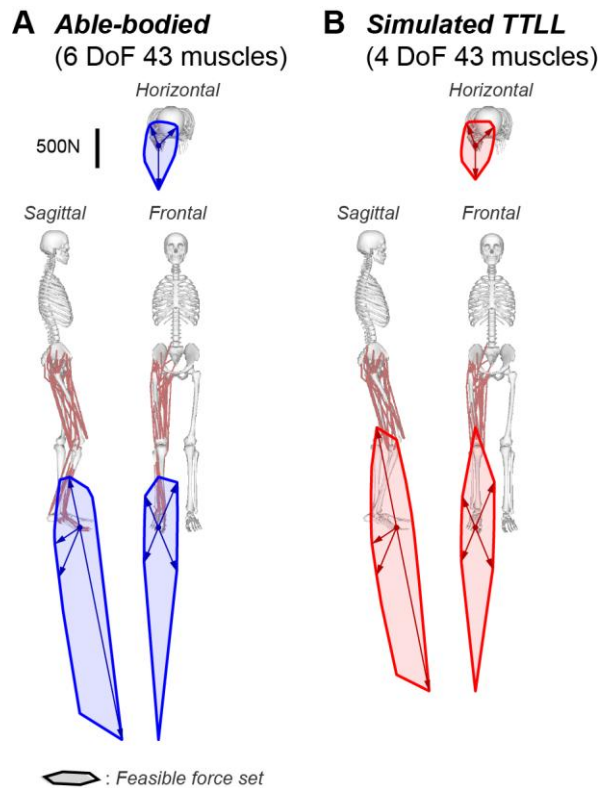


Figure B.3: FFS in ABLED and TTLL. FFSs in ABLED and TTLL showing maximum isometric forces that can be produced in 3D directions by (A) an able-bodied model and (B) a model with simulated TTLL. Compared to ABLED model, TTLL models could produce lesser extensor force, and higher flexor force. Shear forces in the horizontal plane were similar. Arrows indicate maximum feasible force vectors in few example target directions (out of 289 uniformly distributed directions) in horizontal (top), sagittal (bottom left), and frontal (bottom right) planes.

The FFS in ABLED (Fig. B.3A) was qualitatively similar to previous model predictions (Gruben et al. 2003; Kutch and Valero-Cuevas 2011; Schmidt et al. 2003). The decrease in ability to produce extensor force in TTLL is likely due to absence of ankle joint.

Interestingly, however, the TTLL model could produce greater flexion force (Fig. B.3B, upward direction), which is likely due to less stringent constraint from the joint torque requirement with smaller number of DoF. Subtle differences were found in capability of the limb in producing shear forces, i.e., forces in the horizontal plane (Fig. B.3, top). Different initial conditions resulted in essentially the same maximal force in most directions for the FFS in both ABLED and TTLL model (Fig. B.3).

In general, redundancy in muscle space at maximum feasible force levels was relatively greater in ABLED (Fig. B.4, left column) than TTLL (Fig. B.4, right column)

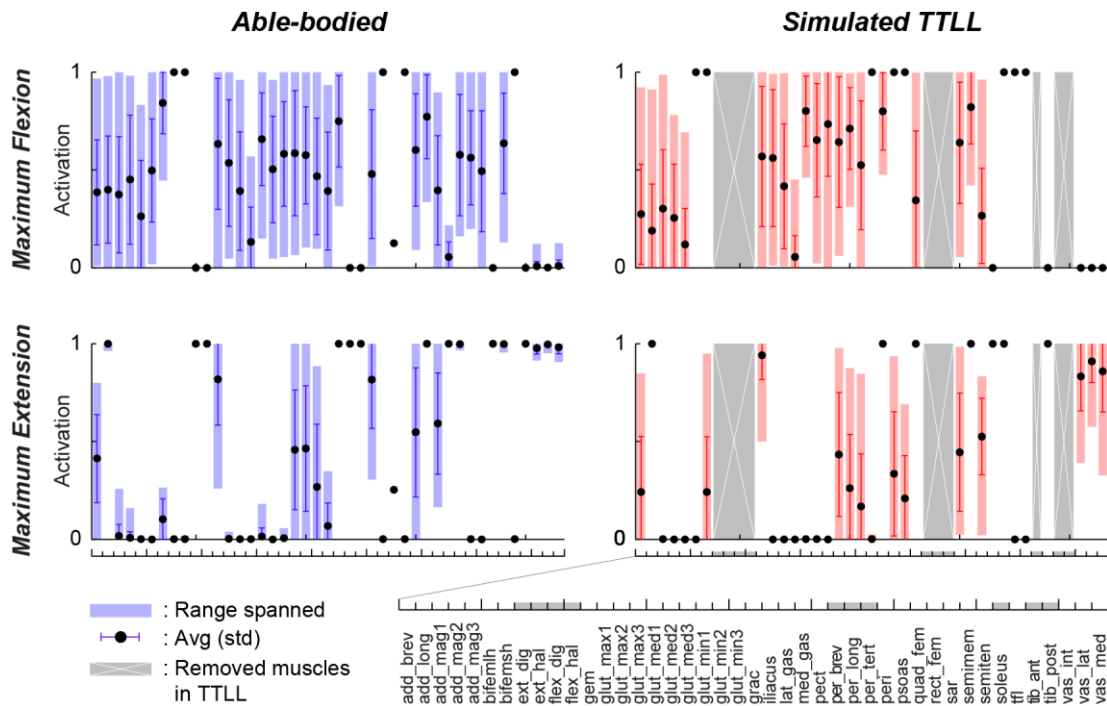


Figure B.4: Redundancy in muscle space. Range spanned by converged solutions in ABLED (left) and TTLL (right) model, starting from the same set of random initial conditions, for maximum flexion (top) and extension (bottom) directions. Filled boxes show the range spanned by activation levels of each muscle in 25 random initial patterns, whereas dots and bars represent average and standard deviations, respectively. Gray bars indicate eliminated muscles in TTLL. In general, ABLED model had relatively greater redundancy in muscle activation space than TTLL.

model. For example, range spanned by converged solutions from the same set of 25 random initial conditions were wider in most muscles for maximum flexion (Fig. B.4, first row) and extension (Fig. B.4, second row) force directions.

B.2.4 Conclusions

Results show that biomechanical capability of the limb as represented by FFS is decreased in extension force direction and increased in flexion force direction. This results merely reflects mechanical actions of muscles with respect to the joints that it cross, which were different in the two conditions: able-bodied (ABLED) and with trans-tibial limb loss (TTLL).

However, many evidence points to possibility of active neural intervention in asymmetric inter-limb coordination in TTLL. Subtle difference between ABLED and TTLL in feasible horizontal plane forces directions suggests that restricted range of force directions used on the prosthetic side in TTLL during balance (Bolger et al. 2014) reflects a neural control strategy. In addition, limited potential in producing extensor force in TTLL also implies that neural compensation is required in tasks involving bilateral leg extension such as rowing or weightlifting (Howard and Enoka 1991; Schantz et al. 1989; Secher et al. 1988). Further, redundancy in muscle activation space even for maximal force tasks grants ample room for the intact nervous system consider multiple functional criteria relevant to the task-level goal (McKay and Ting 2012).

Understanding the possible dissociation of neural and biomechanical asymmetries in unilateral TTLL has great implication for developing rehabilitation strategies, challenging the conventional rehabilitation, which had focused mostly on “recovering” symmetry (Hassid et al. 1997; Hesse et al. 2013; Mauritz 2002).

APPENDIX C

TECHNICAL NOTE ON ESTIMATING STATE MATRIX

This chapter was originally published as an internal document in Neuromechanics lab, Georgia Institute of Technology.

Sohn MH and McKay JL. Muscle pattern optimization via estimated system state matrices to save computation time in the cat hindlimb model, 2011.

This document was partially included as a section in the published journal article in *International Journal for Numerical Methods in Biomedical Engineering*.

Bunderson NE, Bingham JT, Sohn MH, Ting LH, and Burkholder TJ. Neuromechanic: a computational platform for simulation and analysis of the neural control of movement. *Int J Numer Method Biomed Eng* 28: 1015-1027, 2012.

C.1 Introduction

This document describes a computational shortcut that saves time in searching for muscle activation patterns in the cat hindlimb model (Bunderson et al. 2010) that minimize criteria derived from the linearized system state matrix. In particular, we would like to identify muscle patterns in the model that optimize criteria related to limb stability, as quantified with the eigenvalues of the state matrix, while also producing a given force vector at the endpoint.

Calculating the linearized system state matrix at every optimization step within NEUROMECHANIC would require substantial computational overhead. However, this would require numerous calls to NEUROMECHANIC from the optimizer, MATLAB. At each optimization step, the following steps would be required:

- Writing a body file (*filename.nmcb*) for given muscle activation with MATLAB (*write_nmcb.m*).
- Running a forward dynamic simulation in NEUROMECHANIC to generate an output file (*filename.nmco*).
- Replaying the simulation in order to save the linearized system state matrix (*filename_replay.nmco*).
- Loading the output file into the MATLAB workspace (*read_nmco.m*).

As can be expected, computational demand for this procedure will increase extensively if the search space is large, as in the 31-muscle cat hindlimb model.

The shortcut described here saves computation time by estimating the linearized system state matrix at every optimization step within MATLAB by multiplying the current muscle activation pattern by a matrix of pre-calculated regression coefficients. Although this shortcut requires more overhead in the pre-calculation step, it is computationally advantageous over an alternative approach of running a dynamic simulation for every single function evaluation step during the search. The version of the cat hindlimb model used here is built in NEUROMECHANIC and has 14 kinematic states: seven for each of joint displacements and velocities.

Here, we demonstrate that linearized system state matrices estimated from pre-calculated regression coefficients in MATLAB are comparable to results calculated in NEUROMECHANIC.

C.2 Methods

C.2.1 Linearized system matrix

The linearized system state matrix describes how a small change in each of the states will affect the system by linearly approximating the local dynamics of the entire

nonlinear musculoskeletal model around an equilibrium point. The eigenvectors of the state matrix represent the basis vectors that span all possible variations (modes) that can be made on the system. The corresponding eigenvalues determine how the system responds to such modes and determines system's local stability: the system will be stable if all eigenvalues are negative.

The state matrix for a system with kinematic states q can be given as follows. From the equations of motion,

$$\mathbf{M}(q)\ddot{q} = \mathbf{R}(q)\overline{F}_M(q, \dot{q}, a) + \mathbf{J}(q)^T \overline{F}_{End} + \overline{V}(q, \dot{q}) + \overline{G}(q) \quad (\text{D.1}),$$

where \mathbf{M} is the inertia matrix; \mathbf{R} is the moment arm matrix; \mathbf{J} is the endpoint Jacobian; \overline{F}_M is the vector of muscle forces; \overline{F}_{End} is the vector of endpoint forces; \overline{V} is the vector of Coriolis terms; and \overline{G} is the gravitational torque vector. We define the system of the kinematic states as,

$$\ddot{q} = f = \mathbf{M}^{-1}(\mathbf{R}\overline{F}_M + \mathbf{J}^T \overline{F}_{End} + \overline{V} + \overline{G}) \quad (\text{D.2})$$

We obtain the linearized system state matrix about an equilibrium point using the first-order Taylor-series expansion. A system is said to be at an equilibrium when it is balanced to all external forces and moments and there are no changes in the states with respect to time. Therefore, at equilibrium, $f = \mathbf{0}$, and:

$$\begin{bmatrix} \Delta \ddot{q} \\ \Delta \dot{q} \end{bmatrix} = \mathbf{A} \begin{bmatrix} \Delta q \\ \Delta \dot{q} \end{bmatrix} \quad \text{where the state matrix, } \mathbf{A} = \begin{bmatrix} \mathbf{0} & \mathbf{I} \\ \frac{\partial f}{\partial q} & \frac{\partial f}{\partial \dot{q}} \end{bmatrix} \quad (\text{D.3}).$$

C.2.2 State matrix as a function of muscle activation

If the state matrix can be estimated as a linear function of muscle activation vector a , calculation of the state matrix from the muscle activation vector will simply be a matrix-vector multiplication. There are two requirements for this to be possible:

- Limb configuration is static, so that the inertia matrix, moment arm matrix, Jacobian matrix, Coriolis vector, and gravity vector terms in Equation 1 are all constant.
- Hill type Zajac muscle models (Zajac 1989) are used: active muscle force scales with muscle activation and inelastic tendon is assumed, so that the vector of muscle forces in Equation 1 depends only on muscle activation a .

In particular, muscle force in the Zajac model is generated by active and passive component, both based on the current state of the musculotendon length (MTL) and velocity (MTV) each normalized to the optimal fiber length and maximum fiber velocity respectively.

$$F_M = F_{Max} [afl(MTL) \cdot vf(MTV) \cdot a + pfl(MTL)] \cos \alpha_{penn} \quad (D.4)$$

If the posture is assumed to be fixed, all other variables and parameters in Equation 1 except muscle activation a are constant. The above muscle model can then be rewritten comprised of the constant active component multiplied by the activation which is offset by the constant passive component as,

$$\vec{F}_M = \mathbf{F}_a \vec{a} + \vec{F}_p, \text{ and in turn the system equation as,}$$

$$f = \mathbf{M}^{-1} (\mathbf{R}\mathbf{F}_a \vec{a} + \mathbf{R}\vec{F}_p + \mathbf{J}^T \vec{F}_{End} + \vec{V} + \vec{G}) \quad (D.5).$$

Therefore, it can be said that under the condition given above, the state matrix for a given configuration depends solely on the muscle activation and can be expressed in explicit form of muscle activation.

C.2.3 Separating parts of the state matrix that are multiplied by muscle activation

Specifically, we want to focus on the lower part of the state matrix where the elements vary depending on the muscle activation. Defining a new matrix \mathbf{Q} as below,

$$\mathbf{Q} = \begin{bmatrix} \frac{\partial f}{\partial q} & \frac{\partial f}{\partial \dot{q}} \end{bmatrix}^T \quad (D.6).$$

It can be shown that the constant terms in the matrix \mathbf{Q} for a given configuration can be separated by the terms that are multiplied by the muscle activation and the terms that are not. In column-wise notation where Q_i is the i -th column of the matrix \mathbf{Q} ,

$$\bar{Q}_i = \begin{bmatrix} \frac{\partial f_i}{\partial \bar{q}_j} & \frac{\partial f_i}{\partial \dot{\bar{q}}_j} \end{bmatrix}^T = \mathbf{B}_i \bar{a} + \bar{C}_i \quad \text{where } j = 1, 2, \dots, n$$

$$\mathbf{B}_i = \begin{bmatrix} \mathbf{M}^{-1} \frac{\partial(\mathbf{R}\bar{\mathbf{F}}_a)_i}{\partial \bar{q}_j} \\ \mathbf{M}^{-1} \mathbf{R} \frac{\partial \bar{\mathbf{F}}_{a,i}}{\partial \dot{\bar{q}}_j} \end{bmatrix} \quad \text{and} \quad \bar{C}_i = \begin{bmatrix} \mathbf{M}^{-1} \left(\frac{\partial(\mathbf{R}\bar{\mathbf{F}}_p)_i}{\partial \bar{q}_j} + \frac{\partial(\mathbf{J}^T \bar{\mathbf{F}}_{End})_i}{\partial \bar{q}_j} + \frac{\partial \bar{V}_i}{\partial \bar{q}_j} + \frac{\partial \bar{G}_i}{\partial \bar{q}_j} \right) \\ \mathbf{M}^{-1} \left(\mathbf{J}^T \frac{\partial \bar{\mathbf{F}}_{End,i}}{\partial \dot{\bar{q}}_j} + \frac{\partial \bar{V}_i}{\partial \dot{\bar{q}}_j} \right) \end{bmatrix} \quad (\text{D.7})$$

In general, if the system has n kinematic degrees of freedom and m muscles, dimension of the matrix \mathbf{Q} is $2n \times n$ each column, Q_i , being $2n \times 1$ where matrix \mathbf{B}_i has dimension $2n \times m$ and vector C_i $2n \times 1$. For a given configuration, \mathbf{B}_i and C_i are constant for all i , which in result constitutes the whole state matrix. Therefore, given a set of data regarding the muscle activations as predictor variables and its corresponding state matrices as response, we can estimate all \mathbf{B}_i and C_i , which gives the relationship between muscle activations and the state matrix, using linear regression which is to be discussed in the following section.

C.2.4 Regression of the separated state matrix onto muscle activation

A pool of data set with N observations can be generated using NEUROMECHANIC as mentioned in one of previous sections. Since both the response variable (Q_i) and the predictor variable (muscle activation a) are vectors of n and m dimensions respectively, multivariate multiple linear regression (MMLR) must be used. For Q_i , this can be arranged in a form where N observations are constructed with N predictor inputs using the same coefficient matrix:

$$\begin{bmatrix} (\bar{Q}_i^T)_1 \\ (\bar{Q}_i^T)_2 \\ \vdots \\ (\bar{Q}_i^T)_N \end{bmatrix} = \begin{bmatrix} 1 & (\bar{a}^T)_1 \\ 1 & (\bar{a}^T)_2 \\ \vdots & \vdots \\ 1 & (\bar{a}^T)_N \end{bmatrix} \begin{bmatrix} \bar{C}_i^T \\ \mathbf{B}_i^T \end{bmatrix} \quad \text{or in short,} \quad \mathbf{Q}_{i,\text{obs}} = \mathbf{Act}_{\text{in}} \begin{bmatrix} \bar{C}_i^T \\ \mathbf{B}_i^T \end{bmatrix} \quad (\text{D.8}).$$

Using the commonly accepted criteria of least squares error (other criteria can be used, such as), the coefficient matrix can be obtained as below (in MATLAB, this is simply left division `mldivide`):

$$\begin{bmatrix} \bar{C}_i^T \\ \mathbf{B}_i^T \end{bmatrix} = (\mathbf{Act}_{\text{in}}^T \mathbf{Act}_{\text{in}})^{-1} \mathbf{Act}_{\text{in}}^T \mathbf{Q}_{i,\text{obs}} \quad \text{where the error (residual) is } \mathbf{Q}_{i,\text{obs}} - \mathbf{Act}_{\text{in}} \begin{bmatrix} \bar{C}_i^T \\ \mathbf{B}_i^T \end{bmatrix} \quad (\text{D.9}).$$

A single MMLR can be done in order to obtain each of the Q_i 's. In conclusion, n times of MMLR will yield all the coefficient matrices required to construct \mathbf{Q} , and by definition, the state matrix.

C.2.5 Comparison of linearized state matrices estimated in MATLAB and calculated in NEUROMECHANIC

We directly compared linearized state matrices estimated from pre-calculated regression coefficients in MATLAB with those calculated directly from NEUROMECHANIC based on a sample of 100 muscle activation patterns. Briefly,

- We used the musculoskeletal model of the cat hindlimb and stance-like force used by Bunderson et al, 2010. The model was fixed at both the pelvis (translation and rotation) and at the toe (translation only).
- We generated a set of 100 uniformly-distributed random activation patterns as target inputs for the model in NEUROMECHANIC.
- For each activation pattern, the model was balanced to produce the stance-like endpoint force with muscle activation found by NEUROMECHANIC that is

closest to the assigned target (NEUROMECHANIC function ‘*Equilibrate*’) and the state matrix was saved.

- We performed the linearized state matrix separation and regression as described above to generate estimated state matrices for each muscle activation pattern.
- We calculated the mean-squared error between estimated and computed state matrices.

C.3 Results

State matrices estimated from linear regression within MATLAB and computed within NEUROMECHANIC were very similar. Absolute errors between elements of state matrices were $\leq 10^{-3}$. RMS errors between estimated and computed state matrices were $1.28 \times 10^{-6} \pm 3 \times 10^{-7} \%$.

Initially obtaining computed linearized state matrices from NEUROMECHANIC took 397.8 seconds. Once the set of state matrices was available in MATLAB, obtaining estimated linearized state matrices took 0.099 seconds.

C.4 Conclusions

We have presented a method that can save computation time for nonlinear muscle activation optimizations by using pre-calculated estimates of the mapping between muscle activation and the resulting system state matrix for searches within MATLAB rather than requiring repeated calls between MATLAB and NEUROMECHANIC. We found that the state matrix estimates calculated via linear regression within MATLAB were generally very similar to those calculated from the full nonlinear model in NEUROMECHANIC, but required considerably less computational overhead. The advantages of this method are offset somewhat by three factors. First, the regression

equations describing the mapping between muscle activation and system state must be pre-calculated beforehand. Therefore, if a very small number of optimizations is required, the pre-calculation computational overhead may mean that there is no net savings in computational time. Second, use of the method requires that a relatively simple Zajac-style muscle model be used. Therefore, the method may not be appropriate if it is desired to investigate the role of passive mechanisms such as elastic tendons. Third, further research is required to determine the number of muscle patterns required to assure a given level of fidelity in the estimated linearized state matrices. These concerns notwithstanding, the presented method generally appears to be computationally advantageous over an alternative approach of running a dynamic simulation for every single function evaluation step during the search.

REFERENCES

Abel MF, Damiano DL, Pannunzio M, and Bush J. Muscle-tendon surgery in diplegic cerebral palsy: functional and mechanical changes. *Journal of pediatric orthopedics* 19: 366-375, 1999.

Ackermann M, and van den Bogert AJ. Optimality principles for model-based prediction of human gait. *J Biomech* 43: 1055-1060, 2010.

Ackland DC, Lin Y-C, and Pandy MG. Sensitivity of model predictions of muscle function to changes in moment arms and muscle-tendon properties: A Monte-Carlo analysis. *J Biomech* 45: 1463-1471, 2012.

Ait-Haddou R, Jinha A, Herzog W, and Binding P. Analysis of the force-sharing problem using an optimization model. *Mathematical Biosciences* 191: 111-122, 2004.

Alessandro C, Delis I, Nori F, Panzeri S, and Berret B. Muscle synergies in neuroscience and robotics: from input-space to task-space perspectives. *Frontiers in computational neuroscience* 7: 43, 2013.

Alexander RM. A minimum energy cost hypothesis for human arm trajectories. *Biological cybernetics* 76: 97-105, 1997.

Alexander RM. Models and the scaling of energy costs for locomotion. *The Journal of experimental biology* 208: 1645-1652, 2005.

Alexander RM. Optimization and gaits in the locomotion of vertebrates. *Physiological Reviews* 69: 1199-1227, 1989.

Alexandrov AV, Frolov AA, Horak FB, Carlson-Kuhta P, and Park S. Feedback equilibrium control during human standing. *Biological cybernetics* 1-14, 2005.

Alexandrov AV, Frolov AA, and Massion J. Biomechanical analysis of movement strategies in human forward trunk bending. I. Modeling. *Biological cybernetics* 84: 425-434, 2001.

Allen JL, Kautz SA, and Neptune RR. The influence of merged muscle excitation modules on post-stroke hemiparetic walking performance. *Clin Biomech (Bristol, Avon)* 28: 697-704, 2013.

Allen JL, and Neptune RR. Three-dimensional modular control of human walking. *J Biomech* 45: 2157-2163, 2012.

Anderson FC, and Pandy MG. Dynamic optimization of human walking. *Journal of biomechanical engineering* 123: 381, 2001a.

Anderson FC, and Pandy MG. A dynamic optimization solution for vertical jumping in three dimensions. *Computer methods in biomechanics and biomedical engineering* 2: 201-231, 1999.

Anderson FC, and Pandy MG. Individual muscle contributions to support in normal walking. *Gait Posture* 17: 159-169, 2003.

Anderson FC, and Pandy MG. Static and dynamic optimization solutions for gait are practically equivalent. *J Biomech* 34 153-161, 2001b.

Anderson RN, Minino AM, Fingerhut LA, Warner M, and Heinen MA. Deaths: injuries, 2001. *Natl Vital Stat Rep* 52: 1-86, 2004.

Arnold AS, Anderson FC, Pandy MG, and Delp SL. Muscular contributions to hip and knee extension during the single limb stance phase of normal gait: a framework for investigating the causes of crouch gait. *J Biomech* 38: 2181-2189, 2005.

Arnold AS, Liu MQ, Schwartz MH, Ounpuu S, and Delp SL. The role of estimating muscle-tendon lengths and velocities of the hamstrings in the evaluation and treatment of crouch gait. *Gait Posture* 23: 273-281, 2006a.

Arnold AS, Liu MQ, Schwartz MH, Ounpuu S, Dias LS, and Delp SL. Do the hamstrings operate at increased muscle-tendon lengths and velocities after surgical lengthening? *J Biomech* 39: 1498-1506, 2006b.

Arnold EM, and Delp SL. Fibre operating lengths of human lower limb muscles during walking. *Philosophical transactions of the Royal Society of London Series B, Biological sciences* 366: 1530-1539, 2011.

Baumann JU, Ruetsch H, and Schurmann K. Distal hamstring lengthening in cerebral palsy. An evaluation by gait analysis. *International orthopaedics* 3: 305-309, 1980.

Beer RF, Dewald JP, Dawson ML, and Rymer WZ. Target-dependent differences between free and constrained arm movements in chronic hemiparesis. *Experimental Brain Research* 156: 458-470, 2004.

Beer RF, Dewald JPA, and Rymer WZ. Deficits in the coordination of multijoint arm movements in patients with hemiparesis: evidence for disturbed control of limb dynamics. *Experimental Brain Research* 131: 305-319, 2000.

Beer RF, Ellis MD, Holubar BG, and Dewald JP. Impact of gravity loading on post-stroke reaching and its relationship to weakness. *Muscle & nerve* 36: 242-250, 2007.

Berger DJ, Gentner R, Edmunds T, Pai DK, and d'Avella A. Differences in adaptation rates after virtual surgeries provide direct evidence for modularity. *Journal of Neuroscience* 33: 12384-12394, 2013.

Berniker M, Jarc A, Bizzi E, and Tresch MC. Simplified and effective motor control based on muscle synergies to exploit musculoskeletal dynamics. *Proc Natl Acad Sci U S A* 106: 7601-7606, 2009.

Bernstein NI. *The coordination and regulation of movements.* New York: Pergamon Press, 1967.

Bhargava LJ, Pandy MG, and Anderson FC. A phenomenological model for estimating metabolic energy consumption in muscle contraction. *J Biomech* 37: 81-88, 2004.

Biewener AA, Konieczynski DD, and Baudinette RV. In vivo muscle force-length behavior during steady-speed hopping in tammar wallabies. *The Journal of experimental biology* 201: 1681-1694, 1998.

Bingham JT, Choi JT, and Ting LH. Stability in a frontal plane model of balance requires coupled changes to postural configuration and neural feedback control. *J Neurophysiol* 106: 437-448, 2011.

Bingham JT, and Ting LH. Stability radius as a method for comparing the dynamics of neuromechanical systems. *IEEE transactions on neural systems and rehabilitation engineering* 2013.

Bizzi E, and Cheung VC. The neural origin of muscle synergies. *Frontiers in computational neuroscience* 7: 51, 2013.

Bolger D, Ting LH, and Sawers A. Individuals with transtibial limb loss use interlimb force asymmetries to maintain multi-directional reactive balance control. *Clin Biomech (Bristol, Avon)* 29: 1039-1047, 2014.

Bortolami SB, DiZio P, Rabin E, and Lackner JR. Analysis of human postural responses to recoverable falls. *Experimental Brain Research* 151: 387-404, 2003.

Borzelli D, Berger DJ, Pai DK, and d'Avella A. Effort minimization and synergistic muscle recruitment for three-dimensional force generation. *Frontiers in computational neuroscience* 7: 186, 2013.

Bruijn SM, Meijer OG, Beek PJ, and van Dieen JH. Assessing the stability of human locomotion: a review of current measures. *Journal of the Royal Society, Interface / the Royal Society* 10: 20120999, 2013.

Brunnström S. *Movement therapy in hemiplegia: a neurophysiological approach.* New York: Harper & Row, 1970.

Buchanan TS, and Shreeve DA. An evaluation of optimization techniques for prediction of muscle activation patterns during isometric tasks. *Journal of biomechanical engineering* 118: 565-574, 1996.

Bunderson N, and Bingham J. Better science through predictive modeling: Numerical tools for understanding neuromechanical interactions. In: *Neuromechanical Modeling of Posture and Locomotion*, edited by Prilutsky BI, and Edwards DH. Berlin: Springer, in press.

Bunderson NE, Bingham JT, Sohn MH, Ting LH, and Burkholder TJ. Neuromechanic: A computational platform for simulation and analysis of the neural control of movement. *International journal for numerical methods in biomedical engineering* 28: 1015-1027, 2012.

Bunderson NE, Burkholder TJ, and Ting LH. Reduction of neuromuscular redundancy for postural force generation using an intrinsic stability criterion. *J Biomech* 41: 1537-1544, 2008.

Bunderson NE, McKay JL, Ting LH, and Burkholder TJ. Directional constraint of endpoint force emerges from hindlimb anatomy. *The Journal of experimental biology* 213: 2131-2141, 2010.

Burdet E, Osu R, Franklin DW, Milner TE, and Mitsuo K. The central nervous system stabilizes unstable dynamics by learning optimal impedance. *Nature* 414 446-449, 2001.

Burdet E, Tee KP, Mareels I, Milner TE, Chew CM, Franklin DW, Osu R, and Kawato M. Stability and motor adaptation in human arm movements. *Biological cybernetics* 94: 20-32, 2006.

Burkholder TJ, and Lieber RL. Sarcomere length operating range of vertebrate muscles during movement. *The Journal of experimental biology* 204: 1529-1536, 2001.

Burkholder TJ, and Nichols TR. The mechanical action of proprioceptive length feedback in a model of cat hindlimb. *Motor control* 4: 201-220, 2000.

Burkholder TJ, and Nichols TR. Three-dimensional model of the feline hindlimb. *Journal of Morphology* 261: 118-129, 2004.

Byadarhaly KV, Perdoor MC, and Minai AA. A modular neural model of motor synergies. *Neural networks : the official journal of the International Neural Network Society* 32: 96-108, 2012.

Callebaut W, and Rasskin-Gutman D. *Modularity: understanding the development and evolution of natural complex Systems.* Cambridge, MA: MIT Press, 2005.

Cao J, Xie SQ, Das R, and Zhu GL. Control strategies for effective robot assisted gait rehabilitation: the state of art and future prospects. *Medical engineering & physics* 36: 1555-1566, 2014.

Carlsöö S. *How man moves.* London: Heinemann, 1972.

Carpenter MG, Allum JH, and Honegger F. Directional sensitivity of stretch reflexes and balance corrections for normal subjects in the roll and pitch planes. *Experimental Brain Research* 129: 93-113, 1999.

Chang SH, Francisco GE, Zhou P, Rymer WZ, and Li S. Spasticity, weakness, force variability, and sustained spontaneous motor unit discharges of resting spastic-paretic biceps brachii muscles in chronic stroke. *Muscle & nerve* 48: 85-92, 2013.

Cheung VC, d'Avella A, Tresch MC, and Bizzi E. Central and sensory contributions to the activation and organization of muscle synergies during natural motor behaviors. *Journal of Neuroscience* 25: 6419-6434, 2005.

Cheung VCK, Piron L, Agostini M, Silvoni S, Turolla A, and Bizzi E. Stability of muscle synergies for voluntary actions after cortical stroke in humans. *Proceedings of the National Academy of Sciences* 106: 19563-19568, 2009.

Chhabra M, and Jacobs RA. Properties of synergies arising from a theory of optimal motor behavior. *Neural Computation* 18: 2320–2342, 2006.

Chiel HJ, Ting LH, Ekeberg O, and Hartmann MJ. The brain in its body: motor control and sensing in a biomechanical context. *Journal of Neuroscience* 29: 12807-12814, 2009.

Childers WL, and Kogler G. Journal of Rehabilitation Research & Development. *Symmetrical kinematics does not mean symmetrical kinetics in people with transtibial amputation* 2015 (In press).

Chopin N. Fast simulation of truncated Gaussian distributions. *Statistics and Computing* 21: 275-288, 2011.

Chvatal SA, and Ting LH. Common muscle synergies for balance and walking. *Frontiers in computational neuroscience* 7: 48, 2013.

Chvatal SA, and Ting LH. Voluntary and reactive recruitment of locomotor muscle synergies during perturbed walking. *Journal of Neuroscience* 32: 12237-12250, 2012.

Chvatal SA, Torres-Oviedo G, Safavynia SA, and Ting LH. Common muscle synergies for control of center of mass and force in nonstepping and stepping postural behaviors. *J Neurophysiol* 106: 999–1015, 2011.

Clark DJ, Ting LH, Zajac FE, Neptune RR, and Kautz SA. Merging of healthy motor modules predicts reduced locomotor performance and muscle coordination complexity post-stroke. *J Neurophysiol* 103: 844-857, 2010.

Collins JJ. The redundant nature of locomotor optimization laws. *Journal of Biomechanics* 28: 251-267, 1995.

Correa TA, Schache AG, Graham HK, Baker R, Thomason P, and Pandy MG. Potential of lower-limb muscles to accelerate the body during cerebral palsy gait. *Gait & Posture* 36: 194-200, 2012.

Costa RM. A selectionist account of de novo action learning. *Curr Opin Neurobiol* 21: 579-586, 2011.

Crenna P. Spasticity and 'spastic' gait in children with cerebral palsy. *Neurosci Biobehav Rev* 22: 571-578, 1998

Crevecoeur F, and Scott SH. Beyond muscles stiffness: importance of state-estimation to account for very fast motor corrections. *PLoS Comput Biol* 10: e1003869, 2014.

Crowninshield RD, and Brand RA. A physiologically based criterion of muscle force prediction in locomotion. *J Biomech* 14: 793-801, 1981.

Cui L, Perreault EJ, Maas H, and Sandercock TG. Modeling short-range stiffness of feline lower hindlimb muscles. *J Biomech* 41: 1945-1952, 2008.

d'Avella A, Alessandro P, Fernandez L, and Lacquaniti F. Control of fast-reaching movements by muscle synergy combinations. *Journal of Neuroscience* 26: 7791-7810, 2006.

d'Avella A, and Bizzi E. Shared and specific muscle synergies in natural motor behaviors. *Proc Natl Acad Sci U S A* 102: 3076-3081, 2005.

d'Avella A, Saltiel P, and Bizzi E. Combinations of muscle synergies in the construction of a natural motor behavior. *Nat Neurosci* 6: 300-308, 2003.

Damiano DL, Arnold AS, Steele KM, and Delp S. Can strength training predictably improve gait kinematics? A pilot study on the effects of hip and knee extensor

strengthening on lower-extremity alignment in cerebral palsy. *Phys Ther* 90: 269-279, 2010

Damiano DL, Vaughan CL, and Abel MF. Muscle response to heavy resistance exercise in children with spastic cerebral palsy. *Developmental medicine and child neurology* 37: 731-739, 1995.

Davoodi R, Brown IE, and Loeb GE. Advanced modeling environment for developing and testing FES control systems. *Medical engineering & physics* 25: 3-9, 2003.

Dawes H, Enzinger C, Johansen-Berg H, Bogdanovic M, Guy C, Collett J, Izadi H, Stagg C, Wade D, and Matthews PM. Walking performance and its recovery in chronic stroke in relation to extent of lesion overlap with the descending motor tract. *Experimental Brain Research* 186: 325-333, 2008.

De Groot F, Jonkers I, and Duysens J. Task constraints and minimization of muscle effort result in a small number of muscle synergies during gait. *Frontiers in computational neuroscience* 2014.

De Groot F, Van Campen A, Jonkers I, and De Schutter J. Sensitivity of dynamic simulations of gait and dynamometer experiments to hill muscle model parameters of knee flexors and extensors. *Journal of Biomechanics* 43: 1876-1883, 2010.

De Leon RD, Hodgson JA, Roy RR, and Edgerton VR. Full weight-bearing hindlimb standing following stand training in the adult spinal cat. *J Neurophysiol* 80: 83-91, 1998.

de Rugy A, Loeb GE, and Carroll TJ. Are muscle synergies useful for neural control? *Frontiers in computational neuroscience* 7: 19, 2013.

de Rugy A, Loeb GE, and Carroll TJ. Muscle coordination is habitual rather than optimal. *Journal of Neuroscience* 32: 7384-7391, 2012.

Debicki DB, and Gribble PL. Inter-joint coupling strategy during adaptation to novel viscous loads in human arm movement. *J Neurophysiol* 92: 754-765, 2004.

Delp SL, Anderson FC, Arnold AS, Loan P, Habib A, John CT, Guendelman E, and Thelen DG. OpenSim: open-source software to create and analyze dynamic simulations of movement. *IEEE Transactions on Biomedical Engineering* 54: 1940-1950, 2007.

Delp SL, and Loan JP. A computational framework for simulating and analyzing human and animal movement. *Computing in Science & Engineering* 2: 46-55, 2000.

Delp SL, Loan JP, Hoy MG, Zajac FE, Topp EL, and Rosen JM. An interactive graphics-based model of the lower extremity to study orthopaedic surgical procedures. *IEEE Transactions on Biomedical Engineering* 37: 757-767, 1990.

DeLuca PA, Ounpuu S, Davis RB, and Walsh JH. Effect of hamstring and psoas lengthening on pelvic tilt in patients with spastic diplegic cerebral palsy. *Journal of pediatric orthopedics* 18: 712-718, 1998.

Denis W, Brunetti F, Piazza S, Torricelli D, and Pons JL. Functional electrical stimulation controller based on muscle synergies. *Converging Clinical & Engi Research on NR, BIOSYSROB* 1: 283-287, 2013.

Dewald JP, and Beer RF. Abnormal joint torque patterns in the paretic upper limb of subjects with hemiparesis. *Muscle & nerve* 24: 273-283, 2001.

Dewald JPA, Pope PS, Given JD, Buchanan TS, and Rymer WZ. Abnormal muscle coactivation patterns during isometric torque generation at the elbow and shoulder in hemiparetic subjects. *Brain* 118: 495-510, 1995.

Diener HC, Horak FB, and Nashner LM. Influence of stimulus parameters on human postural responses. *J Neurophysiol* 59: 1888-1905, 1988.

Dietz V, and Sinkjaer T. Spastic movement disorder: impaired reflex function and altered muscle mechanics. *The Lancet Neurology* 6: 725-733, 2007.

Dingwell JB, and Kang HG. Differences between local and orbital dynamic stability during human walking. *Journal of biomechanical engineering* 129: 586-593, 2007.

Dodd KJ, Taylor NF, and Damiano DL. A systematic review of the effectiveness of strength-training programs for people with cerebral palsy. *Archives of physical medicine and rehabilitation* 83: 1157-1164, 2002.

Dominici N, Ivanenko Y, Cappellini G, d'Avella, Mondì V, Cicchese M, Fabiano A, Silei T, Di Paolo A, Giannini C, Poppele R, and Lacquaniti F. Locomotor primitives in newborn babies and their development. *Science* 334: 997-999, 2011

Donelan JM, Kram R, and Kuo AD. Mechanical and metabolic determinants of the preferred step width in human walking. *Proc Biol Sci* 268: 1985-1992, 2001

Donelan JM, Kram R, and Kuo AD. Mechanical work for step-to-step transitions is a major determinant of the metabolic cost of human walking. *J Exp Biol* 205: 3717-3727, 2002

Dorn TW, Schache AG, and Pandy MG. Muscular strategy shift in human running: dependence of running speed on hip and ankle muscle performance. *The Journal of experimental biology* 215: 1944-1956, 2012.

Dubois JD, Piche M, Cantin V, and Descarreaux M. Effect of experimental low back pain on neuromuscular control of the trunk in healthy volunteers and patients with chronic low back pain. *Journal of electromyography and kinesiology : official journal of the International Society of Electrophysiological Kinesiology* 21: 774-781, 2011.

Dupeyron A, Rispens SM, Demattei C, and van Dieen JH. Precision of estimates of local stability of repetitive trunk movements. *European spine journal : official publication of the European Spine Society, the European Spinal Deformity Society, and the European Section of the Cervical Spine Research Society* 22: 2678-2685, 2013.

Elble R, Moody C, Leffler K, and Sinha R. The initiation of normal walking. *Mov Disord* 9: 139-146, 1994.

Ellis MD, Acosta AM, Yao J, and Dewald JP. Position-dependent torque coupling and associated muscle activation in the hemiparetic upper extremity. *Experimental Brain Research* 176: 594-602, 2007.

Ellis RG, Howard KC, and Kram R. The metabolic and mechanical costs of step time asymmetry in walking. *Proceedings Biological sciences / The Royal Society* 280: 20122784, 2013.

Epstein M, and Herzog W. Aspects of skeletal muscle modelling. *Philos Trans R Soc Lond B Biol Sci* 358: 1445-1452, 2003.

Erdemir A, McLean S, Herzog W, and van den Bogert AJ. Model-based estimation of muscle forces exerted during movements. *Clinical Biomechanics* 22: 131-154, 2007.

Fisher BE, and Sullivan KJ. Activity-dependent factors affecting poststroke functional outcomes. *Topics in stroke rehabilitation* 8: 31-44, 2001.

Fisher BE, Wu AD, Salem GJ, Song J, Lin CH, Yip J, Cen S, Gordon J, Jakowec M, and Petzinger G. The effect of exercise training in improving motor performance and corticomotor excitability in people with early Parkinson's disease. *Archives of physical medicine and rehabilitation* 89: 1221-1229, 2008.

Fleming BC, and Beynonn BD. In vivo measurement of ligament/tendon strains and forces: a review. *Annals of biomedical engineering* 32: 318-328, 2004.

Franklin DW, Burdet E, Tee KP, Osu R, Chew CM, Milner TE, and Kawato M. CNS learns stable, accurate, and efficient movements using a simple algorithm. *Journal of Neuroscience* 28: 11165-11173, 2008.

Franklin DW, Selen LPJ, Franklin S, and Wolpert DM. Selection and control of limb Posture for stability. In: *35th Annual International Conference of the IEEE EMBS*. Osaka, Japan: 2013.

Franklin DW, So U, Kawato M, and Milner TE. Impedance control balances stability with metabolically costly muscle activation. *J Neurophysiol* 92: 3097-3105, 2004.

Frere J, and Hug F. Between-subject variability of muscle synergies during a complex motor skill. *Frontiers in computational neuroscience* 6: 99, 2012.

Ganesh G, Haruno M, Kawato M, and Burdet E. Motor memory and local minimization of error and effort, not global optimization, determine motor behavior. *J Neurophysiol* 104: 382-390, 2010.

Gardner-Morse MG, and Stokes IA. The effects of abnominal muscle coactivation on lumbar spins stability. *SPINE* 23: 86-92, 1998.

Giszter SF, Davies MR, and Graziani V. Motor strategies used by rats spinalized at birth to maintain stance in response to imposed perturbations. *J Neurophysiol* 97: 2663-2675, 2007.

Giszter SF, and Hart CB. Motor primitives and synergies in the spinal cord and after injury--the current state of play. *Annals of the New York Academy of Sciences* 1279: 114-126, 2013.

Giszter SF, and Kargo WJ. Conserved temporal dynamics and vector superposition of primitives in frog wiping reflexes during spontaneous extensor deletions. *Neurocomputing* 32-33: 775-783, 2000.

Gollhofer A, Horstmann GA, Berger W, and Dietz V. Compensation of translational and rotational perturbations in human posture: stabilization of the centre of gravity. *Neurosci Lett* 105: 73-78, 1989.

Gomi H, and Osu R. Task-dependent viscoelasticity of human multijoint arm and its spatial characteristics for interaction with environments. *Journal of Neuroscience* 18: 8965-8978, 1998.

Gordon AM, Huxley AF, and Julian FJ. The variation in isometric tension with sarcomere length in vertebrate muscle fibres. *J Physiol* 184: 170-192, 1966.

Gottlieb GL. Muscle activation patterns during two types of voluntary single-joint movement. *J Neurophysiol* 80: 1860-1867, 1998.

Graham HK, and Selber P. Musculoskeletal aspects of cerebral palsy. *The Journal of bone and joint surgery British volume* 85: 157-166, 2003.

Graham RB, Oikawa LY, and Ross GB. Comparing the local dynamic stability of trunk movements between varsity athletes with and without non-specific low back pain. *J Biomech* 47: 1459-1464, 2014.

Granata KP, and Gottipati P. Fatigue influences the dynamic stability of the torso. *Ergonomics* 51: 1258-1271, 2008.

Granata KP, and Marras WS. Cost-benefit of muscle cocontraction in protecting against spinal instability. *Spine (Phila Pa 1976)* 25: 1398-1404, 2000.

Gribble PL, and Ostry DJ. Compensation for interaction torques during single- and multijoint limb movement. *J Neurophysiol* 82: 2310-2326, 1999.

Gruben KG, Lopez-Ortiz C, and Schmidt MW. The control of foot force during pushing efforts against a moving pedal. *Experimental Brain Research* 148: 50-61, 2003.

Hak L, van Dieën JH, van der Wurff P, and Houdijk H. Stepping asymmetry among individuals with unilateral transtibial limb loss might be functional in terms of gait stability. *Phys Ther* 94: 1480-1488, 2014

Hamner SR, and Delp SL. Muscle contributions to fore-aft and vertical body mass center accelerations over a range of running speeds. *J Biomech* 46: 780-787, 2013.

Hamner SR, Seth A, and Delp SL. Muscle contributions to propulsion and support during running. *J Biomech* 43: 2709-2716, 2010.

Hansen L, and Anders C. Influence of different control strategies on muscle activation patterns in trunk muscles. *Physiological reports* 2: 2014.

Hargrove LJ, Li G, Englehart KB, and Hudgins BS. Principal components analysis preprocessing for improved classification accuracies in pattern-recognition-based myoelectric control. *IEEE Transactions on Biomedical Engineering* 56: 1407-1414, 2009.

Harris CM, and Wolpert DM. Signal-dependent noise determines motor planning. *Nature* 394: 780-784, 1998.

Hart CB, and Giszter SF. Modular premotor drives and unit bursts as primitives for frog motor behaviors. *Journal of Neuroscience* 24: 5269-5282, 2004.

Hart CB, and Giszter SF. A neural basis for motor primitives in the spinal Cord. *Journal of Neuroscience* 30: 1322-1336, 2010.

Hasan Z. The human motor control system's response to mechanical perturbation: should it, can it, and does it ensure stability? *Journal of motor behavior* 37: 484-493, 2005.

Hassid E, Rose D, Commisarow J, Guttry M, and Dobkin BH. Improved gait symmetry in hemiparetic stroke patients induced during body weight-supported treadmill stepping. *Journal of Neurologic Rehabilitation* 11: 21-26, 1997.

Hasson CJ, Shen T, and Sternad D. Energy margins in dynamic object manipulation. *J Neurophysiol* 108: 1349-1365, 2012.

Hasson CJ, Van Emmerik REA, and Caldwell GE. Predicting dynamic postural instability using center of mass time-to-contact information. *J Biomech* 41: 2121-2129, 2008.

Hausdorff JM. Gait dynamics, fractals and falls: finding meaning in the stride-to-stride fluctuations of human walking. *Human movement science* 26: 555-589, 2007.

Hauser H, Neumann G, Ijspeert AJ, and Maass W. Biologically inspired kinematic synergies enable linear balance control of a humanoid robot. *Biological cybernetics* 104: 235-249, 2011.

Herr H, and Popovic M. Angular momentum in human walking. *The Journal of experimental biology* 211: 467-481, 2008.

Herzfeld DJ, and Shadmehr R. Motor variability is not noise, but grist for the learning mill. *Nat Neurosci* 17: 149-150, 2014.

Herzog W, and Leonard TR. Validation of optimization models that estimate the force exerted by synergistic muscles. *J Biomech* 24: 31-39, 1991.

Hesse S, Herrmann C, Bardeleben A, Holzgraefe M, Werner C, Wingendorf I, and Kirker SG. A new orthosis for subluxed, flaccid shoulder after stroke facilitates gait symmetry: a preliminary study. *Journal of rehabilitation medicine* 45: 623-629, 2013.

Hicks JL, Schwartz MH, Arnold AS, and Delp SL. Crouched postures reduce the capacity of muscles to extend the hip and knee during the single-limb stance phase of gait. *J Biomech* 41: 960-967, 2008.

Hicks JL, Uchida TK, Seth A, Rajagopal A, and Delp SL. Is my model good enough? Best practices for verification and validation of musculoskeletal models and simulations of movement. *Journal of biomechanical engineering* 137: 020905, 2015.

Higginson J, Zajac F, Neptune R, Kautz S, and Delp S. Muscle contributions to support during gait in an individual with post-stroke hemiparesis. *J Biomech* 39: 1769-1777, 2006.

Higham TE, and Biewener AA. Functional and architectural complexity within and between muscles: regional variation and intermuscular force transmission. *Philos Trans R Soc Lond B Biol Sci* 366: 1477-1487, 2011.

Hill AV. The mechanics of active muscle. *Proceedings of the Royal Society of London Series B, Containing papers of a Biological character Royal Society* 141: 104-117, 1953.

Hof AL, Gazendam MG, and Sinke WE. The condition for dynamic stability. *J Biomech* 38: 1-8, 2005.

Hogan N. An organizing principle for a class of voluntary movements. *Journal of Neuroscience* 4: 2745-2754, 1984.

Holmes P, Full R, Koditschek DE, and Guckenheimer J. The dynamics of legged locomotion: models, analyses, and challenges. *SIAM Review* 48: 207-304, 2006.

Holzbaur KR, Murray WM, and Delp SL. A model of the upper extremity for simulating musculoskeletal surgery and analyzing neuromuscular control. *Annals of biomedical engineering* 33: 829-840, 2005.

Horak FB, and Macpherson JM. Postural orientation and equilibrium. In: *Handbook of Physiology, Section 12*. New York: American Physiological Society, 1996, p. 255-292.

Horak FB, and Nashner LM. Central programming of postural movements: adaptation to altered support-surface configurations. *J Neurophysiol* 55: 1369-1381, 1986.

Howard JD, and Enoka RM. Maximum bilateral contractions are modified by neurally mediated interlimb effects. *Journal of applied physiology* 70: 306-316, 1991.

Hoyt DF, and Taylor CR. Gait and the energetics of locomotion in horses. *Nature* 292: 239-240, 1981.

Hu X, Murray WM, and Perreault EJ. Biomechanical constraints on the feedforward regulation of endpoint stiffness. *J Neurophysiol* 108: 2083-2091, 2012.

Hu X, Murray WM, and Perreault EJ. Muscle short-range stiffness can be used to estimate the endpoint stiffness of the human arm. *J Neurophysiol* 105: 1633-1641, 2011.

Huang HJ, Kram R, and Ahmed AA. Reduction of metabolic cost during motor learning of arm reaching dynamics. *Journal of Neuroscience* 32: 2182-2190, 2012.

Huang TW, and Kuo AD. Mechanics and energetics of load carriage during human walking. *The Journal of experimental biology* 217: 605-613, 2014.

Huijing PA. Muscular force transmission necessitates a multilevel integrative approach to the analysis of function of skeletal muscle. *Exercise and sport sciences reviews* 31: 167-175, 2003.

Hunter LC, Hendrix EC, and Dean JC. The cost of walking downhill: Is the preferred gait energetically optimal? *J Biomech* 43: 1910-1915, 2010.

Hussain S. State-of-the-art robotic gait rehabilitation orthoses: design and control aspects. *NeuroRehabilitation* 35: 701-709, 2014.

Ijspeert A, Nakanishi J, and Schaal S. Learning attractor landscapes for learning motor primitives. In: *Advances in Neural Information Processing Systems*, edited by Becker S, Thrun S, and Obermayer K. Cambridge, MA: MIT Press, 2003, p. 1547-1554.

Ison M, and Artemiadis P. Proportional myoelectric control of robots: muscle synergy development drives performance enhancement, retainment, and generalization. *IEEE Transactions on Robotics* 2015.

Ivanenko YP, Poppele RE, and Lacquaniti F. Five basic muscle activation patterns account for muscle activity during human locomotion. *J Physiol* 556: 267-282, 2004.

Jacobs R, and Macpherson JM. Two functional muscle groupings during postural equilibrium tasks in standing cats. *J Neurophysiol* 76: 2402-2411, 1996.

Jahnsen R, Villien L, Aamodt G, Stanghelle JK, and Holm I. Musculoskeletal pain in adults with cerebral palsy compared with the general population. *Journal of rehabilitation medicine* 36: 78-84, 2004.

Jansen K, De Groot F, Aerts W, De Schutter J, Duysens J, and Jonkers I. Altering length and velocity feedback during a neuro-musculoskeletal simulation of normal gait contributes to hemiparetic gait characteristics. *J Neuroeng Rehabil* 11: 78, 2014.

Jinha A, Ait-Haddou R, and Herzog W. Predictions of co-contraction depend critically on degrees-of-freedom in the musculoskeletal model. *J Biomech* 39: 1145-1152, 2006.

Jo S, and Massaquoi SG. A model of cerebellum stabilized and scheduled hybrid long-loop control of upright balance. *Biological cybernetics* 91: 188-202, 2004.

John CT, Anderson FC, Higginson JS, and Delp SL. Stabilisation of walking by intrinsic muscle properties revealed in a three-dimensional muscle-driven simulation. *Computer methods in biomechanics and biomedical engineering* 16: 451-462, 2013.

Jones SL, Henry SM, Raasch CC, Hitt JR, and Bunn JY. Individuals with non-specific low back pain use a trunk stiffening strategy to maintain upright posture. *Journal of electromyography and kinesiology : official journal of the International Society of Electrophysiological Kinesiology* 22: 13-20, 2012.

Kao PC, Dingwell JB, Higginson JS, and Binder-Macleod S. Dynamic instability during post-stroke hemiparetic walking. *Gait Posture* 40: 457-463, 2014.

Kargo WJ, and Nitz DA. Early skill learning is expressed through selection and tuning of cortically represented muscle synergies. *Journal of Neuroscience* 23: 11255-11269, 2003

Kargo WJ, Ramakrishnan A, Hart CB, Rome LC, and Giszter SF. A simple experimentally based model using proprioceptive regulation of motor primitives captures adjusted trajectory formation in spinal frogs. *J Neurophysiol* 103: 573-590, 2010.

Kay RM, Rethlefsen SA, Skaggs D, and Leet A. Outcome of medial versus combined medial and lateral hamstring lengthening surgery in cerebral palsy. *Journal of pediatric orthopedics* 22: 169-172, 2002.

Kaya M, Leonard TR, and Herzog W. Premature deactivation of soleus during the propulsive phase of cat jumping. *Journal of The Royal Society Interface* 5: 415-426, 2008.

Keenan KG, Santos VJ, Venkadesan M, and Valero-Cuevas FJ. Maximal voluntary fingertip force production is not limited by movement speed in combined motion and force tasks. *Journal of Neuroscience* 29: 8784-8789, 2009.

Kerr C, McDowell B, Cosgrove A, Walsh D, Bradbury I, and McDonough S. Electrical stimulation in cerebral palsy: a randomized controlled trial. *Developmental medicine and child neurology* 48: 870-876, 2006.

Khatib O, Demircan E, De Sapiro V, Sentis L, Besier T, and Delp S. Robotics-based synthesis of human motion. *Journal of Physiology-Paris* 103: 211-219, 2009.

Kiemel T, Oie KS, and Jeka JJ. Multisensory fusion and the stochastic structure of postural sway. *Biological cybernetics* 87: 262-277, 2002.

Kistemaker DA, Wong JD, and Gribble PL. The central nervous system does not minimize energy cost in arm movements. *J Neurophysiol* 104: 2985-2994, 2010.

Klein DA, Patino A, and Tresch MC. Flexibility of motor pattern generation across stimulation conditions by the neonatal rat spinal cord. *Journal of Neurophysiology* 103: 1580-1590, 2010.

Krishnaswamy P, Brown EN, and Herr HM. Human leg model predicts ankle muscle-tendon morphology, state, roles and energetics in walking. *PLoS Comput Biol* 7: e1001107, 2011.

Krutky MA, Ravichandran VJ, Trumbower RD, and Perreault EJ. Interactions between limb and environmental mechanics influence stretch reflex sensitivity in the human arm. *J Neurophysiol* 103: 429-440, 2010.

Krutky MA, Trumbower RD, and Perreault EJ. Influence of environmental stability on the regulation of end-point impedance during the maintenance of arm posture. *J Neurophysiol* 109: 1045-1054, 2013.

Kuo AD. An optimal control model for analyzing human postural balance. *IEEE Transactions on Biomedical Engineering* 42: 87-101, 1995.

Kuo AD, and Zajac FE. A biomechanical analysis of muscle strength as a limiting factor in standing balance posture. *J Biomech* 26: 137-150, 1993.

Kutch JJ, Kuo AD, Bloch AM, and Rymer WZ. Endpoint force fluctuations reveal flexible rather than synergistic patterns of muscle cooperation. *J Neurophysiol* 100: 2455-2471, 2008.

Kutch JJ, and Valero-Cuevas FJ. Challenges and new approaches to proving the existence of muscle synergies of neural origin. *PLoS Computational Biology* 8: e1002434, 2012.

Kutch JJ, and Valero-Cuevas FJ. Muscle redundancy does not imply robustness to muscle dysfunction. *J Biomech* 44: 1264-1270, 2011.

Lacquaniti F, Ivanenko YP, d'Avella A, Zelik KE, and Zago M. Evolutionary and developmental modules. *Frontiers in computational neuroscience* 7: 61, 2013.

Lacquaniti F, Ivanenko YP, and Zago M. Patterned control of human locomotion. *The Journal of physiology* 590: 2189-2199, 2012.

Latash ML. The bliss (not the problem) of motor abundance (not redundancy). *Experimental Brain Research* 217: 1-5, 2012.

Liao HF, Liu YC, Liu WY, and Lin YT. Effectiveness of loaded sit-to-stand resistance exercise for children with mild spastic diplegia: a randomized clinical trial. *Archives of physical medicine and rehabilitation* 88: 25-31, 2007.

Liao YW, Schearer EM, Hu X, Perreault EJ, Tresch MC, and Lynch KM. Modeling open-loop stability of a human arm driven by a functional electrical stimulation neuroprosthesis. *Conference proceedings : Annual International Conference of the IEEE Engineering in Medicine and Biology Society IEEE Engineering in Medicine and Biology Society Conference* 2013: 3598-3601, 2013.

Liao YW, Schearer EM, Perreault EJ, Tresch MC, and Lynch KM. An FES controller for arm stability predicts human behavior in interaction tasks In: *Neuroscience 2014*. Washington, DC: 2014.

Lieber RL, and Ward SR. Skeletal muscle design to meet functional demands. *Philos Trans R Soc Lond B Biol Sci* 366: 1466-1476, 2011.

Liu MQ, Anderson FC, Schwartz MH, and Delp SL. Muscle contributions to support and progression over a range of walking speeds. *J Biomech* 41: 3243-3252, 2008.

Lockhart DB, and Ting LH. Optimal sensorimotor transformations for balance. *Nat Neurosci* 10: 1329-1336, 2007.

Loeb GE. Optimal isn't good enough. *Biological cybernetics* 106: 757-765, 2012.

Loeb GE. Overcomplete musculature or underspecified tasks? *Motor control* 4: 81-83; discussion 97-116, 2000.

Loram ID, Lakie M, Di Giulio I, and Maganaris CN. The consequences of short-range stiffness and fluctuating muscle activity for proprioception of postural joint rotations: the relevance to human standing. *J Neurophysiol* 102: 460-474, 2009.

Ma S-P, and Zahalak GI. A simple self-consistent distribution-moment model for muscle: chemical energy and heat rates. *Mathematical Biosciences* 84: 211-230, 1987.

Maas H, and Sandercock T. Force transmission between synergistic skeletal muscles through connective tissue linkages. *J Biomed Biotechnol* 2010.

Macpherson JM. Changes in a postural strategy with inter-paw distance. *J Neurophysiol* 71: 931-940, 1994.

Macpherson JM. Strategies that simplify the control of quadrupedal stance. I. Forces at the ground. *J Neurophysiol* 60: 204-217, 1988a.

Macpherson JM. Strategies that simplify the control of quadrupedal stance. II. Electromyographic activity. *J Neurophysiol* 60: 218-231, 1988b.

Macpherson JM, and Fung J. Weight support and balance during perturbed stance in the chronic spinal cat. *J Neurophysiol* 82: 3066-3081, 1999.

Mandelblat-Cerf Y, Paz R Fau - Vaadia E, and Vaadia E. Trial-to-trial variability of single cells in motor cortices is dynamically modified during visuomotor adaptation. *Journal of Neuroscience* 29: 15053-15062, 2009

Mann R, Hagey J, White V, and D L. The initiation of gait. *The Journal of Bone and Joint Surgery* 61(2): 232-239, 1979.

Mansouri M, and Reinbolt JA. Balance recovery simulation using a novel biologically-inspired musculoskeletal control system. In: *7th World Congress of Biomechanics*. Boston, MA, USA: 2014.

Martelli S, Calvetti D, Somersalo E, and Viceconti M. Stochastic modelling of muscle recruitment during activity. *Interface Focus* 5: 2015.

Martelli S, Calvetti D, Somersalo E, Viceconti M, and Taddei F. Computational tools for calculating alternative muscle force patterns during motion: A comparison of possible solutions. *J Biomech* 2013.

Martin RS. Implementation and validation of a computational model of the feline forelimb. In: *Electrical and Computer Engineering* Georgia Institute of Technology, 2013.

Mauritz KH. Gait training in hemiplegia. *European journal of neurology : the official journal of the European Federation of Neurological Societies* 9 Suppl 1: 23-29; discussion 53-61, 2002.

Mazet V. Simulation d'une distribution gaussienne tronquée sur un intervalle fini Université de Strasbourg, 2012.

McAndrew PM, Wilken JM, and Dingwell JB. Dynamic stability of human walking in visually and mechanically destabilizing environments. *J Biomech* 44: 644-649, 2011.

McCrea PH, Eng JJ, and Hodgson AJ. Saturated muscle activation contributes to compensatory reaching strategies after stroke. *J Neurophysiol* 94: 2999-3008, 2005.

McGill SM, Grenier S, Kavcic N, and Cholewicki J. Coordination of muscle activity to assure stability of the lumbar spine. *Journal of Electromyography and Kinesiology* 13: 353-359, 2003.

McGowan CP, Neptune RR, Clark DJ, and Kautz SA. Modular control of human walking: Adaptations to altered mechanical demands. *J Biomech* 43: 412-419, 2010.

McIntyre J, Mussa-Ivaldi FA, and Bizzi E. The control of stable postures in the multijoint arm. *Experimental Brain Research* 110: 248-264, 1996.

McKay JL, Burkholder TJ, and Ting LH. Biomechanical capabilities influence postural control strategies in the cat hindlimb. *J Biomech* 40: 2254-2260, 2007.

McKay JL, and Ting LH. Functional muscle synergies constrain force production during postural tasks. *J Biomech* 41: 299-306, 2008.

McKay JL, and Ting LH. Optimization of muscle activity for task-level goals predicts complex changes in limb forces across biomechanical contexts. *PLoS Comput Biol* 8: e1002465, 2012.

McLean SG, Su A, and van den Bogert AJ. Development and validation of a 3-D model to predict knee joint loading during dynamic movement. *Journal of biomechanical engineering* 125: 864-874, 2003.

Meier F, Theodorou EA, Stulp F, and Schaal S. Movement segmentation using a primitive library. In: *IEEE/RSJ international conference on intelligent robots and systems*. San Francisco, CA: 2011.

Miall RC, Weir DJ, Wolpert DM, and Stein JF. Is the cerebellum a smith predictor? *Journal of motor behavior* 25: 203-216, 1993.

Milner TEC, Caroline , and Leger ABF, David W. Inability to activate muscles maximally during cocontraction and the effect on joint stiffness. *Experimental Brain Research* 107: 293-305, 1995.

Minai AA. Computational Models of Cognitive and Motor Control. In: *Handbook of Computational Intelligence*, edited by Kacprzyk J, and Pedrycz W 2015.

Mockford M, and Caulton JM. Systematic review of progressive strength training in children and adolescents with cerebral palsy who are ambulatory. *Pediatric physical therapy : the official publication of the Section on Pediatrics of the American Physical Therapy Association* 20: 318-333, 2008.

Muceli S, Boye AT, d'Avella A, and Farina D. Identifying representative synergy matrices for describing muscular activation patterns during multidirectional reaching in the horizontal plane. *Journal of Neurophysiology* 103: 1532-1542, 2010.

Mussa-Ivaldi FA, and Giszter SF. Vector field approximation: a computational paradigm for motor control and learning. *Biological cybernetics* 67: 491-500, 1992.

Mussa-Ivaldi FA, Giszter SF, and Bizzi E. Linear combinations of primitives in vertebrate motor control. *Proc Natl Acad Sci U S A* 91: 7534-7538, 1994.

Mussa-Ivaldi FA, Hogan N, and Bizzi E. Neural, mechanical, and geometric factors subserving arm posture in humans. *Journal of Neuroscience* 5: 2732-2743, 1985.

Nakano E, Imamizu H, Osu R, Uno Y, Gomi H, Yoshioka T, and Kawato M. Quantitative examinations of internal representations for arm trajectory planning: minimum commanded torque change model. *J Neurophysiol* 81: 2140-2155, 1999.

Nashner LM. Adapting reflexes controlling the human posture. *Experimental Brain Research* 26: 59-72, 1976.

Nashner LM. Fixed patterns of rapid postural responses among leg muscles during stance. *Experimental Brain Research* 30: 13-24, 1977.

Nataraj R, Audu M, and Triolo R. Comparing joint kinematics and center of mass acceleration as feedback for control of standing balance by functional neuromuscular stimulation. *Journal of NeuroEngineering and Rehabilitation* 9: 2012

Nataraj R, Audu ML, Kirsch RF, and Triolo RJ. Comprehensive joint feedback control for standing by functional neuromuscular stimulation—a simulation study. *IEEE transactions on neural systems and rehabilitation engineering : a publication of the IEEE Engineering in Medicine and Biology Society* 18: 646-657, 2010.

Neptune R, Sasaki K, and Kautz S. The effect of walking speed on muscle function and mechanical energetics. *Gait & Posture* 28: 135-143, 2008.

Neptune RR. Optimization algorithm performance in determining optimal controls in human movement analyses. *Journal of biomechanical engineering* 121: 249-252, 1999.

Neptune RR, Clark DJ, and Kautz SA. Modular control of human walking: A simulation study. *J Biomech* 42: 1282-1287, 2009.

Neptune RR, Kautz SA, and Zajac FE. Contributions of the individual ankle plantar flexors to support, forward progression and swing initiation during walking. *J Biomech* 34: 1387-1398, 2001.

Nichols TR. The organization of heterogenic reflexes among muscles crossing the ankle joint in the decerebrate cat. *J Physiol* 410: 463-477, 1989

Nishikawa K, Biewener AA, Aerts P, Ahn AN, Chiel HJ, Daley MA, Daniel TL, Full RJ, Hale ME, Hedrick TL, Lappin AK, Nichols TR, Quinn RD, Satterlie RA, and Szymik B. Neuromechanics: an integrative approach for understanding motor control. *Integrative and comparative biology* 47: 16-54, 2007.

Novacheck TF, Trost JP, and Schwartz MH. Intramuscular psoas lengthening improves dynamic hip function in children with cerebral palsy. *Journal of pediatric orthopedics* 22: 158-164, 2002.

Osu R, Franklin DW, Kato H, Gomi H, Domen K, Yoshioka T, and Mitsuo K. Short- and long-term changes in joint co-contraction associated with motor learning as revealed from surface EMG. . *Journal of Neurophysiology* 88: 991–1004, 2002.

Pandy MG. Computer modeling and simulation of human movement. *Annual Review of Biomedical Engineering* 3: 245-273, 2001.

Pandy MG, and Andriacchi TP. Muscle and joint function in human locomotion. *Annual Review of Biomedical Engineering* 12: 401-433, 2010.

Park S, Horak FB, and Kuo AD. Postural feedback responses scale with biomechanical constraints in human standing. *Experimental Brain Research* 154: 417-427, 2004.

Parker P, Englehart K, and Hudgins B. Myoelectric signal processing for control of powered limb prostheses. *Journal of electromyography and kinesiology : official journal of the International Society of Electrophysiological Kinesiology* 16: 541-548, 2006.

Pekny SE, Izawa J, and Shadmehr R. Reward-dependent modulation of movement variability. *Journal of Neuroscience* 35: 4015-4024, 2015.

Perreault EJ, Chen K, Trumbower RD, and Lewis G. Interactions with compliant loads alter stretch reflex gains but not intermuscular coordination. *J Neurophysiol* 99: 2101-2113, 2008.

Perreault EJ, Kirsch RF, and Crago PE. Effects of voluntary force generation on the elastic components of endpoint stiffness. *Experimental Brain Research* 141: 312-323, 2001.

Perreault EJ, Kirsch RF, and Crago PE. Multijoint dynamics and postural stability of the human arm. *Experimental Brain Research* 157: 507-517, 2004.

Perreault EJ, Kirsch RF, and Crago PE. Voluntary control of static endpoint stiffness during force regulation tasks. *J Neurophysiol* 87: 2808-2816, 2002.

Perry J. *Gait Analysis: Normal and pathological function.* Thorofare, NJ: SLACK Incorporated, 1992.

Peterka RJ. Postural control model interpretation of stabilogram diffusion analysis. *Biological cybernetics* 82: 335-343, 2000.

Piazza SJ, and Delp SL. The influence of muscles on knee flexion during the swing phase of gait. *J Biomech* 29: 723-733, 1996.

Piazza SJ, and Delp SL. Three-dimensional dynamic simulation of total knee replacement motion during a step-up task. *Journal of biomechanical engineering* 123: 599-606, 2001.

Picelli A, Melotti C, Origano F, Neri R, Verze E, Gandolfi M, Waldner A, and Smania N. Robot-assisted gait training is not superior to balance training for improving postural instability in patients with mild to moderate Parkinson's disease: a single-blind randomized controlled trial. 2014.

Pippenger W, and Scalzitti D. What are the effects, if any, of lower-extremity strength training on gait in children with cerebral palsy? *Phys Ther* 84: 849-858, 2004.

Prilutsky BI, Herzog W, and Allinger TL. Forces of individual cat ankle extensor muscles during locomotion predicted using static optimization. *J Biomech* 30: 1025-1033, 1997.

Prinsen EC, Nederhand MJ, and Rietman JS. Adaptation strategies of the lower extremities of patients with a transtibial or transfemoral amputation during level walking: a systematic review. *Archives of physical medicine and rehabilitation* 92: 1311-1325, 2011.

Prinz AA, Bucher D, and Marder E. Similar network activity from disparate circuit parameters. *Nature Neuroscience* 7: 1345-1352, 2004.

Raasch CC, and Zajac FE. Locomotor strategy for pedaling: muscle groups and biomechanical functions. *J Neurophysiol* 82: 515-525, 1999.

Raasch CC, Zajac FE, Ma B, and Levine WS. Muscle coordination of maximum-speed pedaling. *J Biomch* 30: 595-602, 1997.

Rack PM, and Westbury DR. The effects of length and stimulus rate on tension in the isometric cat soleus muscle. *The Journal of physiology* 204: 443-460, 1969.

Racz K, Brown D, and Valero-Cuevas FJ. An involuntary stereotypical grasp tendency pervades voluntary dynamic multifinger manipulation. *J Neurophysiol* 108: 2896-2911, 2012.

Ralston HJ, Todd FN, and Inman VT. Comparison of electrical activity and duration of tension in the human rectus femoris muscle. *Electromyogr Clin Neurophysiol* 16: 271-280, 1976

Raphael G, Tsianos GA, and Loeb GE. Spinal-like regulator facilitates control of a two-degree-of-freedom wrist. *Journal of Neuroscience* 30: 9431-9444, 2010.

Reisman DS, and Scholz JP. Workspace location influences joint coordination during reaching in post-stroke hemiparesis. *Experimental Brain Research* 170: 265-276, 2006.

Risher DW, Schutte LM, and Runge CF. The use of inverse dynamics solutions in direct dynamics simulations. *Journal of biomechanical engineering* 119: 417-422, 1997.

Roh J, Cheung VCK, and Bizzi E. Modules in the brain stem and spinal cord underlying motor behaviors. *J Neurophysiol* 106: 1363-1378, 2011.

Roh J, Rymer WZ, and Beer RF. Robustness of muscle synergies underlying three dimensional force generation at the hand in healthy humans. *J Neurophysiol* 2012.

Roh J, Rymer WZ, Perreault EJ, Yoo SB, and Beer RF. Alterations in upper limb muscle synergy structure in chronic stroke survivors. *J Neurophysiol* 109: 768-781, 2013.

Rose J, Gamble J, Medeiros J, Burgos A, and Haskell W. Energy cost of walking in normal children and in those with cerebral palsy: comparison of heart rate and oxygen uptake. *Journal of pediatric orthopedics* 9: 276-279, 1989.

Roy RR, Kim JA, Monti RJ, Zhong H, and Edgerton VR. Architectural and histochemical properties of cat hip 'cuff' muscles. *Acta Anatomica* 159: 136-146, 1997.

Ruckert E, and d'Avella A. Learned parametrized dynamic movement primitives with shared synergies for controlling robotic and musculoskeletal systems. *Frontiers in computational neuroscience* 7: 138, 2013.

Runge CF, Shupert CL, Horak FB, and Zajac FE. Ankle and hip postural strategies defined by joint torques. *Gait Posture* 10: 161-170, 1999.

Runge CF, Zajac FE, III, Allum JHJ, Risher DW, Bryson AE, and Honegger F. Estimating net joint torques from kinesiological data using optimal linear system theory. *IEEE Transactions on Biomedical Engineering* 42: 1158-1164, 1995.

Sacks RD, and Roy RR. Architecture of the hind limb muscles of cats: functional significance. *Journal of Morphology* 173: 185-195, 1982.

Safavynia SA, and Ting LH. Sensorimotor feedback based on task-relevant error robustly predicts temporal recruitment and multidirectional tuning of muscle synergies. *J Neurophysiol* 109: 31-45, 2013.

Santos VJ, Bustamante CD, and Valero-Cuevas FJ. Improving the fitness of high-dimensional biomechanical models via data-driven stochastic exploration. *IEEE Transactions on Biomedical Engineering* 56: 552-564, 2009.

Schantz PG, Moritani T, Karlson E, Johansson E, and Lundh A. Maximal voluntary force of bilateral and unilateral leg extension. *Acta physiologica Scandinavica* 136: 185-192, 1989.

Schmidt MW, Lopez-Ortiz C, Barrett PS, Rogers LM, and Gruben KG. Foot force direction in an isometric pushing task: prediction by kinematic and musculoskeletal models. *Experimental Brain Research* 150: 245-254, 2003.

Scianni A, Butler JM, Ada L, and Teixeira-Salmela LF. Muscle strengthening is not effective in children and adolescents with cerebral palsy: a systematic review. *Australian Journal of Physiotherapy* 55: 81-87, 2009.

Secher NH, Rube N, and Elers J. Strength of 2-leg and one-leg extension in man. *Acta physiologica Scandinavica* 134: 333-339, 1988.

Selen LP, Franklin DW, and Wolpert DM. Impedance control reduces instability that arises from motor noise. *Journal of Neuroscience* 29: 12606-12616, 2009.

Shemmell J, Krutky MA, and Perreault EJ. Stretch sensitive reflexes as an adaptive mechanism for maintaining limb stability. *Clinical neurophysiology : official journal of the International Federation of Clinical Neurophysiology* 121: 1680-1689, 2010.

Silverman AK, Wilken JM, Sinitski EH, and Neptune RR. Whole-body angular momentum in incline and decline walking. *J Biomech* 45: 965-971, 2012.

Simpson CS, Sohn MH, Allen JL, and Ting LH. Muscle feasible ranges in human walking are unconstrained by biomechanics. *J Biomech* in review.

Soares A, Yamaguti E, Mochizuki L, Amadio A, and Serrão J. Biomechanical parameters of gait among transtibial amputees: a review. *Sao Paulo Med J* 127: 302-309, 2009

Sober SJ, Wohlgenuth MJ, and Brainard MS. Central contributions to acoustic variation in birdsong. *Journal of Neuroscience* 28: 10370-10379, 2008.

Soechting JF, Buneo CA, Herrmann U, and Flanders M. Moving effortlessly in three dimensions: does Donders' law apply to arm movement? *Journal of Neuroscience* 15: 6271-6280, 1995.

Sohn MH. Assessing functional stability of predicted muscle activation patterns for postural control using a neuromechanical model of the cat hindlimb. In: *Woodruff School of Mechanical Engineering* Georgia Institute of Technology, 2011.

Sohn MH, McKay JL, and Ting LH. Defining feasible bounds on muscle activation in a redundant biomechanical task: practical implications of redundancy. *J Biomech* 46: 1363-1368, 2013.

Steele KM, Seth A, Hicks JL, Schwartz MH, and Delp SL. Muscle contributions to vertical and fore-aft accelerations are altered in subjects with crouch gait. *Gait Posture* 2012a.

Steele KM, Seth A, Hicks JL, Schwartz MS, and Delp SL. Muscle contributions to support and progression during single-limb stance in crouch gait. *J Biomech* 43: 2099-2105, 2010.

Steele KM, Tresch MC, and Perreault EJ. Consequences of biomechanically constrained tasks in the design and interpretation of synergy analyses. *J Neurophysiol* jn 00769 02013, 2015.

Steele KM, Tresch MC, and Perreault EJ. The number and choice of muscles impact the results of muscle synergy analyses. *Frontiers in computational neuroscience* 7: 105, 2013.

Steele KM, van der Krogt MM, Schwartz MH, and Delp SL. How much muscle strength is required to walk in a crouch gait? *J Biomech* 45: 2564-2569, 2012b.

Stinear CM, Barber PA, Smale PR, Coxon JP, Fleming MK, and Byblow WD. Functional potential in chronic stroke patients depends on corticospinal tract integrity. *Brain* 130: 170-180, 2007.

Stokes IA, and Gardner-Morse M. Lumbar spinal muscle activation synergies predicted by multi-criteria cost function. *J Biomech* 34: 733-740, 2001.

Sukal TM, Ellis MD, and Dewald JP. Shoulder abduction-induced reductions in reaching work area following hemiparetic stroke: neuroscientific implications. *Experimental Brain Research* 183: 215-223, 2007.

Swinnen E, Beckwée D, Meeusen R, Baeyens J, and Kerckhofs E. Does robot-assisted gait rehabilitation improve balance in stroke patients? A systematic review. *Topics in stroke rehabilitation* 21: 87-100, 2014

Takikawa Y, Kawagoe R, Itoh H, Nakahara H, and Hikosaka O. Modulation of saccadic eye movements by predicted reward outcome. *Experimental Brain Research* 142: 284-291, 2002.

Thelen DG. Adjustment of muscle mechanics model parameters to simulate dynamic contractions in older adults. *Journal of biomechanical engineering* 125: 70, 2003.

Thelen DG, and Anderson FC. Using computed muscle control to generate forward dynamic simulations of human walking from experimental data. *J Biomech* 39: 1107-1115, 2006.

Thelen DG, Anderson FC, and Delp SL. Generating dynamic simulations of movement using computed muscle control. *J Biomech* 36: 321-328, 2003.

Thoroughman K, and Shadmehr R. Learning of action through adaptive combination of motor primitives. *Nature* 407: 742-747, 2000.

Ting LH. Dimensional reduction in sensorimotor systems: a framework for understanding muscle coordination of posture. *Progress in Brain Research* 165: 299-321, 2007.

Ting LH, and Chiel HJ. Muscle, biomechanics, and implications for neural control. In: *The Neurobiology of Motor Control: Fundamental Concepts and New Directions*, edited by Hooper SL, and Büschges A. New York: Wiley, in press.

Ting LH, Chiel HJ, Trumbower RD, Allen JL, McKay JL, Hackney ME, and Kesar TM. Neuromechanical principles underlying movement modularity and their implications for rehabilitation. *Neuron* in press.

Ting LH, Chvatal SA, Safavynia SA, and Lucas McKay J. Review and perspective: neuromechanical considerations for predicting muscle activation patterns for movement. *International journal for numerical methods in biomedical engineering* 28: 1003-1014, 2012.

Ting LH, Kautz SA, Brown DA, and Zajac FE. Phase reversal of biomechanical functions and muscle activity in backward pedaling. *J Neurophysiol* 81: 544-551, 1999.

Ting LH, and Macpherson JM. A limited set of muscle synergies for force control during a postural task. *J Neurophysiol* 93: 609-613, 2005.

Ting LH, and Macpherson JM. Ratio of shear to load ground-reaction force may underlie the directional tuning of the automatic postural response to rotation and translation. *J Neurophysiol* 92: 808-823, 2004.

Ting LH, van Antwerp KW, Scrivens JE, McKay JL, Welch TDJ, Bingham JT, and DeWeerth SP. Neuromechanical tuning of nonlinear postural control dynamics. *Chaos: An Interdisciplinary Journal of Nonlinear Science* 19: 026111, 2009.

Todorov E. Optimality principles in sensorimotor control. *Nature Neuroscience* 7: 907-915, 2004.

Todorov E, and Jordan MI. Optimal feedback control as a theory of motor coordination. *Nature Neuroscience* 5: 1226-1235, 2002.

Torres-Oviedo G, Macpherson JM, and Ting LH. Muscle synergy organization is robust across a variety of postural perturbations. *J Neurophysiol* 96: 1530-1546, 2006.

Torres-Oviedo G, and Ting LH. Muscle synergies characterizing human postural responses. *J Neurophysiol* 98: 2144-2156, 2007.

Torres-Oviedo G, and Ting LH. Subject-specific muscle synergies in human balance control are consistent across different biomechanical contexts. *J Neurophysiol* 103: 3084-3098, 2010.

Torres EB, and Zipser D. Reaching to grasp with a multi-jointed arm. I. Computational model. *J Neurophysiol* 88: 2355-2367, 2002.

Tresch MC, and Jarc A. The case for and against muscle synergies. *Curr Opin Neurobiol* 19: 601-607, 2009.

Tresch MC, Saltiel P, and Bizzi E. The construction of movement by the spinal cord. *Nat Neurosci* 2: 1999.

Trumbower RD, Krutky MA, Yang BS, and Perreault EJ. Use of self-selected postures to regulate multi-joint stiffness during unconstrained tasks. *PloS one* 4: e5411, 2009.

Trumbower RD, Ravichandran VJ, Krutky MA, and Perreault EJ. Contributions of altered stretch reflex coordination to arm impairments following stroke. *J Neurophysiol* 104: 3612-3624, 2010.

Tsianos GA, Goodner J, and Loeb GE. Useful properties of spinal circuits for learning and performing planar reaches. *Journal of Neural Engineering* 11: 056006, 2014.

Tumer EC, and Brainard MS. Performance variability enables adaptive plasticity of 'crystallized' adult birdsong. *Nature* 450: 1240-1244, 2007.

Tuzson AE, Granata KP, and Abel MF. Spastic velocity threshold constrains functional performance in cerebral palsy. *Archives of physical medicine and rehabilitation* 84: 1363-1368, 2003.

Uno Y, Kawato M, and Suzuki R. Formation and control of optimal trajectory in human multijoint arm movement. Minimum torque-change model. *Biological cybernetics* 61: 89-101, 1989.

Valero-Cuevas FJ. An integrative approach to the biomechanical function and neuromuscular control of the fingers. *J Biomech* 38: 673-684, 2005.

Valero-Cuevas FJ. A mathematical approach to the mechanical capabilities of limbs and fingers. *Advances in experimental medicine and biology* 629: 619-633, 2009.

Valero-Cuevas FJ. Predictive modulation of muscle coordination pattern magnitude scales fingertip force magnitude over the voluntary range. *J Neurophysiol* 83: 1469–1479, 2000.

Valero-Cuevas FJ, and Hentz VR. Releasing the A3 pulley and leaving flexor superficialis intact increases pinch force following the Zancolli lasso procedures to prevent claw deformity in the intrinsic palsied finger. *Journal of Orthopaedic Research* 20 902-909, 2002.

Valero-Cuevas FJ, Hoffmann H, Kurse MU, Kutch JJ, and Theodorou EA. Computational Models for Neuromuscular Function. *IEEE reviews in biomedical engineering* 2: 110-135, 2009.

Valero-Cuevas FJ, Jae-Woong Y, Brown D, McNamara RV, Paul C, and Lipson H. The tendon network of the fingers performs anatomical computation at a macroscopic scale. *IEEE Transactions on Biomedical Engineering* 54: 1161-1166, 2007.

Valero-Cuevas FJ, Zajac FE, and Burgar CG. Large index-fingertip forces are produced by subject-independent patterns of muscle excitation. *J Biomech* 31 693-703, 1998.

van Antwerp K, Burkholder T, and Ting L. Inter-joint coupling effects on muscle contributions to endpoint force and acceleration in a musculoskeletal model of the cat hindlimb. *J Biomech* 40: 3570-3579, 2007.

van der Kooij H, Jacobs R, Koopman B, and Grootenboer H. A multisensory integration model of human stance control. *Biological cybernetics* 80: 299-308, 1999.

van der Krogt MM, Delp SL, and Schwartz MH. How robust is human gait to muscle weakness? *Gait & Posture* 36: 113-119, 2012.

Vrieling AH, van Keeken HG, Schoppen T, Otten E, Hof AL, Halbertsma JP, and Postema K. Balance control on a moving platform in unilateral lower limb amputees. *Gait Posture* 28: 222-228, 2008.

Wagner GP, Pavlicev M, and Cheverud JM. The road to modularity. *Nature reviews Genetics* 8: 921-931, 2007.

Walmsley B, Hodgson JA, and Burke RE. Forces produced by medial gastrocnemius and soleus muscles during locomotion in freely moving cats. *J Neurophysiol* 41: 1203-1216, 1978.

Walter JP, Kinney AL, Banks SA, D'Lima DD, Besier TF, Lloyd DG, and Fregly BJ. Muscle synergies may improve optimization prediction of knee contact forces during walking. *Journal of biomechanical engineering* 136: 021031, 2014.

Wang R, and Gutierrez-Farewik EM. Compensatory strategies during walking in response to excessive muscle co-contraction at the ankle joint. *Gait Posture* 39: 926-932, 2014.

Ward NS, Newton JM, Swayne OB, Lee L, Thompson AJ, Greenwood RJ, Rothwell JC, and Frackowiak RS. Motor system activation after subcortical stroke depends on corticospinal system integrity. *Brain* 129: 809-819, 2006.

Waters RL, and Mulroy S. The energy expenditure of normal and pathologic gait. *Gait Posture* 9: 207-231, 1999.

Welch TD, and Ting LH. A feedback model explains the differential scaling of human postural responses to perturbation acceleration and velocity. *J Neurophysiol* 101: 3294-3309, 2009.

Welch TDJ, and Ting LH. A feedback model reproduces muscle activity during human postural responses to support-surface translations. *J Neurophysiol* 99: 1032-1038, 2008.

Wiley ME, and Damiano DL. Lower-extremity strength profiles in spastic cerebral palsy. *Developmental medicine and child neurology* 40: 100-107, 1998.

Will B, Galani R, Kelche C, and Rosenzweig MR. Recovery from brain injury in animals: relative efficacy of environmental enrichment, physical exercise or formal training (1990-2002). *Progress in neurobiology* 72: 167-182, 2004.

Wilmink RJ, and Nichols TR. Distribution of heterogenic reflexes among the quadriceps and triceps surae muscles of the cat hind limb. *J Neurophysiol* 90: 2310-2324, 2003.

Winter DA. *The biomechanics and motor control of human gait.* Waterloo, Ontario, Canada: University of Waterloo Press, 1987.

Winter DA, and Yack HJ. EMG profiles during normal human walking: stride-to-stride and inter-subject variability. *Electroencephalography and clinical Neurophysiology* 67: 402-411, 1987.

Wren TA, Rethlefsen S, and Kay RM. Prevalence of specific gait abnormalities in children with cerebral palsy: influence of cerebral palsy subtype, age, and previous surgery. *Journal of pediatric orthopedics* 25: 79-83, 2005.

Wu HG, Miyamoto YR, Gonzalez Castro LN, Olveczky BP, and Smith MA. Temporal structure of motor variability is dynamically regulated and predicts motor learning ability. *Nat Neurosci* 17: 312-321, 2014.

Yamasaki H, Tagami Y, Fujisawa H, Hoshi F, and Nagasaki H. Interaction torque contributes to planar reaching at slow speed. *Biomedical engineering online* 7: 27, 2008.

Yeo SH, Mullens CH, Sandercock TG, Pai DK, and Tresch MC. Estimation of musculoskeletal models from in situ measurements of muscle action in the rat hindlimb. *The Journal of experimental biology* 214: 735-746, 2011.

Yeo SH, Tresch MC, and Pai DK. Optimal design of musculoskeletal models using force field data. In: *30th Annual International IEEE EMBS Conference.* Vancouver, British Columbia, Canada: 2008, p. August 20-24.

Zackowski KM, Dromerick AW, Sahrman SA, Thach WT, and Bastian AJ. How do strength, sensation, spasticity and joint individualation relate to the reaching deficits of people with chronic hemiparesis? *Brain* 127: 1035-1046, 2004.

Zajac FE. Muscle and tendon: properties, models, scaling, and application to biomechanics and motor control. *Crit Rev Biomed Eng* 17: 359-411, 1989.

Zajac FE. Muscle coordination of movement: a perspective. *J Biomech* 26 Suppl 1: 109-124, 1993.

Zajac FE, and Gordon ME. Determining muscle's force and action in multi-articular movement. *Exercise and sport sciences reviews* 17: 187-230, 1989.

Zarrugh MY, Todd FN, and Ralston HJ. Optimization of energy expenditure during level walking. *European journal of applied physiology and occupational physiology* 33: 293-306, 1974.

Zenzeri J, De Santis D, and Morasso P. Strategy switching in the stabilization of unstable dynamics. *PloS one* 9: e99087, 2014.

VITA

M. HONGCHUL SOHN

M. Hongchul Sohn was born in Atlanta, Georgia. He graduated from Seoul National University in Seoul, Korea, earning a Bachelor of Science degree in Mechanical and Aerospace Engineering. Before coming to Georgia Tech to study neural control of movement, he served in Republic of Korea Air Force as an officer, investigating aircraft accidents and conducting failure analysis on turbine engine components. His research focuses on understanding the neuromechanical principles underlying functional and impaired movements. When he is not working on his research, he enjoys spending time with his family and is involved in his church.